Pharmacological characterization of chemokine receptor 7 (CCR7) as a potential therapeutic target in cancer

Haneen Adel Daoud BASHEER

Submitted for the degree of Doctor of Philosophy

Institute of Cancer Therapeutics

University of Bradford

2017

Abstract

Haneen Adel Daoud Basheer

Title: Pharmacological characterization of chemokine receptor 7 (CCR7) as a potential therapeutic target in cancer

Keywords: Cancer, Chemokine, CCR7, pharmacology

The expression of CCR7 was evaluated in different cancer cell lines by using flow cytometry, western blot, Immunofluorescence and immunohistochemistry. We showed for the selected cell lines that the expression is maintained in cells grown as spheroids, and xenoplanted in mice. Furthermore, we showed the expression of CCR7 correlates with stage of the disease in patient derived head and neck cancer tissue. We also showed that expression of CCR7 in cancer cell lines correlates with migratory aptitude towards CCL21 in a scratch assay, Boyden chamber assay and spheroid invasion assay.

We then showed that the expression of CCR7 is elevated under serum starvation and under hypoxia in cancer cell lines grown as monolayers and as spheroids; and that there is a correlation between hypoxia and CCR7 expression in spheroids, xenografted cells and clinical cancer tissue. However, we found that in cell line OSC-19, the increase in the expression of CCR7 did not correlate to increased migration. Our investigations following this observation showed that whilst hypoxia increases the expression of CCR7, it concurrently causes a decrease in reactive oxygen species (ROS) which strongly abrogates migratory aptitude in OSC-19, resulting in an overall loss of migration in OSC-19 cells.

In addition, we characterised OSC-19 as a suitable model to evaluate small molecule CCR7 antagonists using a number of different assays. In particular, we showed that ICT13069 antagonised response of this cell line across a number of drivers of malignancy such as migration, invasion in 2D and 3D models.

In loving memory of my father

Hope this makes you proud

Acknowledgements

My first debt of gratitude must go to my supervisor, Dr Kamyar Afarinkia. He patiently provided the vision, encouragement and advice necessary for me to proceed through my project. His guidance and stimulating discussions helped me to keep on the right track.

I would like also to thank my second supervisor, Dr Victoria Vinader for her generous and unconditional support. I'm thankful for her advice and insightful comments in all the time of my research.
I could not have imagined having better friendly advisors for my PhD study.

I'm also thankful to Dr Steven Shnyder, for sharing his expertise and knowledge that helped me throughout my project.

My sincere thanks go to Mrs Patricia Cooper for xenografts preparations and Mr Gary Lawson for his help in cell culture lab, Dr. Simon Allison, for his guidance and insightful comments on my flow cytometry work and for teaching me knockdown studies, Professor Keith Hunter and Dr. Lisette Martin for microarrays clinical samples scoring, Mr. Edvinas Pakanavicius for statistical analysis of clinical samples data. Msc student Roshan Petal for helping in SW-480 scratch assay results, ICT intern Mr Marco Mazzini for helping in PC-3 scratch assay and Immunofluorescence staining of CCR7 in colon cell lines and Dr.Jose María Ayuso Domínguez for his helpful suggestions on spheroid invasion assay.

Special thanks go to my colleagues and friends Monika, Dany, Laura, Hanadi, Chema, Lina, Djev, Mario, Sadr, Ghasak, Lina, Sara and Maria who worked with me in the lab, for their support, guidance and helpful suggestions. I owe them my heartfelt appreciation.

I'd like also to express my gratitude for Zarqa University for their generous sponsorship and Prof.Nancy Hakooz for her unconditional support and genuine care.

I'm deeply thankful for my mother Yusra Basheer, without her continuous support and encouragement I never would have been able to achieve my goals. Thank you for all of the sacrifices that you have made on my behalf. Your love was my driving force. Words cannot express how grateful I am to have a mom like you, who sacrificed everything for my siblings and myself to make us happy. Mom, I owe you everything and wish I could show you how much I love and appreciate you.

I'm also thankful for my loving siblings Riham, Ahmed, Shahd and Omar and my beloved aunt Mariam. All of you have been there to support me through the good and bad times.

Last but not least, this work is dedicated for my late dad Dr. Adel Basheer, I hope that this work makes you proud. Throughout the years you have been my true and only role model not only for the tremendous success you achieved in life but also for your unconditional love and care that you gave for our family. It is your shining example that I try to follow in all that I do.

Publications:

Basheer HA, Vinader V, Afarinkia K. CCR7 axis in cancer: Friend or Foe?. *Manuscript in preparation***.**

Basheer HA, Simon J. Allison, Steven D. Shnyder, Lisette Martin, Keith D. Hunter, Victoria Vinader, Kamyar Afarinkia. The role of hypoxia in CCR7 mediated metastasis of head and neck cancers. *Manuscript in preparation***.**

Ahmed M, **Basheer HA**, Ayuso JM, Ahmet D, Mazzini M, Patel R, Shnyder SD, Vinader V, Afarinkia K. Agarose Spot as a Comparative Method for in situ Analysis of Simultaneous Chemotactic Responses to Multiple Chemokines. Sci Rep. 2017 Apr 21;7(1):1075. doi: 10.1038/s41598-017-00949-4 . **Joint First author.**

Elkashef SM, Allison SJ, Sadiq M, **Basheer HA**, Ribeiro Morais G, Loadman PM, Pors K, Falconer RA. Polysialic acid sustains cancer cell survival and migratory capacity in a hypoxic environment. Sci Rep. 2016 Sep 9;6:33026. doi: 10.1038/srep33026.

Ayuso JM, **Basheer HA**, Monge R, Sánchez-Álvarez P, Doblaré M, Shnyder SD, Vinader V, Afarinkia K, Fernández LJ, Ochoa I. Study of the Chemotactic Response of Multicellular Spheroids in a Microfluidic Device. PLoS One. 2015 Oct 7;10 (10):e0139515. doi: 10.1371/journal.pone.0139515. eCollection 2015.

Conference abstracts:

H. A. D. Basheer, S. Allison, M. Ahmed, S. D. Shnyder, M. V. Vinader, K. Afarinkia (2016). Role of CCR7 in head and neck cancer, North of England Cell Biology meeting, Bradford, UK.

H. A. D. Basheer, S. Allison, M. Ahmed, S. D. Shnyder, M. V. Vinader, K. Afarinkia (2016). Role of CCR7 in head and neck cancer, chemotactic cytokines GRS, Girona, Spain.

H. A. D. Basheer, S. Allison, M. Ahmed, S. D. Shnyder, M. V. Vinader, K. Afarinkia (2016.) Role of CCR7 in head and neck cancer, chemotactic cytokines GRC, Girona, Spain.

H. A. D. Basheer, Mohaned S Ahmed, S. D. Shnyder, M. V. Vinader, K. Afarinkia (2015). Role of CCR7 in head and neck cancerThe NCRI Cancer Conference, Liverpool, UK.

H. A. D. Basheer, Mohaned S Ahmed, S. D. Shnyder, M. V. Vinader, K. Afarinkia (2014). ICT5888 is a novel small molecule antagonist of CCR7 chemokine receptor, GRC, Mount Snow, USA.

M.V. Vinader, Mohaned S Ahmed, **H. A. D. Basheer**, D. Ahmet, S. D. Shnyder, L. H. Patterson, K. Afarinkia (2014). Potential of novel chemokine antagonists for the treatment of cancer, YCR annual scientific conference Harrogate, UK.

Contents

List of figures:

List of tables

List of Abbreviations

-ve	Negative control
+ve	Positive control
µ	Micro
AIDS	Acquired immune deficiency syndrome
APES	3-aminopropyltriethoxysilane
ATP	Adenosine triphosphate
A	Avidin
B	Biotinylated peroxidase
BSA	Bovine serum albumin
CAIX	Carbonic anhydrase IX
Carboxy-H2DCFDA	6-carboxy-2',7'-dichlorodihydrofluorescein diacetate
cAMP	Cyclic adenosine monophosphate
CDC42	Cell division control protein 42
DAB	3,3'-diaminobenzidine
DC	Dendritic cell
DMSO	Dimethyl Sulfoxide
DPX	Distyrene, tricresyl phosphate and xylene
ELISA	Enzyme-linked immunosorbent assay
EMT	Epithelial-mesenchymal transition
ECM	Extracellular matrix
EGF(R)	Endothelial growth factor (receptor)
ERK	Extracellular-signal-regulated kinases
FIH-1	Factor inhibiting HIF-1
FBS	Foetal bovine serum FBS

G	Guanosine
GAGs	Glycosaminoglycans
GDP	Guanosine diphosphate
GPCR	G-protein coupled receptors
GTP	Guanosine triphosphate
HIF	Hypoxia inducible factor
H	Hour
ICT	Institute of Cancer Therapeutics
IF	Immunofluorescence
JNK	c-Jun N-terminal kinases
L-DHA	Lactate dehydrogenase
LOX	Lysyl oxidase
M	Metastasis
Ml	milliliters
MAPK	Mitogen-activated protein kinases
Min	Minutes
MMP	Matrix metalloproteinase
MTT	3-(4,5-dimethythiazol-2-yl)-2,5-diphenyl tetrazolium bromide
N	Regional lymph node metastasis
NKC	Natural killer cell
NSCLC	Non-small cell lung cancer
OS	Overall survival
PDAC	Pancreatic ductal adenocarcinoma
PBS	Phosphate buffer saline
PBST	Phosphate buffer saline TWEEN 20

PFA	Paraformaldehyde
PI	Propidium iodide
PHD	Prolyl-4-hydroxylase domain
PI3K	Phosphatidylinositol-3-kinase
PI3P	Phosphatidylinositol 3-phosphate
PLC	Phospholipase C
PTEN	Phosphatase and tensin homolog
RANKL	Receptor activator of nuclear factor kappa-B ligand
R.T.	Room temperature
ROS	Reactive oxygen species
SAR	Structure activity relationship
S	Seconds
SD	Standard deviation
SREs	Skeletal related complications
TM	Trans-membrane
TMB	3,3′,5,5′-Tetramethylbenzidine
T	Tumour
U-PA	Urokinase-type plasminogen activator
VEGF	Vascular endothelial growth factor

Chapter 1:

Introduction

1.1 Cancer & Metastasis

Cancer accounted for 8.8 million deaths worldwide in 2015 (WHO, 2017) . Recent figures indicate that 14.1 million new cancer cases were diagnosed and 32.6 million people are still living with cancer within 5 years of diagnosis in 2012 worldwide (WHO, 2014). In the UK, approximately 163,444 cancer related deaths occurred in 2014 (Cancer Research UK, 2014).

Cancer results from an abnormal growth of cells. Over the past four decades much is discovered about the molecular mechanisms underlying this disease. In both animal and in human studies, it has been observed that cancer is triggered by multiple successive genetic and epigenetic changes in cells, leading to their transformation into a population with an imbalance between proliferation and death; eventually developing into cells that can invade adjacent tissues and metastasise to distant organs (Hanahan and Weinberg, 2000). Within this broad definition, the disease can be subclassified and in fact, there are over 100 different types of cancer and multiple subtypes within each cancer that have been described. However, despite such variety, Hanahan and Weinberg, have proposed common traits shared by nearly all cancer types that they described as Cancer Hallmarks Figure 1.

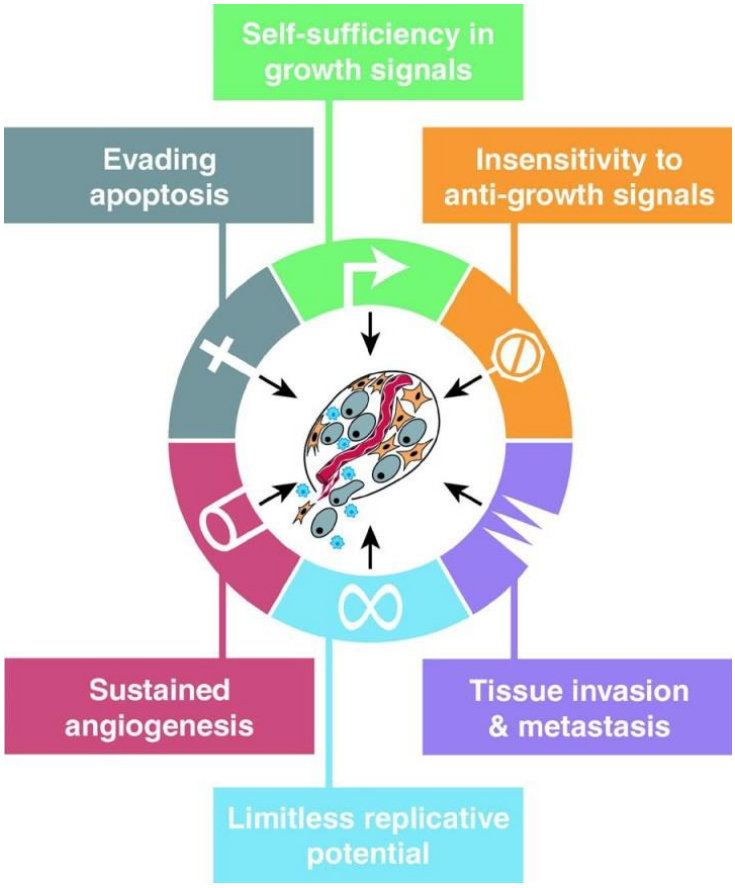

Figure 1: The First six established hallmarks of cancer.

These characteristics are shared by most cancer cells (Hanahan and Weinberg, 2000).

These traits or common characteristics include: (1) Self-sufficiency in growth signals, (2) Unresponsiveness to anti-growth signals, (3) Evasion of apoptosis, (4) Uncontrolled replicative potential (5) Angiogenesis, (6) Tissue invasion and metastasis.

These hallmarks can be acquired at different time points *via* different mechanisms in different cancer types, but they can ultimately lead cancer cells to proliferate, survive, invade and colonise other tissues. Since the initial publication of these

hallmarks, researchers have proposed other traits and hallmarks, which are also important for the progression and development of cancer, to be added to the initial list. They include “enabling” hallmarks (Hanahan and Weinberg, 2011) which are necessary to allow the acquisition of all the earlier mentioned characteristics and result from the genomic instability and the pro-inflammatory state of cancer cells. These hallmarks include the escape from the immune system and reprogramming of the metabolic processes to provide energy to support the endless growth and survival of cells Figure 2. There are many molecular factors that can contribute for acquiring of tumour cells’ hallmarks, among which are the chemokines and their cognate receptors that will impact most of hallmarks by acting on cancer cells and the surrounding microenvironment (Balkwill, 2012). For instance, CCR7 can influence the tumour cell proliferation, invasion and migration of cancer cells to the lymph node as well as recruiting certain immune cells, involved in resolving the immune reaction, towards the tumour site in order to evade the destruction by effector immune cells

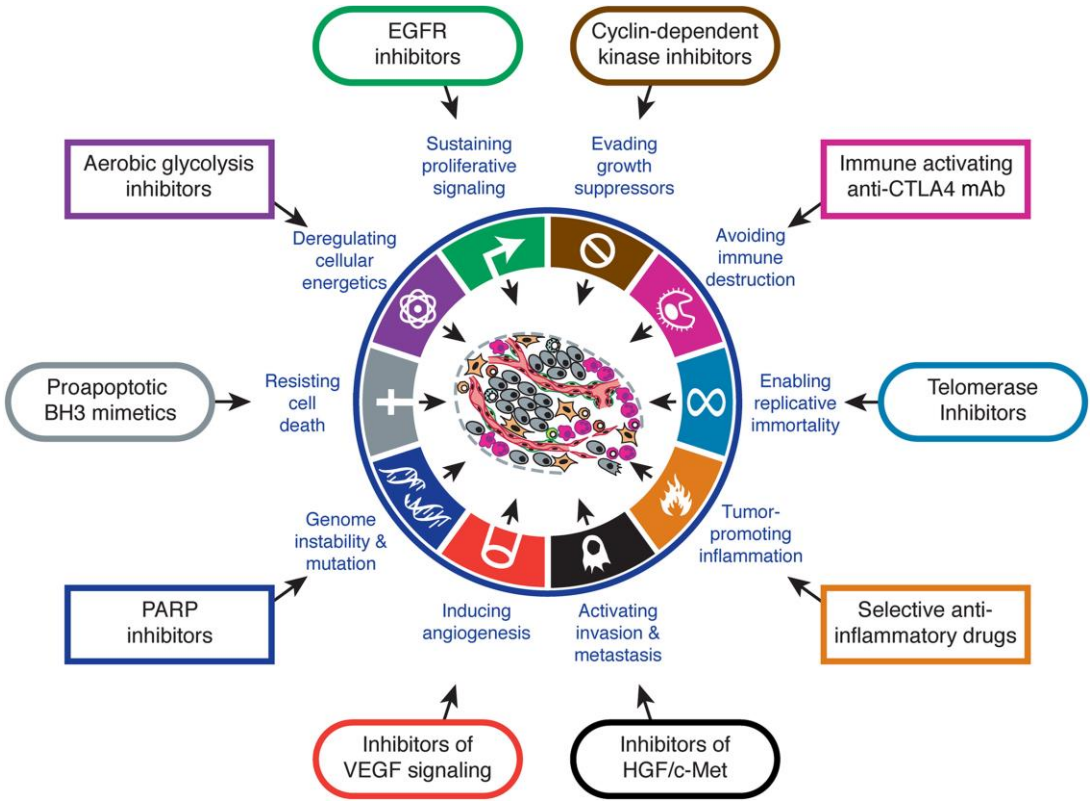

Figure 2: Cancer hallmarks (Hanahan and Weinberg, 2011).

Researchers have proposed additional hallmarks that are important to support the progression and development of cancer. Here drug treatment options are suggested next to each hallmark.

The development of cancer leads to significant morbidity and, if untreated, the death of the patient (Ruddon, 2007). However, the majority of the deaths, by some estimates 90% of human cancer deaths, are reported to be caused not by the growth of primary tumour, but by metastasis (Mehlen and Puisieux, 2006). Metastasis is the process by which the cancerous cells from a primary site spread to other parts of the body (Mehlen and Puisieux, 2006) and this process is one of the specific hallmarks that differentiate a benign from a malignant neoplasm (Chambers et al., 2002). A 5-year survival is considered good for patients with

localized disease in most cancers, but this rate decreases dramatically once the patient is diagnosed with metastatic cancer, according to the US National Cancer Institute Surveillance Figure 3 (Steeg, 2016). Importantly, for most types of primary (localised) cancer, survival rates have improved from 2005 to 2015, however, for metastasised cancers, survival rates have hardly changed.

(a)

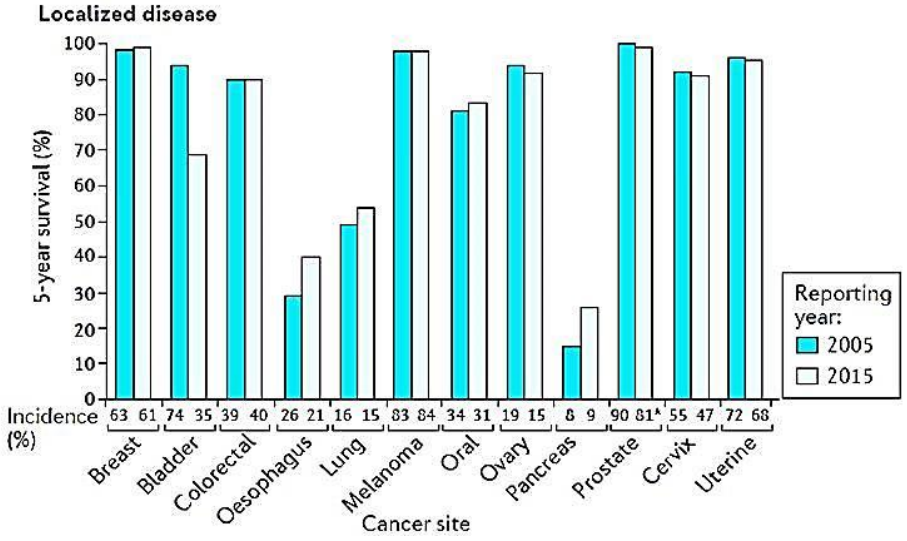

(b)

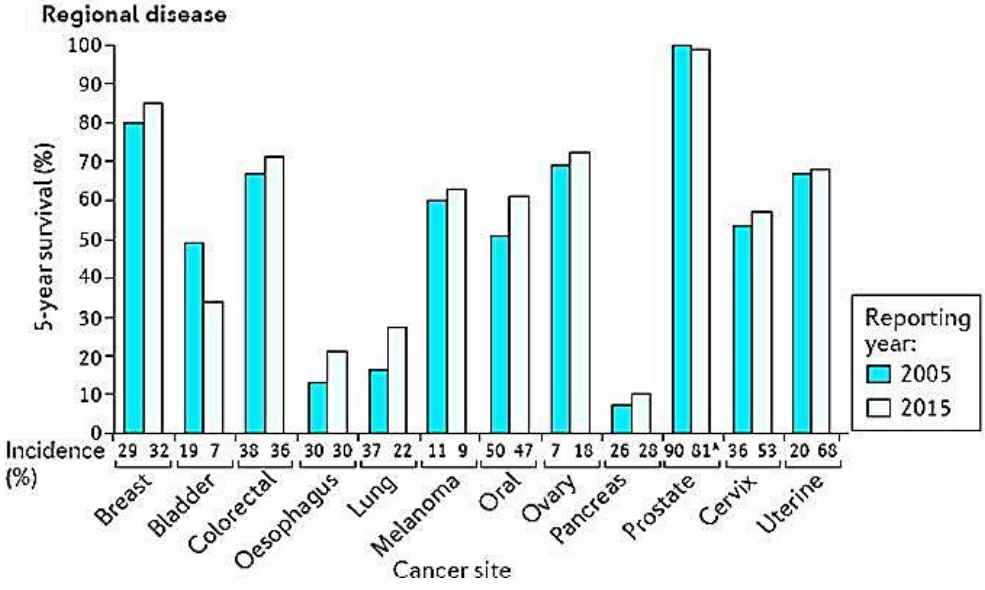

(c)

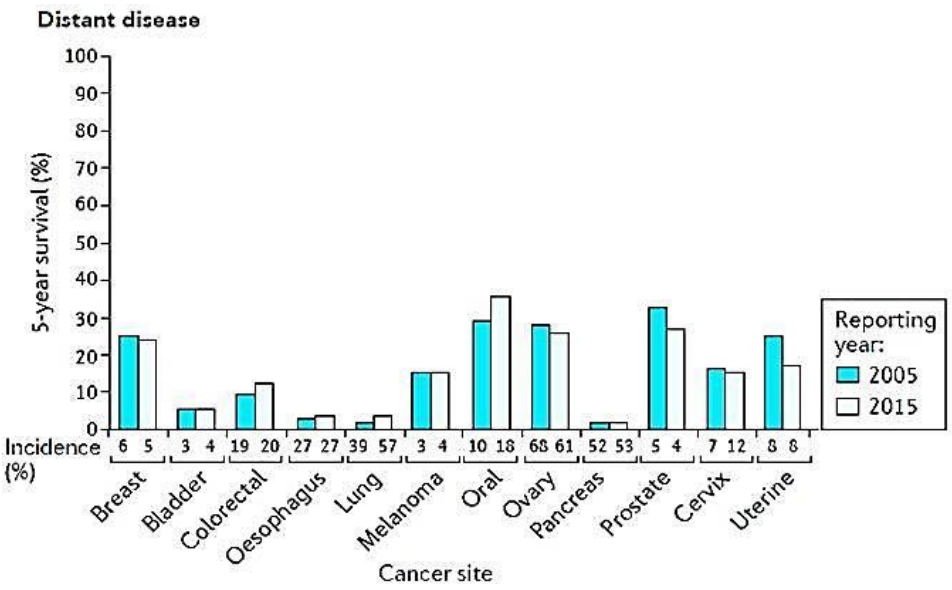

Figure 3: US National Cancer Institute surveillance for cancer patients(Steeg, 2016).

(a) The 5-years survival rate is considered good for most cancer types for patients diagnosed with localized disease. (b) Those with lymph node spread known as regional disease at diagnosis have lower overall survival compared with patients with localized disease, with the exception of bladder or prostate cancer patients. (c) The survival rate of patient with distant metastasis is decreased dramatically in all cancer types compared with localized disease (Steeg, 2016).

1.1.1 Challenges in Developing Treatments for Metastasis

Despite the significant role of metastasis on patient prognosis, there are limited therapeutic options available in the clinic to prevent or treat metastasis. There are a number of reasons for that. Metastasis is a complex and multistep process which involves invasion, intravasation, extravasation and colonization at the metastatic site Figure 4 (Nguyen et al., 2009, Schroeder et al., 2012). Whilst this implies multiple opportunities for intervention in the metastatic process, it also puts significant limitation to validity and reliability of preclinical models, which by nature focus on single aspects of the process, and clinical data, which need to be strictly quantifiable.

The majority of the available cancer therapeutic strategies are focused on eradicating the primary tumour rather than targeting the metastatic process, but even so, these drugs are tested on patients diagnosed with metastatic disease (Mueller and Zlotnik, 2009, Stock et al., 2013, Steeg, 2016). The end points of these clinical trials are the shrinkage of tumour size which is easily quantifiable, as well as an increase in overall survival, or progression free survival which can be multifactorial. However, for an anti-metastatic drug to be considered effective, it should prevent the formation of metastases which is not easily quantifiable. Furthermore, the vast majority of drugs currently available clinically were not tested in preclinical anti-metastatic models in their developmental stage. Indeed, the majority of the information about anti-metastatic behaviour of these drugs is often gained from adjuvant trials, using overall survival, progression free survival and cancer recurrence as the end points or from available clinical data from studies

initially directed towards combination or chemotherapy resistant therapies. This is because of the hurdles in initiating clinical trials by using an anti-metastatic agent on its own in non-terminal patients. To make the situation more difficult to interpret, conflicting data was gathered for these drugs in metastasis-focused pre-clinical experiments. For instance, some FDA approved drugs such as paclitaxel, cisplatin, and anti-androgens have stimulated metastasis in preclinical models (Steeg, 2016).

Furthermore, preclinical data suggesting anti-metastatic potential for a drug, do not necessarily translate to clinical studies. For example, αvβ3 and αvβ5 integrin inhibitor, cilengitide had been shown to be a good candidate for preventing metastasis in mice preclinical models, however failed in clinical studies (Scaringi et al., 2012). Integrins can regulate the development and progression of tumours as they are involved in increasing the adhesion of tumour cells to the extracellular matrix (ECM) and they affect angiogenesis, survival, invasion and metastasis (Ganguly et al., 2013, Desgrosellier and Cheresh, 2010). Cilengitide has been shown to prevent metastasis and increase apoptosis as monotherapy or in combination with other agents such as temozolomide in glioblastoma, non-small cell lung cancer, head and neck and melanoma in preclinical models (Wichmann et al., 2017, Scaringi et al., 2012). The preclinical data was encouraging to progress cilengitide into clinical trials. However, Phase III trials in glioma were negative for an overall survival end point. Phase II trials were conducted in patients with bone metastatic prostate cancer, metastatic melanoma and advanced non-small-cell lung cancer, showing very little clinical activity. These failures at the clinical stage

could be attributed to the pharmacokinetic profile of cilengitide, or in choosing the wrong cancer type; for instance, glioma was chosen to test for anti-metastatic activity whereas glioma does not really involve distant metastasis as part of its progression (Scaringi et al., 2012).

On the other hand, the relative success of Denosumab proves that metastasis can be targeted successfully to increase patient survival and quality of life. Bone metastasis is one of the most common sites of metastasis in advanced cancer. Skeletal metastases are most common among prostate, lung, breast, kidney, myeloma, and thyroid cancers. Bone metastases can be either osteolytic (bone destructing) or osteoblastic (bone forming) or a mixture of both (Weidle et al., 2016, So et al., 2012). Bone metastasis is considered to be facilitated by the fenestrated capillaries of the bone marrow, high blood flow, and the presence of adhesive molecules on cancer cells that can bind to osteoblasts and osteoclasts, as well as the bone matrix (Weidle et al., 2016). These types of cell play an important role in bone re-modelling and its niche structure The osteolytic metastases require the activation of osteoclasts by binding of activator NF-κB ligand (RANKL) Gul et al., 2016), which is produced by osteoblasts, to the RANK receptor on the osteoclasts' surface. RANKL can also trigger angiogenesis, migration and invasion by inducing the production of proteins involved in these processes, such as matrix metalloproteinases (MMPs; Gul et al., 2016). Bone metastases will eventually lead to skeletal related complications (SREs; Weidle et al., 2016). SREs are associated with pathologic fractures, the need for bone surgery, radiation to bone or surgery,

spinal cord compression and hypercalcemia. SRE leads to compromised quality of life, loss of mobility and reduced survival rates

Tumour cells trigger RANKL expression by osteoblasts through the secretion of cytokines and hormones, in some cases, cancer cells can express RANKL to directly activate the osteoclasts. Denosumab is a fully humanized monoclonal antibody that binds to RANKL, thereby inhibiting the activation of RANK and the destruction of bone. Denosumab has already been approved by the FDA for the prevention of SRE in breast, prostate and myeloma cancers with bone metastases. Denosumab was superior to zoledronic acid, which is a bisphoshonate that induces the death of osteoclasts and is the current standard of care to delay or prevent SRE in bone metastatic cancer patients (Rolfo et al., 2014). In addition, no difference was observed in overall survival (OS) between patients treated with denosumab or zoledronic acid in breast and prostate cancer studies. However, in a Phase III clinical trial in non-small cell lung cancer, denosumab has been reported to increase the overall survival compared with zoledronic acid in patients with metastatic lung cancer (Scagliotti et al., 2012).

Furthermore, Smith et al., have shown in a Phase III clinical trial study in castration-resistant prostate cancer patients that denosumab causes a delay in the development of bone metastasis, compared with placebo (Smith et al., 2012).

The success of denosumab is a result of coherent understanding of the molecular mechanism in the metastatic process, preclinical studies focusing on the metastatic

process, rather than primary tumours and that adequate clinical trials design with relevant endpoints is a key factor in this context.

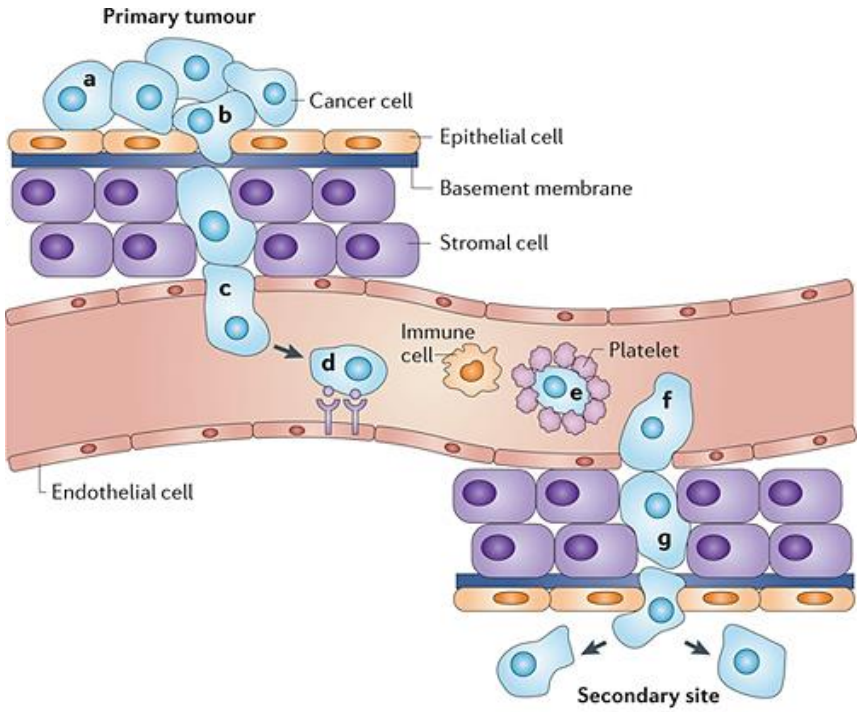

Figure 4: The metastatic process steps.

Cancer cells escape the primary tumour intravasate, extravasate and colonise a favored secondary site (Schroeder et al., 2012). Reduction in adhesion to neighbouring cells (a) facilities the cells movement to invade through the basement membrane and stromal cells (b). Hence cells are free to intravasate (c) the blood or lymph. Once cancer cell are in the blood or lymph vessels, the distribution of the cancer cells is determined by the flow and interactions between cancer cells and the secondary organs that they colonise. In the blood stream tumour cells can express receptors that bind to metastasis-supporting sites (d) or to platelets (e), which protect the cancer cells from the immune system. After reaching the secondary site, tumour cells can reside at the capillary beds of the secondary site and can exit the bloodstream (f) by inducing endothelial cell retraction or death. To colonise in the secondary site (g), cancer cells start to release pro-inflammatory molecules and proteinases that induce their neighbours to release growth factors. From (Schroeder et al., 2012).

Table 1: Typical sites of metastasis for solid tumours (Robins, 2006, Ahmad et al., 2011, Aranovich et al., 2013, Kowalski, 2001, Agalianos et al., 2016)

Tumour type	Principle site for distal metastasis	Principle site for regional lymph node metastasis
Breast	bone, lungs, liver and brain	axillary and internal mammary lymph nodes
Lung adenocarcinoma	brain, bone, adrenal glands and liver	cervical lymph nodes
Skin melanoma	lungs, brain, skin and liver	site dependent, for example: head and neck melanoma; the most common site is cervical lymph nodes
Colorectal cancer	liver and lungs	mesenteric lymph node
Pancreatic carcinoma	liver and lungs	para- aortic lymph node
Prostate cancer	bone	para- aortic lymph node inguinal lymph node
Head and neck	lungs	cervical lymph node
Uveal melanoma	liver	internal iliac, external iliac, or obturator lymph nodes

1.1.2 A new approach to anti-metastatic drugs

Clearly, developing anti-metastatic drugs remains an unmet clinical need as it would notably reduce tumour recurrence and improve patient survival. Therefore, as a better understanding of the complex metastatic process emerges, there is an opportunity to exploit these new findings to develop new targeted approaches for metastasis. For example, an interesting observation in metastasis is that primary tumours of certain organs usually metastasise to other specific organs (Murphy, 2001, Muller et al., 2001), *e.g.* breast cancer normally migrates to the bone, lungs, brain, while colorectal cancer usually metastasises to the liver (Table 1). Although studies on the metastatic process have revealed many molecular factors that

contribute to invasion and metastasis, *e.g.* adhesion molecules and proteases, the exact mechanism of this directional migration was unclear until the role of the chemokine system has shown to be one of the key players in the metastatic process and particularly in organ specific metastasis. (Dowsland et al., 2003). Whilst the role of chemokine system in the metastasis to different organs have been demonstrated we are going to focus on metastasis to the lymph nodes which as discussed in the introduction to this chapter, is a major negative prognostic factor.

1.1.3 Lymph node metastasis

Metastasis of tumour cells to the lymph nodes is an early event and therefore, is considered as a key indicator of tumour stage and therapeutic options (Das et al., 2013). Metastasis of tumour cells to the regional lymph nodes is associated with poor prognosis and local tumour recurrence after the resection of surgically removable malignancies (Achen and Stacker, 2008). Furthermore, the lymphatic spread is not only involved in local disease recurrence, but also leads to lethal distinct metastases (Sperveslage et al., 2012, Guo et al., 2013, Kawada and Taketo, 2011). It has been shown that distant metastasis is often observed along with induced lymph node metastasis (Hirakawa et al., 2007).

Despite, the high prognostic importance of the lymphatic spread in cancer progression, the underlying mechanisms by which tumour cells migrate to lymph nodes remain unclear. It has been proposed that molecular pathways, mediated by proteins such as VEGF-C, can induce lymphangiogensis, and *de-novo* generation of new lymph vessels, and are critical for lymphatic metastasis in melanoma

(Hirakawa et al., 2007), breast (Ran et al., 2010) and prostate (Mumprecht and Detmar, 2009). In contrast, the migration of human pancreatic ductal adenocarcinoma (PDAC) to the lymph node does not require lymphangiogenesis (Sipos et al., 2005). This suggests that other mechanisms facilitate lymph node metastasis in PDAC. In this way, the molecular pathways that are involved in the lymphatic spread might be dependent on tumour type.

The involvement of chemokines and their cognate receptors in the lymphatic metastasis has been reported in different types of cancer (Xiao et al., 2014, Achen and Stacker, 2008). More interestingly, the most commonly expressed chemokine receptors on tumours that lead to the lymphatic spread are CXCR4 and CCR7 (Xiao et al., 2014, Cunningham et al., 2010, Guo et al., 2013, Irino et al., 2014).

In the following sections, a brief introduction to chemokines and their role in cancer, focusing on the role of CCR7 in normal and cancer cells, and the therapeutic potential of targeting CCR7 as an anti-metastatic target will be discussed.

1.1.4 Chemokines and their Receptors

1.1.4.1 *Definition and Nomenclature of Chemokines and their Receptors*

Chemokines are a family of chemo-attractant cytokines that exert their effects through binding to cell surface chemokine receptors which belong to the seven trans-membrane (7TM) helical G-protein coupled receptor (GPCR) family (Figure 5; Bennett et al., 2011). The N terminus and three extracellular loops are directed towards the outside of the cell, whereas the C terminus and three intracellular loops are exposed to the cytoplasm (Allen et al., 2007). The chemokine system is comprised of 49 chemokine ligands divided into four subfamilies (CXCL1–18, CCL1-CCL28, XCL1-2, and CX3CL1) which bind and activate 18 chemokine cell surface receptors (CXCR1-6, CCR1-10, XCR1 and CX3CR1), and also bind 6 atypical receptors (ACKR1-6), see table 2 (Viola and Luster, 2008, Hauser and Legler, 2016). This classification of chemokines is based on structure rather than function and is according to the number and the spacing of the first two cysteine residues (C) in the amino-terminal part of the protein (Slettenaar and Wilson, 2006).

Although there are chemokine ligands and receptors which are uniquely paired within each subfamily, there is apparent promiscuity in the chemokine system. This means that some chemokines can bind and activate more than one chemokine receptor or the same receptor could be activated by different chemokines (Allen et al., 2007). For example, chemokine receptor CXCR4, which is one of the most studied chemokine receptors, is selectively activated by chemokine CXCL12,

whereas chemokine receptor CCR7 is activated by two chemokines, CCL19 and CCL21.

The nomenclature of chemokines starts with their subclass, followed by “L” for “ligand” and a number for the corresponding gene nomenclature (Dowsland et al., 2003). The nomenclature system of chemokine receptors also starts with the subclass, followed by “R” for “receptor” and the corresponding gene number.

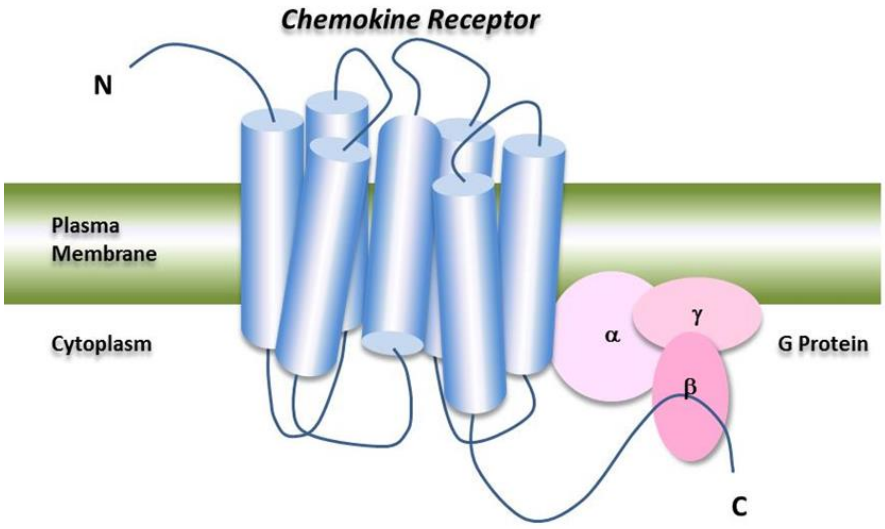

Figure 5: A proposed structure for the chemokine receptor.

The G-protein coupled receptor consists of 7 TMs, N terminus and three extracellular loops, and C terminus and three intracellular loops. Figure courtesy of Dr. Victoria Vinader.

Table 2: Chemokine receptors and their known ligands (Bonecchi and Graham, 2016, Viola and Luster, 2008).

Chemokine receptors	Ligands
CCR1	CCL3, CCL5, CCL7, CCL13, CCL14, CCL15, CCL16, CCL23
CCR2	CCL2, CCL7, CCL8, CCL13, CCL16
CCR3	CCL5, CCL7, CCL8, CCL11 ,CCL13, CCL15, CCL16, CCL24, CCL26, CCL28
CCR4	CCL17, CCL22
CCR5	CCL3, CCL4, CCL5, CCL8, CCL11, CCL14, CCL16
CCR6	CCL20
CCR7	CCL19, CCL21
CCR8	CCL1
CCR9	CCL25
CCR10	CCL27, CCL28
CXCR1	CXCL6, CXCL7, CXCL8
CXCR2	CXCL1, CXCL2, CXCL3, CXCL5, CXCL6, CXCL7, CXCL8
CXCR3	CXCL4, CXCL9, CXCL10, CXCL11
CXCR4	CXCL12
CXCR5	CXCL13
CXCR6	CXCL16
XCR1	XCL1, XCL2
CX3CR1	CX3CL1
ACKR1	>20 inflammatory chemokines belonging to the CC and CXC families
ACKR2	Agonists for CCR1 and CCR5
ACKR3	CXCL12, CXCL11
ACKR4	CCL19, CCL21, CCL25, CXCL13
ACKR5	C5a
ACKR6	chemerin

Chemokines are also classified according to their pattern of expression and related function as homeostatic or inflammatory chemokines (Fernandez and Lolis, 2002). The homeostatic chemokines are constitutively produced and perform various functions, such as trafficking of lymphocytes to lymphoid tissues, immune surveillance, and localization of T or B cells in the lymphatic system and the architecture of secondary immune organs. The inflammatory chemokines are only produced during an inflammatory stimulus or infection. The secretion of the inflammatory chemokines causes the migration of leukocytes to the injured or infected area. However, depending on the biological context, some chemokines may be considered both homeostatic and inflammatory.

1.1.4.2 *Glycosaminoglycans Binding*

Chemokines other than CXCL16 and CX3CL1, exist as soluble chemokines that can bind to the negatively charged glycosaminoglycans (GAGs), *e.g.* heparin sulphate, *via* their basic N terminus (Scholten et al., 2012). It has been reported that chemokines such as CCL2, CCL3, CCL5, CXCL8, CCL21 and CCL19 have a GAG binding domain (Vinader and Afarinkia, 2012, Vives et al., 2004, Stringer et al., 2002, Koopmann and Krangel, 1997). GAGs are bound to proteins on the cell surface and/or on the ECM and act as traps for chemokines. The binding of GAGs to chemokines has multiple effects (Vinader and Afarinkia, 2012). Firstly, it creates a chemotactic gradient which facilitates cell migration towards the source of chemokine production. Secondly, it induces chemokine conformational changes that facilitate its binding to the corresponding receptor. Thirdly, the binding of GAGs to chemokines could have importance in terms of selectivity in chemokine-

chemokine receptor pairing. Finally, the binding of GAG is an essential requirement for chemokine receptor functionality *in vivo*, even though it is not required for receptor activation (Hamel et al., 2009).

Binding of chemokines to their receptors results in activation of a number of intracellular signal transduction pathways. Therefore, chemokines can significantly influence the biology of the cell in different contexts. One major outcome of chemokine activation is cell migration towards the source of chemokine production, following the chemotactic gradient (Slettenaar and Wilson, 2006). This process is known as chemotaxis.

Once the chemokine receptor is activated, the bound guanosine diphosphate (GDP) is exchanged to guanosine triphosphate (GTP) in the α G protein subunit (Figure 6; Allen et al., 2007). This leads to G_{α} and $G_{\beta\gamma}$ dissociation and departure from the receptor complex, entering the next stage of signal transduction. The G_{α} subunit interacts with adenyl cyclase which converts adenosine triphosphate (ATP) to cyclic adenosine monophosphate (cAMP). The $G_{\beta\gamma}$ subunit phosphorylates phosphatidylinositol-3-kinase (PI3K) which activates mitogen-activated protein kinases (MAPK) pathway. $G_{\beta\gamma}$ also phosphorylates phospholipase C (PLC) which accumulates inositol triphosphate and diacylglycerol in the cytoplasm (Kruizinga et al., 2009). These in turn, among other downstream effectors, induce Ca^{2+} mobilization, which is involved in cell shape and motility (Kruizinga et al., 2009).

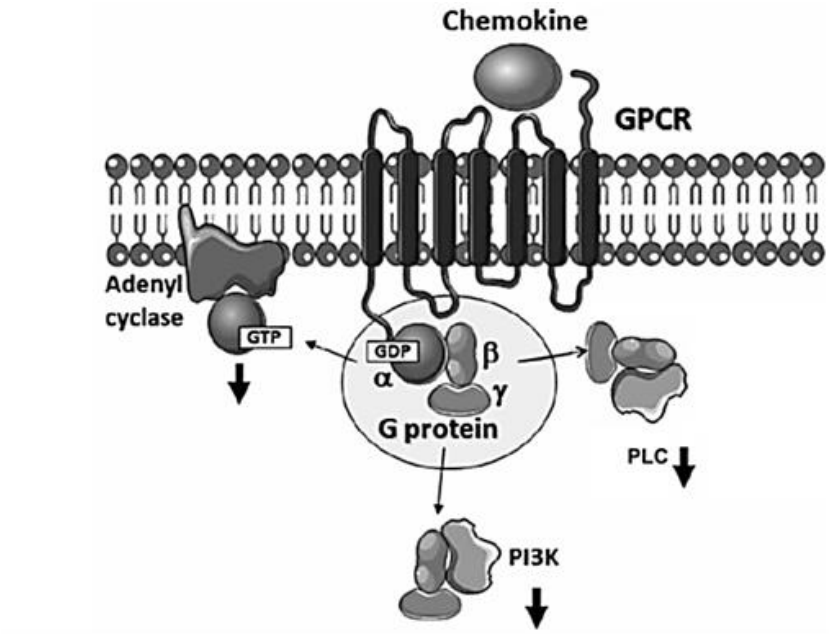

Figure 6: Chemokine receptor activation.

Chemokines bind to the chemokine receptor, activate it and triggers a cascade of signalling. The bound GDP is exchanged by GTP in the α subunit of G protein. This leads to Gα and Gβ dissociation and departing from the receptor. The Gα subunit interacts with adenyl cyclase. The Gβ subunit phosphorylates PI3K and PLC. Adapted from (Kruizinga et al., 2009). (GDP: guanosine diphosphate; GTP: guanosine triphosphate; G: guanosine; PI3K: phosphorylates phosphatidylinositol-3-kinase; PLC: phospholipase C.

The consequent cascade of downstream effectors activation eventually results in several biological functions (Figure 7). It has been observed that the G_i subclass are the primary G_α subunit associated with chemokine receptor's induced chemotaxis and it's well known that this subclass inhibits adenylate cyclase therefore it is the release of free $\beta\gamma$ subunit from G_i that is responsible of chemotaxis as shown by (Neptune and Bourne, 1997). Nonetheless, depending on the cell-type and chemokine receptors expressed on these cells, G proteins other

than Gα-$_i$ could be activated which could results in different signalling pathway and function (Mellado et al., 2001).

The biochemical pathway of chemokine receptors is not only dependent on G protein activation (Mellado et al., 2001). It has been shown that chemokine receptors activation can result in transactivation of other signalling pathways, *e.g.* binding of CXCL12 to CXCR4 results in EGF receptor activation (Mellado et al., 2001, Porcile et al., 2005). Another significant property of chemokine receptors is their ability to homo or hetero-dimerize with other chemokines, GPCR and other cell surface proteins. It has been speculated that chemokine receptor dimerization is responsible for their biological functions (Mellado et al., 2001).

Activation of the chemokine receptor and the consequent signal transduction to downstream effectors leads to the directional sensing and cell polarization that contributes to cell migration (Raman et al., 2011). Accumulation of small GTPase, RAC, cell division control protein 42 (CDC42) and PI3K at the front edge of the cells results in actin polymerization and F-actin formation, whereas accumulation of phosphatase and tensin (PTEN) tyrosine/ phosphatidylinositol 3-phosphate (PI3P) phosphatase and Rho GTPase at the trailing end causes actomyosin contraction and tail retraction.

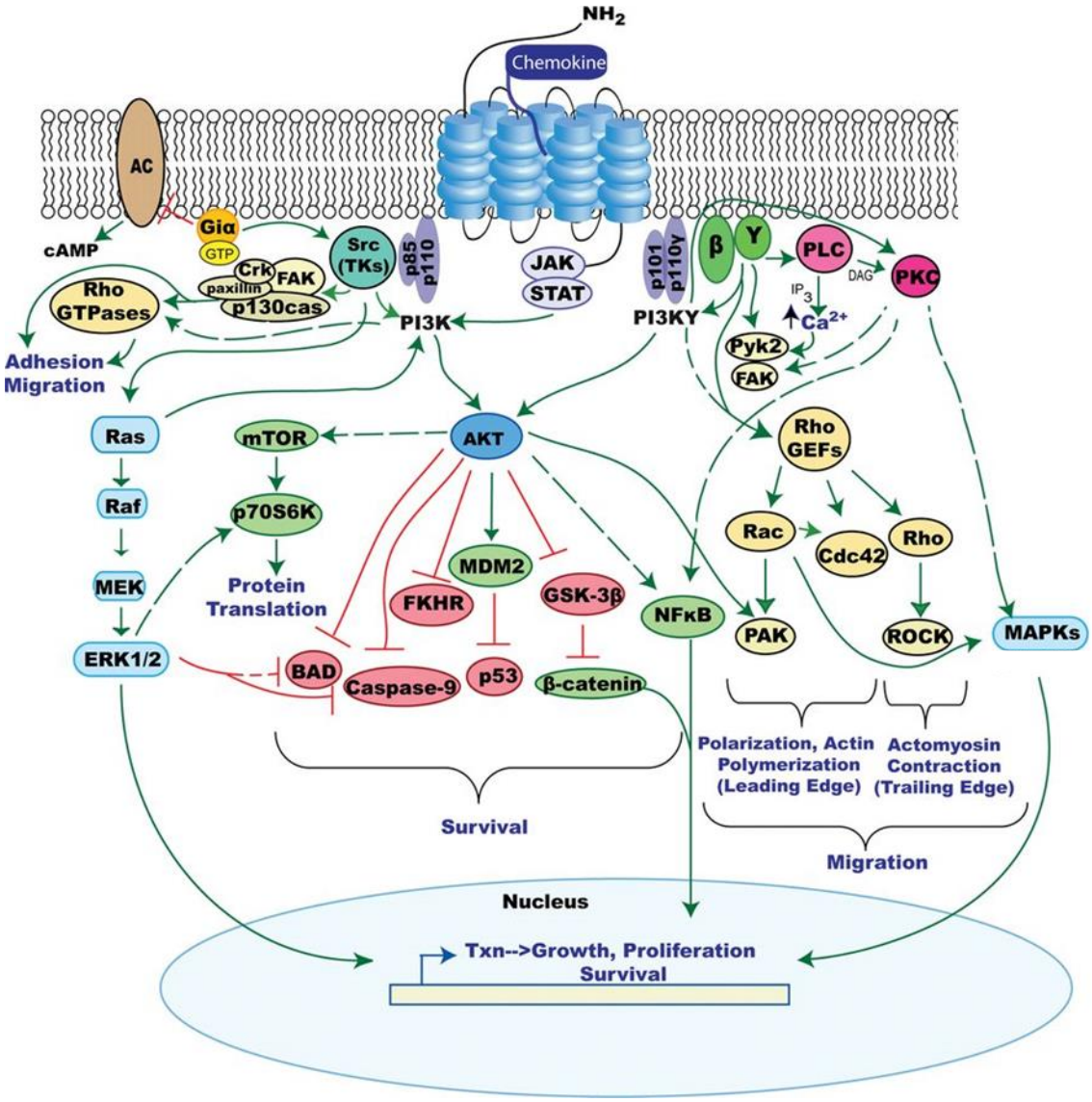

Figure 7: Chemokine receptor signaling in migration and survival/proliferation.

Different signaling pathways can be activated by chemokine-chemokine receptor interaction. Chemokine receptors are GPCR, as such; they are involved in activating G proteins, primarily G_i. However, it has been shown chemokine receptors can also signal through other G proteins or even non- G proteins signaling pathways. These signaling pathways can also vary depending on certain pairing between a chemokine and a chemokine receptor and the cell type. This accounts for the different physiological roles that chemokine receptor activation can induce. Solid lines indicate direct effect, dashed lines indicate indirect effect. (O'Hayre et al., 2008).

In addition to the conventional chemokine receptors that signal through G proteins, there are 6 atypical chemokine receptors which signal in a G-protein-independent manner and do not result in cell migration. These 6 receptors include, ACKR1, previously called Duffy antigen receptor for chemokines (DARC); ACKR2, known as (D6 or CCBP2); ACKR3, also called CXC-chemokine receptor 7 (CXCR7) or RDC1; ACKR4, previously known as (CC chemokine receptor-like 1 (CCRL1) and also known as CCX-CKR; ACKR5 known as (CCRL2) and ACKR6 known as PITPNM3 (Hauser and Legler, 2016, Ulvmar et al., 2011, Bonecchi and Graham, 2016). The function of the atypical chemokine receptors is to regulate the chemokine expression by scavenging, transporting, or storing them to help with resolution of inflammatory response at the inflammation site (Bonecchi and Graham, 2016).

1.1.5 Chemokine receptors in cancer

The aberrant chemokine receptor expression in cancer cells is associated with oncogenic mutations, hypoxia, epigenetic modulation and other changes in the tumour microenvironment (Zlotnik et al., 2011). For example, it has been observed that the angiogenesis-promoting molecule VEGF induces the overexpression of CXCR4 (Zlotnik et al., 2011). However, the expression of chemokine receptors such as CCR10 in melanoma may only mirror the already high expression of CCR10 on the normal counterpart cells (Rossi and Zlotnik, 2000).

Table 3: The expression profile of chemokine receptor on different type of tumours (Balkwill, 2012).

Cancer type	Chemokine receptors expressed by tumour cells
Breast	CXCR4, CXCR7, CCR4, CCR5, CX3CR1
High grade serous ovarian	CXCR4
Prostate cancer	CXCR4, CXC3R1
Melanoma	CXCR4, CCR10, CCR7, CCR9, CXCR1,CXCR2, CXCR3
Oesophageal cancer	CXCR4
Non-small cell lung cancer	CXCR4, CCR7
Head and neck cancer	CXCR4, CCR7, CXCR5
Bladder cancer	CXCR4
Colorectal cancer	CXCR4, CCR6, CCR7, CXCR5
Osteosarcoma	CXCR4
Neuroblastoma	CXCR4
Pancreatic cancer	CXCR4, CX3CR1
Acute lymphoblastic leukaemia	CXCR4, CXCR3
Chronic lymphocytic leukaemia	CXCR4, CCR7, CXCR3
Stomach cancer	CXCR4, CCR7, CCR4
Non-Hodgkin's lymphoma	CCR7
T cell leukaemia	CCR7
Cutaneous lymphoma	CCR3, CCR4, CCR10
Hodgkin's lymphoma	CCR5
Multiple myeloma	CCR1
Glioma	CXCR4, CXCR7, CX3CR1

Studies on chemokine receptors on cancers have shown that tumours overexpress certain chemokine receptors to match the chemokines produced by organs to which these cells normally metastasise Table 3 (Balkwill, 2012). The most commonly expressed chemokine receptor on tumours is CXCR4, followed by

CCR7, although other chemokine receptors are also expressed, as indicated in table 3 (Balkwill, 2012).

Once the chemokine receptors are activated, the cancer cells can adopt normal cellular pathways to migrate towards the source of chemokine production resulting in metastasis (Zlotnik et al., 2011). In addition, cancer cells can express chemokine ligands for the same chemokine receptors that they are expressing (Balkwill, 2012). It has been speculated that this autocrine loop is involved in the increased cell survival and resistance to chemotherapy of the primary and metastatic tumours (Balkwill, 2012). However, when cancer cells are ready to metastasise following a concentration gradient of chemokines, they shut down this autocrine loop by repressing chemokine production, while maintaining the receptor expression, *e.g.* in breast cancer cells, *CXCL12* gene has been found to be epigenetically silenced without affecting the expression of CXCR4 (Wendt et al., 2008).

1.1.6 Role of CCR7 in normal physiology

The chemokine receptor 7 (CCR7) was first identified in 1993 (Birkenbach et al., 1993). It is a homeostatic chemokine receptor which has a crucial role in immune responses and its aberrant expression, like other chemokine receptors such as CXCR4, has been associated with the development of autoimmune diseases (Comerford et al., 2013).

Normally, CCR7 is expressed on naive and memory and regulatory T cells, B cells, and mature dendritic cells (DCs) (Förster et al., 2008). Two ligands, CCL19 and CCL21, have been identified to activate CCR7 (Comerford et al., 2013). CCL21 is

expressed in lymph nodes, Peyer's patches and their endothelial venules, the T-cell zones of the spleen and the lymphatic endothelium of multiple organs. CCL19 is expressed mainly by stromal cells in the T-cell zone of the spleen, lymph nodes and Peyer's patches (Mashino et al., 2002). Although, both ligands bind to CCR7, they may play different roles. CCL19 and CCL21 share only 32% amino acid sequence similarity and only the latter has a GAGs binding domain (Steen et al., 2014).

The lack of sequence similarity in CCL19 and CCL21 can explain differences in their functional roles by which CCL19 and CCL21 can activate CCR7 to trigger different signalling pathways (Comerford et al., 2013). It has been shown that CCL19 can induce internalization and desensitisation of the receptor, whereas CCL21 cannot (Steen et al., 2014). In regards to migration, some *in vitro* studies have shown that DCs migrate more efficiently towards CCL21, controversially, others have shown that DCs migrate more efficiently towards CCL19 (Nandagopal et al., 2011, Ricart et al., 2011). Furthermore, Ricart et al. have shown that murine DCs present biased migratory movement, which depends on the ligand concentration (Steen et al., 2014). Thus, CCL21 induces migration at higher levels when its concentration is significantly high. On the other hand, CCL19 causes this increase in migration at relatively low concentrations. Of note, despite the above findings, *in vivo* experiments have shown that CCL21 plays the dominant role in migration (Comerford et al., 2013).

Despite that different signalling and functions result from binding of CCL21 or CCL19 to CCR7, a similar chemokine receptor activation model has been

proposed by both CCL21 and CCL19 (Scholten et al., 2012). Chemokines bind to the outside N terminus and the extracellular loops of the chemokine receptor. This binding is mainly due to the ionic interaction between the negatively charged residues of chemokines and the positively charged amino acids at the N terminus and the extracellular loops of the receptor. This changes the chemokine to the conformation needed to interact with a second binding site consisting of extracellular loops and/or TM domains leading to receptor activation Figure 8. It has been shown in Ott et al., study that CCR7 has four important second binding sites including, $Lys^{3.33\ (137)}$, $Gln^{5.42\ (227)}$, $Lys^{3.26\ (130)}$ and $Asn^{7.32\ (305)}$ (Ott et al., 2004). This study fits with the proposed model of 2 step model of binding decribed above because these four resides in CCR7 were demonstrated to be involved in receptor activation without affecting CCL21 or CCL19 affinty binding.

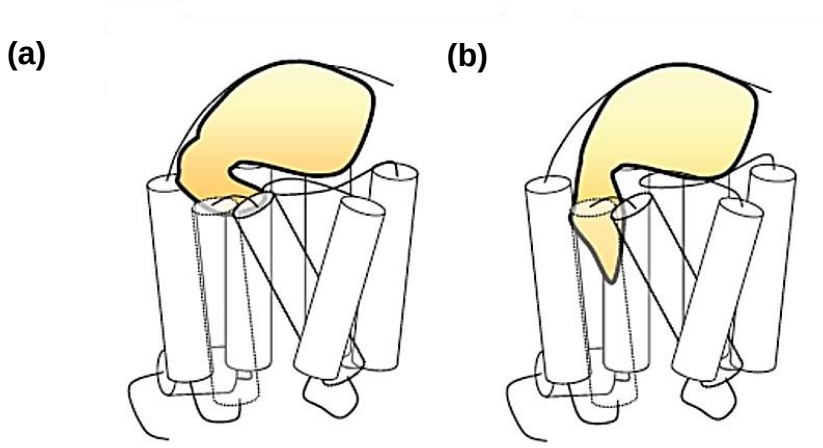

Figure 8: The proposed two step model for chemokine receptor activation.

(a) Chemokine binds at the recognition site, the N terminus and extracellular loops. (b) Change in the chemokine conformation to position its binding at the external loops and transmembrane domains, which activates the receptor (Scholten et al., 2012).

After activation by CCL21 or CCL19, CCR7 expressing immune cells are then recruited to lymph nodes to initiate an immune response and in establishing central and peripheral tolerance to differentiate between self and non-self-antigen, preventing the development of autoimmune diseases (Förster et al., 2008, Comerford et al., 2013, Worbs and Förster, 2007).

1.1.7 Role of CCR7 in cancer

The CCR7 axis plays a dual, and at first sight conflicting role in cancer. As discussed above, CCR7 and its ligands are highly involved in immune responses and therefore, may have an anti-tumour role by recruiting leukocytes that are capable of initiating an immune response to cancer. However, tumour cells can readily circumvent this process by: (1) secretion of CCL21 to recruit immune cells (T regulatory cells) that are involved in tolerogenic responses, producing immunologic tolerance (Shields et al., 2010); (2) secreting oxysterols (oxygenated derivatives of cholesterol) that act as ligands of the liver X receptor (LXR) which results in inhibiting CCR7 expression in maturing DCs (Zlotnik et al., 2011, Villablanca et al., 2010). Consequently, the DCs lose the ability to migrate and initiate an anti-tumour response see Figure 9. Furthermore, cancer cells can upregulate CCR7 expression and hijack its signalling pathways to enable cells to migrate and colonise the lymph nodes (**see below**). In fact, there is now mounting evidence that CCR7 is a promotor of cancer progression and metastasis which we will discuss below.

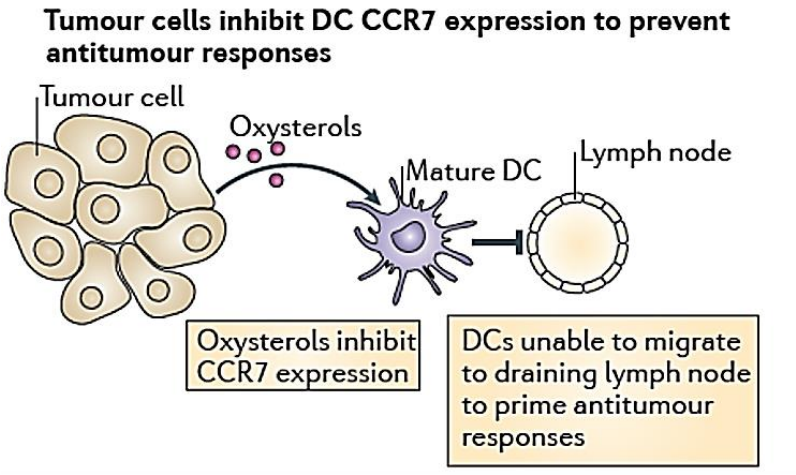

Figure 9: Inhibition of CCR7 expression on immune cells.

Tumour cells inhibit DC CCR7 expression to prevent antitumor responses by secreting oxysterol to interact with LXR expressed on DC resulting in halting the migration of DC to the tumour site (Zlotnik et al., 2011).

1.1.8 CCR7 expression in cancer and lymphatic metastasis

The expression of chemokine receptors can be downregulated, upregulated or show no significant difference in cancer cells in comparison to normal cells (Wang et al., 2004, Muller et al., 2001). However, all the studies carried out so far have shown that CCR7 expression is always upregulated in cancer tissues and cell lines, compared with their normal counterparts, with no discrepancy between gene and protein level (Takanami, 2003, Muller et al., 2001, Xia et al., 2014, Ueda et al., 2010)

The association between CCR7 expression and lymphatic metastasis has been investigated in human tissues by immunohistochemical and clinicopathologic correlation studies. It has been shown that CCR7 expression correlates with lymph node metastasis and poor prognosis in a number of malignancies, *e.g.* in breast (Liu et al., 2010), pancreatic ductal adenocarcinoma (Sperveslage et al., 2012, Guo et al., 2013), esophageal squamous cell carcinoma (Irino et al., 2014), tongue carcinoma (Xia et al., 2014), breast cancer(Li et al., 2014), gastric carcinoma (Mashino, 2002, Zhou et al., 2013), head and neck cancer (Li et al., 2011), non-small cell lung cancer (Takanami, 2003), cervical cancer (Shang et al., 2009), tonsillar cancer (Pitkin et al., 2007), prostate cancer (Heresi et al., 2005), colorectal cancer and pancreatic cancer (Zhao et al., 2011). Recent studies have suggested a potential role for the chemotactic effect of CCR7 in the migration of leukemic cells to the central nervous system; (Buonamici, 2009).

In addition, cells in which CCR7 expression is upregulated are shown to have enhanced metastatic potential and vice versa, ones in which the expression is

downregulated have diminished metastatic potential. In a study conducted by Henry et al., the induced expression of CCR7 in B16 murine melanoma increased the migration of cells to lymph nodes (Wiley et al., 2001). However, B16-CCR7-transfected and control cells show no preference for lung metastasis or increased proliferation. Similarly, enhanced migration to the lymph node along with proliferation has been observed in CCR7-transfected PT45P1, which is a PDAC cell line, compared with the control cells (Sperveslage et al., 2012). In addition, Cunningham et al, have reported that the induced expression of CCR7 in mouse breast cancer cells alters the metastatic destination from the lung to the lymph nodes (Cunningham et al., 2010). In their model, injecting 10 mice with $CCR7^{-}$ breast cancer cells has led to lung metastasis (10/10 mice), however in the corresponding experiment with the $CCR7^{+}$ cells, mainly lymph node metastasis (6/10 mice) and a reduced rate of metastasis to the lungs (4/10 mice) was observed.

Whilst a correlation between CCR7 expression and lymphatic metastasis can be inferred from these studies, the underlying mechanisms by which $CCR7^{+}$ tumour cells migrate to the lymph node is yet to be fully elucidated. It has been suggested that the CCR7/CCL21 interaction plays an important role in this process (Legler et al., 2014). Importantly, knocking down of CCR7 in different cancer types also confirmed the importance of CCR7 for lymphatic selectivity (Xia et al., 2014, Maekawa et al., 2008). To the best of our knowledge few studies have addressed the correlation between CCL19 and lymphatic metastasis. Where experiments

have been performed, no association was observed between CCL19 expression and lymphatic metastasis in PDAC (Sperveslage et al., 2012).

In addition, utilizing Enzyme-Linked Immunosorbent Assay (ELISA), presence of CCL21 and CCL19 is detected in cell culture supernatant produced by PDAC cell lines, BxPc3, Capan1, Colo357, HPAF2, Panc89, T3M-4 and PT45P1. This suggests that not only do these ligands originate in lymph vessels and nodes but also in the tumour microenvironment and that CCL21/CCL19 may participate in the metastatic process by autocrine stimulation of CCR7 leading to intravasation (Sperveslage et al., 2012).

Different *in vitro* experiments have shown a decrease in motility, invasion and adhesion of tumour cells where CCR7 was knocked down (Xia et al., 2014). Furthermore, in lung adenocarcinoma, blocking CCR7 using antibodies showed a significant suppression of cell migration (Maekawa et al., 2008). The number of metastases to lymph nodes was significantly reduced *in vivo* after knocking down CCR7 (Maekawa et al., 2008). Muller et al. have reported that breast cancer cells co-express CCR7 and CXCR4 and blocking of CXCR4 using antibodies resulted in suppressing lymph node metastasis (Muller et al., 2001). However, in a different study loss of other chemokine receptors expression such as, CCR6, was suggested as important as the presence of expression of CCR7 for migration of squamous cell carcinoma of the head and neck to the lymph node (Wang et al., 2004).

Although the lymphatic metastasis is highly correlated with the CCR7/CCL21 axis, it is not determined yet if this single chemokine interaction is the only responsible interaction for lymphatic selectivity. Some studies have demonstrated that CCR7/CCL21 might be the ultimate important interaction for lymph node selectivity. Wiley et al. have shown that the induced expression of CCR7 cells but not CXCR5, in melanoma, correlated with lymph node metastasis (Wiley et al., 2001). Keeping in mind that the CXCR5 ligand CXCL13 is expressed in the lymph nodes as well, that could confirm that the lymphatic metastasis is dependent on CCR7 expression. Also, despite that in a non-small cell lung carcinoma study, CCR7 rather than CXCR4 expression, was correlated with lymph node metastasis (Takanami, 2003). However, in submucosal esophageal cancer expression of CXCR4 was correlated with lymph node metastasis (Sasaki et al., 2008).

While CCR7 expression and subsequent activation might be one of the most critical steps for lymphatic selectivity, loss of expression of other chemokine receptors such as CCR6 loss of expression in head and neck cancer, may also play a role (Wang et al., 2004). This, however, needs further investigation to determine whether single or multiple chemokine interactions are involved in guiding the metastatic destination to the lymph node either by loss or gain of expression.

1.1.9 Other metastasis-supporting roles for the CCR7 axis

In addition to chemotaxis, CCR7 activation has been shown to have multiple roles which support tumour progression and metastasis. The PI3K/Akt pathway triggered by the activation of CCR7 in head and neck cancer and T cell lymphoma has been shown to be involved in survival and growth in both primary and metastatic

tumours (Wang et al., 2005, Zhao et al., 2011). Activation of CCR7 by CCL21 is associated with blood and lymph node vessels formation in breast, pancreatic cancer and melanoma. (Tutunea-Fatan et al., 2015, Zhao et al., 2011, Takekoshi et al., 2012). Although the mechanism underlying the induction of angiogenesis and lymphangiogenesis is currently unclear, there is strong evidence that CCR7/CCL21 axis is involved in the process of metastasis (Zhao et al., 2011). In B-cell chronic lymphocytic leukaemia and colon cancer, activation of CCR7 by CCL21 has also been shown to promote MMP-9 production, which has a major role in degrading the ECM, hence promoting invasion and metastasis (Li et al., 2011). In breast cancer cells, CCR7 activation by its ligand CCL21 was recently found to inhibit detachment induced apoptosis (anoikis) by upregulating anti-apoptotic proteins and downregulating apoptotic proteins through PI3K and c-Jun N-terminal kinase (JNK) pathways (Kochetkova et al., 2009), consequently increasing the cell survival and the number of metastatic cells. Of note, this CCL21 induced survival was only observed by loss of attachment and not by serum deprivation or treatment with cytotoxic drugs. Conversely, CCR7 activation by CCL21 in non-small cell lung cancer (NSCLC) was found to increase cell proliferation and survival *via* the extracellular-signal-regulated kinase (ERK) pathway but not AKT, p38, or JNK. (Xu et al., 2012). A recent study has shown that the other ligand for CCR7, CCL19, is associated with increased proliferation, invasion and anoikis inhibition through ERK and Akt pathways in breast cancer (Su et al., 2014). Interestingly, this study showed that CCL21, which is proved by published work to have more significant importance on the downstream effects

upon CCR7 activation, did not increase the expression level of either ERK or Akt. Accordingly, these inconsistent findings on the signalling pathways of CCR7 activation could be related to the use of different cell types and/or different experimental conditions in the studies.

In summary, activation of the CCR7 receptor by its ligands in cancer cells triggers several signaling pathways leading to, depending on cancer type, cell migration, survival, proliferation and metastasis particularly to the lymph nodes. Furthermore, conventional treatments have proved to be inefficient when it comes to cancer metastasis that is responsible for cancer relapse and most of patient's deaths. Accordingly, targeting CCR7 using small molecule antagonists can reduce or inhibit progress of metastasis providing better opportunities for patient's survival.

As discussed earlier, a key requirement for developing anti-metastatic therapeutics is the availability of reliable *in vitro* models to predict anti-metastatic potential of drug agents. In the following section, we review the advantages and disadvantages of available techniques to assess metastatic potential in cancer cells when treated with drug agents.

1.1.10 In vitro invasion and migration assays

As described earlier the major challenge in developing anti-metastatic inhibitors is the testing of these inhibitors in suitable preclinical models. Here we are going to focus on the *in vitro* assays that inform on migratory and invasiveness. In drug discovery, *in vitro* assays are favoured because of their ease in handling, increased reducibility and most importantly they are high throughput drug testing

and are less expensive compared with the *in vivo* assays. Furthermore, the use of animal in drug studies is controversial ethically and therefore proceeding with more promising confident compounds from *in vitro* to *in vivo* studies would reduce the conflict. In the following subsection definitions of migration and invasion and the most common 2D and 3D assay are briefly described (Kramer et al., 2013, Eccles et al., 2005, Decaestecker et al., 2007).

1.1.10.1 *Definition of migration and invasion*

Cancer cells mimic the movement of normal cells, as observed during embryonic morphogenesis, would healing and immune-cell trafficking (Kramer et al., 2013, Eccles et al., 2005). That movement in cancer cells is crudely classified into migration and invasion although there is no clear cut differentiation between the two. Migration is usually used in non-pathological description of cell movement in the body. On the other hand, invasion is often used to describe a pathological disorder of cancer cell movement. Malignant carcinomas are defined by the ability of tumour cells to invade and penetrate through tissues and basement membranes and infiltrate into the underlying interstitial tissues. For example intestinal cancers are considered invasive, when the tumour mass penetrates through the basal membrane and enters the submucosal muscle layer. Obviously, although assessing migration is useful in determining metastatic potential, assessment of invasion is more relevant.

The distinction between migration and invasion become clearer when we refer to *in vitro* cell movement. Any cell movement on a 2D surface (basal membranes, ECM fibers or plastic plates) or 3D tissue without any obstructive network, such as

collagen, that does not require any destruction or proteolysis of matrices is defined as migration. On the other hand, invasion occurs when cells move through a 3D matrix, and requires modulation of adhesion, modification or proteolysis of extracellular-matrix components. Therefore, invading cells must modify their shape and interact with and are involved in remodeling of the ECM.

1.1.10.2 *2D and 3D migration and invasion assays.*

1.1.10.2.1 2D Migration assays

1.1.10.2.1.1 Microcarrier bead assay

Cells are grown to reach confluency on microcarrier beads. Thereafter, cell-coated beads are placed in 24-well plates and left for a certain period of time. Later the beads are removed and the migrated cells that are now attached to the plastic surface are fixed and stained with crystal violet. The migrated cells are then quantified. (Kramer et al., 2013, Eccles et al., 2005, Decaestecker et al., 2007)

1.1.10.2.1.2 **W***ound healing*

Cells are grown to reach confluency on a cell culture treated plastic surface Attached cells are then wounded manually by hand using a pipette tip or automatically by using electric signals. Cells that migrate into the wounded area can then be monitored by time-lapse microscope or manually taking imaging at certain time points. Cell migration can be calculated by measuring the free surface area before and after migration. This assay is very popular because it is easy to set-up, analyze and inexpensive, however, this assay is not suitable for cells that need more than 24 h to close the wounded area because it cannot distinguish

between proliferation and migration, unless performed under very low serum conditions. Furthermore, the gap closure rate is not uniform and is speeded up as the gap narrows. Also, the free surface area after migration has to be normalized to the free surface area before, for each scratch, to circumvent the differences in widths of scratches if performed manually. (Kramer et al., 2013, Eccles et al., 2005, Decaestecker et al., 2007).

1.1.10.2.1.3 Ring assay

Cells are seeded to the circular inner region of a Teflon or glass ring in 6 well culture plates. The ring is removed after several hours and the attached cells are left to migrate for several hours. The cells are then washed fixed and stained. The cell migration is calculated by the net increase of total area covered by the cells or as the average of the linear distances covered by from the point of origin. (Kramer et al., 2013, Eccles et al., 2005, Decaestecker et al., 2007) .

1.1.10.2.1.4 Single cell tracking assays

Colloidal gold migration assay is used to track single cell locomotion of cultured cells on a glass coverslip that is covered with gold particles. The cells are left to migrate and are fixed before adding the coverslip onto microscope slides. In assessing the cell migration, computer-aided analysis can monitor the images of the tracks made by the cells and to measure the areas of the tracks. Under the microscope, the colloidal gold particles form a homogenous layer of small dark

dots and the migrating single cells phagocytose the gold particles leaving white tracks that can be evaluated by computer-assisted image analysis.

Single cells migration can also be tracked by using microscopes equipped with a time lapse video system. Manual or automated tracking can be achieved with computer aided software. Cell division, proliferation and path crossing can also be taking into account if recorded for sufficient time.

Another single migration assay is the Dunn assay. Briefly, a microscope slide that has 2 chambers connected via a bridge horizontally. Media containing cells are added to one chamber and media containing chemoattractants are added to the other chamber. Cells sense the gradient of the chemoattractant and start to move towards it. Cells can be counted at the surface of the connecting bridge under the microscope. This assay is valuable when it comes to test expensive compounds, because of the small volumes needed. (Kramer et al., 2013, Eccles et al., 2005, Decaestecker et al., 2007) .

1.1.10.2.1.5 Under agarose spot assay

This assay permits the tracking of cell migration in response to multiple chemokines. Chemokines at specific concentrations are diluted in agarose and applied as a drop on the glass bottom petri dish as a spot. Then, media containing cells is added to the petri dish and cells are left to migrate. Chemokine will start to diffuse and therefore cells will migrate under the agarose spot towards the source of the chemokine if they only express the cognate

receptor for the corresponding chemokine. Later, cells migrated under the agarose spot are quantified for each individual chemokine (Ahmed et al., 2017)

1.1.10.2.2 3D migration/invasion assays

1.1.10.2.2.1 Transwell assay

The transwell assay known also as Boyden chamber assay consists of two chambers; the upper one has a porous membrane. The pore size (5–12 µm) is smaller than the cell size to prevent active cell movement. Briefly, cells suspended into media are added to the upper chamber and can migrate vertically through the porous membrane towards the lower chamber, which contains the medium with the appropriate chemoattractant. The horizontal migration/invasion of cells until reaching the pores is an important element in this assay. Migrated cells on the reverse side of the porous membrane are fixed, stained and counted. The transwell assay can be modified for invasion, if the inserts are coated with a matrix (e.g. collagen, fibronectin) prior to seeding the cells. Hence the cells are moving towards the lower chamber, the transwell assay can be used to investigate chemotaxis (Kramer et al., 2013, Eccles et al., 2005, Decaestecker et al., 2007) .

1.1.10.2.2.2 Gel invasion assay

Cells are seeded onto the surface of collagen gel and left to migrate into the gel to monitor the depth of the invasion using a phase-contrast microscope. (Kramer et al., 2013, Eccles et al., 2005, Decaestecker et al., 2007) .

1.1.10.2.2.3 Spheroid/single cell suspension invasion assay

Spheroids which are 3D clusters of tumour cells are confronted with normal cells (see section 1.1.10.4 for methods used for growing spheroids), initially on semi-solid agar to allow cells attachment, and later in media for few days. This type of study is useful to study immune cells infiltration into tumours *in vitro*. In addition normal cells can be grown into spheroids and a cell suspension of tumour cells is added to it, to study cancer invasion into normal tissue. The cell count is not an easy task and needs either deep confocal imaging or good sample preparation if analyzed with flow cytometry to differentiate between truly invaded cells and cells attached to the spheroid surface. (Kramer et al., 2013, Eccles et al., 2005, Decaestecker et al., 2007) .

1.1.10.2.2.4 Spheroid invasion assay

Tumour spheroids are embedded into a 3D matrix such as collagen I or matrigel and topped up with media containing a chemoattractant, if the spheroid is derived from non-invasive cancer cell lines it will stay compact, with no signs of invasion, if the spheroid is derived from an invasive cancer cell line such as the breast cancer line MDA-MB-231, it will invade into the matrix. Invasion can be recorded through live imaging or by taking images at different time points and the invasive area over time is analysed. (Kramer et al., 2013, Eccles et al., 2005, Decaestecker et al., 2007) .

Despite the fact that the 3D spheroid assays requires relatively more experimental effort compared with other assays, it is highly important to use it for *in vitro* analysis before proceeding for *in vivo* work. Therefore, the importance of spheroids in

evaluating compounds and the different method used to generate them are discussed in the following section.

1.1.10.3 *Importance of spheroids in drug screening*

Culturing cells on 2D cell culture plates has been used to study cancer cell biology as well as drug screening, although this assumes that cells grown as monolayers on plastics can mimic the physiology and environment of real tissues. While the 2D cultured cells can provide valuable information about cell migration, they do not account for the complex conditions found in *in vivo* (Lin and Chang, 2008). It has been demonstrated that PC-3 prostate cancer cell line cultured as 3D spheroids have a significant reduction of β1-integrin expression compared with cells cultured as 2D monolayers (Sameni et al., 2008). Therefore, growing cells as spheroids has been suggested to provide a model closer to the *in vivo* conditions, namely, the cell-to-cell and cell-to-matrix, as well as availability of nutrients, oxygen level and growth factors gradients (Hirschhaeuser et al., 2010). These features allow for a better understanding of the physiological process *in vivo* and can provide a more successful selection of compounds during tests.

Improving our *in vitro* experimental set up to better mimic the *in vivo* situation can be very beneficial for the use of animals in research as this raises many ethical concerns and in this way, the use of animals can be reduced to the most promising candidates.

In this context, is very important to observe the difference between spheroids and cell aggregates. The latter are sometimes mistakenly in the literature considered as

spheroids, since they are not true spheroids, they will not provide the perquisites for their use as spheroids in drug testing (Friedrich et al., 2009). Cell aggregates lack cell-cell and cell-matrix interactions and the spherical geometry. In addition, as they are loose aggregates, they can detach easily and are difficult to transfer them for drug testing (Hirschhaeuser et al., 2010). Most importantly, these aggregates cannot develop the pathophysiological characteristics of a true spheroid Figure 10. Spheroid with diameters larger than 200 µm will develop a gradient of oxygen, glucose, lactate and ATP that is highest at the outer layers and lowest at the most inner areas (Mehta et al., 2012, Lin and Chang, 2008). Hence the spheroid can mirror the *in vivo* situation, with cells at the rim are closer to oxygen and nutrients, likewise tumour cells that are close to blood vessels. The inner cells are far from the nutrients and oxygen supply and therefore become quiescent and eventually die.

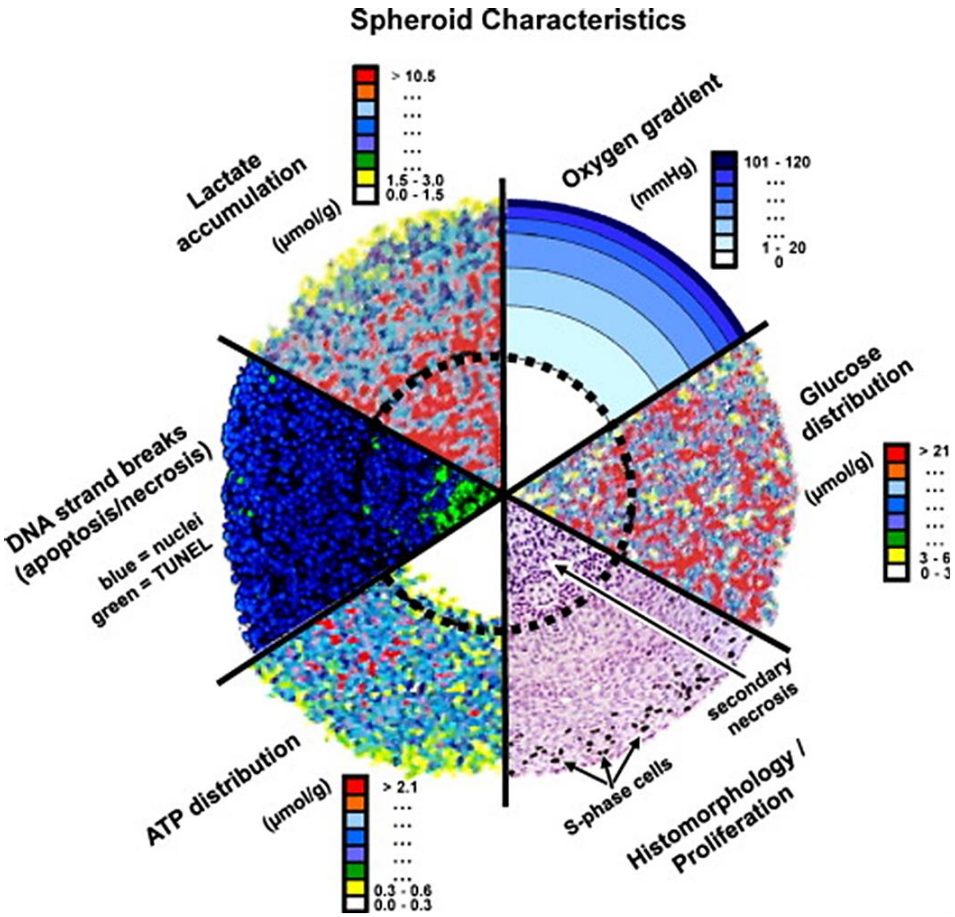

Figure 10: Spheroid characteristics.

Images of different analytical methods; autoradiography, the tunnel assay, bioluminescence imaging, and probing with oxygen microelectrodes showing the different gradient of oxygen, lactate, apoptosis, glucose, proliferation, apoptosis and necrosis through spheroid section. (Hirschhaeuser et al., 2010).

The responses of potential anti-tumour drug candidate molecules on 3D models can be influenced by multiple factors including diffusion barrier, different expression of the particular target, modulation of DNA damage and repair mechanisms, cell cycle distribution and cell-cell and cell-matrix interactions, therefore growing spheroids of a particular size can provide a valuable insight into

drug screening studies (Mehta et al., 2012, Hirschhaeuser et al., 2010, Friedrich et al., 2009).

In spite of, the valuable physiologically relevant information that can be gained from spheroids model, they can sometimes give negative results in compounds screening due to the complexity of the system and therefore falsely mistaken active compounds into inactive ones. However, this might not be related to compound/target interaction of a hit molecule, but for physiological parameters such as permeability and diffusion of compounds which cannot be assessed in hit selection of compounds and of course can be improved by SAR studies performed by medicinal chemists. Hence, both 2D and 3D studies have to be considered, especially in therapeutic screening in drug discovery.

1.1.10.4 *Methods for growing spheroids*

The formation of spheroids comprises of 3 important steps Figure 11 (Cui et al., 2017). (1) Cells in suspension that are close to each other can form loose aggregates, resulting from ECM fibers binding to the integrin on the cells. These aggregates that have high cell-cell interaction results in cadherin expression increase. (2) Further cadherin upregulation is followed at the membrane surface with more compacted aggregates (3) Tight spheroids are formed from the solid aggregates due to homophilic cadherin –cadherin binding.

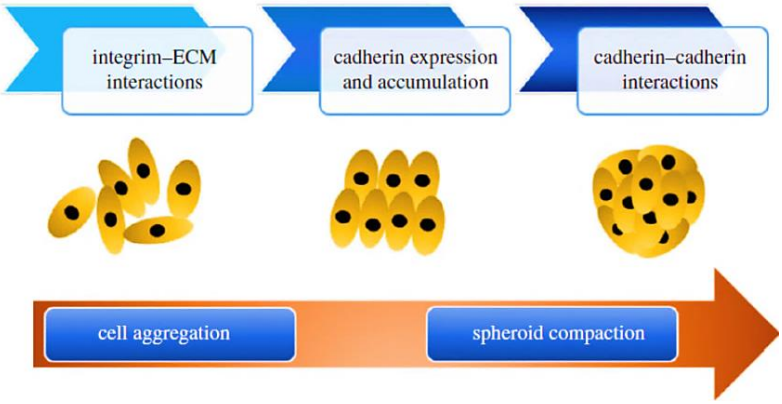

Figure 11: Spheroids formation steps. Cells that are in close proximity due to integrin-ECM interaction, results in loose cell aggregates, later cadherin is upregulated and tighter aggregates are formed. Finally cadherin-cadherin interaction results in spheroid compaction. From (Cui et al., 2017).

To date, many methods have been developed to grow spheroids. These are:- (1) The conventional method of forced floating by preventing attachment of cells to cell cultures surfaces, hanging drop and spinner flask, (2) The matrix and scaffold methods, (3) The microfluidic devices Figure 12. A brief description on the different spheroids formation techniques is summarised in Figure 12.

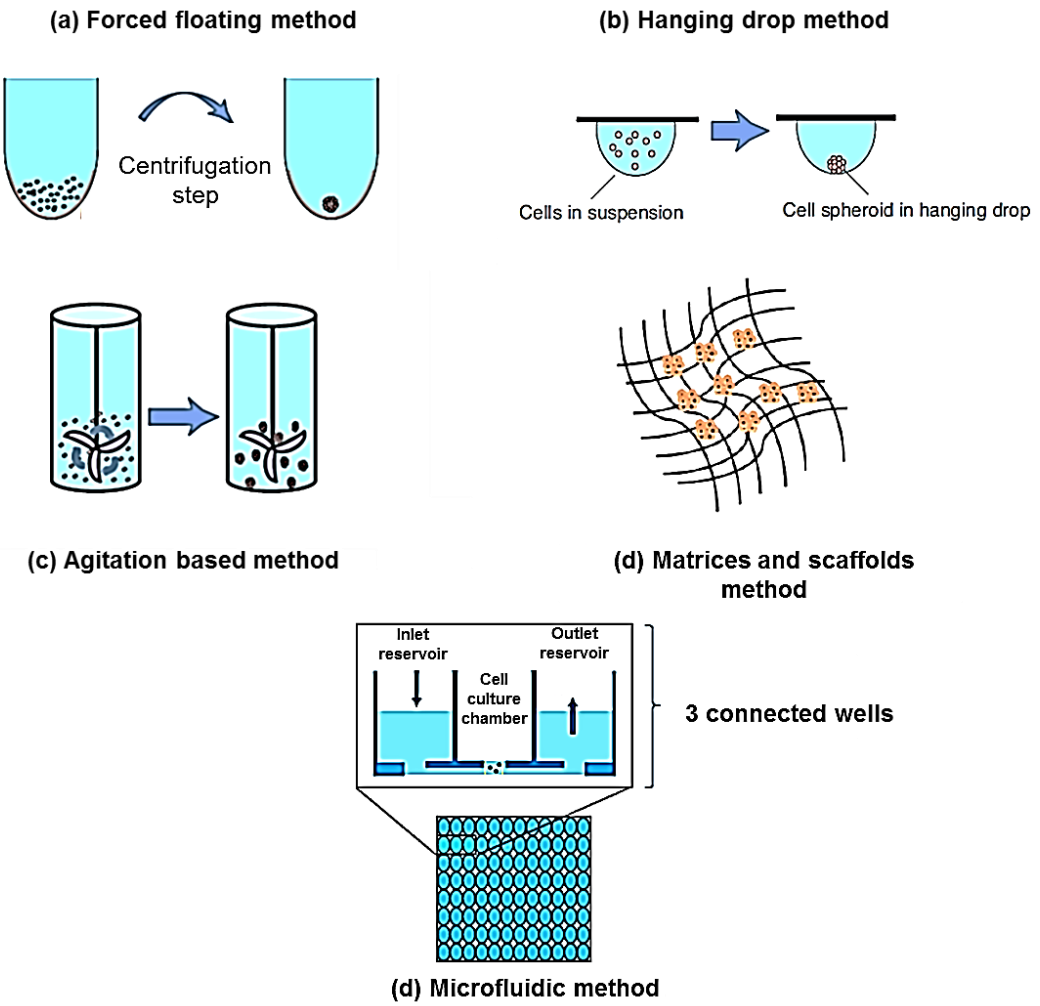

Figure 12: Methods for developing 3D spheroids.

(a) Forced floating method (b) Hanging drop method (c) Spinner flask method (d) Matrices and scaffolds (e) Microfluidic system. Adapted from (Cui et al., 2017, Breslin and O'Driscoll, 2013).

Table 4: Description of spheroid formation methods (Breslin and O'Driscoll, 2013, Hirschhaeuser et al., 2010, Foty, 2011, Patra et al., 2013, Cui et al., 2017).

Method	Hanging drop	Spinner flask	Forced floating	Scaffolds and matrices	Microfluidic cell culture platforms
Spheroids size	small	small and large spheroids can be produced	small and large spheroids can be produced	small and large spheroids can be produced	small and large spheroids can be produced
Ease of technique	easy	easy	easy	easy	easy
Cost	inexpensive	inexpensive	inexpensive	expensive	expensive
High scale production	incompetent	competent	competent	competent	incompetent
Variation in size	uniform	variant	variant	variant	uniform
Labour intensive	yes	yes	no	no	no
Mimic Cell-matrix interaction	no	no	no	yes	yes
Drawbacks	media exchange is difficult due to small volume of the drop	damage by shear force and no control over spheroids size and shape	no control over spheroids size	difficulty to retrieve spheroids after culturing	difficulty for further analysis due to small volume produced by plate

In summary (table 5), there are a number of different migration and invasion assays available and the importance to include a 3D model in the drug screening is highlighted. Therefore, in next chapters we have used some of these assays including wound healing, transwell and 3D spheroid invasion assays to assess the effect of CCL21 or CCL19 on cell migration/invasion in CCR7 expressing cells and evaluate the effectiveness of our in house developed CCR7 antagonists in blocking cell migration and invasion.

Table 5: Comparison of common *in vitro* migration and invasion assays.

Assay	Dimensionality	Invasion/migration	Chemotaxis	Direction of movement	Measurement	Ease of technique
Micro-carrier	2d/3d	migration	-	vertical then horizontal	migration area	+
Ring	2D	migration	-	horizontal	migration area	+
Single cell	2D	migration	-	horizontal	cell migration path	+
Wound healing	2D	migration	-	horizontal	migration area	+
Transwell	2D	migration/ invasion	+	vertical then horizontal	number of cells	+
Under agarose	2D	migration	+	horizontal	number of cells	++
Spheroid gel invasion	3D	invasion	assay dependent	vertical and horizontal	invasion area	+++

1.2 Aims and objectives

Currently, many aspects of the role of CCR7 in cancer remain unclear. For example, whilst it is known that CCR7 is upregulated in tumours, there is little known about the factors that regulate the expression of CCR7 and how these affect tumour cell's functions response to CCL21 or CCL19.

Antagonism of CCR7 receptor could not only provide valuable information on the role of the receptor in cancer, it may also lead to the discovery of novel therapeutic agents with promising potential, in preventing lymph node metastasis. Therefore the **aims** of this research project are:-

- To study the protein expression of CCR7 in different cell lines, xenografts and clinical tissue and assess how wide spread is the CCR7 expression, and assess the functional response of cell lines in order to choose a model for screening of CCR7 antagonist compounds *in vitro* and later *in vivo*. (**Chapter 2**).
- To investigate the regulation of CCR7 expression by stress induced conditions; hypoxia, serum deprivation, mechanical stress and 3D geometry, to mimic the settings that tumours encounter *in vivo* and to investigate if an increase in the expression of CCR7 correlates with an increase in drivers of malignancy (e.g. migration, proliferation, survival) (**Chapter 2**).
- To carry out siRNA CCR7 knockdown studies on OSC-19 cells *in vitro* in order to better understand the CCR7/CCL21 functional roles in cancer and to gain confidence in the hypothesis that CCR7 antagonism is a good

strategy to stop the migration and invasion of cancer cells and thus improve the survival of cancer patients (**Chapter 3**).

- To evaluate the effect of CCR7 antagonism on receptor activation, migration, invasion in different *in vitro* pharmacological assays that include; scratch, transwell, and spheroid invasion assays in order to characterise and identify small molecules, to understand their structure activity relationship and develop potent compounds that can potentially increase the quality of life and the survival of patients (**Chapter 4**).

Chapter 2:

Expression of CCR7 in cancer cell lines and impact of cellular stress on its expression

2.1 Introduction

A number of studies have previously shown that CCR7 is present in different types of solid tumours **(chapter 1)** (Tutunea-Fatan et al., 2015, Zhang et al., 2016, Lu et al., 2016, Shuyi et al., 2008, Xia et al., 2014, Oliveira-Neto et al., 2013, Tutunea-Fatan et al., 2015, Peng et al., 2015) and that its expression contributes to the expansion of cancers. However, factors and mechanisms that regulate the expression of CCR7 remain largely unknown.

During the progression and development of cancer, tumour cells encounter cellular stress through a multitude of factors such as hypoxia, nutrient deprivation, uncontrolled growth in confined space, and unresolved inflammation. Cellular stress is known to have a significant impact on cancer progression (see below). In view of the significance of CCR7 to the growth, invasion and metastasis of head and neck cancers, it would therefore be reasonable to hypothesise that one or more these factors can exert that impact through regulation of CCR7 axis. However, so far, little is known about how these stress factors can affect the expression of CCR7 in the tumour. Therefore, we set out to explore how the expression of CCR7 may be regulated in cancer cell lines by some of these factors and then extend that investigation to clinical tissue.

In this chapter, we first provide a brief overview from literature of how stress factors can impact on cancer expansion. We will then report on changes in the expression of CCR7 and its functional response in cancer cell lines under stress conditions, focusing specifically on the role of hypoxic stress.

2.1.1 Chronic Inflammation of cancer

The idea of cancer as an inflamed tissue was postulated many years ago by (Dvorak et al., 1984). In his paper, Dvorak et al proposed that stroma cells within tumours share many traits with those in wound-healing skin, and suggesting that tumour cells enhance the stroma formation by activating wound healing processes, resulting in increased cell proliferation, and inadvertently to invasion and metastasis. The role of inflammation in promotion of tumours by an experiment in which, injecting Rous sarcoma virus into chickens, results in tumour development not only directly at the injection site, but also at other sites where injuries were sustained by the animals (Schafer and Werner, 2008). This suggests that inflammatory response in those sites of injury can promote tumour formation. In addition, the injection of pro-inflammatory growth factors is also shown to initiate tumour development, which can then be prevented by anti-inflammatory treatment, indicating that inflammation was responsible for the development of wound-triggered tumour (Schafer and Werner, 2008).

It is noteworthy that chemokine axes, and CCR7 axis in particular, play a critical role in the inflammatory response which is associated with tumours. For example, it has been demonstrated that chemokines and chemokine receptors are not only expressed on stroma cells, where they contribute to wound healing, but also on the tumour cells themselves (Coussens and Werb, 2002). This has led to the hypothesis that autocrine activation of chemokine receptors may be involved in the growth and metastasis of pancreatic, head and neck, and non-small-cell lung cancers (Coussens and Werb, 2002, Wang et al., 2008). Furthermore, the

presence of inflammatory cells within the tumour and surrounding areas, has been shown in different types of cancer and their role in supporting cancer progression is well established (Coussens and Werb, 2002). It has been shown that the expression of chemokines in tumours help in the recruitment of immune cells to support tumour progression and immune escape (Yaguchi et al., 2011, Kitamura et al., 2015). For instance, the expression of CCL22 and CCL28 in ovarian cancer has shown to attract CCR4 or CCR10 expressing regulatory T cells that can suppress the anti-tumour responses caused by other subset of immune cells such as leukocytes that are involved in the kill of tumour cells.

Many studies have shown the involvement of CCL21 during chronic inflammation and wound healing process. For instance, it is likely that CCL21 accelerated the wound repair when injected into skin wounded mice by recruiting innate lymphoid cells and other innate immune cells cell that can differentiate into different types of skin cells (Li et al., 2016). Furthermore, the expression of CCL21 in melanoma tumors was shown to recruit the regulatory T cells to tumour site which are associated with an immunotolerant response (Shields et al., 2010).

2.1.2 Hypoxia in cancer

Oxygen is a key energy substrate for ATP generation and any disruption of its level risks damage to nucleic acids, lipids, and proteins. Consequently, many pathophysiological diseases such as cardiovascular, cerebrovascular, lung and cancer can develop as result of this disruption (Brown and Wilson, 2004). In the body, oxygen is maintained at a steady level, ranging from 16% in the pulmonary alveoli to less than 6% in the other organs (Semenza, 2001, Semenza, 2012).

However, the level of oxygen within the tumour can be as low as 0.1% in tumours (Evans et al., 2007). See table 6.

Hypoxia activates a number of signalling pathways that lead eventually to migration, proliferation, apoptosis, angiogenesis and metabolic reprogramming Figure 13 (Majmundar et al., 2010), through a family of hypoxia inducible factors HIF-1, HIF-2 and HIF-3 (Kietzmann et al., 2016). Hypoxia inducible factors are composed of a HIF-α and a HIF-β subunit (Semenza, 2001, Majmundar et al., 2010, Muz et al., 2015). The cellular levels of the alpha subunits are tightly regulated through changes in oxygen level, in contrast to the beta unit, which is constitutively expressed. The regulation of HIF's involves continuous production of the HIF-α unit which is then degraded under normoxia in oxygenated cells after hydroxylation by oxygen sensors, prolyl-4-hydroxylase domain (PHD) and factor inhibiting HIF-1(FIH-1). However, the HIF-α is stabilized and activated under hypoxia. It should be noted that further regulation of HIF-α level is also achieved through other pathways such as Extracellular Receptor Kinase (ERK) and nuclear factor κB (NFκB), receptor tyrosine kinases (RTK), GPCR, toll-like receptors (TLR), and alarmins receptors activation (Kietzmann et al., 2016). Moreover, nitric oxide (NO) and reactive oxygen species (ROS) have been shown to decrease or increase HIF-α levels (Panieri and Santoro, 2016, Muz et al., 2015, Kietzmann et al., 2016).

During hypoxia, the stabilized HIF-1α combines with HIF-1β enabling the combined complex to translocate to the nucleus and thus, regulate various genes such as those involved in angiogenesis or transport of oxygen. The stabilization of HIF1-α

is a hallmark of hypoxia, therefore detecting HIF-1α is used to screen for hypoxia. However, as the HIF-1α is one of the hardest proteins to detect in cells cultured under hypoxia, other downstream proteins that are increased through stabilisation of HIF-1α are routinely screened for as indirect evidence of HIF-1α stabilisation. For example, as one of the target genes of HIF-1 is enzyme lactate dehydrogenase A (LDH-A), its detection can be used as evidence of HIF-1α stabilisation (Elkashef et al., 2016, Semenza, 2013).

The induction of HIF-1α is usually performed by two simple methods:- (Wu and Yotnda, 2011) (1) The Incubator Chamber that is attached to hypoxia tank that has certain level of O_2 and (2) Cobalt Chloride ($CoCl_2$) which is a chemical inducer HIF-1α. The $CoCl_2$ method has the advantage to be fast, inexpensive and the ability to handle flasks freely without affecting the hypoxia level. However, $CoCl_2$ can also regulate other genes apart from HIF-1α and therefore checking what other effects $CoCl_2$ have on particular cells is highly recommended (Wu and Yotnda, 2011).

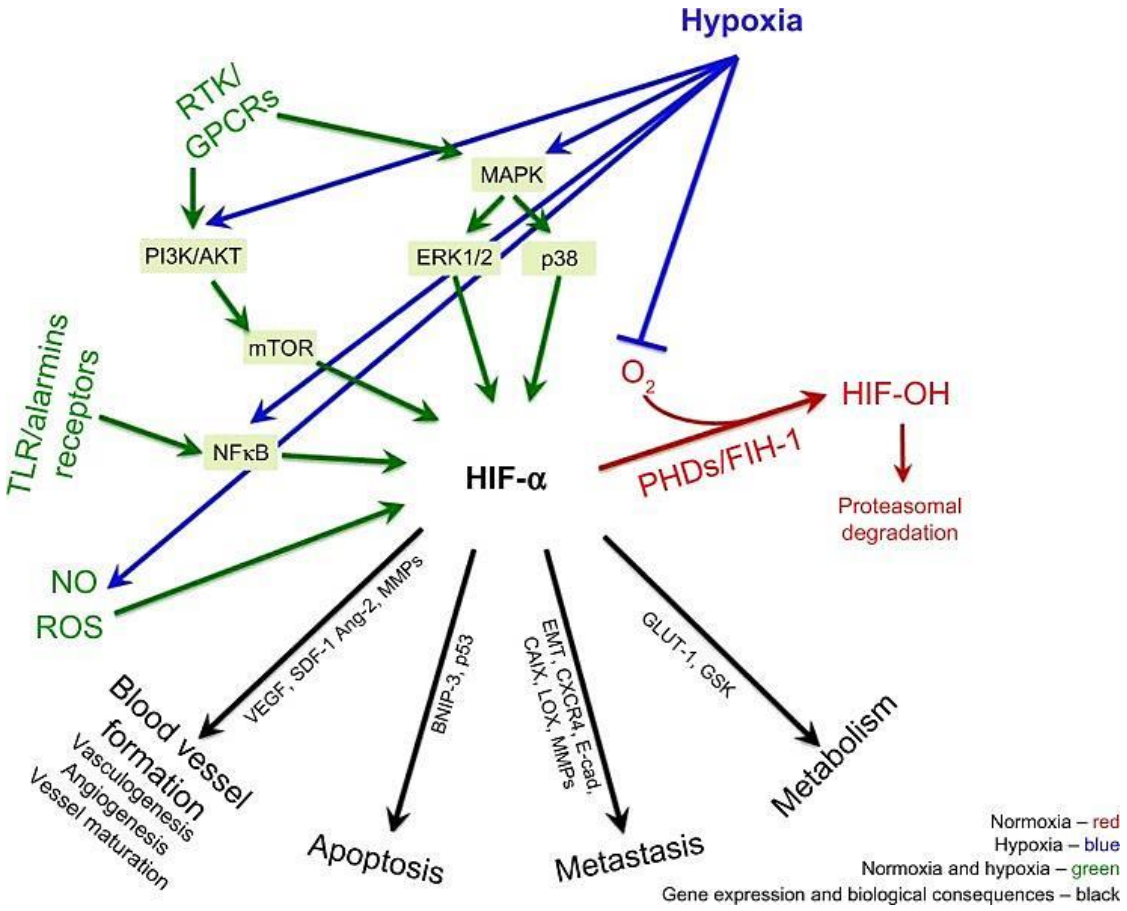

Figure 13: HIF-α regulation. HIF-α is regulated under hypoxic and normoxic conditions. Under normoxia where oxygen is present, HIF-α is degraded after hydroxylation by oxygen sensors PHD and FIH-1. In the contrary, under hypoxia the activity of PHD and FIH-1 is dropped and HIF is stabilised. In addition, HIFα is regulated through PI3K/AKT/mTOR, MAPK and NFκB pathways by cytokines, lipopolysaccharides, and growth factors. From (Muz et al., 2015)

2.1.2.1 *The role of hypoxia in cancer progression*

Solid tumours larger than 1 mm^3 contain regions of low oxygen levels or “hypoxia” Table 6. The diffusion of oxygen through tissue is limited to 200 µm, therefore cells that are closer to blood vessels are well oxygenated and cells located further from blood vessels are poorly oxygenated. As the tumour grows in size, hypoxic regions develop and become larger. Cancer cells respond to the low oxygen level by a

number of routes and in particular by generating new blood vessels in a process known as angiogenesis.

Indeed, hypoxia transcription factors, mainly HIF-1 and HIF-2 have been reported to be involved in all steps of blood vessel formation (Krock et al., 2011), for instance: (1) Endothelial progenitor cells are recruited from bone marrow by hypoxia transcription factors and are later differentiated into endothelial cells by VEGF that is also regulated by hypoxia, specifically HIF-α; (2) induction of MMPs in order to split pre-existing blood vessels; (3) complete maturation of the new blood vessels by recruiting smooth muscle cells and pericytes.

These newly developed blood vessels are profoundly abnormal, dysfunctional and provide insufficient supply of nutrients and oxygen. Furthermore, the new vasculature do not provide the tumour cells with nutrients and oxygen that meet the demand of the growing tumour, leading to even more hypoxia (Dachs and Tozer, 2000) and eventually to formation of necrotic foci. Thus, larger tumours become highly hypoxic with abnormal vasculature which eventually contributes to metastasis and evasion of the immune system making them resistant to therapy.

Table 6: Oxygenation level in different tissues and corresponding tumours. Adapted from (Muz et al., 2015, Evans et al., 2007)

Tissue	% of O_2	
	Normal	Cancer
Brain	**4.6**	**1.7**
Breast	**8.5**	**1.5**
Cervix	**5.5**	**1.2**
Head and neck	**10**	**2.5-0.1**
Kidney cortex	**9.5**	**1.3**
Liver	**4-7.3**	**0.8**
Lung	**5.6**	**2.2**
Pancreas	**7.5**	**0.3**
Rectal mucosa	**3.9**	**1.8**

The permeable and heterogeneous vasculature of newly developed blood vessels facilitates all the pre-metastatic steps; extravasation, circulation, and the establishment of tumour cells to new tissues to escape from the hypoxic environment in the primary tumour (Tsai and Wu, 2012, Muz et al., 2015). In addition, hypoxic cells themselves have a better ability to metastasize. For example, multiple myeloma cancer cells cultured *in vitro* under hypoxia and then injected into mice were able to metastasize to the new bone marrow faster than the normoxic cells (Azab et al., 2012). It also has been reported that mouse models that bear cervical or sarcoma cancer cells, have increased number of lymph node and lung metastases respectively after exposing the models to cycles of hypoxia (Cairns and Hill, 2004, Muz et al., 2015). It has been shown that hypoxia affects the migratory behaviour of cancer cells via an epithelial-mesenchymal transition (EMT) (Guo et al., 2013, Azab et al., 2012). EMT is a biological process that allows a trans-differentiation of epithelial cells to mesenchymal cell phenotype. This

phenotype is responsible for increased migratory capacity, invasiveness, and resistance to apoptosis. Hypoxia induces EMT by reducing the expression of epithelial-associated genes, such as E-cadherin, β-catenin and increasing the expression mesenchymal-like genes, such as N-cadherin, vimentin, smooth muscle actin, and CXCR4 (Azab et al., 2012, Hu et al., 2014). Therefore, tumour oxygenation is a key driving factor for cancer progression and aggressiveness of the majority of human cancers and their metastases that correlates with poor prognosis and overall survival.

2.1.2.2 *Drugs targeting Hypoxia*

One of the biggest challenges in cancer therapy is resistance to chemotherapy and radiation (Tsai and Wu, 2012). The resistant cells are the major cause of patient relapse and metastasis. Cancer cells develop hypoxia (see the previous section), and in particular, hypoxic cells are resistant to chemotherapy and radiation (Muz et al., 2015).

The subpopulation of hypoxic cancer cells become resistant to chemotherapy treatment by different processes such as:- (1) induced quiescence - a state of cell cycle arrest, (2) inhibiting apoptosis and senescence of cells, (3) controlling autophagy, p53, and mitochondrial redox, (4) reduced drug delivery and cellular uptake of chemotherapeutic agents (Hockel and Vaupel, 2001, Muz et al., 2015).

In regard to radio-therapy resistance, one of the most important factors for successful radiation treatment is the oxygenation level within the tumour (Brown and Wilson, 2004). Under normoxia where oxygen is abundant, the radiation

induces radical formation which are able to react with DNA leading to irreversible DNA damage. Under hypoxic conditions cells are resistant to DNA damage. In addition, radio-sensitivity is determined by the cell cycle phase of the tumour cells. Irradiated cells are more prone to cell death in the G2/M phase, where the repair mechanisms are less effective. Many chemotherapeutics agents and radio-therapy target the highly proliferating tumour cells rather than the low proliferating cells sparing the dormant cells that can cause tumour regrowth and relapse (Wilson and Hay, 2011).

Currently, the evaluation of tumour oxygenation and HIF expression can be used to determine the effectiveness of chemo and radio-therapy. For instance, high expression of HIF-1α and HIF-2α in head-and-neck cancer samples is correlated to resistance of the chemotherapeutic agent carboplatin, when compared to samples expressing low level of HIF-1α or HIF-2α (Koukourakis et al., 2002). In addition, oropharyngeal cancer biopsies with high expression of HIF-1α correlated negatively with disease free survival after irradiation. In addition, HIF-1α expression can serve as a strong predictive and prognostic marker in individuals treated with radio-therapy (Muz et al., 2015, Dachs and Tozer, 2000). Moreover, inhibition of HIF-1α in an *in vivo model of* gastric cancer, increased sensitivity to carboplatin, when compared to wild type (Rohwer et al., 2010). Likewise, inhibition of HIF-2α increased the sensitivity of renal cancer cells to doxorubicin, by restoring the expression of the tumour suppressor gene p53 (Roberts et al., 2009).

One of the earliest approaches to treat cancer was proposed by Folkman by using anti-angiogenic agents (Wilson and Hay, 2011). Bevacizumab is a monoclonal

antibody against VEGF (vascular endothelial growth factor), it was successfully approved for treatment of metastatic colorectal and lung cancers (Wilson and Hay, 2011, Rohwer et al., 2010, Hockel and Vaupel, 2001). Later, it was also approved by the FDA for treating metastatic breast cancer along with paclitaxel as first line treatment (Montero et al., 2012). However, the long term use of such agents is linked to an increase in the ability of cancer cells to metastasize, while decreasing the primary tumour size (Wilson and Hay, 2011).

HIF-1α is an interesting target for treatment, (Wang et al., 2011, Tsai and Wu, 2012). It has been reported that 90% of the invading cells of gastric cancer biopsies expressed HIF-1α, while normal tissues showed no HIF-1α expression (Muz et al., 2015). HIF-1α deficient gastric cells by siRNA grown *in vitro* showed less migratory behaviour (Rohwer et al., 2009). It was also observed that less metastases developed after the inhibition of HIF-1α *in vivo* by using antisense oligonucleotide (EZN-2968) to inhibit its activity and no toxicity was observed in a Phase I clinical trial in solid tumours (Guise et al., 2014, Lalani et al., 2007, Albertella et al., 2008), however the trial was stopped due to suspended development of EZN-2968. Currently a new phase I trial has been initiated in hepatocellular carcinoma patients to establish a proof of concept (Wigerup et al., 2016).

Another way of targeting the metastatic process is to target molecules downstream of HIF-α signalling. For example, carbonic anhydrase IX (CAIX) promotes survival and invasion of breast tumour *in vivo* and its inhibition by CAIX inhibitors has shown to reduce tumour growth and less lung metastases (Gieling et al., 2012).

Another example is lysyl oxidase (LOX) that is secreted by cancer cells under hypoxia to recruit cells from the bone marrow that serve as a pre-metastatic niche for metastasis and its inhibition by irreversible inhibitor of LOX in a breast tumour model *in vivo,* reduced the metastasis of the cancer cells to lungs (Erler et al., 2006).

Chemokines are also upregulated by hypoxia (Wilson et al., 2006, Tsai and Wu, 2012). For instance, the chemokine receptor CXCR4 has shown to be upregulated under hypoxia primarily through HIF-1α in melanoma, breast, gastric, pancreatic, lung, ovarian and renal cancers (Sun et al., 2015, Schioppa et al., 2003, Pore and Maity, 2006, Oh et al., 2012, Liu et al., 2006). Oh et al, have demonstrated that the up-regulation of CXCR4 expression in gastric cell lines was HIF-1α dependent and associated with increased invasion and migration (Oh et al., 2012). Of course, blocking CXCR4 signalling with antibodies, low molecular weight antagonists and synthetic peptide antagonists decreased the formation of metastases in different types of cancer and can hence counter this hypoxia driven invasion and migration of cancer (Chatterjee et al., 2014).

2.1.2.3 *CCR7 and hypoxia in cancer*

In contrast to CXCR4, CCR7 expression under hypoxia is far less studied. The expression of CCR7 under hypoxia was evaluated in lung, ovarian, prostate and breast cancers (Li et al., 2009, Li et al., 2008, Wilson et al., 2006, Cheng et al., 2014, Huang et al., 2013). It was demonstrated that CCR7 expression in breast and lung cell lines is induced under hypoxia *via* HIF-1α. Furthermore, the

expression of CCR7 in lung clinical tissues is correlated positively with HIF-1α and HIF-2α and clinical stage and lymph node metastasis (Li et al., 2009). Currently, there are no studies on the relationship between CCR7 and hypoxia in head and neck cancers.

2.1.3 Nutrient deprivation in cancer

The reduction of blood flow does not only result in hypoxia, but also in nutrient deprivation (Wek and Staschke, 2010). For instance, the protein kinase GCN2 and its downstream target, the transcription activator ATF4 are involved in the stress pathway. When cells are glucose deprived, GCN2 phosphorylates the α subunit of the translation initiation factor, eIF2, to compensate for nutrient deprivation by upregulating ATF4 which in turn increase amino acid synthesis and transport pathways by upregulating genes such as asparagine synthetase (ASNS) which is involved in alleviation of nutrient deprivation (Wek and Staschke, 2010).

Tumour cells which are nutrient starved *in vitro,* upregulate the expression of different chemokine receptors. The expression of CXCR3 in colon cancer cells was upregulated in serum starved cells at the membrane bound level, but not in terms of total cellular level (Kawada et al., 2007). The expression of CCR7 was upregulated in thyroid carcinoma after serum starvation (Sancho et al., 2006). Furthermore, CCR7 activation was reported to protect from cell death in serum starved cell in pancreatic cancer (Zhang et al., 2016). Currently, there are no studies on the relationship between CCR7 and nutrient deprivation in head and neck cancers.

2.1.4 Aims and objectives

Studies on the regulatory factors that control the expression of CCR7 receptor are scarce particularly in head and neck cancer. Therefore, we set out to determine how stress factors such as hypoxia and serum deprivation affect receptor expression and its functional response to CCL21 or CCL19.

❖ **The main aims and objectives of this Chapter are:-**

- To study the expression of CCR7 in different cell lines evaluate the usefulness of these cells as *in vitro* models.
- To evaluate the functional role of CCR7 *i.e* responses to CCL21 and CCL19 in different pharmacological assays under normoxic and hypoxic conditions.
- To study the impact of stress factors by mimicking *in vivo* stress related conditions in 2D and 3D *in vitro* models on the protein expression of CCR7 in different head and neck cell lines and study the underlying mechanisms that regulate its expression.
- To study the correlation between the expression of CCR7 and hypoxia in *in vivo* system of head and neck xenografts as well as clinical tissues

2.2 Materials and methods

2.2.1 Materials

Tissue culture materials and reagents were all obtained from (Sigma-Aldrich) unless otherwise specified.

2.2.2 Cell lines

All cell lines (PANC-1, U-87 MG, DU-145, PC-3, MDA-MB-231, MCF-7, DLD-1, HT-29, SW-480, COLO-205, FaDu, SCC-4, A-253, Detroit 562) were obtained from European Collection of Cell Cultures (ECACC) UK, American Type Culture Collection (ATCC) USA or NCI Developmental Therapeutics Programme. OSC-19 was a generous gift from Prof Faye M. Johnson (M.D., Anderson Cancer Center, Houston, Texas, USA). See table 7 for more background information about the used cell lines. These cell lines were chosen to understand how spread is the CCR7 expression among different types of cancer. OSC-19 cell line was chosen later after confirmed expression of CCR7 as a model to investigate the role of CCR7 in cancer and the potentiality to inhibit its effects by small molecule antagonists because it was shown by Kawashiri et al that OSC-19 cell line is a representative model of lymph node metastasis when implanted into the tongue of nude mice (Kawashiri et al., 1995).

Cells were grown in complete appropriate media at 37°C, 5% CO_2 atmosphere and 100% humidity (see appendix I for medium used for each cell line). All cells were passaged when the cells were ~70% confluent, according to the standard

operating procedure for cell culture in the Institute of Cancer Therapeutics (ICT; see section 2.2.5).

Table 7: Cell lines information. (ATCC, 2017 and Cellosaurus, 2017)

[(1)]nt = not tested [(2)]+ = authenticated

Cell line	Tissue of origin	Drived from	Disease	DNA finger print
PANC-1	pancreas	pancreas/duct	adenocarcinoma	nt[(1)]
U-87 MG	brain	brain	glioblastoma	nt
DU-145	prostate	metastatic site brain	carcinoma	nt
PC-3	prostate	metastatic site bone	carcinoma	nt
MDA-MB-231	breast	metastatic site pleural effusion	adenocarcinoma	+[(2)]
MCF-7	breast	metastatic site invasive ductal carcinoma	adenocarcinoma	+
DLD-1	colon	colorectal	adenocarcinoma	+
HT-29	colon	colorectal	adenocarcinoma	nt
SW-480	colon	colorectal	adenocarcinoma	nt
COLO-205	colon	metastatic site ascites	adenocarcinoma	nt
OSC-19	tongue	metastatic cervical lymph node	squamous cell carcinoma	nt
SCC-4	tongue	tongue	squamous cell carcinoma	+
FaDu	pharynx	pharynx	pharyngeal squamous cell carcinoma	+
Detroit 562	pharynx	metastatic site pleural effusion	pharyngeal squamous cell carcinoma	+
A-253	submaxillary salivary gland	submaxillary salivary gland	epidermoid carcinoma	+

2.2.3 Xenografts

Paraffin embedded xenografts were prepared by the staff at ICT. Briefly, cell lines were injected subcutaneously into Balb-c nude mice aged 6 to 12 weeks (Harlan, UK). Mice were sacrificed when the tumour size reached 150 mm^3, afterwards, tumours were excised and immersed in 10% formalin for 24 h and processed for paraffin embedding.

2.2.4 Patients samples

2.2.4.1 *Head and neck tissue microarrays*

Head and neck tissue microarrays slides (consecutive slides from block HN803c) were purchased from Insight Biotechnology Limited (P O Box 520, HA9 7YN, UK). The microarrays were prepared by the Biomax Company (https://www.biomax.us/). For patients clinical characteristics see appendix VII.

2.2.4.2 *TNM classification*

The samples were classified according to TNM system of head and neck cancer (Medscape, 2016). The extent of the primary tumor (T) Table 8, presence and extent of regional lymph node metastasis (N) Table 9, and presence or absence of distant metastasis (M) Table 10. The clinical characteristics of the patients are listed in appendix VII.

Table 8: Primary tumour extent (T)

Tx	Primary tumour cannot be assessed
T0	No evidence of primary tumour
Tis	Carcinoma in situ
T1	Tumour 2 cm or less in greatest dimension
T2	Tumour > 2 cm but not more than 4 cm in greatest dimension
T3	Tumour > 4 cm in greatest dimension

Table 9: Regional lymph nodes (N)

Nx	Regional nodes cannot be assessed
N0	No regional lymph node metastasis
N1	Metastasis in a single ipsilateral lymph node 3 cm or less in greatest dimension
N2	Metastasis in a single ipsilateral lymph node > 3 cm but not more than 6 cm in greatest dimension; or in multiple ipsilateral lymph nodes, none > 6 cm in greatest dimension; or in bilateral or contralateral lymph nodes, none > 6 cm in greatest dimension
N2a	Metastasis in a single ipsilateral lymph node > 3 cm but not more than 6 cm in greatest dimension
N2b	Metastasis in multiple ipsilateral lymph nodes, none > 6 cm in greatest dimension
N2c	Metastasis in bilateral or contralateral lymph nodes, none > 6 cm in greatest dimension
N3	Metastasis in a lymph node > 6 cm in greatest dimension

Table 10: Distant metastasis

Mx	Distant metastasis can't be assessed
M0	No distant metastasis
M1	Distant metastasis

2.2.5 Passaging of cells

All cell lines were cultured and maintained at 5% CO_2 and 100% humidity at 37°C. Cells were cultured in appropriate medium recommended by supplier and prepared according to the manufacturer instruction (for media composition for each cell line, refer to appendix I. For instance, to prepare Complete RPMI1640, 500 ml

incomplete RPMI was mixed with 50 ml of FBS, 5 ml sodium pyruvate solution (100 mM), 5 ml L-glutamine solution (200 mM) and stored at 4°C. Thus, complete RPMI solution contains 1mM pyruvate, 2mM glutamine and 10% FBS. When cells reached ~70% confluency, they were washed twice using 10 ml of phosphate buffer saline (Severn Biotech ltd.) before adding 2 ml of 0.25% trypsin/EDTA for 5 min in 37°C incubator to detach the cells from the flask. Trypsin was inactivated by addition of 10 ml of complete medium. The cell suspension was transferred to a 20 ml universal tube and centrifuged for 5 min at 1000 rpm. Afterwards, media was carefully discarded and the retained cell pellet was then resuspended in 10 ml of fresh medium. Finally, cells were counted and the appropriate amount of the cell suspension was added to another 10 ml of complete medium in a new 75 cm^2 cell culture flask and kept in the incubator.

2.2.6 Counting cells using hemocytometer and growth curve of OSC-19

The cell density was determined using a haemocytometer. 10 µl of cell suspension was added to each chamber of the haemocytometer. Cells were counted manually under the light microscope at 100x magnification power. In each chamber, cells in 1 central and 4 corner squares were counted as shown in Figure 14. The cell density was then calculated according to the following equation:

$$Cell\ density\left(\frac{cells}{ml}\right) = Average\ of\ cells\ counted\ * 10^4$$

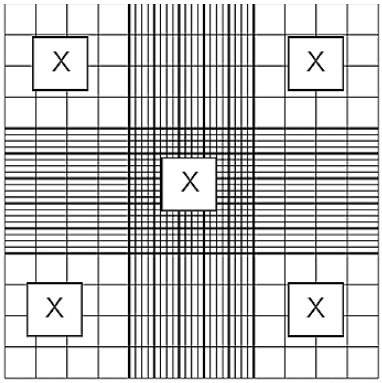

Figure 14 : Haemocytometer chamber. Cells were counted in each square labelled (X).

2.2.7 Immunofluorescence detection for CCR7 staining

Immunofluorescence (IF) technique uses fluorescent antibodies to detect the protein of interest. It is useful and easy method for detection of proteins and their localization in cells. Here, IF was used to qualitatively detect the expression of CCR7 in a panel of cell lines. Cells at a density of 3 x 10^5 cells/ml (PANC-1, U-87 MG, DU-145, PC-3 MDA-MB-231, MCF-7, DLD-1, HT-29, SW-480, COLO-205, OSC-19, FaDu, SCC-4, A-253, Detroit 562) were seeded on coverslips placed inside wells of a 6 well plate. The following day, cells were washed with PBS twice and fixed with 4% paraformaldehyde (PFA) for 15 minutes (min) at room temperature (R.T.) and left to air dry. These coverslips were used immediately or kept at -20°C in the dark until ready for analysis. On the day of the experiment, coverslips were taken out from the -20°C freezer and allowed to warm up to R.T and rehydrated by immersion in PBS for 5 min. Afterwards, cells were permeabilised using 0.1% Triton X-100 for 15 min at R.T. Subsequently, cells were blocked for non-specific binding for 1 h with 5% Bovine serum Albumin (BSA). After blocking, cells were either stained for CCR7 (Anti-CCR7 antibody, Abcam; 1:100

dilution with PBS) or Ki-67 (Anti-Ki-67 antibody, Abcam) (2:100 dilution with PBS) overnight at 4°C. The following day, cells were washed with PBS 3 times for 2 min each before adding the secondary antibody (Alexa Fluor® 546 Donkey Anti-Rabbit IgG, life technologies) for 1 h in the dark. After washing for 3 times/2 min each, one drop of mounting media containing DAPI (Vectashield, Vector laboratories) was added to microscope slides for nucleus staining, the coverslips were added on top of the DAPI-mounting medium and left to dry for 1 h at 4°C. Images were taken using a Leica DM 2000 fluorescence microscope using Tritc (red) channel.

2.2.8 Flow cytometry for quantification of CCR7 and CXCR4 expression

We used the direct staining procedure to investigate the expression of cell surface proteins (CCR7 and CXCR4). In the direct staining method the primary antibody is conjugated to a fluorochrome. For this method, cells (OSC-19, FaDu, PANC-1, MDA-MB-231, MCF-7, PC-3, DU-145, U-87MG, HT-29, DLD-1) were used at 60-70 % confluency, washed twice with PBS, trypsinised and centrifuged. Afterwards, half million cells were transferred to an eppendorf tube, re-suspended in 100 µl of 4% PFA for 10 min at R.T, and centrifuged. Supernatant was removed and cells were washed twice with 1% BSA. Cells were incubated either with anti-CCR7 (2:100 dilution with PBS), (Alexa Fluor® 488 anti-human CCR7 antibody, BioLegend), anti-CXCR4 (5: 100) (Human CXCR4 Alexa Fluor® 488-conjugated Antibody, R&D systems), the isotype matched control for CCR7 (2:100) (Alexa Fluor® 488 Mouse IgG2a, κ Isotype Control Antibody, BioLegend) or the isotype matched control for CXCR4 (5:100) for 30 min at R.T in the dark. Finally, cells were harvested, washed three times for 2 min with 1% BSA solution and resuspended in

500 µl of 1%BSA solution, ready to be analysed on FACS Calibur Cytometer at Ex/Em: ~492–495/517–527 nm using the FL1H (green) channel. The fold change in fluorescence intensity mean was calculated by normalizing the mean fluorescence intensity of CCR7 or CXCR4 stained cells relative to the isotype control in each cell line. All reported results are averages from 3 independent experiments.

2.2.9 Western blot for CCR7 detection

2.2.9.1 *Protein extraction*

To compare cell surface expression of CCR7 with whole cell lysate expression, the western blot technique was used. All cell lines were cultured as previously described in section 2.2.2. Pellets were washed twice with PBS and any remaining supernatant was removed after centrifugation and stored at -80ºC. On the extraction day, any remaining supernatant was removed and cells were resuspended in 300 µl complete RIPA lysis buffer (see appendix VIII for western blot preparation of buffers and solutions), mixed well by pipetting up and down and kept on ice for 20 min with mixing from time to time to ensure complete resuspension in lysis buffer. Subsequently, while kept on ice, cells were sonicated for 10 seconds (s) each time for 3 cycles. In between each sonication cycle cells were kept on ice for 30 s. Next, samples were centrifuged at 13,200 rcf for 15 min at 4ºC. Supernatants were taken to new microcentrifuge tubes to get rid of any un-lysed cell pellet or any residual debris. Samples were stored at -80ºC until used.

2.2.9.2 *Determination of total protein concertation*

The protein concentration was determined using the Bradford assay. BSA was used as a protein standard ranging from 0 mg/ml to 2 mg/ml. BSA was dissolved in distilled water (2 mg/ml), followed by serial dilution and 950 µl of Braford reagent was added to the standard samples and mixed well. Unknown samples were diluted 20x with distilled water and 800 µl of Bradford reagent was added to the unknown samples and mixed well. Finally 200 µl of standards and unknown samples were added to flat 96 well plate (Corning) in triplicates and the absorbance was measured using a Multiskan Spectrum spectrophotometer (thermoscientific) at 595 nm using SkanIt Software 2.4.4 RE. The standard calibration graph was generated by plotting the average absorbance 595 nm for each standard concentration on the y-axis and the corresponding BSA concentration on the x-axis on excel as shown below and the protein concentration of the unknown samples was calculated using the equation shown below in Figure 15.

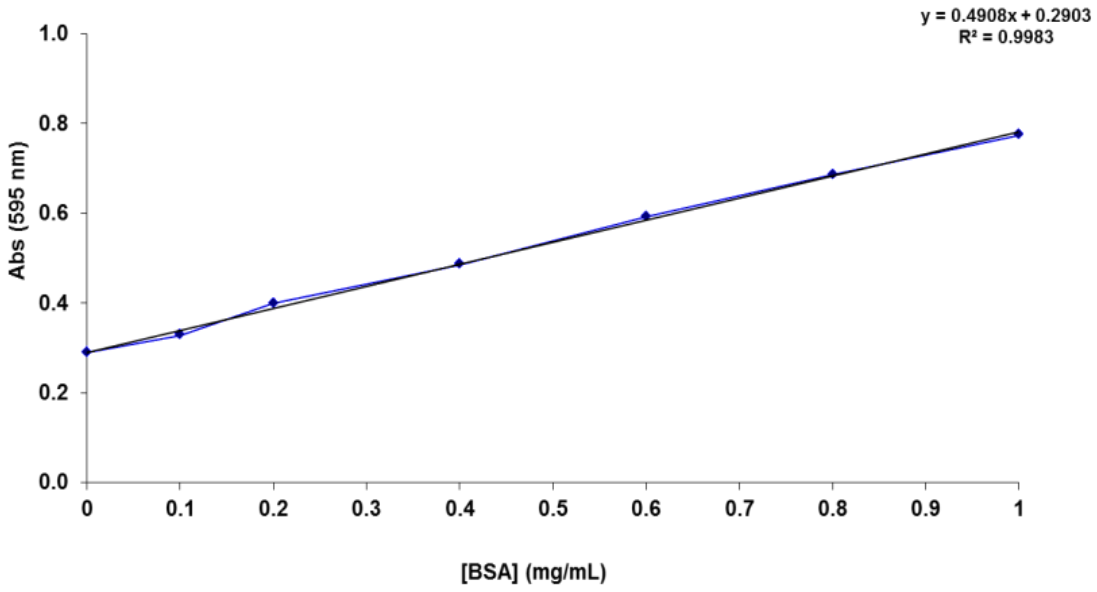

Figure 15: BSA standard curve.

2.2.9.3 *Polyacrylamide gel preparation*

The space integrated glass plates (Bio-Rad) were cleaned with water and 70% ethanol and then assembled according the manufacturer's instructions. Resolving gel 12% or 10 % (see appendix VIII for components of resolving gel) was prepared and pipetted between the connected plates in the casting stand. Next, 1 ml isopropanol was added above the resolving gel which was left to set at room temperature for 30 min. Isopropanol was removed and the gel was washed several times with distilled water. The excess water was removed and the stacking gel was prepared and added on top of the resolving gel (see appendix VIII for components of stacking gel). The gel comb was inserted quickly but carefully and the gel was left to set at R.T for at least 30 min. Next, the comb was removed and the glass plate apparatus which contain the gel was then kept in a humid environment at 4°C until used.

2.2.9.4 *Gel electrophoresis*

Samples 25 µg (CCR7 expression), 30 µg (LDH-A) or 50 µg for (HIF-1α) were taken out from -80°C and kept on ice to thaw and mixed with loading buffer (see appendix VIII for component of loading buffer), vortex and incubated at 95°C for 5 min. Membranes were probed with LDH-A, it's a well known HIF-1α target gene that is upregulated under hypoxia to increase lactate generation, as an indirect indicator of HIF-1α induction that has been used by many including ourselves (Elkashef et al., 2016). Next, the comb was removed from the glass plates apparatus was fitted in the clamping frame and electrode assembly and transferred to an electrophoresis buffer tank (Bio-Rad) filled with 1x running buffer (see appendix VIII for components of running buffer). The denatured samples 20 µl each were loaded to the wells of the gel as well as 5 µl of pre-stained protein ladder (Fermentas PageRuler™ Plus, Thermo Scientific). The gel was run at 70 volts for 10 min, followed by 120 volts until the dye front reached the bottom of the plate, approximately for 90 min.

2.2.9.5 *Protein transfer to nitrocellulose membrane*

After gel electrophoresis, nitrocellulose membrane (Amersham Hybond ECL, GE health care Life Sciences) was soaked in distilled water for 1 min, followed by soaking the membrane, blotting paper and sponges in 1x transfer buffer for 15 min (see appendix VIII for components of transfer buffer). The transfer sandwich (membrane, blotting paper and sponges) was assembled and transferred to the transfer buffer tank (surrounded with ice) which contains 1x transfer buffer and run at 100 volts for 1 h.

2.2.9.6 *Post transfer and immunodetection of proteins*

Nitrocellulose membrane was placed in an incubation box containing 5% w/v skimmed milk for blocking (appendix VIII) and shaked for 1 h. The blocking solution was removed and replaced with 10 ml of 5% milk solution containing the unconjugated primary antibody CCR7 (Abcam; 1:5000 in blocking solution). The membrane was incubated with the primary antibody overnight at 4ºC on a shaker. Then the membrane was washed with PBS TWEEN 20 (PBST) 3 times; 5 min each. Subsequently the membrane was incubated with 10 ml of 5% blocking solution containing (1:3500 in blocking solution) horseradish peroxidase (HRP) based secondary antibody or (1:500 in blocking solution) western dot 625 fluorescence based secondary antibody (Life technologies) for 1 h on a shaker. Finally, the membrane was washed with PBST 3 times; 5 min each for detection method.

2.2.9.7 *Detection method*

The membrane was developed using the enhanced chemiluminescent system (Roche) or the transiluminator system depending on the secondary antibody type. For the chemiluminescent system, the solution was prepared according to the manufacturer's instructions by mixing 10 µl of component B ($NaBO_3$ solution) with 990 µl of component A (Luminol substrate solution). Initially, the excess PBST was removed and the detection solution was pipetted on the protein side surface of the membrane. After incubation at R.T. for 1 min, the detection reagent was discarded and the membrane was placed on X-ray film Amersham hyperfilm^{TM} ECL (GE Healthcare) in a X-ray cassette before being developed in Ilford developer for 2

min and Ilford fixer solution for another 2 min in the dark (for developer and fixer preparation see appendix VIII). The same membrane was washed with PBST (3 × 5 min) and re-probed with primary and secondary antibodies to detect actin protein. For transiluminator system, the membrane was placed in the transiluminator in which the proteins side of the membrane faces the UV light for image uptake. The same membrane was washed with PBST (3 × 5 min) and re-probed with primary and secondary antibodies to detect actin protein.

2.2.10 Immunohistochemistry detection of CCR7 in xenografts and OSC-19 spheroids

2.2.10.1 *Coating slides*

Slides were immersed in acetone for 2 minutes, drained and incubated in 2% 3-aminopropyltriethoxysilane (APES) solution for 2 min. APES solution was prepared by dissolving APES in acetone. Slides were left to dry and were washed twice in running water for several mins. The slides were then left to dry at R.T. overnight.

2.2.10.2 *Immunohistochemistry and staining evaluation of CCR7 in xenografts:*

Immunohistochemical studies were performed for comparison with the results from the protein expression analysis obtained by flow cytometry and western blot and to identify a good xenograft model. The paraffin-embedded tissues were sectioned using a Leica RM 2135 microtome (5 µm thick) and allowed to dry on hot plate at 37°C for at least 2 h. Then, sections were subjected to immunostaining for CCR7. The mounted sections on positively charged coated slides were deparaffinised and

dehydrated by immersing them in the following mixtures: xylene (10 min x 2), 50% xylene/ethanol (5 min), 100% ethanol (10 min x 2), 90% ethanol (2 min), 70% ethanol (2 min), and distilled water (5 min). Endogenous peroxidase was blocked with 3% aqueous H_2O_2 for 30 min. Antigen retrieval was completed in the microwave to boil the sections in 10 mM citrate buffer (pH 6.0) for 20 min at intermediate power, allowed to cool down for 30 min and washed in PBS for 10 min. Subsequent to the nonspecific binding being blocked with goat normal serum (15:1000 dilution with PBS; vectastain® ABC kit) for 20 min. Next, excess goat serum was removed and the sections were covered with CCR7 primary antibody (rabbit monoclonal IgG; Abcam,) and incubated at R.T for 1 h at (1:1000 dilution with PBS).

The primary antibody was washed off with distilled water and the slides were left in PBS for 10 min. The slides were then dried around sections and covered with biotinylated secondary antibody (50:10000 dilution with PBS; IgG anti rabbit, vectastain® ABC kit). Meanwhile ABC reagent (vectastain® ABC kit) was prepared by mixing one drop of A (Avidin) in 5 ml of PBS, adding 1 drop of B (biotinylated peroxidase) and mixing to give a mixture called (C). Secondary antibody was washed off by distilled water and slides were washed again in PBS for 10 min. Afterwards, sections were dried and incubated with ABC reagent for 30 min. The slides were rinsed with PBS for 10 min and colour was developed using DAB detection kit (Vector laboratories). The DAB solution was prepared by mixing 2.5 ml of distilled water, 1 drop of buffer stock solution 2 drops of 3,3'-diaminobenzidine (DAB) and 1 drop of H_2O_2. DAB was disposed of into bleach;

following its incubation with the sections for 2 min. Sections were counterstained in Harris' haematoxylin for 20 s, washed well in tap water and blued in Scott's tap water for 2 min. Finally, sections were dehydrated and cleaned in 70% ethanol, followed by 90% ethanol, absolute ethanol 2 times, 50% xylene/ ethanol and xylene II, each for 2 min. Finally, slides were immersed in clean xylene for 5 min and mounted using DPX (a mixture of distyrene, tricresyl phosphate and xylene) to preserve stains. For Harris' haematoxylin and Eosin staining of xenografts see appendix V.

2.2.11 Detection of CCL21 in head and neck mouse xenografts of head and neck cancers

We have discussed in chapter 1 and the current chapter, the significance of CCL21 expression on tumours cells in modulating the immune response and enhancing tumour growth by autocrine activation (Shields et al., 2010, Wang et al., 2008). Therefore we sought to look for CCL21 expression in head and neck tissues because they have shown as described later in the result section to express high level of CCR7 compared to other cancer cell lines. Xenografts sections of (OSC-19, FaDu, Detroit 235 and A-253) were stained following the staining described in section 2.2.10. The CCL21 antibody was diluted with PBS (1:40) before applied to sections, incubated overnight at 4°C and followed the rest of IHC staining that is described earlier.

2.2.12 Effect of CCL21 or CCL19 on proliferation

2.2.12.1 *Growth curves of OSC-19 and FaDu*

Performing a growth curve for OSC-19 and FaDu cells is important; in order to define their growth characteristics and to determine the best time for evaluation of the effect of CCL21 on cell proliferation and the effects of CCR7 antagonists.

Growth curves of OSC-19 and FaDu cells were obtained using manual counting and MTT proliferation assay, for the preparation of MTT solution (see appendix II). For manual counting, 100 µl of cell suspension was mixed with another 100 µl of trypan blue solution; trypan blue has the ability to penetrate only the dead cells' membrane, therefore highlighting the viable/dead cells. Next, 10 µl of the cell suspension/ trypan blue mix was loaded to each channel in the haemocytometer and viable cells (white) were counted. Note that dead cells appear blue. The cell density was calculated according to the following equation:-

$$Cell\ density\left(\frac{cells}{ml}\right) = Average\ of\ cells\ counted\ * dilution\ factor * 10^4$$

*The dilution factor = 2 (100 µl of cell suspension: 100 µl of trypan blue solution).

The MTT assay was performed to create growth curves with different starting cell concentrations. 3-[4,5-Dimethylthiazol-2-yl]-2,5 diphenyl tetrazolium bromide (MTT) is used to determine the number of viable cells. In viable cells, the yellow MTT enters the cells and passes to the mitochondria where it is reduced to insoluble dark purple formazan Figure 16. Then, the formazan is solubilised with an organic

solvent, *e.g.,* Dimethyl Sulfoxide **(**DMSO). The purple colour of the solubilised formazan is then measured using colorimetric plate reader at 540 nm (Thermo Scientific multiskan). Reduction of MTT can only take place in metabolically viable cells; therefore the intensity of the colour indicates the population of viable cells. We first determined the appropriate condition where cells would be in log growth phase. Cells were passaged and counted as previously described and the desired cell concentrations were prepared: $5x10^2$, $1x10^3$, $5\ x10^3$, $1\ x10^4$, $5\ x10^4$, $1\ x10^5$ cells/ml. Cells were seeded in 96 well plates by loading 200 µl of each cell concertation to the specified wells. On day 0 (seeding day) and day 2, 3, 4, 5, 7 (after seeding), on the specified day one plate was taken out from the incubator and 20 µl of 5 mg/ ml MTT stock solution was added and the plate was incubated for 4 h, the medium was removed and 150 µl of DMSO was added to each well to dissolve the puple-blue formazan crystals. Absorbance was then recorded at 540 nm using the colorimetric plate reader. The mean absorbance was calculated from three independent experiments. The blank mean value (media with no cells) was subtracted from the absorbance mean values. Results were plotted as absorbance on y-axis against time on x-axis.

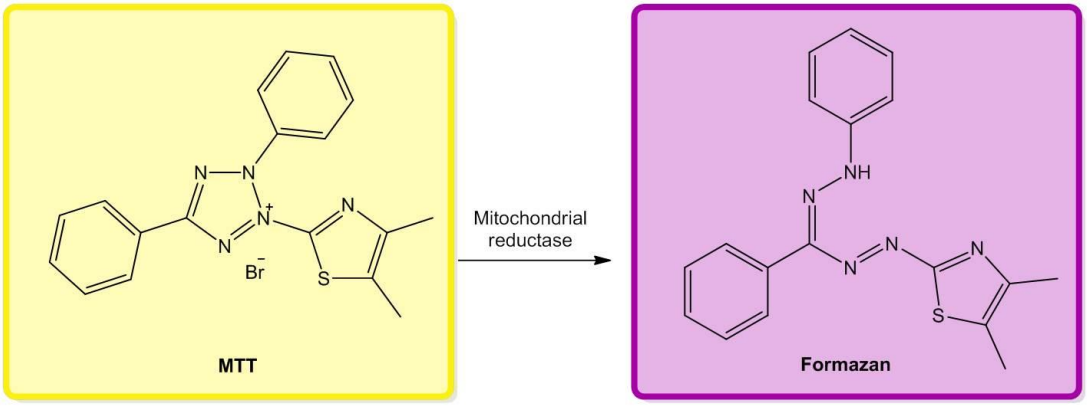

Figure 16: MTT metabolism in viable cells.

MTT (yellow) is converted by mitochondrial reductase to formazan crystals (purple).

2.2.12.2 *Proliferation rate after CCL21 or CCL19 addition using MTT*

The effect of CCL21 or CCL19 on the proliferation rate of OSC-19 and FaDu cells was determined using MTT assay. OSC-19 or FaDu cells were seeded in a 96-well plate at a density of 1 x 10^4 cells/ ml and incubated for 24 h. Then, 20 µl of CCL21 or CCL19 was added to each well containing 180 µl of media to achieve a final concentration of 1, 10 or 100 nM. After 72 h, the MTT assay was performed as described in section 2.2.12.1. Proliferation was calculated using this equation:-

$$Proliferation(\%) = \frac{A - B}{C - B} * 100$$

Where A is the absorbance of treated cells with CCL21 or CCL19, B is the absorbance of blank and C is the absorbance of untreated cells.

2.2.13 Effect of CCL21 or CCL19 on cell migration

2.2.13.1 *Wound healing assay:*

OSC-19, FaDu, SCC-4, PC-3, DU-145, DLD-1 and SW-480 cells were seeded at a density of (8.5 x 10^5 cells/ml) in 24 well plates (350 µl/ well) and left overnight to reach confluency. On the following day, the supernatant was removed and the wells washed with PBS. A wound was scratched using a p200 pipette tip. The cells were then washed twice with PBS and treated with 2% FBS media containing CCL21 at (10 and 100 nM), CCL19 at (10 and 100 nM) or 2% FBS media alone as control. We used 2% FBS rather than 10% FBS to exclude the role of proliferation in our analysis. Images were taken using a lumascope 488 microscope at 0 h (after making scratch) and at 18, 24, 18, 14, 14, 42 and 21 h (after cell migration) for OSC-19, FaDu, SCC-4, PC-3, DU-145, DLD-1 and SW-480, respectively. Image J software was used to measure the free surface area of the wound at 0 h (Figure 17-a) and at specific time points after migration (for example 18 h for OSC-19) Figure 17-b (Schneider et al., 2012). The % of the free surface area was calculated according to the following equation:

$$\%\ of\ free\ surface\ area\ after\ migration = 100 - \left(\frac{A - B}{A}\right) * 100$$

Where A= Free surface area at 0 h and B = free surface area after migration at specific time point for each cell line.

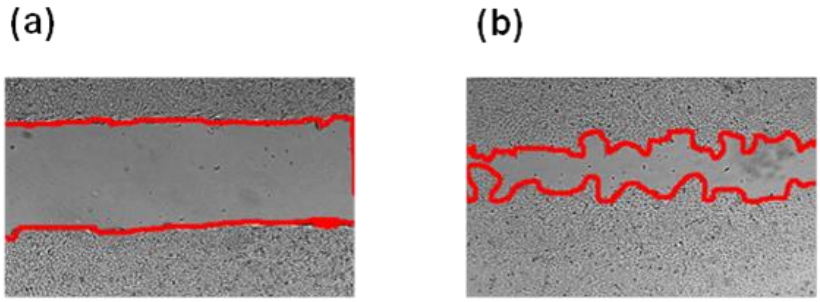

Figure 17: Wound healing assay.

Photos were captured at 0 h (A) and 18 h (B).

2.2.13.2 *IF staining for Ki-67 in wound healing assay*

Our results from the wound healing assay showed positive results, with CCL21 enhancing the migration of OSC-19, SCC-4, PC-3 and DU-145. Accordingly, we choose one of these cell lines as a model for our investigation on the role of CCR7 in cancer progression and to test and evaluate CCR7 antagonists in preventing cell migration. OSC-19 was chosen and to confirm that the results seen in the migration assay relate to migration, rather than proliferation, we stained with Ki-67, a marker for proliferation. OSC-19 cells were seeded at 8.5 x 10^5 cells/ml on coverslips in 6 well plates were seeded on coverslips in 6 well plates. The following day, cells were washed with PBS twice and the wound healing assay was performed as described in section 2.2.13.1. Immediately after scratch half of the coverslips were fixed with PFA for 15 min at room R.T. and left to air dry and kept at -20°C until ready to use. The other half of cells on the coverslips were left to migrate for 18 h with or without CCL21 and fixed in the same way as previously described. On the day of the experiment, immunofluorescence staining (IF) was

performed as described in 2.2.7. The cells were incubated with Ki-67 antibody (2:100 dilution with PBS) (Abcam) for 0 h and 18 h or with CCR7 (1:100 dilution with PBS) overnight at 4°C. On the following day, cells were washed with PBS 3 times for 2 min each before adding the secondary antibody (Alexa Fluor® 546 Donkey Anti-Rabbit IgG, life technologies) for 1 h. After washing with PBS (2 min, x 3), one drop of mounting media containing DAPI was added to microscope slides for nucleus staining. The coverslips were added on top of the DAPI-mounting medium and left to dry for 1 h at 4°C. Images were taken using a Leica DM 2000 fluorescence microscope using Tritc (red) channel for CCR7 and Ki-67 and blue for DAPI.

2.2.14 Expression of CCR7 using flow cytometry after serum deprivation

Cells were cultured at 37^{o}C, 5% CO_2 and 100% humidity, when reached 60-70% confluency, the media was removed and cells were washed twice with PBS. Next, 0% FBS or 10% FBS media was added to the cells for 24 h before analysing them for CCR7 expression using flow cytometry as described earlier in section 2.2.8.

2.2.15 Effect of CCL21 or CCL19 on CCR7 receptor activation using (Ca^{2+}) flux assay

Binding of ligands to GPCRs can induce an intracellular increase in calcium concentration that can be measured using a Ca^{2+} sensitive fluorescence dye; this method can be used for high throughput screening as an indication of receptor activation. We used this assay to look for CCR7 functionality through binding to its ligands. Cells cultured in 10% FBS were seeded in 96-well black plate at 1x10^5

cells/well cell density and left to attach overnight in the incubator. The following day, media was removed and cells were washed with 100 µl of the assay buffer twice. Quickly but carefully 100 µl of the loading dye (Molecular Probes^{TM} Fluo-4 NW, Invitrogen) was added to each well and incubated for 1 h at 37°C. Fluorescence intensity was measured in response to 20 µl addition of CCL21 or CCL19 (100 nM in well concentration), added using Thermo Scientific Flouroskan Ascent FL at excitation wavelength 485 nm and emission wavelength 538 nm at 37°C.

2.2.16 CCL21 detection using enzyme-linked immunosorbent assay

Enzyme-linked immunosorbent assay (ELISA) is a technique used for detecting and quantifying substances based on antigen-antibody interaction. Antigen binds to the bottom of the pre-prepared plates that allow protein binding, later antibodies are added to bind to the attached antigen. The binding can be detected by directly labelled primary antibodies, labelled secondary antibodies that bind to the primary antibody or by the sandwich method, where the antigen is bound between two antibodies. Here, human CCL21 ELISA kit was purchased from (Thermo-scientific) for detecting CCL21 produced from OSC-19 cultured cells. In, 1 ml of 8.5 x10^5 cells/ml OSC-19 cells was added to each well of a 6 well plate and left to form confluent monolayer. After 24 h, cells were washed twice with PBS and multiple scratches of total 8 were made using 200 pipette tips. Next, 2% FBS media was added to all wells and the supernatant was collected after 18 and 24 h and stored at -80ºC until ready to analyse. On the day of the experiment, lyophilized recombinant human CCL21 standard was centrifuged and 400 µl of 1X assay

diluent B was added. After mixing, 50 ng/ml of CCL21 standard was used to prepare serial dilutions (8,000, 3200, 1280, 204.8, 81.92, 32.76 pg/ml). Supernatant and/or standard (100 µl) was added to pre-coated 96 wells strip plate in Triplicate, covered and incubated overnight at 4ºC with gentle shaking. The solution was discarded and washed 4 times with 300µL of 1X wash buffer. At each washing step complete removal of liquid was assured for good performance. After the last wash, the plate was inverted and blotted against clean paper towels to remove any remaining wash buffer. Next, 100 µl of 1X biotinylated antibody was added to each well and incubated for 1 h at R.T. with gentle shaking. The solution was discarded and the washing step was repeated as described earlier. Next, 100 µl of streptavidin-HRP solution was added to each well and incubated for 45 minutes at R.T. with gentle shaking. The solution was discarded and the washing step was repeated as described earlier and 100 µl of 3,3′,5,5′-Tetramethylbenzidine (TMB) substrate to each well. After, 30 min of incubation at R.T. in the dark with gentle shaking, 50 µl of stop solution was added to each well. The plate was evaluated within 30 min of stopping the reaction by measuring the absorbance on a colorimetric plate reader (Thermo-electron Corporation, Multiskan Ex) at 450 nm. The standard curve was generated by plotting the average absorbance (450 nm) for each standard concentration on the y-axis and the corresponding CCL21 concentration on x-axis as below using excel Figure 18. The equation generated from the standard curve was then used to calculate the amount of CCL21 present at each time.

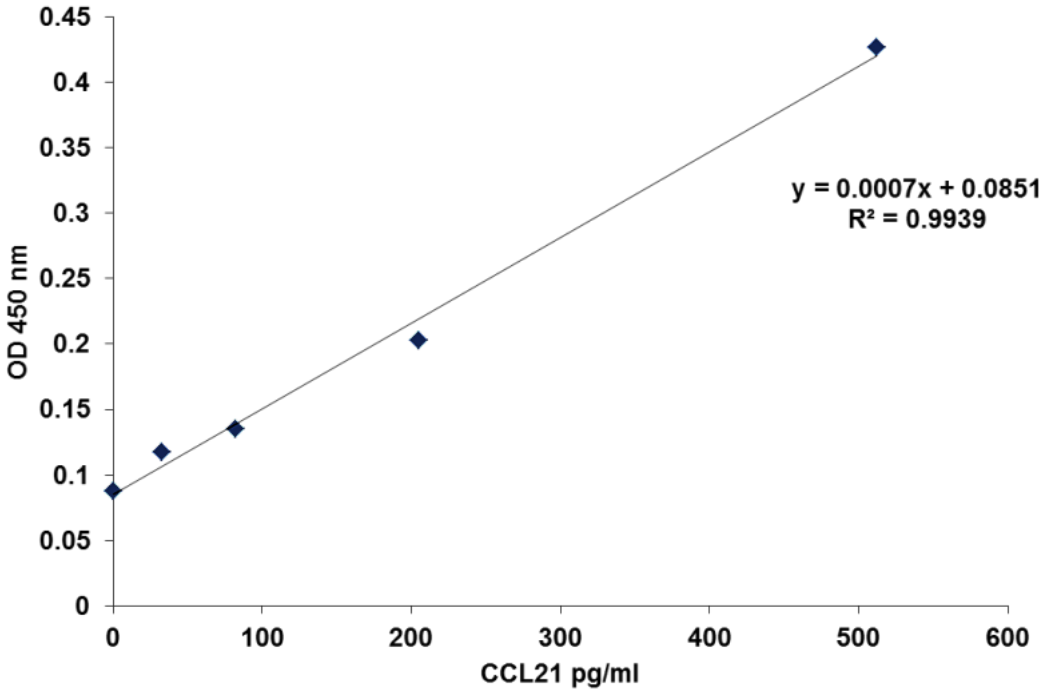

Figure 18: CCL21 standard calibration curve.

2.2.17 Role of Hypoxia in CCR7 expression

2.2.17.1 *Incubation of cells under hypoxia*

The head and neck cell lines were seeded in 75 cm^2 flasks and incubated under normoxic conditions (37ºC, 5% CO_2 and 100% humidity). Later, when cells reached 60%-70%, cells were either kept at normoxic conditions (control) or transferred to a hypoxia chamber (Whitley H35 hypoxystation) (0.1% O_2, 95% N_2, 5% CO_2 and 100% humidity) for 24 h prior to cell harvesting for flow cytometry and western blot analysis. The cells inside the hypoxia chamber were washed once with PBS that was placed in the hypoxia chamber 24 h earlier. Then, pre-hypoxic media was added to cells and left for the appropriate incubation period.

2.2.17.2 *CCR7 protein expression in head and neck cell line after hypoxia*

After 24 h of culturing cells under hypoxia, cells were washed twice with PBS, trypsinised and spinned down. For CCR7 expression, half million cells were transferred to an eppendorf tube, re-suspended in 100 µl of 4% PFA for 10 min at R.T. and centrifuged. All these operations take place in the hypoxic chamber. After fixation, cells were moved out of the hypoxic chamber and the CCR7 staining was performed as described earlier in section 2.2.8. Cells cultured under normoxia were also examined for CCR7 expression for comparison. All hypoxic and normoxic samples were analysed using flow cytometry as before in section 2.2.8.

2.2.17.3 *Detection HIF-1α or LDH-A*

To confirm the existence of a hypoxic environment in the hypoxia chamber, cells were washed twice with PBS and trypsinised in the hypoxia chamber. After centrifugation, the supernatant was removed in the chamber and cell pellets were moved to the -80ºC until used. Normoxic cells were also included for comparison and cultured in parallel to the hypoxic cells. Subsequently, hypoxic and normoxic cells were taken out from -80ºC storage and kept on ice for protein extraction using RIPA buffer see section 2.2.9.1, followed by the western blot steps described in section 2.2.9. After sample loading into the gel, membranes were incubated for (1:1000 dilution with PBS) HIF-1α (BD transduction laboratories) or (1:500 dilution with PBS) LDH-A (Abcam). The membrane was incubated with the primary antibody overnight at 4ºC on a shaker, followed by secondary antibody incubation and developing for HIF-1α or LDH-A as described in 2.2.9.

2.2.17.4 *Induction of HIF-1α using cobalt chloride ($CoCl_2$)*

In addition to the hypoxia chamber, the chemical Cobalt chloride ($CoCl_2$) was used to stabilise HIF-1α under normoxia (Wu and Yotnda, 2011) in order to examine whether expression of CCR7 was increased by HIF-1α. To determine the non-toxic concentration of $CoCl_2$ for HIF-1α induction in OSC-19 cells, an MTT assay was carried out. Cells were seeded into 96 well plates by adding 180 µl of cell suspension containing 1 x 10^4 cells/ml to each well and incubated at 37ºC, 5% CO_2 and 100% humidity for 24 h. Next, cells were treated with $CoCl_2$ serial dilutions ranging from 10 µM to 500 µM (in well concentrations) for 24 h, the media was removed and exchanged with fresh media and the cells were incubated for further 48 h. After 96 h from seeding the cytotoxicity was evaluated using MTT solution as described earlier in section 2.2.12.

To induce HIF-1α expression, OSC-19 cells were seeded into 75 cm^2 flasks and incubated at 37ºC, 5% CO_2 and 100% humidity. According to the MTT assay results, OSC-19 cells were treated with (200 and 100 µM $CoCl_2$) for 24 h before being trypsinised for protein extraction. Western blot for HIF-1α detection was performed as previously described in section 2.2.17.2.

2.2.18 Cells migration under hypoxia

OSC-19 cells were seeded at a density of (8.5 x 10^5 cells/well) in 24 well plates and left overnight to reach confluency, the supernatant was removed and the wells washed with PBS. Later, a wound was scratched using a p200 pipette tip and 0 h photos were taken. Cells were either kept at normoxia or transferred to the hypoxia chamber. Afterwards, the cells were washed twice with PBS and treated with 2%

FBS media containing CCL21 at (10 and 100 nM in well concentrations), CCL19 at (10 and 100 nM in well concentrations) or 2% FBS media alone as control. Finally, at 18 h, photos were taken and analysed as before 2.2.13.1.

Another experimental setting was also performed, in which OSC-19 cells were seeded at (1.6 x 10^4 cells/well) at normoxic conditions for 48 h and then transferred to hypoxia or kept in normoxia. After 24 h of transferring cells to the hypoxia chamber, scratches were produced inside the chamber, cells were washed with PBS and the plate was taken out of the chamber for not more than 10 min for capturing photos at 0 h and immediately returned back to hypoxia and treated with 2% FBS media containing CCL21 at (10 and 100 nM in well final concentration), CCL19 at (10 and 100 nM in well, final concentrations) or 2% FBS media alone as control. After 18 h after migration photos were captured and analysed as before 2.2.13.1.

2.2.19 Proliferation under hypoxia

In order to evaluate the proliferation rate after adding CCL21 under hypoxia, 180 µ l of OSC-19 cell suspension were added to each well of a 96 well plate at a density of 1 x10^4 cells/ml. After 24 h, 20 µl of CCL21 solution was added to each well to achieve a final concentration in the well of 1, 10 or 100 nM. After 72 h, the MTT assay was performed as described in section earlier in section 2.2.12.2. Cells under normoxia (control) also received the same treatment. Proliferation rate under hypoxia was calculated by comparing results to normoxic cells, in both cases, control is considered when no CCL21 is added.

2.2.20 Reactive oxygen species (ROS) detection and its effect on CCR7 expression

It has been demonstrated the ROS facilities cancer progression by affecting the cell migration, as well as induction of chemokine receptors expression such as CXCR4 (Chetram and Hinton, 2013). Therefore, we evaluated the relationship between ROS and CCR7 expression by flow cytometry.

In addition, we also carried out evaluation of ROS to understand their effect on cell migration and compare with what we had seen in our experiments in the hypoxia chamber and $CoCl_2$ treatment.

The cells were seeded in phenol red free RPMI medium (Gibco) into 25 cm^2 flasks at a concentration of 4 x 10^4 cells/ml and incubated at 37˚C and 5% CO_2 until reached 70% confluency. The following day, cells were moved to the hypoxia chamber treated with $CoCl_2$ (200 µM and 100 µM) or with H_2O_2 200 µM (positive control for ROS induction) for another 24 h. Cells cultured under normoxia in phenol red free medium with no additional treatment were used as control. After 72 h from seeding, the cells were trypsinised, washed and treated with 6-carboxy-2',7'-dichlorodihydrofluorescein diacetate carboxy-H2DCFDA (Fisher scientific) before analysing the samples using flow cytometry. In addition, OSC-19 cells that were been treated with or without H_2O_2 (200 µM) were also analysed with flow cytometry for CCR7 expression.

2.2.21 Relation between hypoxia and CCR7 in spheroids

2.2.21.1 *Spheroids formation and growth curve*

OSC-19 cell suspension was prepared and diluted to the desired cell concertation as usual and seeded at 10000 cells/ well or 2000 cells/well in round 96 bottom well plates that were coated previously with 1.5% agarose solution to avoid cell adhesion. SCC-4 cells seeded at 2000 cells/well (for agarose preparation and plate coating see appendix VI). On the seeding day, the plate was centrifuged for spheroid initiation. The media was changed every other day for 7 days. The diameter of OSC-19 spheroids was measured from day 1 (after seeding day and every other day during the culture period using a calibrated graticule fixed to the eye piece of a light microscope using a 10x objective lens. Results were plotted as a graph with the mean of the diameters of at least 20 spheroids on the y-axis and time on the x-axis. Photos were taken at 100x magnification power on Lumascope 488 microscope.

2.2.21.2 *Pimonidazole treatment*

To confirm the presence of a hypoxic core within OSC-19 500 µm spheroids, we used Hypoxyprobe™-1 Green kit (HPI) for hypoxia detection. 2000 cells spheroids on day 7 and 10000 cells spheroids on day 5 were treated with pimonidazole which is the active compound of Hypoxyprobe, it interacts with proteins in the hypoxic core and forms stable adducts. Briefly, the spheroids were transferred to 1.5 ml microcentrifuge, washed twice with PBS and then treated with pimonidazole at (100 µM) for 2 h at 37°C. During incubation the tubes were inverted every 30 min for homogenous penetration of pimonidazole. Next, the spheroids were washed

with PBS and fixed with Bouin's solution as described earlier. -ve control samples (no pimonidazole treatment) were also included.

2.2.21.3 *Fixation and paraffin embedding of OSC-19 spheroids*

Spheroids on day 1 and day 7 were transferred to a 20 ml universal tube and allowed to sediment down. Media was removed with care and spheroids were washed with PBS. Then 3 ml of Bouin's solution was added for 75 min. Bouin's solution was drained off and spheroids were washed with 70% ethanol several times to remove as much as possible of the Bouin's solution. Finally, spheroids were left in in 70% ethanol for 1 h. The spheroids were then immersed in 90% ethanol for another h. Subsequently, the spheroids were covered with absolute ethanol for another hour and replaced with xylene for an h. Afterwards, spheroids were transferred to embedding moulds with minimum amount of xylene, covered with paraffin and left in the oven at 68°C for 30 min. The paraffin/ xylene mixture was removed after 30 min and replaced with paraffin twice after 30 minutes each time and left for 1 h in the oven. Finally, spheroids were centred in the middle of the mould, covered with fresh paraffin and left for 5 min in the oven to allow spheroids to settle at the bottom. Moulds were transferred to a cold plate overnight and then kept in the freezer at -20°C until ready to use.

2.2.21.4 *Immunofluorescence staining*

Spheroids were sectioned at 5 µm thickness on APES coated slides as described earlier in section 2.2.10.1. The slides were kept at 4°C until used. On staining day, the slides were baked at 45°C for 20 min and the mounted sections on positively coated slides were deparaffinised and dehydrated by the following procedure:

xylene (10 min x 2), 50% xylene/ethanol (5 min), 100% ethanol (2 min x 2), 90% ethanol (2 min), 70% ethanol (2 min), and distilled water (5 min). Antigen retrieval was completed in the microwave to boil the sections in 10 mM citrate buffer (pH 6.0) for 20 min, allowed to cool down for 30 min and washed in PBS for 10 min. Sectioned were circled with zimed pen, treated with 0.1% triton X-100 for 10 min and washed 3 times with PBS (5min, x 3). Sections were blocked in 5% BSA at R.T for 1 h. Afterwards, the formed pimonidazole adducts were detected with FITC conjugated MAb1 (1: 150 diluted with PBS monoclonal mouse antibody, Hypoxyprobe™-1 Green kit), for 2 h at 37°C. Sections were washed with PBS (3 min x 3) followed by nucleus staining with DAPI. For CCR7, Ki-67 detection, sections were incubated with CCR7 (1:100 dilution with blocking solution) or Ki-67 (1:50 dilution with blocking solution) antibodies overnight at 4°C. After the PBS washing (3 min × 3), sections were incubated with the secondary anti rabbit antibody (1:200 dilution with PBS) for 1 h. Again, sections were washed with PBS before staining the nucleus with DAPI. The DAPI-mounting medium slides were left to dry for 1 h at 4° C. Images were taken using a Leica DM 2000 fluorescence microscope using Fitc (green), Tritc (red) and DAPI (blue) fluorescent channels.

2.2.22 Evaluation of CCR7, HIF-1α and Ki-67 in mouse xenografts of head and neck cell lines

The paraffin-embedded head and neck cell lines OSC-19, FaDu, Detroit, A-253 mouse xenografts were sectioned using a Leica RM 2135 microtome (5 µm thick) on APES coated slides and allowed to dry on hot plate at 37°C for at least 2 h. Sequential sections were stained for CCR7, HIF-1α and Ki-67 as described earlier

in section 2.2.10.2 The incubation time for the primary antibodies CCR7 (1:1000 dilution) HIF-1α (1:100 dilution) and Ki-67 (1:100 dilution) was overnight at 4°C.

2.2.23 Evaluation of CCR7 and HIF-1α in head and neck clinical samples

2.2.23.1 *Microarray slides staining*

The microarray slides were processed according to the manufacturer instructions (Biomax). Initially, slides were de-paraffinized by immersing them into xylene for (10 min, x 2), 100% ethanol (5 min), 95% (5 min), 70% (5 min) and then distilled water (5 min). Next, slides were washed with PBS (5 min, x 2), treated with 3% H_2O_2 in distilled water for 5 min and washed again in PBS (5 min). Antigen retrieval was completed in the microwave to boil the sections in 10 mM citrate buffer (pH 6.0) for 15 min at low power, allowed to cool down for 30 min and washed in PBS for 10 min. After antigen retrieval, IHC staining was followed as in section 2.2.10 for CCR7 (1:1000 dilution) for 1 h at R.T and HIF-1α (1:100 dilution) for overnight at 4°C.

2.2.23.2 *Evaluation of CCR7 and HIF-1α staining in microarrays*

For the evaluation of the staining level of CCR7 and HIF-1α, H-score was used in this study. Briefly, tumour cells were only scored according to pre agreed staining level intensity (Figure 19) by two head and neck pathologist; Professor Keith D Hunter and Dr Lisette Martin, and the H-score was subsequently generated by adding the percentage of strongly stained cell (3×), the percentage of moderately stained cell (2×), and the percentage of weakly stained cell (1×), giving a possible range of 0–300. The score was independently obtained by the two pathologists and

the correlation between the two pathologists' scores was above 0.9. The mean of the two values was obtained.

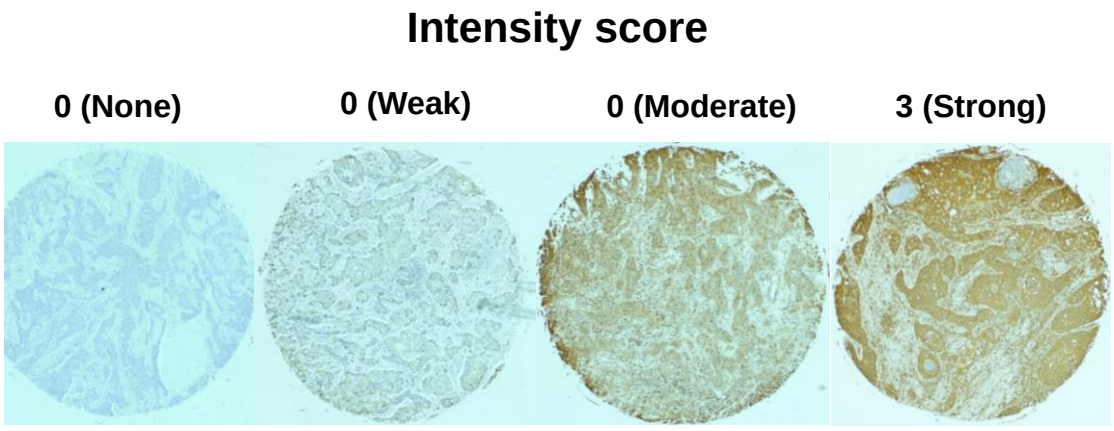

Figure 19: Microarrays scoring intensity. Photos were taken by light microscope at 4x objective lens.

2.2.24 Statistical analysis

The significance of the results was assessed through a comparison of means using two-tailed student t-test in excel. Results were expressed as the mean ± standard deviation. P values were calculated to determine statistical significance of the results. ***P < 0.05 and **P < 0.01 were deemed significant.**

Statistical analyses for clinical samples between H-scores of CCR7 and HIF-1α for each clinical stage (1, 2, 3 and 4) and lymph node metastasis were performed using Pearson correlation test and the significance of the results is represented by P value. Statistical differences between the H-score for CCR7 or HIF-1α expression between tumour cells and normal cells were evaluated using Mann-Whitney U test. Association between high expression and clinical characteristics

was evaluated using Fisher exact test. High expression levels were assigned for H-score ≥ 150. ***P < 0.05 and **P < 0.01 were deemed significant.** Clinical statistical tests were performed using Python 2.7 SciPy 0.19.The analysis was done by the bioinformatician Mr. Edvinas Pakanavicius from UCL University.

2.3 Results

2.3.1 Expression of CCR7 on cancer cell lines and xenografts

2.3.1.1 *CCR7 expression and its localization using qualitative immunofluorescence staining method.*

The subcellular location of the CCR7 protein was assessed by immunofluorescence microscopy in 15 different cell lines. Since the cells were permeablised after fixation, it is expected that antibodies will cross cell membrane and can detect not only membrane bound CCR7, but also cytoplasmic CCR7.

CCR7 was detected by immunofluorescence microscopy in all cell lines except in two of the colon cancer cell lines; HT-29 and SW-480, and very little in another colon cell line COLO-205 (Figure 20-a). The localization of CCR7 was confined to the cytoplasm and the cell membrane in all of the cell lines. Of note, the membrane bound expression was more significant in OSC-19, SCC-4, FaDu, Detroit 562, A-253 and PANC-1. To ensure specificity of binding of secondary antibody to primary antibody, negative control (-ve) was achieved by adding secondary antibody to slides that had no anti CCR7 antibody (Figure 20-b).

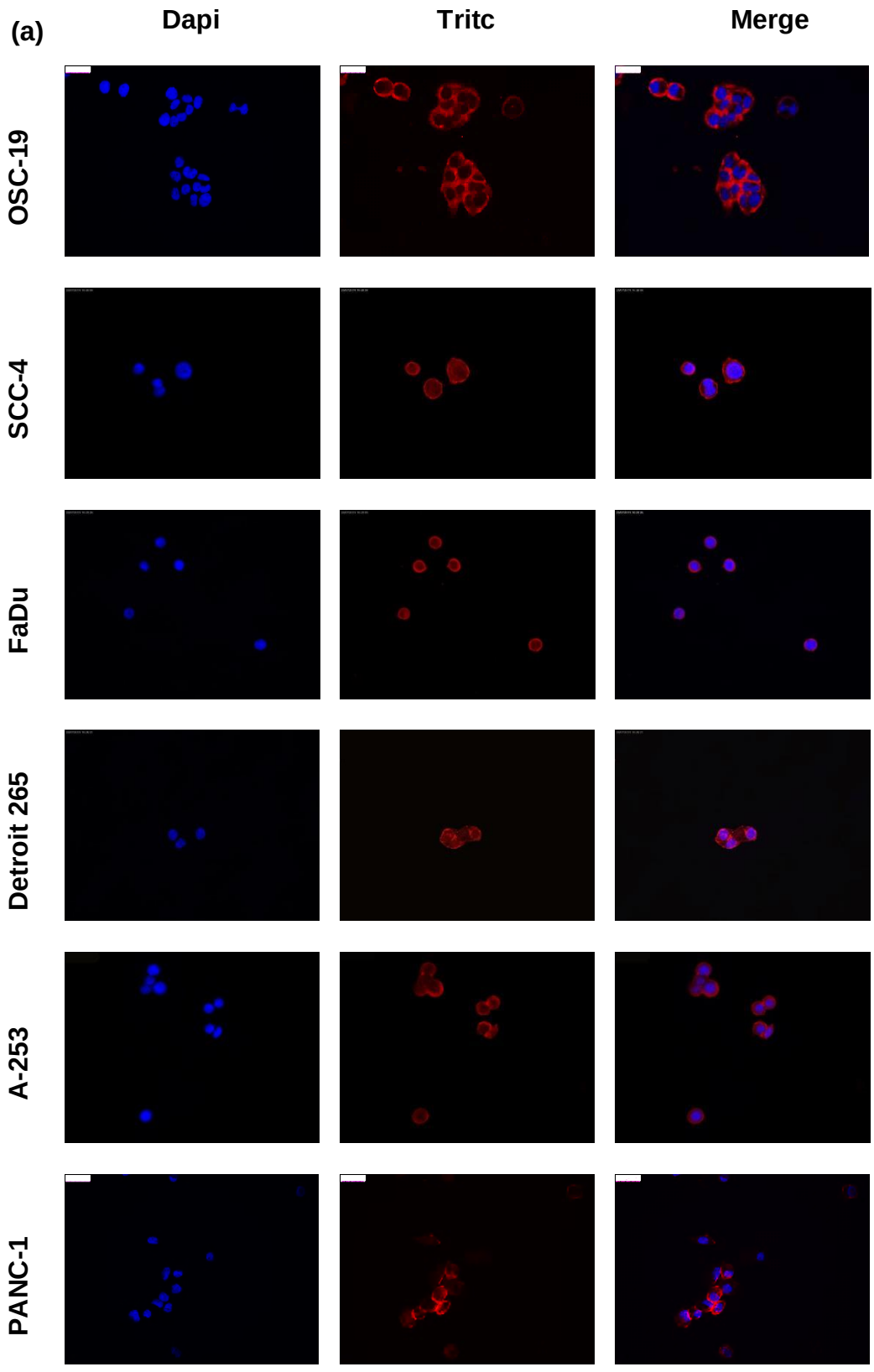
(a)
Dapi
Tritc
Merge
OSC-19
SCC-4
FaDu
Detroit 265
A-253
PANC-1

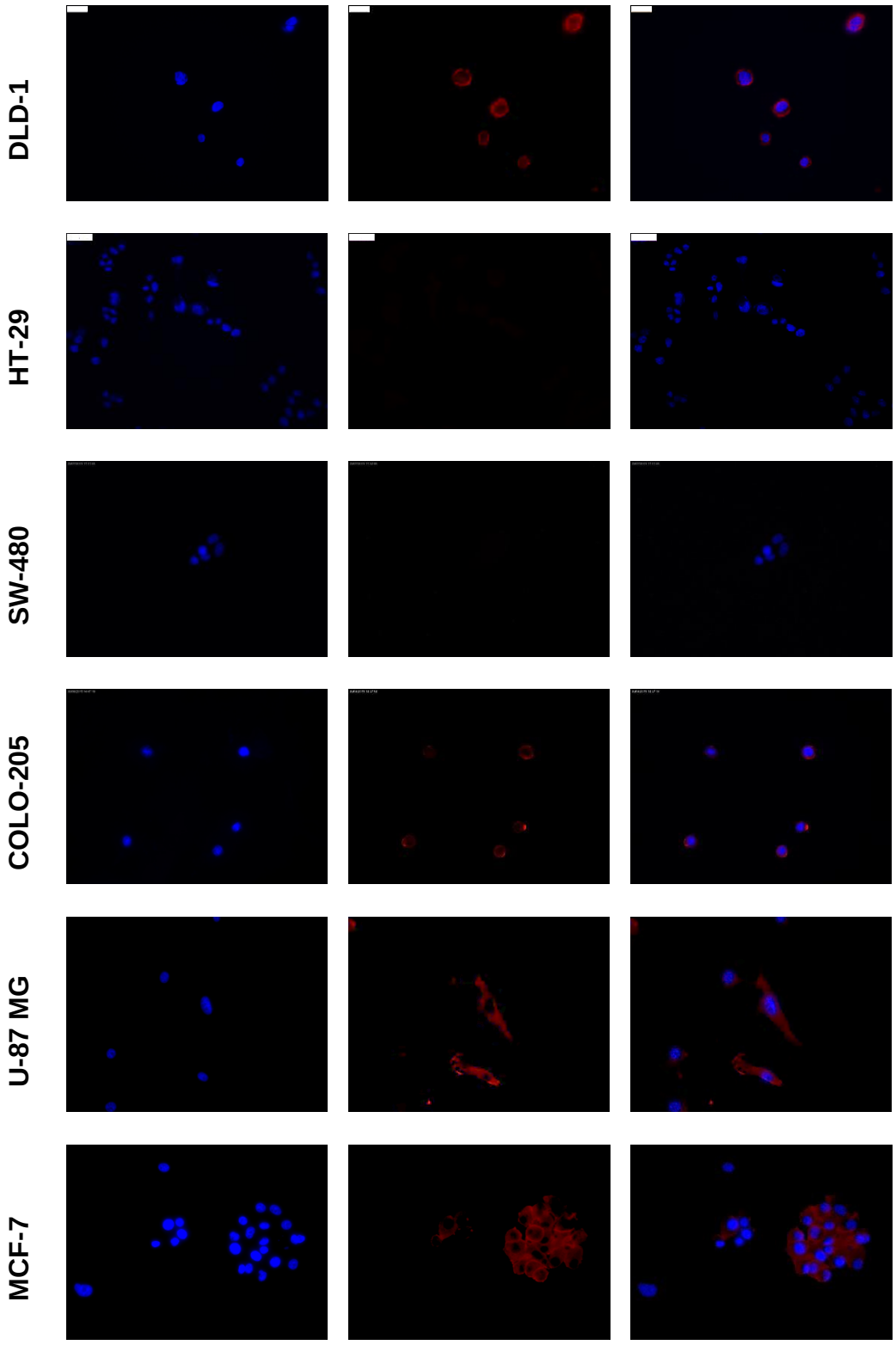
DLD-1
HT-29
SW-480
COLO-205
U-87 MG
MCF-7

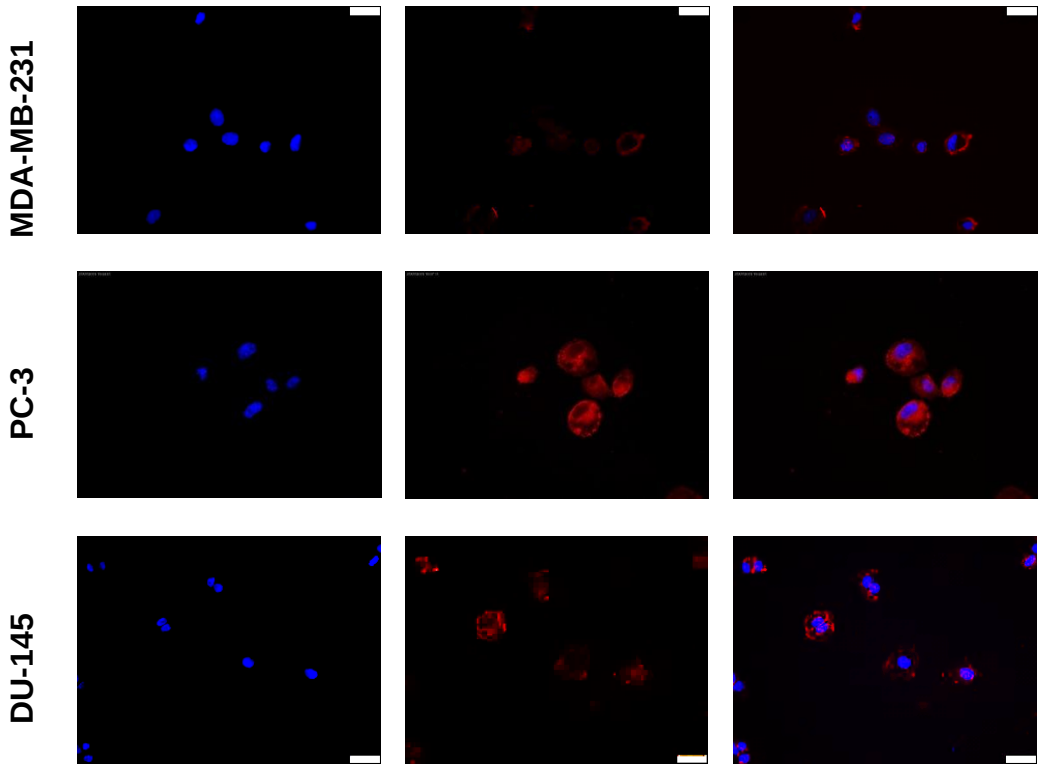
MDA-MB-231
PC-3
DU-145

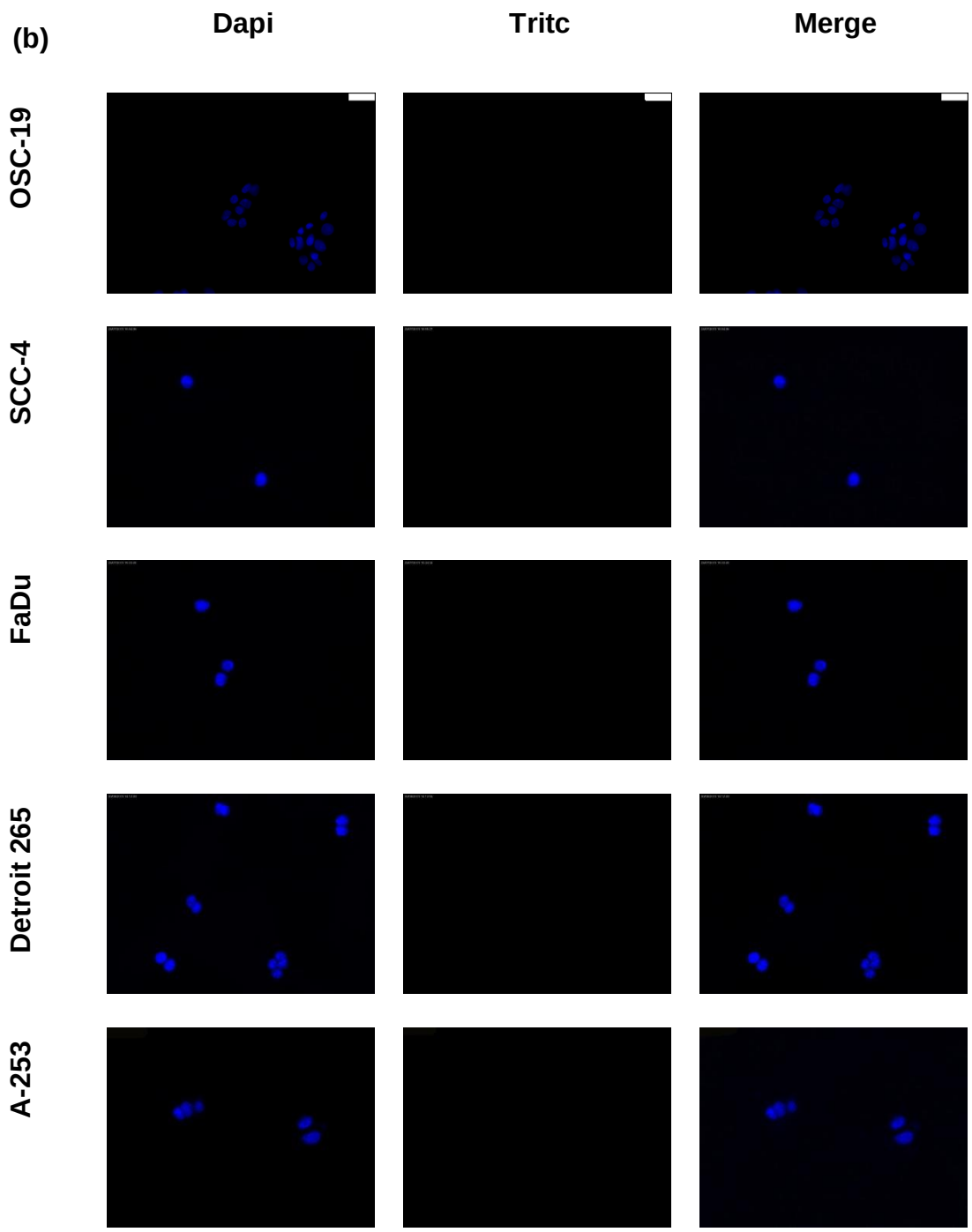
(b)
Dapi
Tritc
Merge
OSC-19
SCC-4
FaDu
Detroit 265
A-253

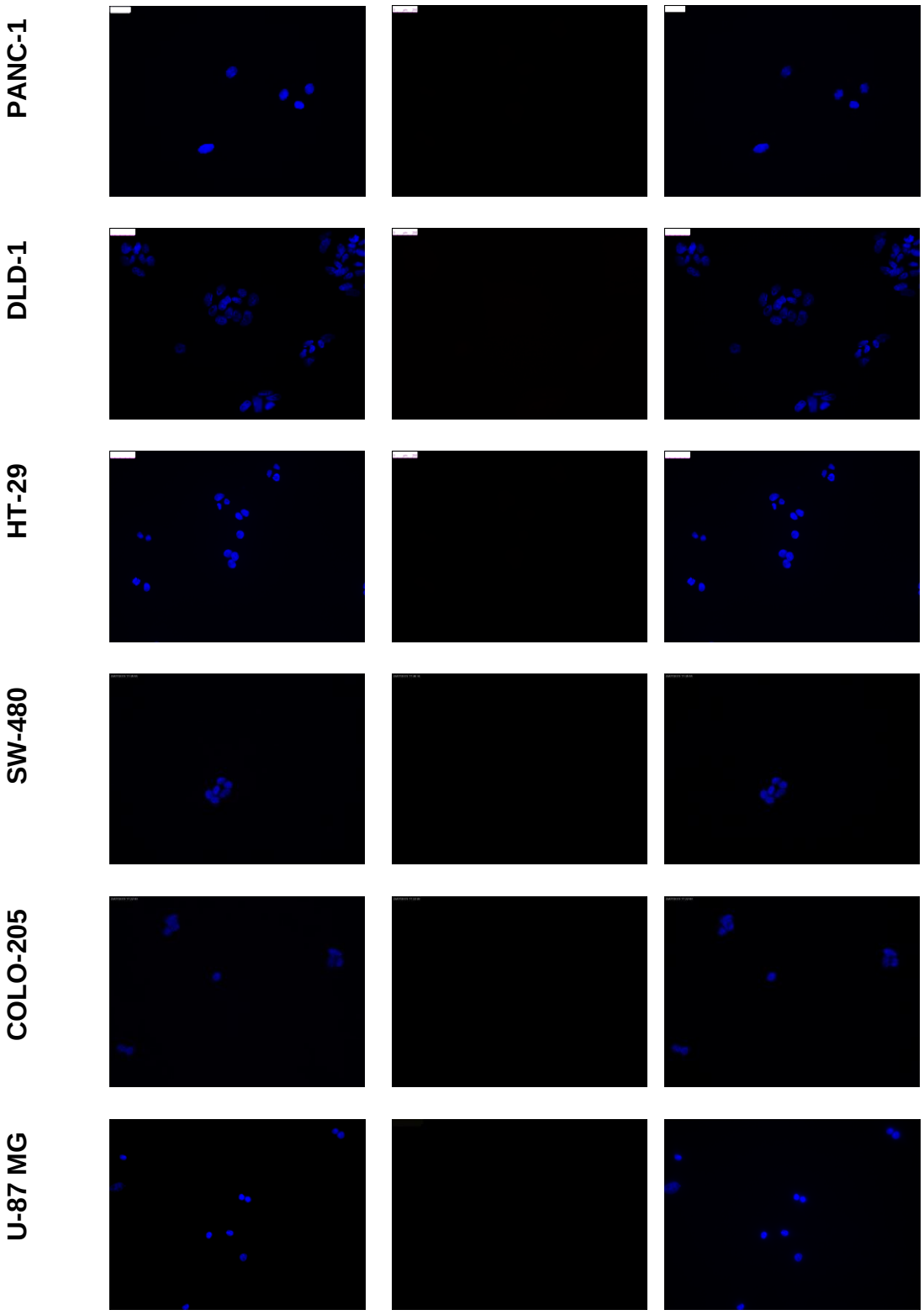
PANC-1
DLD-1
HT-29
SW-480
COLO-205
U-87 MG

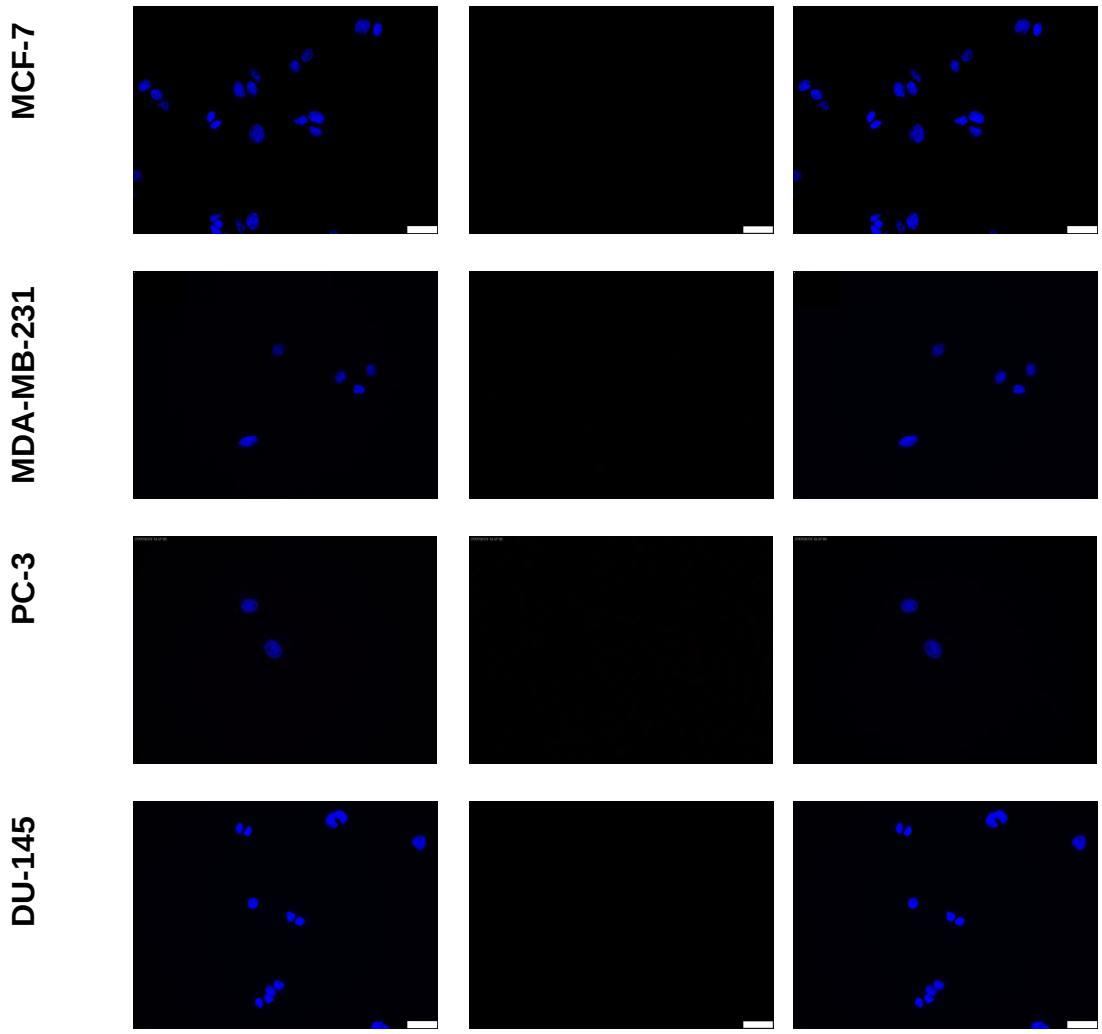

Figure 20: Subcellular location of CCR7 in cell lines.

(a) Immunofluorescence demonstrates the expression and localization of CCR7. CCR7 was expressed in all cell lines apart from HT-29 and SW-480 at different locations ranging from membrane bound, cytoplasmic or both, without nucleus staining. (b) Immunofluorescence of -ve control demonstrates no CCR7 staining, confirming that staining is selective and due to binding of the secondary antibody to primary anti CCR7. Scale bar = 25 μm.

2.3.1.2 *Quantitative analysis of CCR7 and CXCR4 expression on cancer cell lines*

Flow cytometry was used to detect the membrane bound expression of CCR7 in a panel of cell lines as well as the membrane bound expression of CXCR4 in order to compare the spread of its expression with CCR7 expression in cancer cell lines (Figure 21). Since the cells were not permeabilised after fixation, it is expected that antibodies will not cross cell membrane and can only detect membrane bound CCR7. We chose 9 cell lines from the 13 cell lines that were used to evaluate CXCR4 expression for this comparison.

The protein expression level of CCR7 (Figure 21, a, c) was evaluated in, FaDu, OSC-19, SCC-4, PANC-1, U-87 MG, MCF-7, MDA-MB-231, DLD-1, HT-29, SW480, COLO-205, PC-3 and DU-145 cell lines. CCR7 protein was found in all cell lines apart from COLO-205, SW-480 which broadly agrees with IF results. The expression level of CCR7 was highest, with more than 3 fold increase compared to isotype control, in SCC-4, FaDu, OSC-19, PANC-1 and PC-3 cell lines, followed by U87-MG, MCF-7, MDA-MB-231, DLD-1, DU-145 and HT-29 (Figure 21, a, c).

CXCR4 was expressed in most cell lines (Figure 21, b, d) but its expression level was lower than CCR7, except for FaDu and PC-3. The highest expression was in PC-3 (20 fold increase) followed by FaDu, OSC-19, MCF-7, MDA-MB-231 and DLD-1) cells. In these experiments, HT-29 cell lines showed no expression of CXCR4 (Figure 21, b, d).

(a)

FL1-H = CCR7 staining

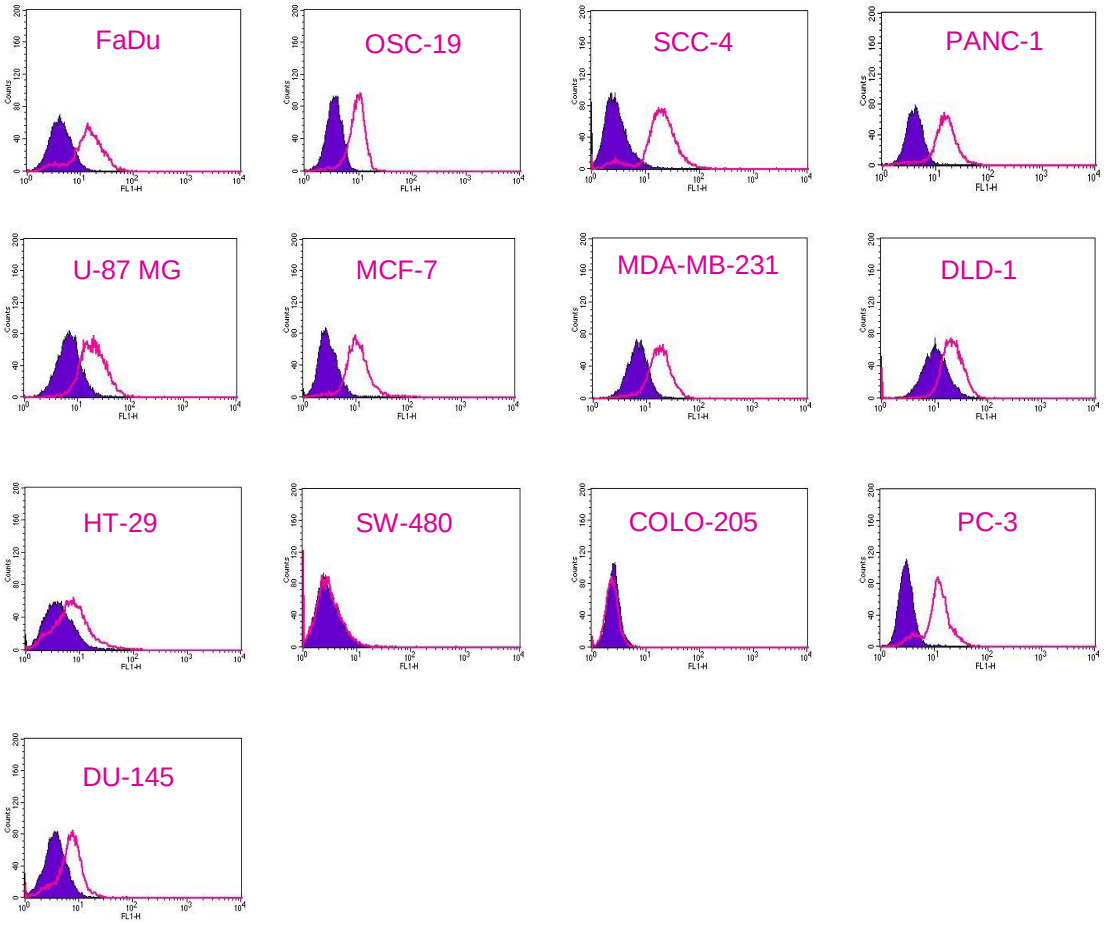

(b) **FL1-H = CXCR4 staining**

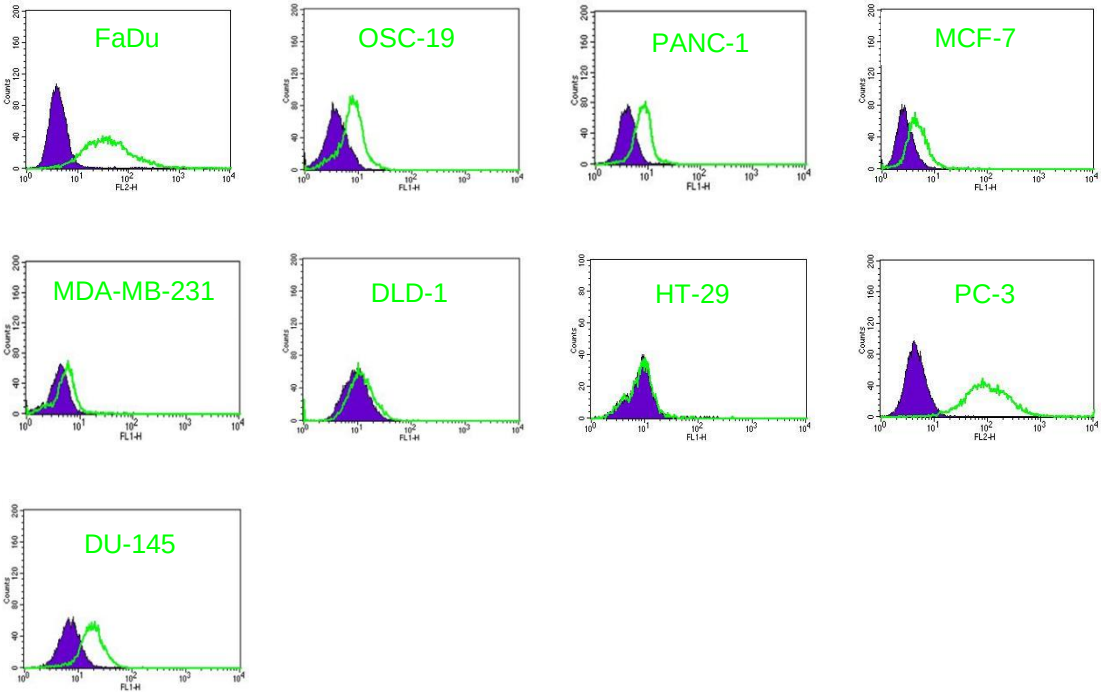

(c)

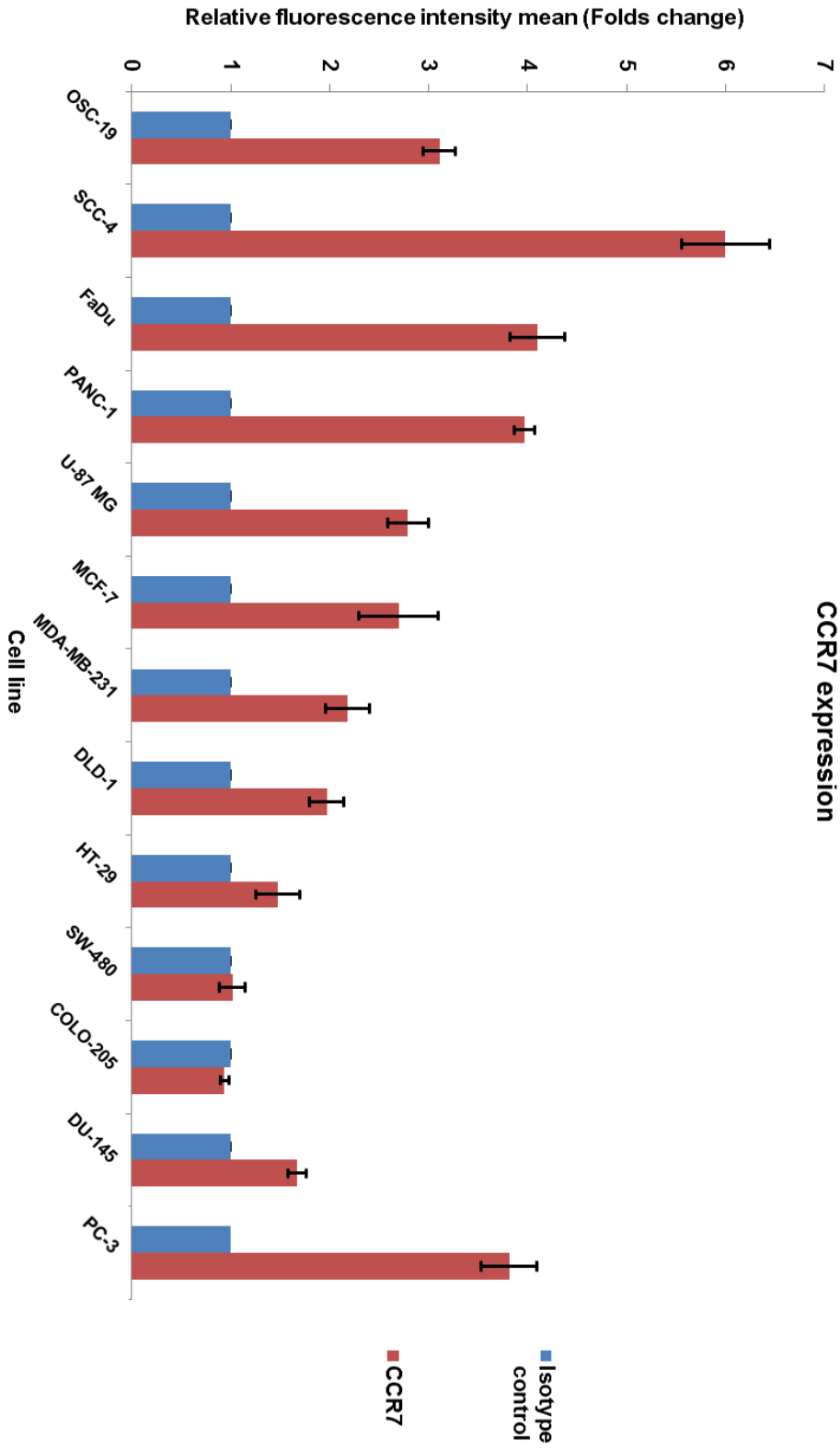
Relative fluorescence intensity mean (Folds change)
0
1
2
3
4
5
6
7
OSC-19
SCC-4
FaDu
PANC-1
U-87 MG
MCF-7
MDA-MB-231
DLD-1
HT-29
SW-480
COLO-205
DU-145
PC-3
Cell line
CCR7 expression
CCR7
Isotype control

(d)

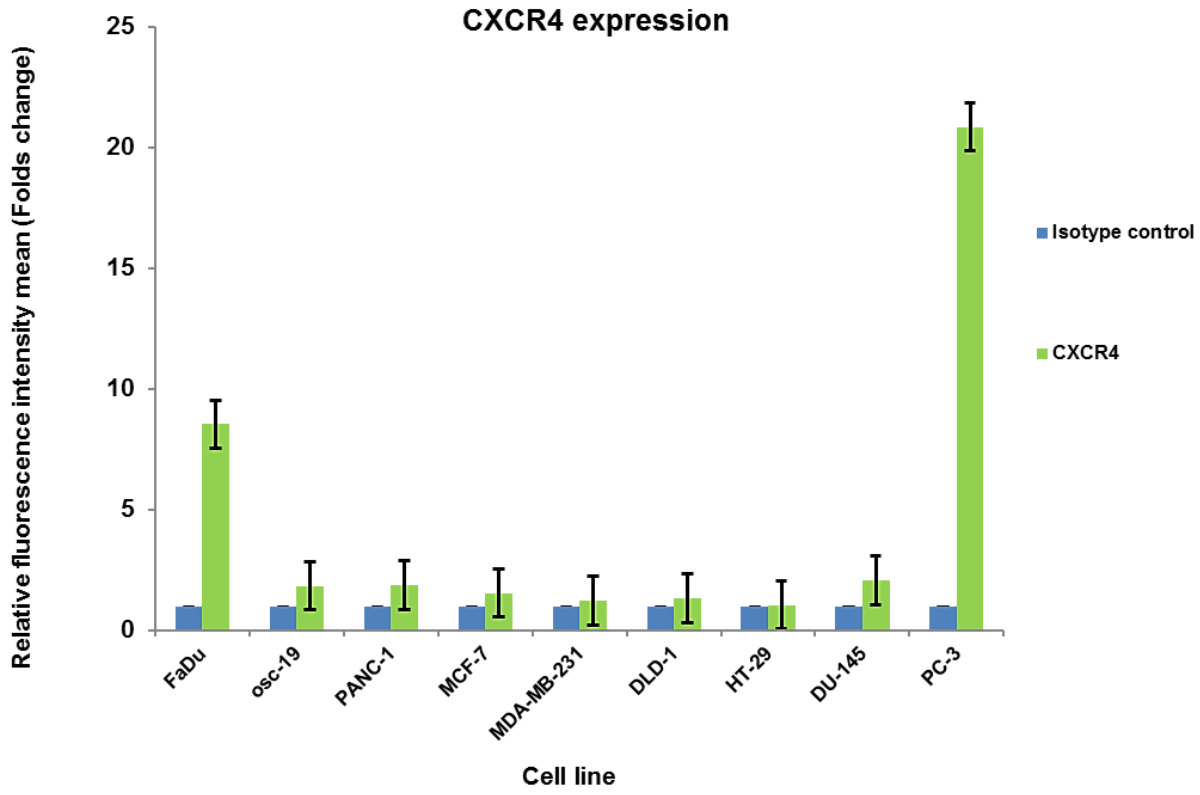

Figure 21: CCR7 and CXCR4 membrane bound protein expression.

(a) CCR7 is expressed in most of the cell lines tested (pink unfilled curves). The more shifted the unfilled curve (CCR7 stained) from the filled curve (isotype control in purple) the higher the expression. (b) CXCR4 is expressed in 8 cell lines (in green). Only HT-29 did not express CXCR4. (c-d) Analysis of flow cytometry data using mean fluorescence intensity. CCR7 or CXCR4 immunofluorescence intensity mean was normalized to its isotype control. Values are the mean of 3 independent experiments and error bars represent standard deviation (SD).

2.3.1.3 *Expression of CCR7 using western blot*

After the membrane bound evaluation of CCR7 using flow cytometry, we investigated the expression of CCR7 using the semi quantitative western blot technique as described in section 2.2.9. β-Actin was used as a loading control. The

western blot technique does not differentiate between protein expressions at different locations because all the proteins present in the cell lysate are extracted. The western blot was used to confirm the results of the flow cytometry and to see if there is any difference between the expression of membrane bound CCR7 and the whole cell expression of CCR7. Our western blot results (Figure 22) confirmed the flow cytometry results. The expression of CCR7 was highest in SCC-4. Cell lines OSC-19, FaDu, PC-3, PANC-1, U-87 MG, MCF-7 followed by MDA-MB-231 and DU-145. The expression of CCR7 in colon cell lines was highest in DLD-1, followed by HT-29, SW-480 and COLO-205. The expression of CCR7 of SW-480 and COLO-205 was the lowest in all of the cell lines but was different from the flow cytometry results that showed no membrane bound expression of CCR7.This agrees with previous literature date on different membrane bound expression to whole cell expression of CCR7 in colon cell lines (Na et al., 2008).

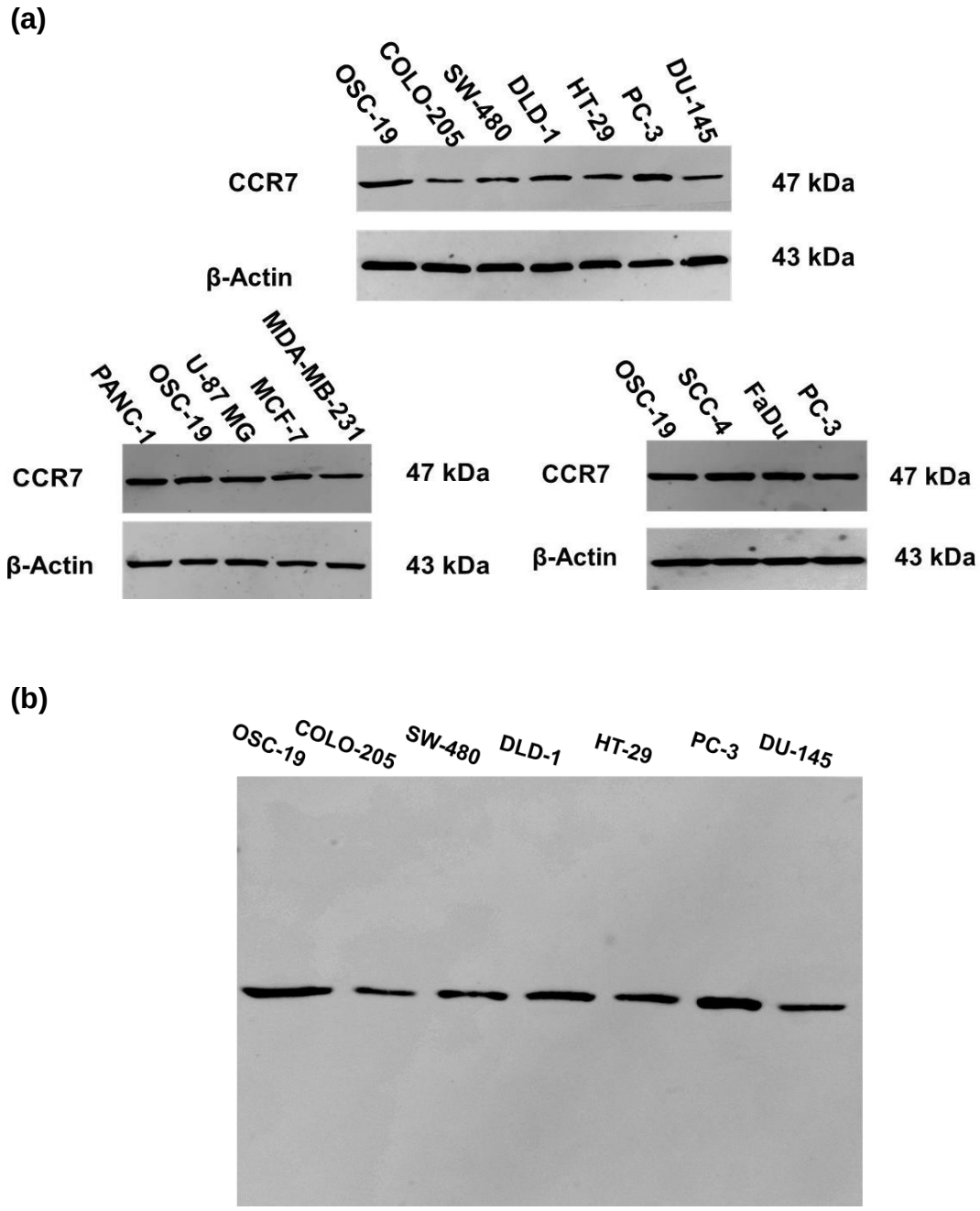

Figure 22: Expression of CCR7 using western blot.

(a)The expression of CCR7 was evaluated using the western blot technique and β-Actin was used as a loading control. All cell lines expressed CCR7 at different levels and the colon cell lines SW-480 and COLO-205 had the lowest expression.(b) An example of a whole western blot membrane showing only one specific CCR7 band at 47 kDa.

2.3.1.4 *Expression of CCR7 in xenografts*

Tumours encounter different conditions to cells cultured *in vitro* such as nutrient deprivation, hypoxia, confined space and cell-cell and/or cell-matrix interactions that are not present *in vitro*. Hence, cells grown *in vivo* are exposed to conditions which are more similar to real life tumours than those grown as a monolayer. Expression of individual proteins in cell lines growing as monolayer cultured cells may not necessarily be the same as those grown as a 3D spheroid or xenograft. So we next set out to study the effect of 3D spheroids (described later in section 2.3.14) and xenotransplantation on CCR7 expression which also facilitates the choice of suitable 3D spheroid model and *in vivo* model for future testing of CCR7 antagonist compounds. Paraffin embedded xenografts were stained using IHC as described in section 2.2.10. Hematoxylin-eosin stained sections are shown in (appendix V). Staining for the CCR7 protein was identified in the cytoplasm and cell membrane of OSC-19, Detroit 562, U-87 MG, DLD-1, PANC-1, HT-29, DU-145 and PC-3 (Figure 23). However, MCF-7, MDA-MB-231 and A-253 cell lines showed only cell membrane staining whilst FaDu cell line showed mainly cytoplasmic expression with very little membrane bound expression and colon cell line COLO-205 showed only a little staining in the cytoplasm (Figure 23). The membrane bound expression of CCR7 was the highest in the head and neck cell lines (OSC-19, Detroit 562 and A-253) along with the pancreatic PANC-1 and prostate PC-3. The intensity of the expression (intensity of the brown colour and the spread of the staining) was the highest in OSC-19, FaDu, Detroit 562, PANC-1 and PC-3. These results were in agreement with the flow cytometry, western blot

and IF results described earlier in section 2.3.1.2. On the other hand, COLO-205 had the lowest cytoplasmic expression amongst the xenografts models investigated and no membrane bound expression confirming the results from flow cytometry. All the -ve controls, in which no primary anti CCR7 antibody was added, showed no positive brown colour staining (Figure 23, right sided photos). Evaluation of difference of CCR7 expression between xenografts and cell lines is present under section 2.4 (Discussion).

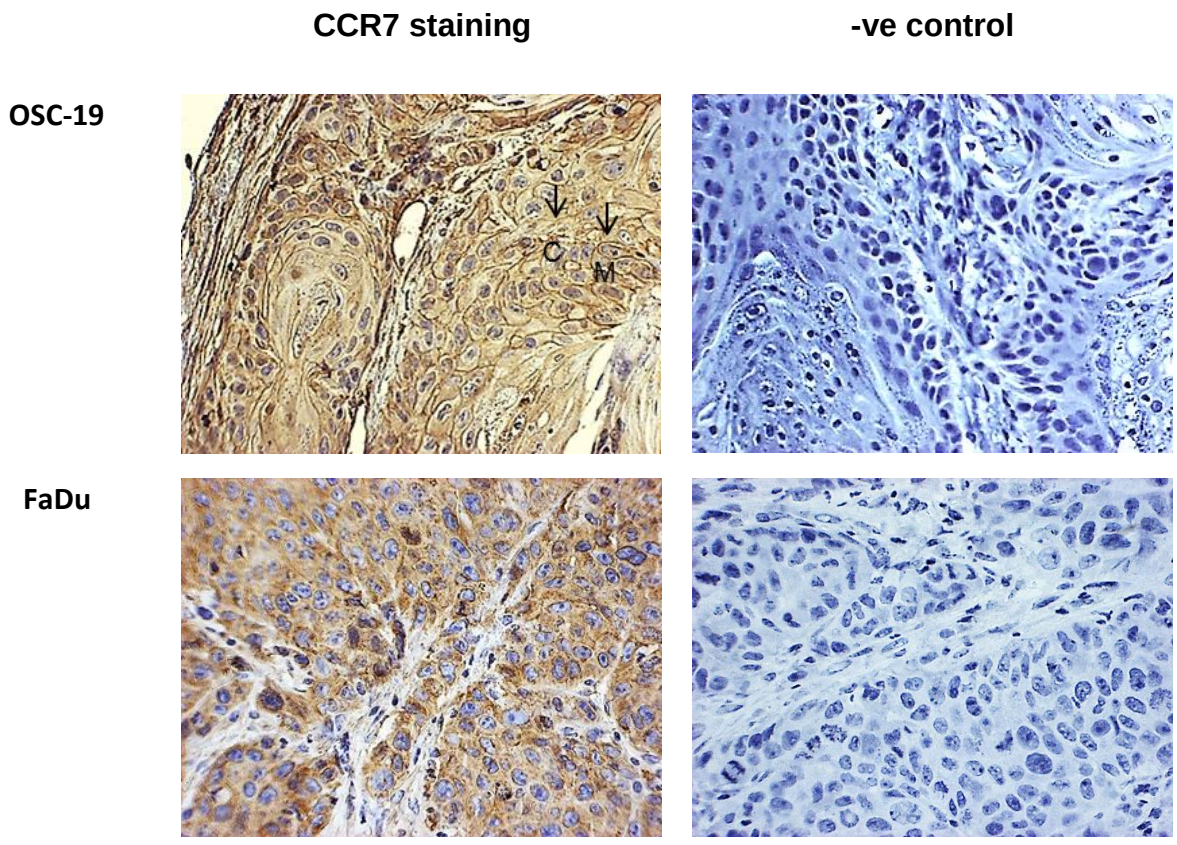

A-253

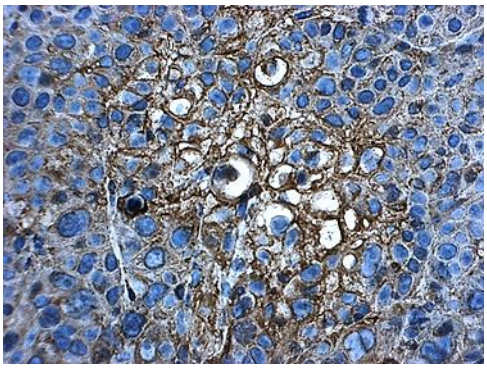

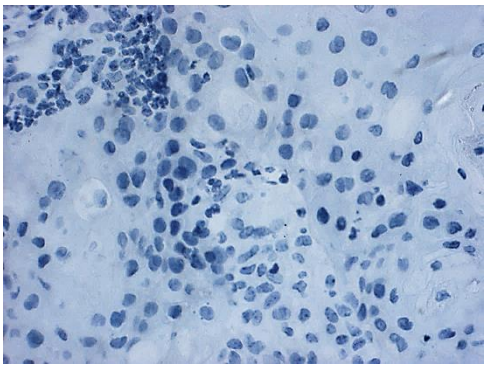

Detroit 256

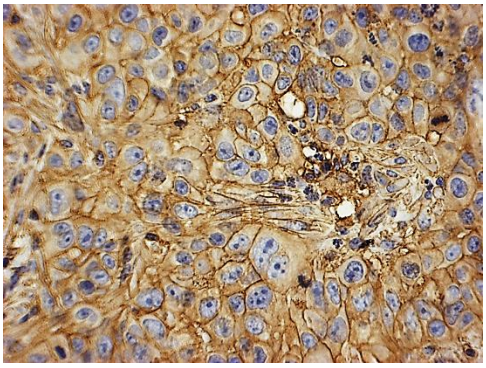

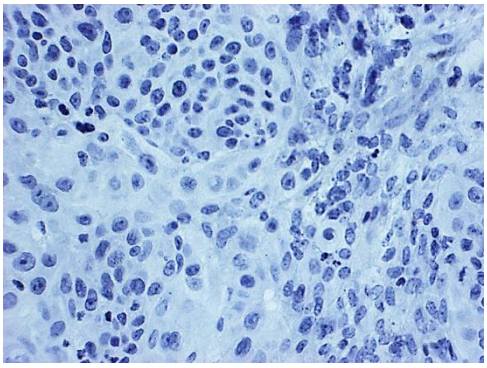

PANC-1

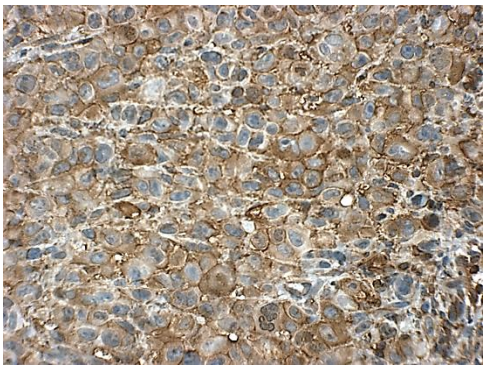

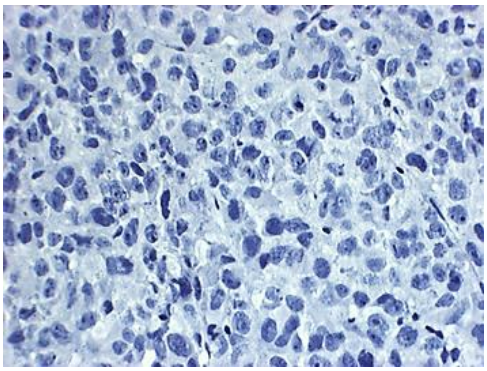

DLD-1

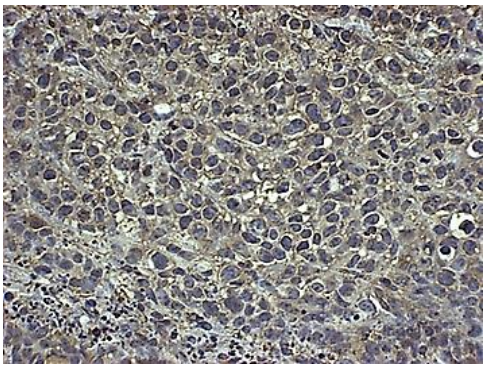

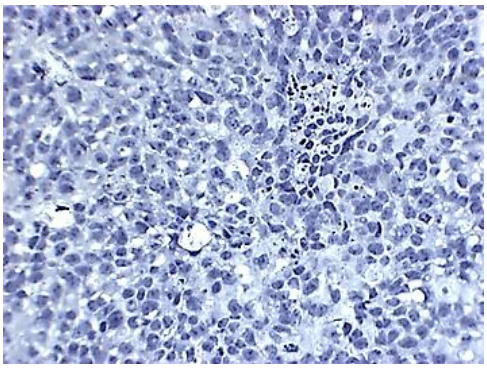

HT-29

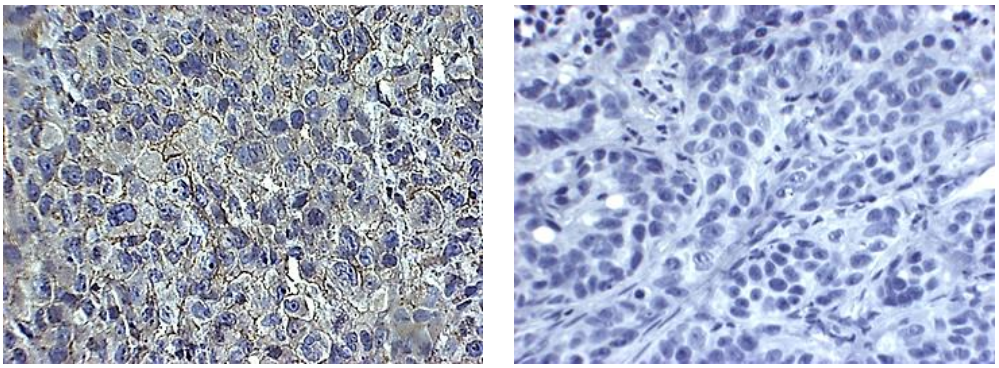

COLO-205

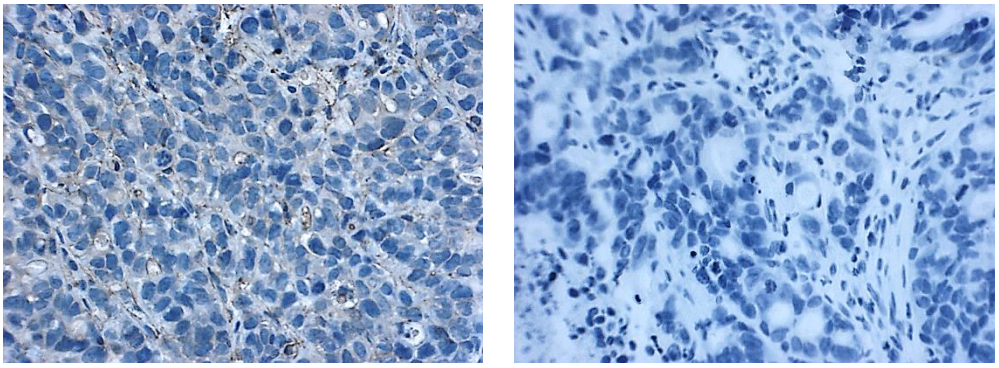

U-87 MG

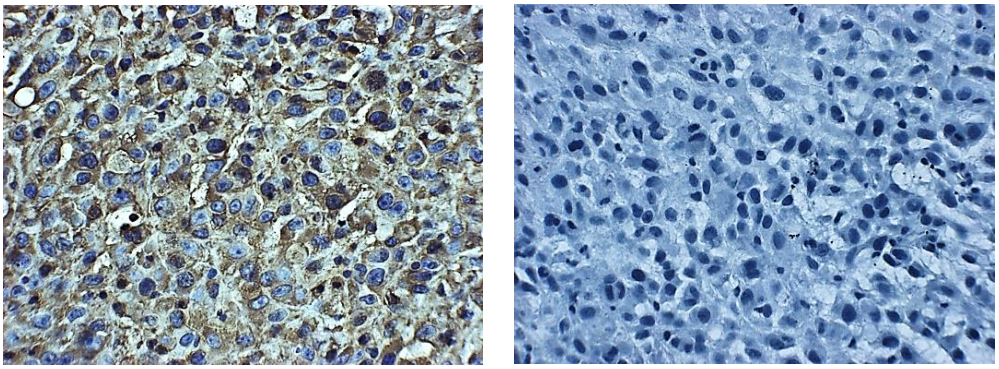

MCF-7

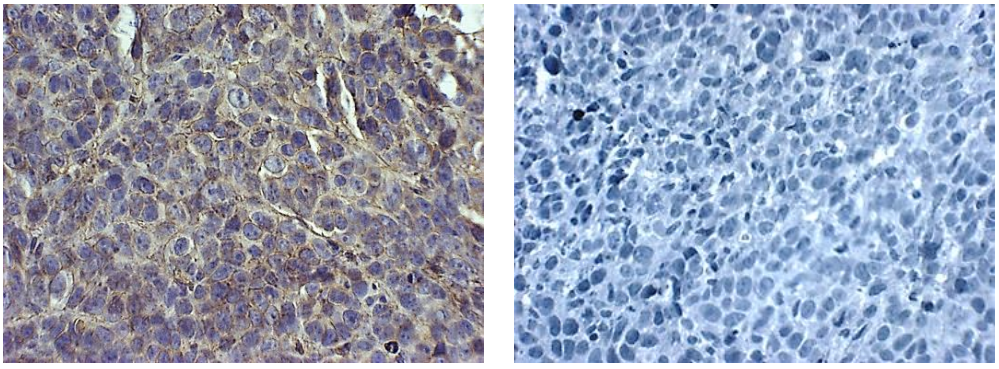

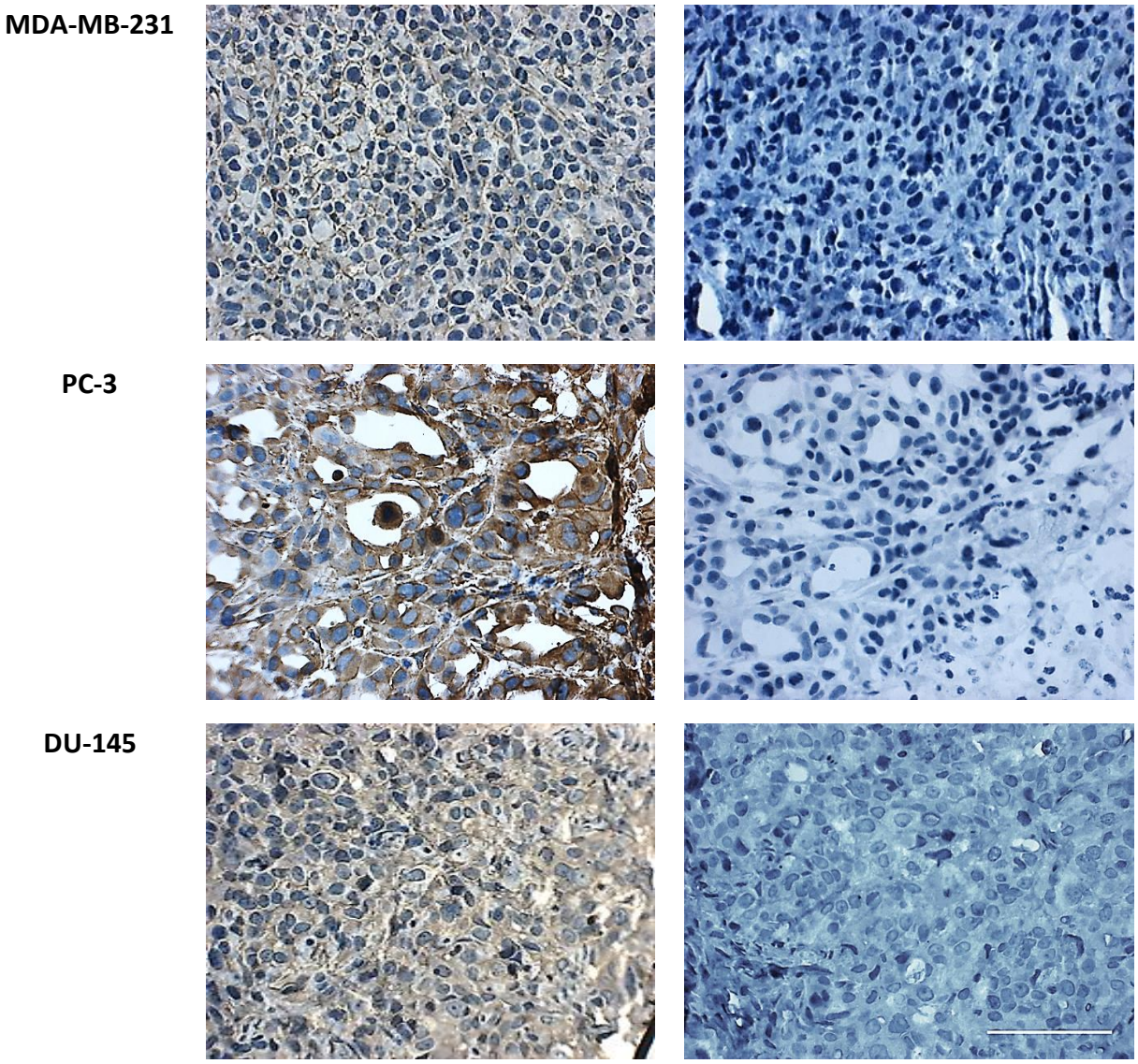

Figure 23: Immunohistochemical staining of CCR7 in tumour xenogafts.

The xenografts (OSC-19, FaDu, Detroit 562, A-253, PANC-1, U-87 MG, MCF-7, MDA-MB-231, DLD-1, HT-29, COLO-205, PC-3 and DU-145) were evaluated for CCR7 expression. Brown colour indicates positive staining of CCR7 expression. Membrane bound staining (M) and cytoplasmic staining (C).The scale bar = 100 µm at 40x objective lens.

2.3.2 Effect of CCL19/CCL21 on cell migration

Following on from the demonstration of CCR7 expression in culture and xenografted cancer cell lines, we explored the functional activity of the receptor in various pharmacological assays. First, we performed the scratch assay in order to determine whether CCL21 and CCL19 have a functional role in cell migration and to select a model for testing the CCR7 small molecule antagonists that are synthesized in house (Chapter 4). For this purpose, we measured the free surface area 14-42 h after generation of a wound/scratch in the absence of chemokine (used as control) to that in the presence of 100 nM of CCL21 or CCL19. We selected 6 cell lines with different levels of CCR7 expression; SCC-4, OSC-19, PC-3, FaDu, DLD-1, and SW-480 which does not express any membrane bound CCR7 according to our flow cytometry results as a -ve control. We chose the 100 nM dose because it lies within the physiological concentration for these ligands (10 nM - 2 μM) (Shannon et al., 2010). After scratching the monolayer, the cells were left to migrate for the optimal time determined by the fastest migratory cells, i.e. the CCL21 containing wells. Hence, SCC-4, OSC-19, FaDu, DLD-1, SW-480 and PC-3 were left to migrate for 24, 18, 24, 42, 21, and 14 h, respectively.

The before and after migration results of all the examined cell lines are represented below (Figure 24-a). CCL21 (100 nM) increased cell migration by 58%, 33%, 29% and 18% respectively for SCC-4, OSC-19, PC-3 and FaDu compared with control (no ligand added) (Figure 24-b). However, CCL21 did not affect the cell migration of DLD-1 or SW-480 cells; (Figure 24-b). The increase in cell motility correlates

with the membrane bound expression result of CCR7 in section 2.3.1.2 in these cell lines.

Interestingly, addition of the same concentration of CCL19 (100 nM) had no effect in cell migration in any of the cell lines used compared with the control (no CCL19 added) (Figure 24-b). This differential response of cell migration towards CCL21 and CCL19 at similar concentrations was observed earlier in DC (Haessler et al., 2011).

From these experiments, we concluded that the highest migratory cell lines, after the addition of CCL21 were SCC-4 and OSC-19. We selected OSC-19 cell line as our model for further investigation of migratory aptitude because we could not have grown SCC-4 as a xenograft and hence further progression with this cell line for *in vivo* work would not be useful. In addition, as shown below in section 2.2.21.1, we could grow OSC-19 as compact spheroids to study CCR7 invasion in 3D, whereas SCC-4 cells on the other hand, form loose spheroids.

Please note that in chapter 4 we report the effects of in house CCR7 antagonists on the CCL21 and CCL19 induced migration/invasion of OSC-19 spheroids.

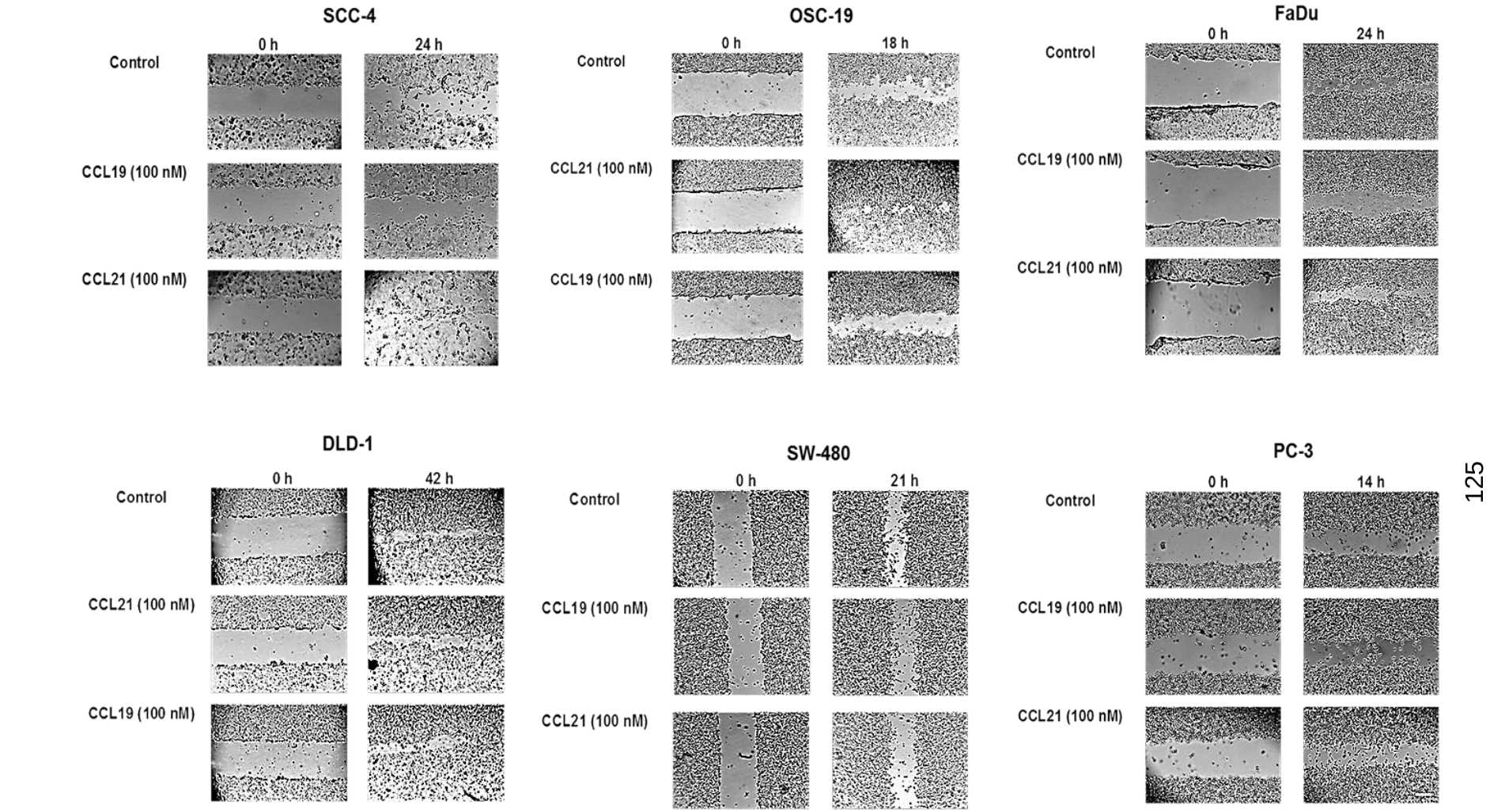
SCC-4
0 h
24 h
Control
CCL19 (100 nM)
CCL21 (100 nM)
OSC-19
0 h
18 h
Control
CCL21 (100 nM)
CCL19 (100 nM)
FaDu
0 h
24 h
Control
CCL19 (100 nM)
CCL21 (100 nM)
DLD-1
0 h
42 h
Control
CCL21 (100 nM)
CCL19 (100 nM)
SW-480
0 h
21 h
Control
CCL19 (100 nM)
CCL21 (100 nM)
PC-3
0 h
14 h
Control
CCL19 (100 nM)
CCL21 (100 nM)

(a)

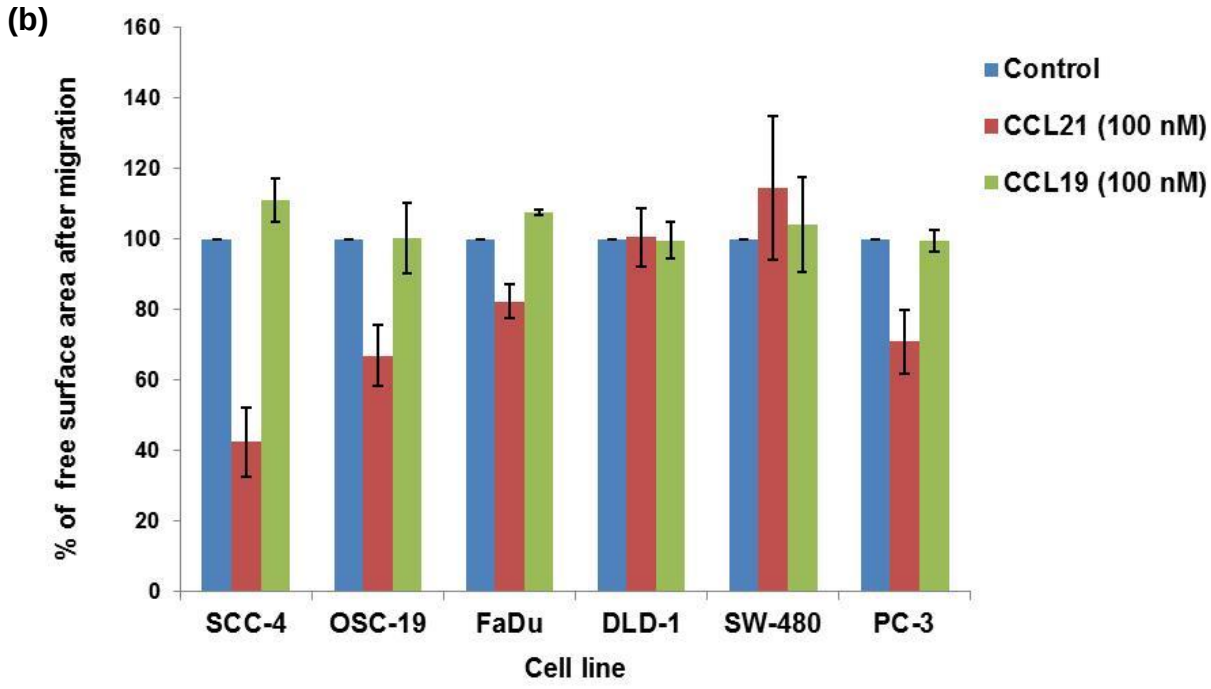

Figure 24: Effect of CCL21 and CCL19 in wound healing assay.

(a) Scratches were made on confluent monolayers of SCC-4, OSC-19, FaDu, DLD-1, SW-480 and PC-3 cells. Cells were treated with CCL19 100 nM, CCL21 100 nM or no ligand added (control). Free surface area was measured after the migration of cells on 2 fields per well and averaged and normalized to free surface area at 0 h. (b) Data expressed as % of free surface area after migration. Error bars represent SD of 2 independent experiments. The scale bar = 100 µm at 10x objective lens using lumascope 488 microscope.

To further demonstrate that the increase in cell motility was chemokine induced, the effect of CCL21 at 100 and 10 nM and CCL19 at 100 and 10 nM on the migration of OSC-19 were also compared (Figure 25-a). As shown, CCL21 at 100 nM significantly increased the cell migration compared with control (no ligand added) after 18 h. The percentage of the free surface area fell by 33% when CCL21 100 nM was added. The results are statistically significant, with $P < 0.05$ (Figure 25-b). However, we found no great difference between 100 nM and 10 nM of CCL21 in the percentage of the free surface area. The acceleration in gap

closure determined by the free surface area between the CCL21 10 nM and the control (no CCL21 added) was also statistically significant with P = 0.016. Unfortunately, due to limited time available, we were not able to further reduce the concentration of CCL21 to establish a dose response curve. On the other hand, CCL19 had no effect in cell migration compared with control at the concentrations used.

(a)

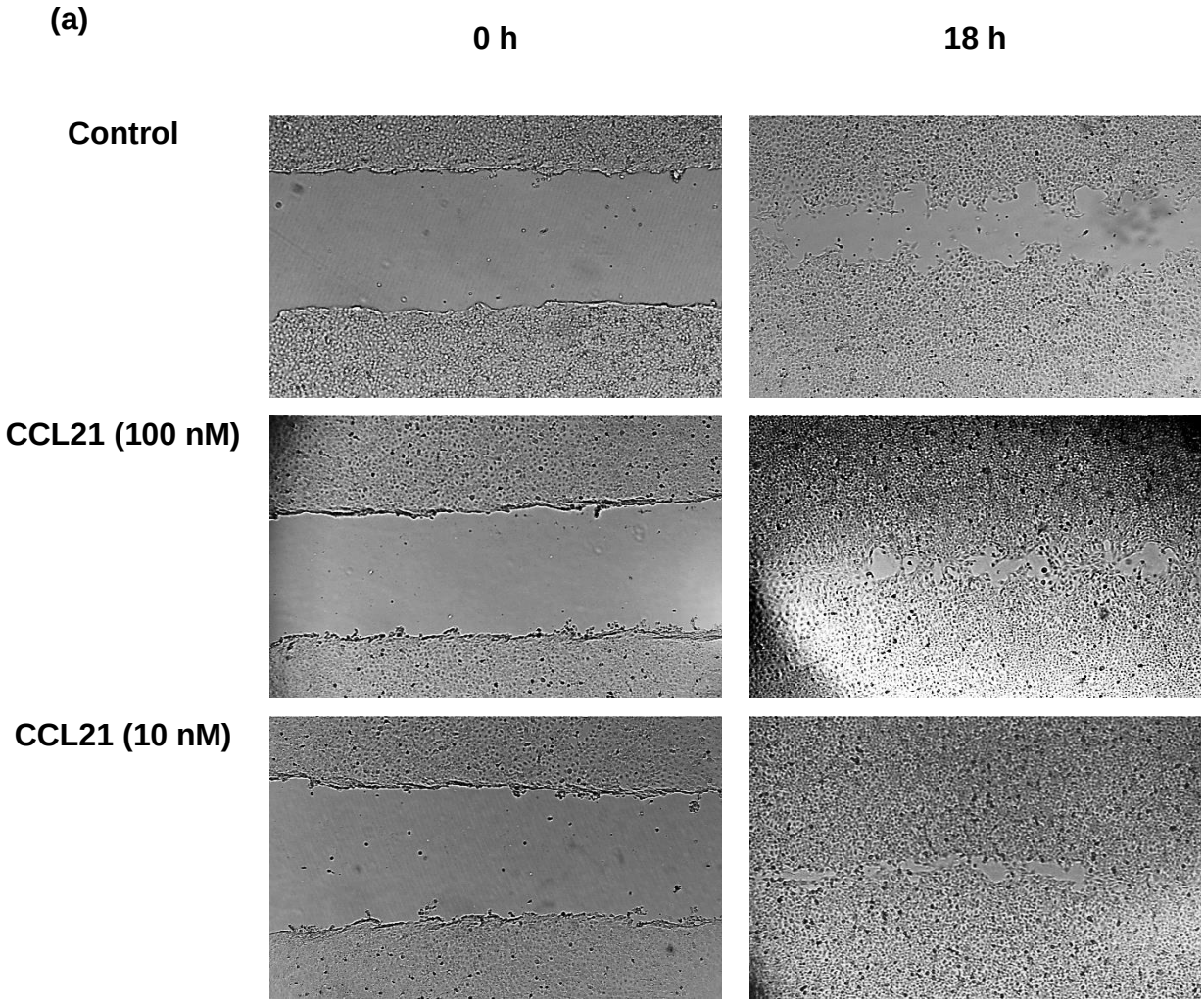

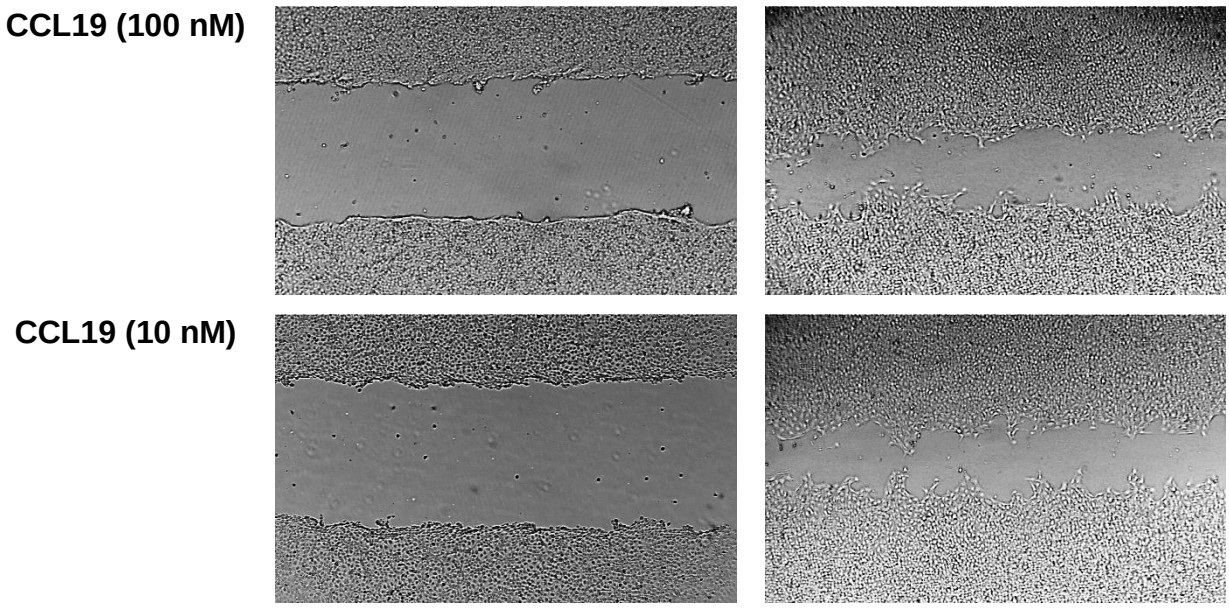

(b)

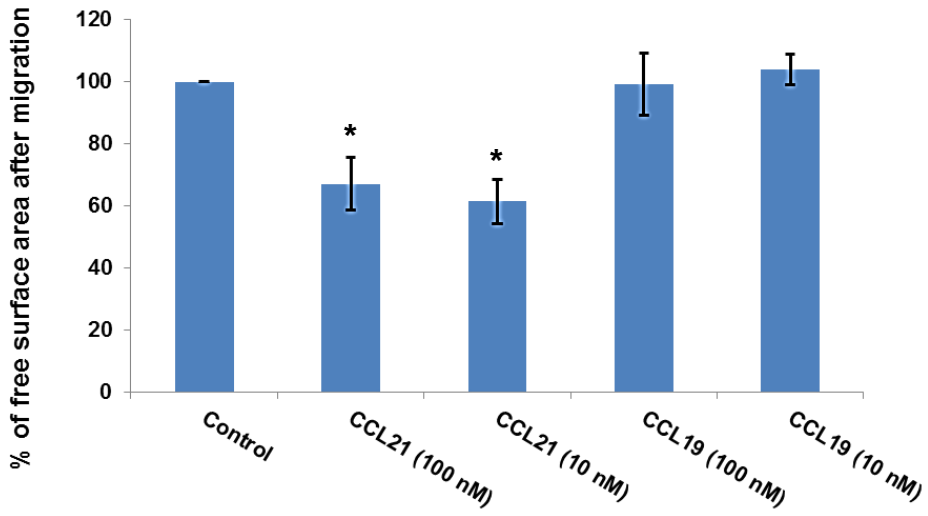

Figure 25:CCL21 increased wound healing.

Scratches were made on confluent monolayers of OSC-19 cells. Cells were treated with CCL21 at 100 nM and 10 nM, CCL19 at 100 nM and 10 nM or no ligand added (control).Free surface area was measured after 18 h on 2 fields per well and averaged and normalized to free surface area at 0 hrs. (b) Data expressed as % of free surface area after migration. Error bars represent SD of 3 independent experiments. *P < 0.05 compared with control group.

In order to clarify whether the effects seen in the wound healing assay are due to migration rather than proliferation, Ki-67, a proliferation marker, was used to stain cells at the beginning and end of scratch assay experiment. OSC-19 cells grown in 2% FBS media as a confluent monolayer in the wound healing assay showed no significant proliferation, compared with positive (+ve) control OSC-19 cells that were grown at sub-confluency in 10% FBS on coverslips for 2 days before staining for Ki-67 (Figure 26). Sub-confluent cells which are grown in 10% FBS will stain +ve for Ki-67. Furthermore, we stained for CCR7 after cell migration to confirm that the migratory cells are still expressing CCR7 after the 18 h of migration as shown in Figure 27.

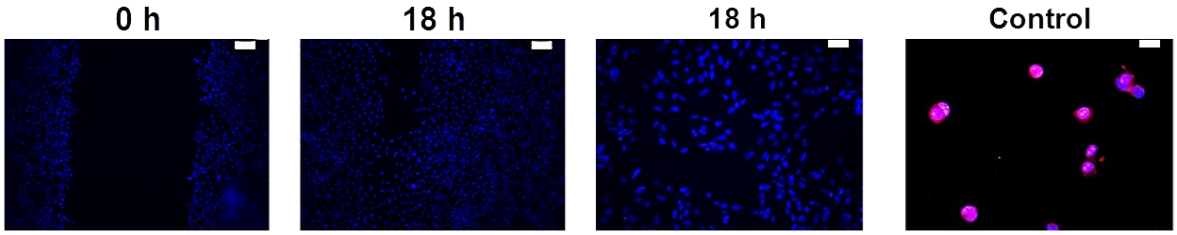

Figure 26: Movement of OSC-19 cells in the wound healing assay is due to migration rather than proliferation. OSC-19 cells at 0h and 18h showed no Ki-67 staining compared with +ve control. The scale bar = 100, 50, 25 µm at 10x, 20x, 40x objective lens respectively.

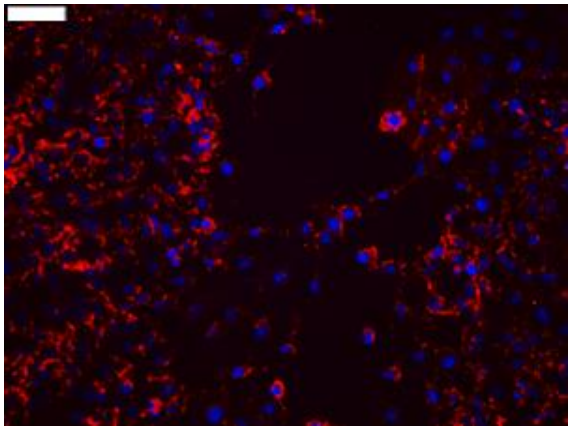

Figure 27: Expression of CCR7 in wound healing assay after 18 h of migration.

The expression of CCR7 (red) is shown in migratory cells in which nucleus is counterstained with DAPI. The scale bar = 50 µm at 20x objective lens.

2.3.3 Neither CCL21 nor CCL19 increase the proliferation of OSC-19 cells.

In order to evaluate the proliferation effect of CCL21 on OSC-19 and FaDu cell lines, we initially performed a growth curve of both cell lines using different cell concentrations to determine the conditions in which cells were in the log phase when we studied the effect of CCL21. This information was also useful later in chapter 4, when we added small molecules CCR7 antagonist compounds. The absorbance (which correlates to cell numbers) was measured and plotted against the day of reading (see Figure 28). Most cells have common characteristics of growth, which is an initial lag time when they adapt to their environment, and then start to increase in numbers, usually after 24 h. Following the initial lag stage, cells enter the log growth phase, in which the cell numbers grow exponentially. In this phase any drugs or agents that modulate cell survival or proliferation would have the most pronounced effect. After that, cells enter the plateau phase, where little or

no growth of the cells is observed. The length of each phase depends on the starting concentration. The lower the cell concentration, the longer the initial and log growth phase and (Figure 28-a). This, we determined that based on their characteristics of cell growth, the cell density of 1 x10^4 cell/ml is appropriate for the required duration of testing ligands or compounds in OSC-19 and FaDu cell lines. Briefly, after 24 h of seeding the cells at 1 x10^4 cell/ml, CCL21 and CCL19 at (100 and 10 nM) were added and after 72 h, MTT solution was added and relative cell numbers were measured as described in section 2.2.12. The effects of CCL21 or CCL19 on OSC-19 or FaDu cells are presented by % increase of proliferation versus control where no chemokine was added (Figure 28-b). Our results indicated that addition of CCL21 resulted in a minor increase (20 %) of proliferation compared to control in OSC-19, however this effect was not observed at 100 nM with $P \geq 0.05$. Likewise, CCL21 did not cause any significant effect on the proliferation rate compared with control in FaDu cells. CCL19 also did not induce any significant increase of proliferation in either cell lines (see later for precedence).

(a)

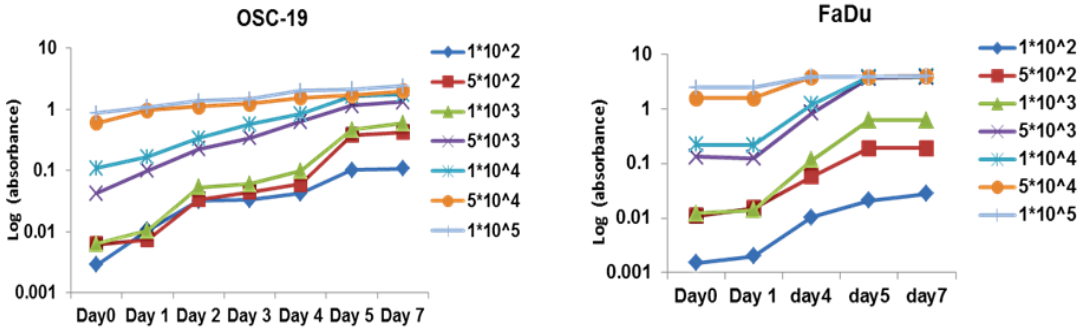

(b)

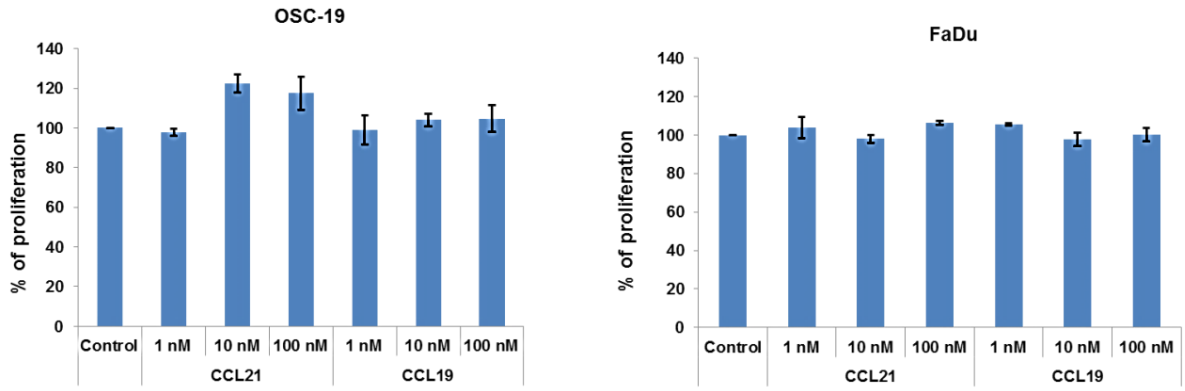

Figure 28: Effect of CCL21 and CCL19 on OSC-19 and FaDu cells.

(a) Osc-19 and FaDu growth curve. (b) Effect of CCL21 and CCL19 on cell proliferation. The assay was quantified using the MTT proliferation assay. The growth curves were a result of one time experiment (n=1) and hence no error bar. CCL21 and CCL19 at 100 nM did not induce increase of proliferation P ≥ 0.05. Error bars represent SD of 3 independent experiments. P value represent T-student test.

2.3.4 CCL21 or CCL19 induced receptor activation that was detected by an increase in cytoplasmic Ca^{2+} moblisation

Our results so far showed that only CCL21 has a functional effect in cells. Therefore, we decided to look at the effects of CCL21 and CCL19 at the receptor activation level. For this, the activation of CCR7 on OSC-19 cell line using a Ca^{2+} mobilisation assay was studied (Figure 29). Ca^{2+} release from endoplasmic reticulum is an early event in the chemokine signalling cascade that precedes cell migration. Activation of CCR7 typically results in at least a 10 fold increase in the intracellular concentration of Ca^{2+}. In a calcium mobilisation assay, cells are labelled with Fluo-4 NW (Invitrogen; a dye which fluoresces upon binding to Ca^{2+}, before adding CCL21; 100 nM in well concentration), CCL19 (100 nM in well concentration) or assay buffer as control. The fluorescence of stimulated cells is shown in (Figure 29). Both CCL21 and CCL19 caused an increase of mobilized Ca^{2+} (flux) compared with the control (assay buffer) in which no ligands were added to the cells. There was 40 and 17 times increase in the relative fluorescence change for CCL21 ($P < 0.01$) and CCL19 ($P < 0.05$), respectively compared to assay buffer.

The mobilized Ca^{2+} flux in response to CCL21 (100 nM) was 2.4 times higher than CCL19 (100 nM) ($P < 0.01$) in OSC-19 cells. These results indicate that CCR7 is functional in OSC-19 cells and responded to treatment with its ligands. However, it is interesting to note that the effect of CCL21 is more pronounced that the effect caused by CCL19 the same concentration. This mirrors the observations in DC chemotactic sensitivity for these two chemokines at this tested concentration (Haessler et al., 2011).

(a)

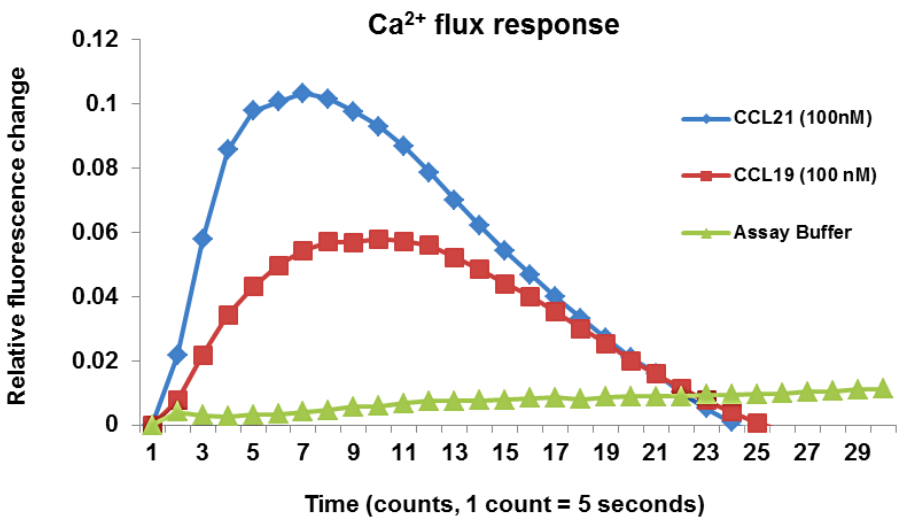

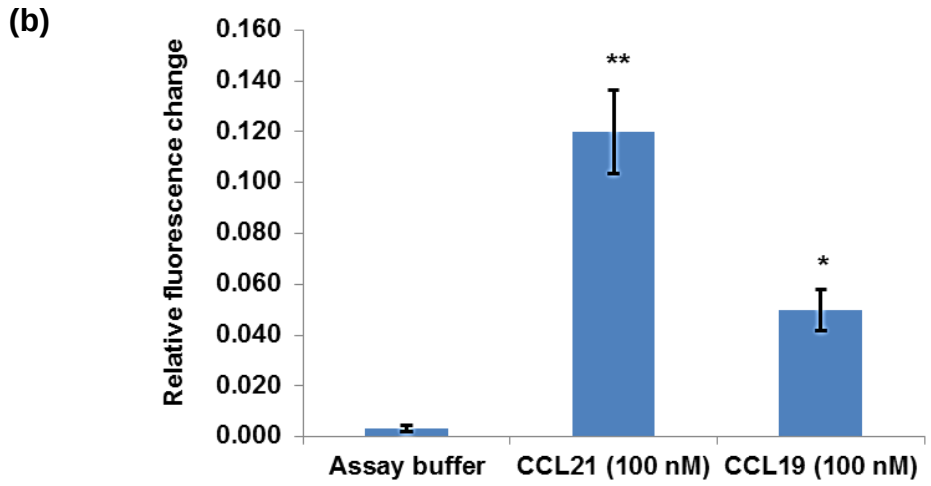

Figure 29: Elicitation of Ca^{2+} flux in OSC-19 cells.

Relative fluorescence change was calculated by normalizing each time point to the zero point of adding CCL21 or CCL19 (a) Ca^{2+} flux was measured with adding CCL21 (100 nM), CCL19 (100 nM) or assay buffer. An increase in fluorescence change was detected after adding CCL21 or CCL19 compared with adding only assay buffer. (b) Relative fluorescence change at its highest point was higher in CCL21 treated cells compared with CCL19 treated cells and both were higher than control (assay buffer). Error bars represent SD of 3 independent experiments. *P < 0.05 and **P < 0.01 compared with control (assay buffer).

2.3.5 Increase of CCR7 expression after serum deprivation

So far, we have shown that OSC-19 cells, which we had chosen as a model system, express CCR7 and functionally respond to CCL21 and to a lesser extent to CCL19. We next set out to investigate how various stress factors can influence the expression of CCR7.

First, we set out to determine the effect of serum deprivation on CCR7 expression, in order to simulate the conditions in which tumours grow *in vivo.* OSC-19 cells were cultured in either in 0% or 10% FBS for 24 h before analysing them using flow cytometry as described earlier in section 2.2.8 (Figure 30-a). Our results showed

that CCR7 expression was increased from 3.7 fold change in fluorescence intensity in relation to isotype, for serum enriched (10% FBS) OSC-19 cells, compared to 4.6 for serum deprived (0% FBS) OSC-19 cells Figure 30-b). The difference of the fold change between 0% and 10% was 0.91 with ($P < 0.05$).

(a)

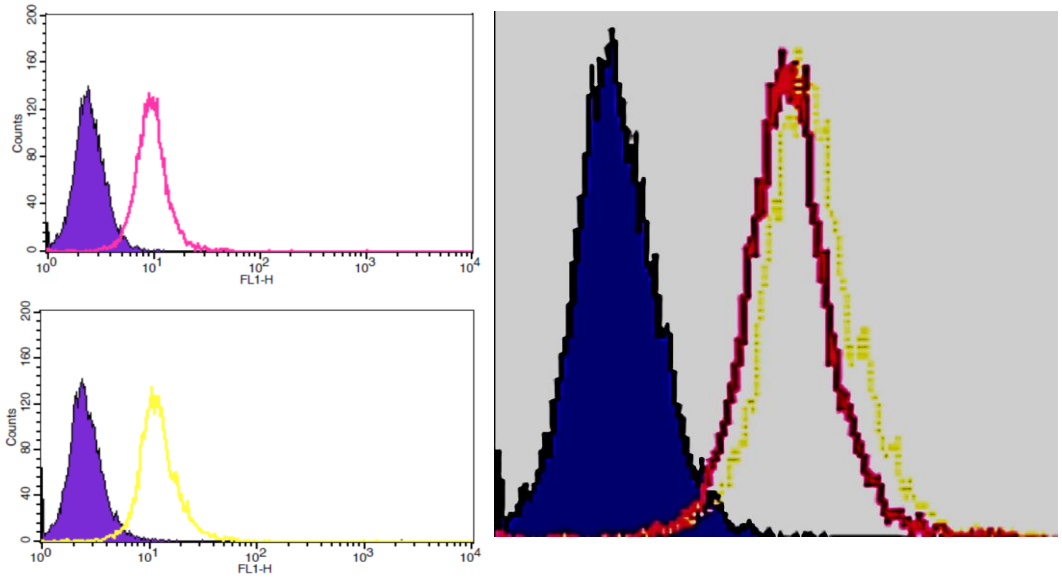

(b)

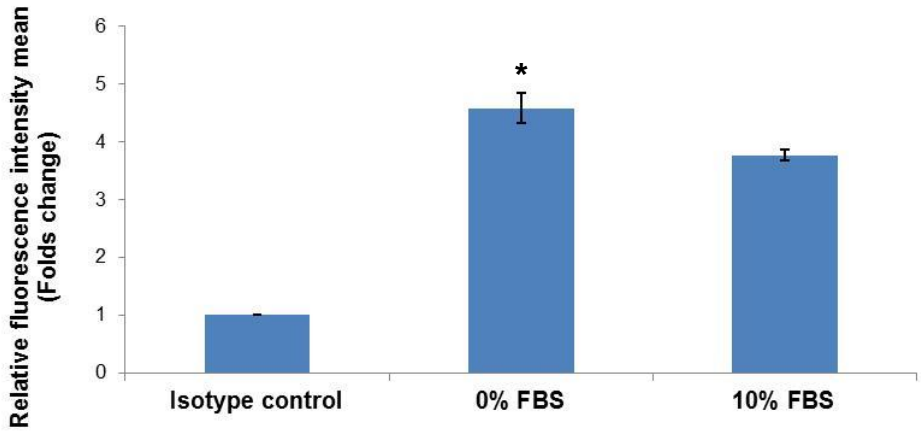

Figure 30: CCR7 expression is increased after serum deprivation.

(a) The upper graph shows the expression of CCR7 for cells cultured in 10% FBS (unfilled pink curve) over the filled curve isotype control in purple. The lower graph shows the expression of CCR7 for cells cultured in 0% FBS (unfilled yellow curve) over the filled curve isotype control. On the right side, cells cultured in 10% FBS was overlaid with 0% FBS to show the shift of CCR7 expression for cells in 0% FBS (yellow) from 10% FBS (pink). (b) Analysis of flow cytometry data using mean fluorescence intensity. CCR7 immunofluorescence intensity mean was normalized to its isotype control. Error bars represent SD of 3 independent experiments. *P < 0.05 of 0% FBS group compared with 10% FBS.

2.3.6 Production of CCL21 after mechanical stress and xenograft tissues

2.3.6.1 *CCL21 release from cells after induced stress by scratch assay*

In order to broaden our understanding of the role of CCR7 in stress conditions, we evaluated the production of CCL21 after stressing the OSC-19 cells; initially we scratched the cells and left them to heal in 2% FBS for 18 h and 24 h. The supernatant was collected after the scratches at 18 and 24 h and control (no scratches). We assayed the supernatant to determine whether CCL21 was produced by using a CCL21 Elisa detection kit as described in section 2.2.16. Our data showed that CCL21 concentration was 64.9 and 82.3 pg/ml after 18 and 24 h respectively (Figure 31). The fold change of CCL21 concertation was 1.59 and 1.64 for 18 and 24 h respectively compared with the control (no scratches) with ($P < 0.05$) and ($P < 0.01$) respectively for 18 and 24 h.

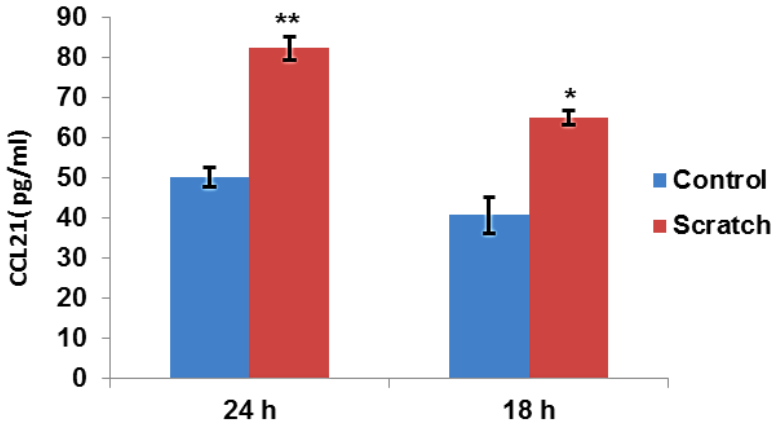

Figure 31: CCL21 was detected after cell wounding.

OSC-19 was wounded and supernatant was collected after cell migration or healing at 18 and 24 h for wounded cells and unwounded cells (control). CCL21 was detected by Elisa at 18 and 24 h. Error bars represent SD of 3 independent experiments. *P < 0.05 and **P < 0.01 compared with control.

2.3.7 Production of CCL21 in 3D xenografts

Cells growing as 3D encounter different types of stress which they try to escape in order to survive. We have seen in section 2.3.1.4 that head and neck xenografts express CCR7 and therefore expression of CCL21 in these xenografts might indicate the presence of autocrine activation of CCR7 that might results in increase tumour growth and immunetolerant reaction as proposed by others before (Balkwill, 2012, Wang et al., 2008).

Figure 32 shows that head and neck xenografts produce CCL21 and its expression is confined to the cytoplasm and nucleus on tumour cells with little expression on stromal cells in cytoplasm OSC-19, FaDu and Detroit 562. However, in A-253 xenografts, the stromal cells show high expression of CCL21.

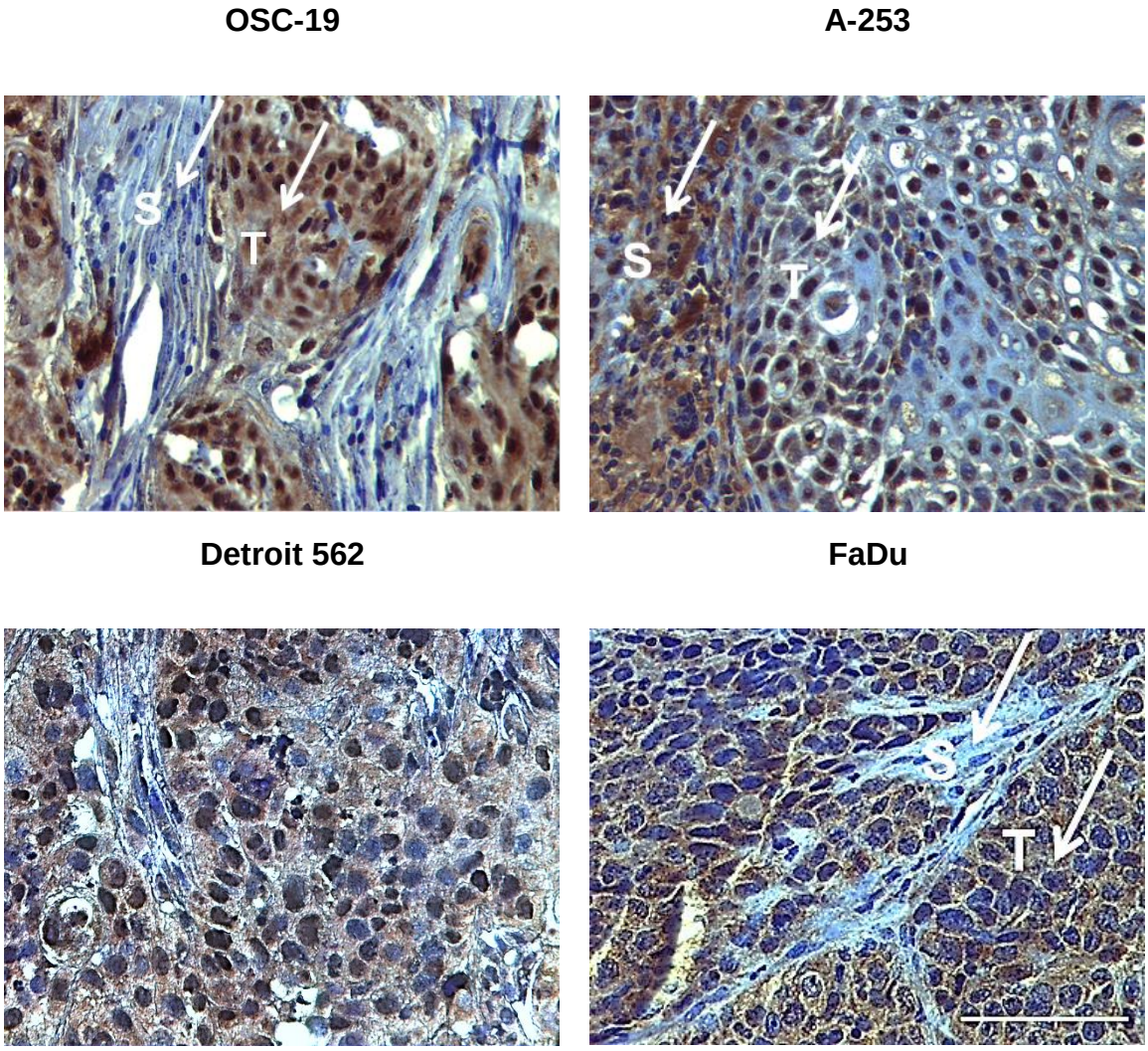

Figure 32: Expression of CCL21 in head and neck xenografts.

OSC-19, A-253, Detroit 562 and FaDu xenografts express CCL21 in tumour cells (T) and its expression is confined to the cytoplasm and nucleus. Furthermore, CCL21 is also expressed on stromal cells (S) in the cytoplasm. The scale bar = 100 µm at 40x objective lens.

2.3.8 Increase of CCR7 expression in hypoxic cultured cells compared to normoxia

As mentioned earlier in section 2.1.2, the effect of hypoxia on CCR7 expression has been studied by other groups in breast, prostate and lung cancers. We decided to look for the effect of hypoxia on CCR7 expression in head and neck cell lines by comparing CCR7 expression of cells under hypoxia compared with cells cultured in normoxia. OSC-19, FaDu, Detroit 562, A-253 and SCC-4 cells were incubated under hypoxia or normoxia as described in section 2.2.17.1 for 24 h before analyzing them by flow cytometry for evaluating CCR7 expression (For growth curve of head and neck cell lines see appendix IV). At the same time cells were also studied for HIF-1α, as it is well known that HIF-1α is upregulated under hypoxia. We intended to use HIF-1α as a positive control however we could not directly detect HIF-1α in our analyzed samples. Therefore, we looked instead for LDH-A to confirm the induction of hypoxia. LDH-A is a well-established biomarker for the induction of hypoxia indirectly indicates the presence of actively and functionally expressed HIF-1α, and others have shown that expression of LDH-A correlates with HIF-1α expression (Denko, 2008, Hu et al., 2003, Semenza, 2013, Elkashef et al., 2016).

FL1-H = CCR7 staining

(a)

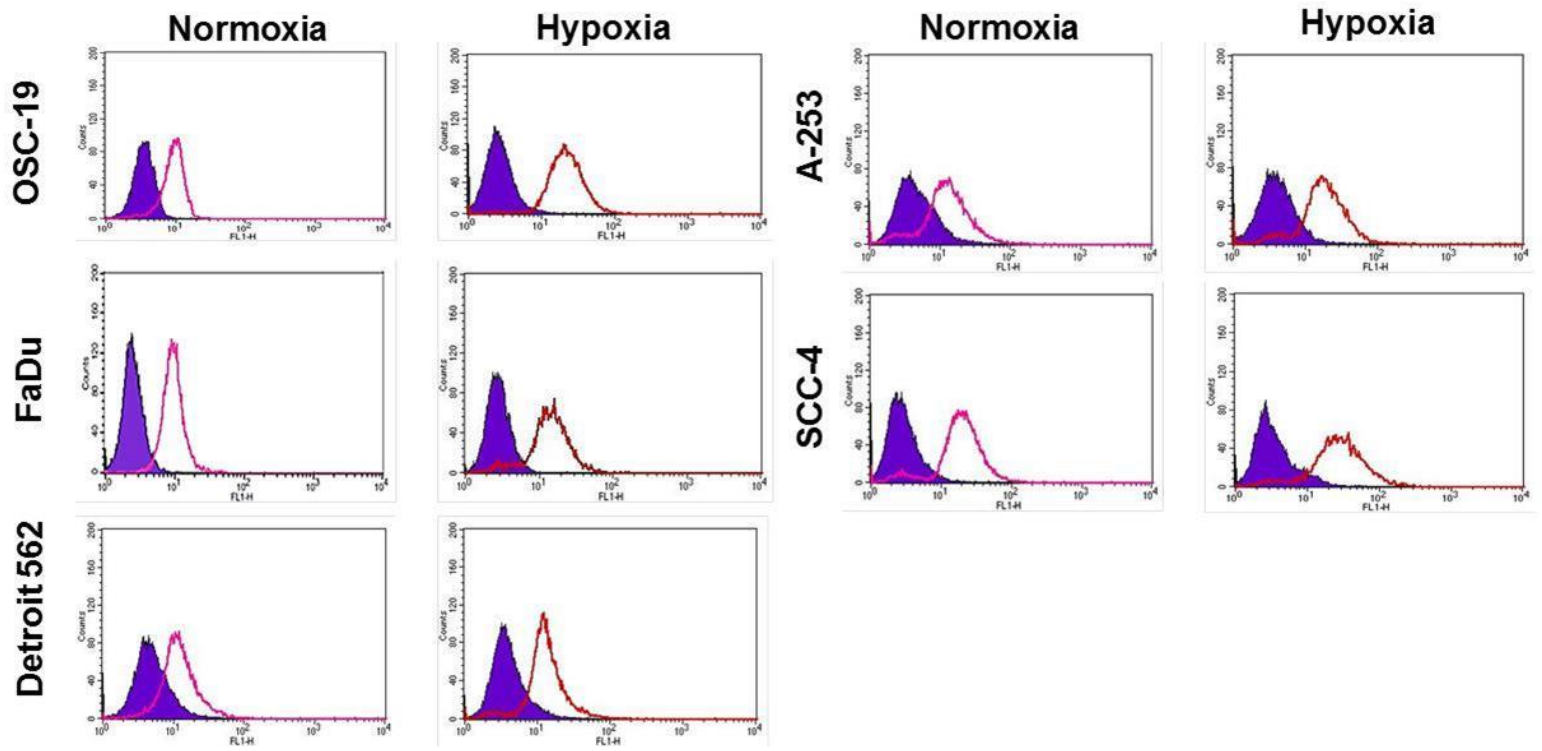

Our results showed that the expression of LDH-A was upregulated under hypoxia compared with normoxia (Figure 33-c), indirectly indicating the presence of HIF-1α (positive control). Furthermore, CCR7 expression was significantly increased in 3 cell line OSC-19, FaDu and Detroit 562 (Figure 33-a, b). The fold change of CCR7 expression was (3.2 vs 6.5) with ($P < 0.05$), (4.1 vs 5.8) with ($P < 0.01$), and (2.1 vs 3.0) with ($P < 0.05$), for normoxia vs hypoxia in OSC-19, FaDu and Detroit 562, respectively. The changes in A-253 and SCC-4 were not significant and the least change in expression was seen in SSC-4 (Figure 33-a, b), which already highly expresses CCR7.

(b)

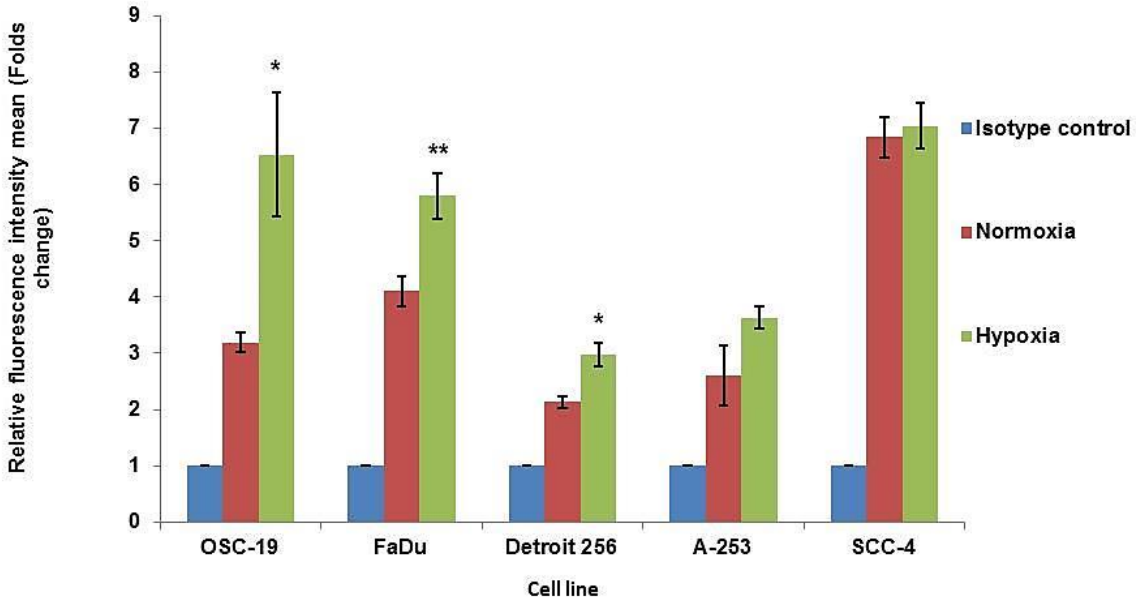

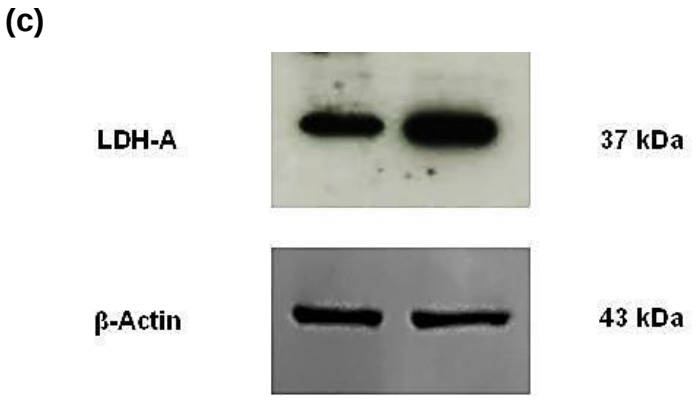

Figure 33: Effect of hypoxia on CCR7 expression.

(a) The expression of CCR7 for cells cultured in under normoxia (unfilled pink curve) and under hypoxia (unfilled red curve) over the filled curve (isotype control in purple). (b) Analysis of CCR7 expression from flow cytometry data using mean fluorescence intensity. CCR7 immunofluorescence intensity mean was normalized to its isotype control. The expression of CCR7 was upregulated under hypoxia significantly in OSC-19, FaDu and Detroit 562. Error bars represent SD of 3 independent experiments. *P < 0.05 and **P < 0.01 for cells cultured under hypoxia compared with normoxic cells. (c) Expression of LDH-A in normoxia (left band) and hypoxia (right band).

2.3.9 Reduction of ROS under hypoxia

There is controversy surrounding the level of cellular reactive oxygen species (ROS) in cells growing under hypoxic conditions and whether the level of ROS increases or decreases during hypoxia (Kondoh et al., 2013, Liu et al., 2004). On the other hand, the role of high level concentration of ROS in increasing cell migration is well established in the literature (Hurd et al., 2012). For instance, the migration of lung cancer cell lines A549, H1299 and H460 was increased by inducing ROS production (Huang et al., 2014). Therefore, we evaluated the level of ROS under hypoxia and normoxia to see whether the observed reduction in migration that we have seen under hypoxia (section 2.3.11) might be related to the ROS levels.

H_2O_2 is well known to induce ROS generation and hence we used it as a positive control (Hurd et al., 2012). The ROS levels were measured using flow cytometry as described earlier in section 2.2.20. Our results showed that hypoxic cells have less ROS compared to normoxic cells. Furthermore, addition of H_2O_2 (200 µM) to hypoxic cells resulted in an increased ROS generation which actually can surpass that observed in normoxic cells. The fold change of ROS generation between normoxic and hypoxic cells is illustrated in (Figure 34- b).

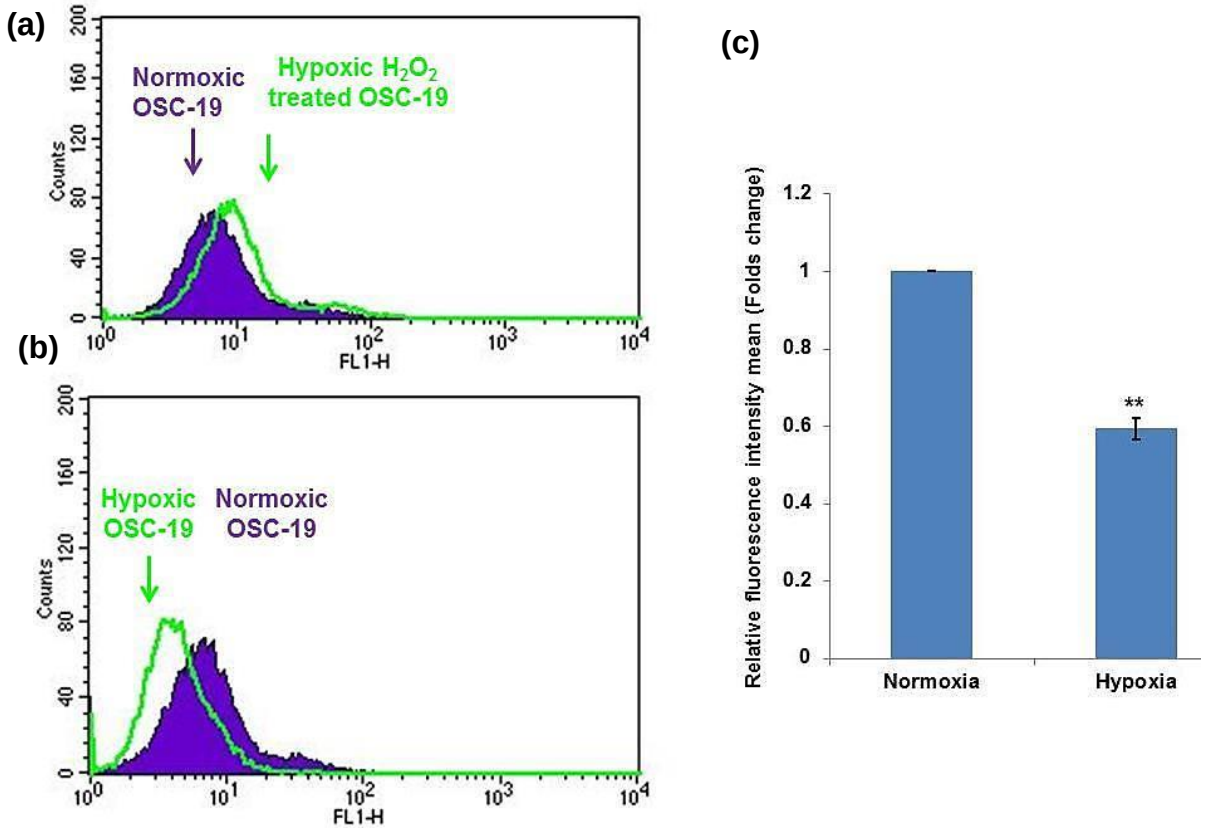

Figure 34: Comparison of ROS level between hypoxic and normoxic OSC-19 cells.

(a) H_2O_2 increased the ROS production compared with cells cultured under normoxia. (b) Hypoxia conditions resulted in ROS level reduction in OSC-19 cells. (c) Fold change of ROS generation was calculated by normalizing fluorescence intensity mean (the geometric mean of area under the curve) obtained from flow cytometry data to normoxia fluorescence intensity mean (the geometric mean). Error bars represent SD of 3 independent experiments. **P < 0.01 for cells cultured under hypoxia compared with normoxic cells.

2.3.10 Induction of HIF-1α using $CoCl_2$ and its effect on CCR7 expression and ROS

Our results from previous section showed that CCR7 is upregulated under hypoxia in OSC-19, FaDu and Detroit 256. Since CCR7 gene has hypoxia response elements at the promoter region (Li et al., 2009), and HIF-1 and HIF-2 have been shown to induce their effects on genes by binding to this hypoxia response element (Tsai and Wu, 2012), we postulate that hypoxia induces HIF-1 and HIF-2 expression and promotes transcription of the CCR7 gene.

To investigate whether the expression of CCR7 is regulated by HIF-1, OSC-19 cells were treated with a known stabiliser of HIF-1α protein, $CoCl_2$ (Han et al., 2015).

The concentrations of $CoCl_2$ were selected according to the results of the MTT assay. The dose response curve of OSC-19 cells treated with $CoCl_2$ for 24 h is shown in (Figure 35). We chose 2-fold concentration below the IC_{50} (200 and 100 μM) to make sure that none of the observed effects were associated with cytotoxicity.

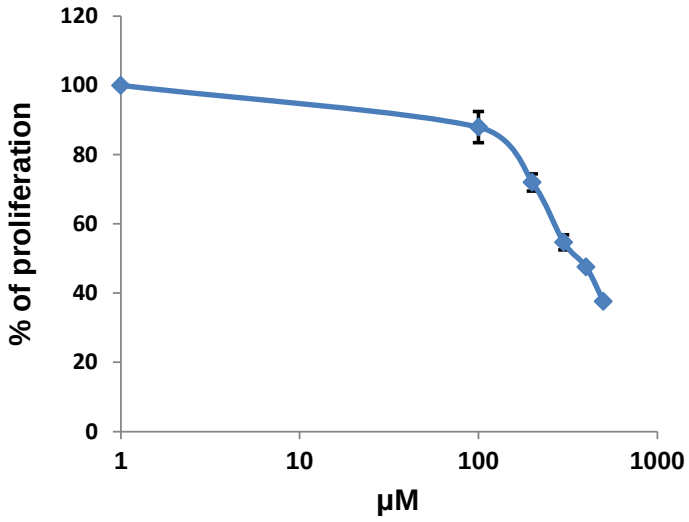

Figure 35: Dose response curve of 24 h $CoCl_2$ treatment.

(a)The OSC-19 cells were treated for 24 h with $CoCl_2$. After 24 h media was removed and exchanged with fresh media before adding the MTT solution 72 h later. Values are the mean of 3 independent experiments and error bars are SD.

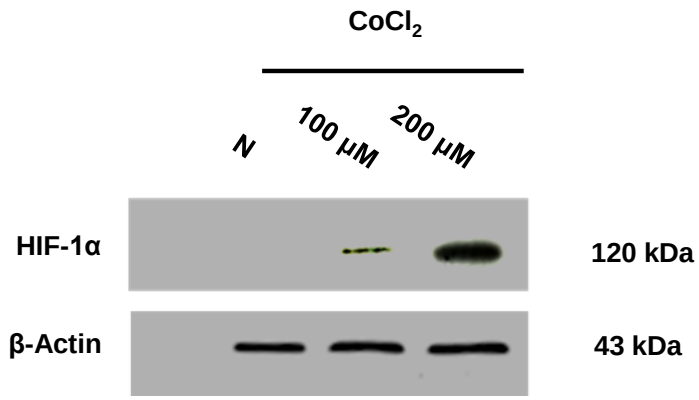

Figure 36: Western blot analysis of HIF-1α protein expression upon treatment with $CoCl_2$ in OSC-19 cells.

Induction of HIF-1α expression upon treating cells with $CoCl_2$ Compared with normoxic cell (N) with no $CoCl_2$ treatment. Actin was used as internal control protein.

The $CoCl_2$ treatment induced significant expression of HIF-1α at 200 μM (Figure 36). The effect of $CoCl_2$ is not limited to HIF-1α induction; others have shown that $CoCl_2$ may also affect ROS levels within the cells by increasing or decreasing them (Oh et al., 2014, Kotake-Nara and Saida, 2007). Because we have seen a reduction in ROS generation in the hypoxia chamber, so we decided to investigate whether $CoCl_2$ at the same concertation used, affects the ROS levels. Again, we used H_2O_2 (200 μM) as a positive control for ROS generation. The samples treated with or without H_2O_2 or $CoCl_2$ were also checked for CCR7 expression. Our results indicate that $CoCl_2$ treatment caused a significant reduction of the ROS levels, as expected, H_2O_2 addition resulted in an increase in the ROS levels (Figure 37-a). The fold change observed is illustrated in Figure 37-b).

(a)

FL1-H = ROS staining

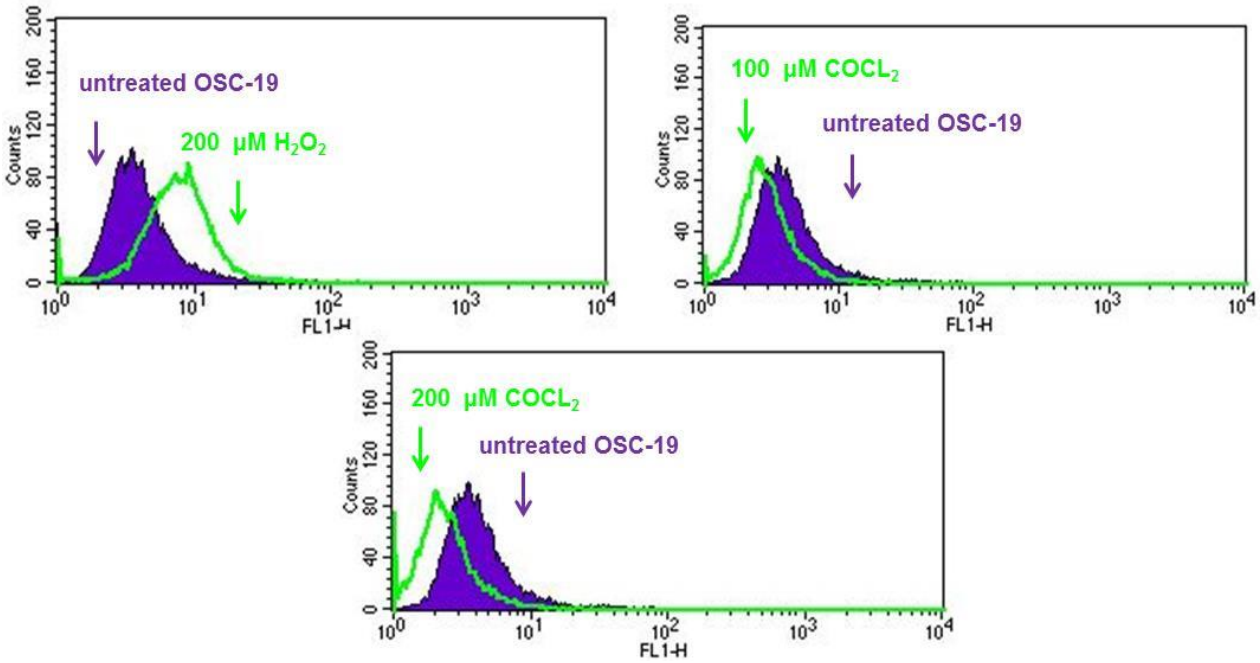

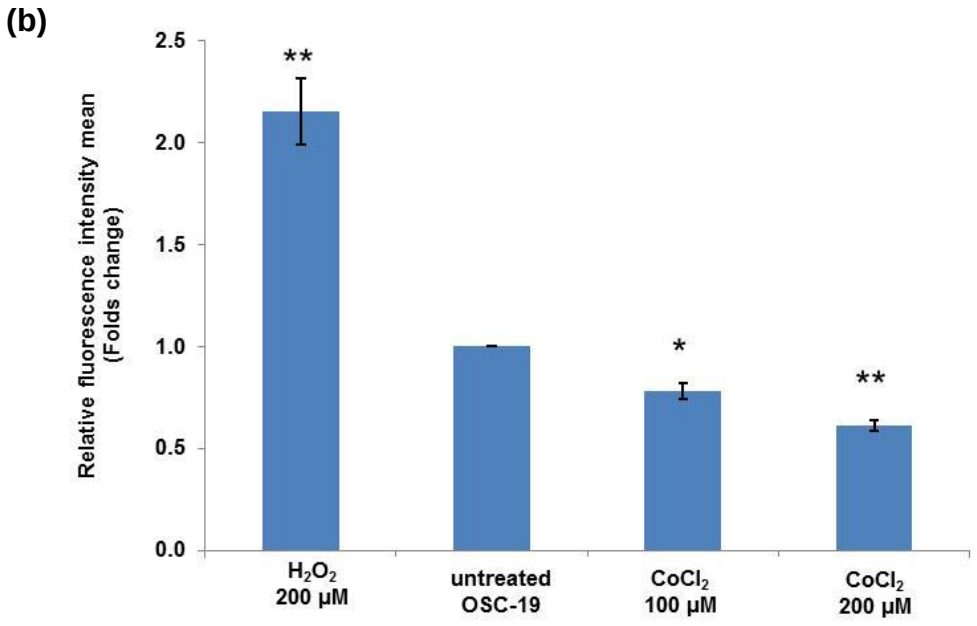

Figure 37: Detection of ROS after H_2O_2 or $CoCl_2$ treatment.

(a) H_2O_2 increased the ROS level but $CoCl_2$ decreased the ROS level after 24 h treatment compared with untreated cells. (b) Fold change of ROS generation was calculated by normalizing fluorescence intensity mean (the geometric mean of area under the curve) obtained from flow cytometry to fluorescence intensity mean of untreated OSC-19 cells. Error bars represent SD of 3 independent experiments. **P < 0.01 *P < 0.05 for cells compared with untreated OSC-19 cells.

Interestingly, the expression of CCR7 was increased significantly after treating the cells with 200 µM of H_2O_2 or $CoCl_2$ (Figure 38-a). It should be noted however that 100 µM of $CoCl_2$ did not cause any significant changes in CCR7 expression. The fold change was 6.3, 4.3 and 3.3 respectively for H_2O_2 treated cells, $CoCl_2$ treated cells or untreated cells relative to the isotype control (Figure 38-b).

FL1-H = CCR7 staining

(a)

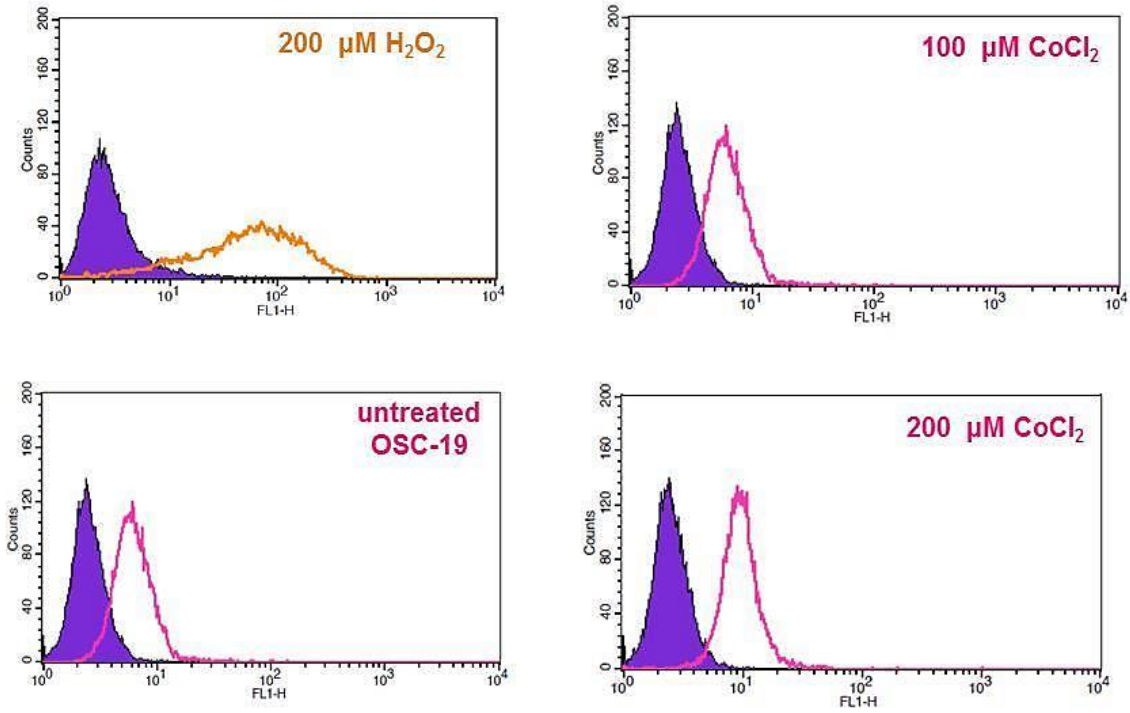

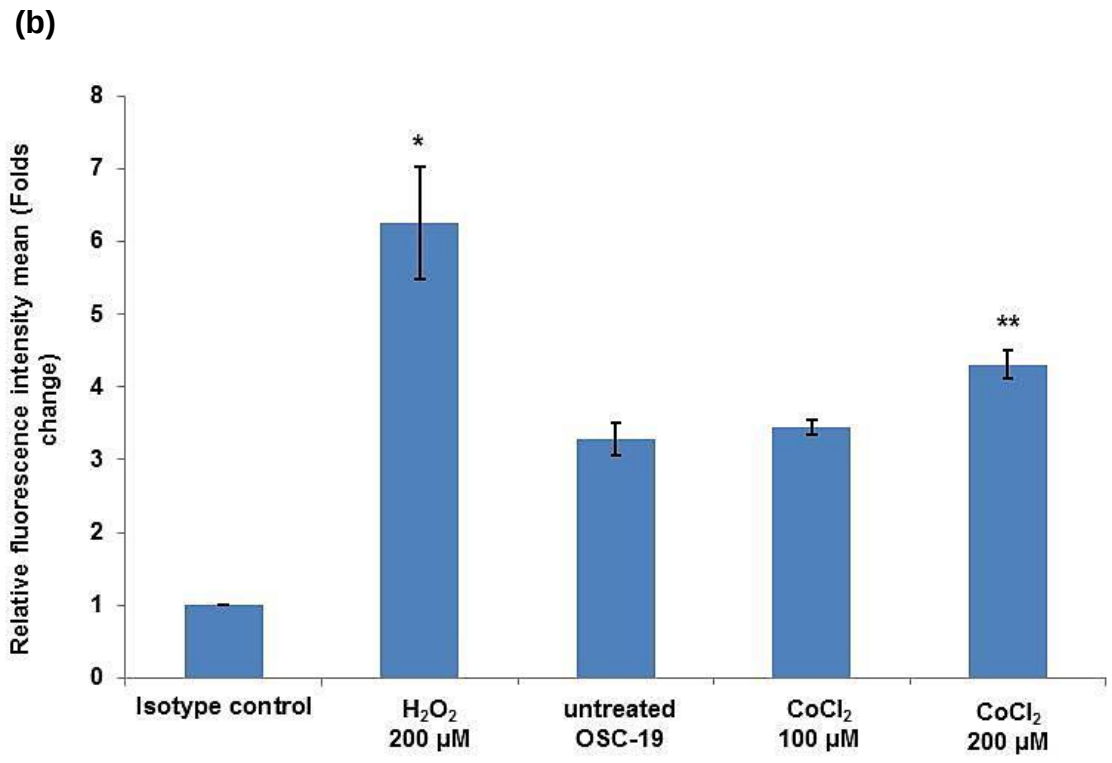

Figure 38: CCR7 expression level after H_2O_2 or $CoCl_2$ treatment.

CCR7 expression is upregulated after H_2O_2 or $CoCl_2$ .The more shifted the unfilled curve (CCR7 stained) from the filled curve (isotype control in purple) the higher the expression.(b) Analysis of flow cytometry data using mean fluorescence intensity. CCR7 immunofluorescence intensity mean was normalized to its isotype control. Error bars represent SD from 3 independent experiments. **P < 0.01 *P < 0.05 for cells compared with untreated OSC-19 cells.

2.3.11 Migration of OSC-19 cells under hypoxia

In section 2.3.2 we have shown that the addition of CCL21 on CCR7 expressing cell lines increases the migration of a number of cell lines including OSC-19 under normoxic conditions. Furthermore, we observed that CCR7 expression increases under hypoxia in OSC-19, FaDu and Detroit 562 head and neck cell lines, with the highest increase observed with OSC-19 cells (section 2.3.8). So we next set out to investigate if the increase in OSC-19 expression under hypoxia corresponds to a larger functional response in cell migration.

As described in section 2.1.2, hypoxia leads to a complex series of cellular changes. Whilst the role of hypoxia as a driving force for aggressive tumours that eventually leads to metastasis is well described in the literature, the impact of hypoxia in increasing or reducing migration of cells *in vitro*, in comparison of normoxia, remains contradictory (Qu et al., 2005, Fujiwara et al., 2007). Therefore we were keen to know which way hypoxia could affect the migration of OSC-19 cells compared with the migration under normoxia.

We first cultured cells under normoxia and after forming the scratches, one plate was moved to the hypoxia and 18 h later the migration was compared with cells allowed to migrate under normoxia (Figure 39-a). In fact, the migration of hypoxic cells in 10% FBS media, and with CCL21 added, was slower than normoxic cells as determined by larger free surface area remaining after migration; (Figure 40-a). There was no change when CCL19 was added but that was to be expected as CCL19 did not influence cell motility even under normoxia. The increase of surface

area after hypoxia incubation compared to normoxia was statistically significant ($P < 0.05$) for 10% FBS and CCL21 groups as shown in (Figure 40-a).

It could be argued that the duration of the experiment was too short to allow any cellular changes, e.g. increase in CCR7 expression, to be sufficiently effective. To confirm our results, cells were incubated inside the hypoxia chamber for 24 h before scratches were made. The plates were only taken out for less than 10 min for taking images (0 h) and returned back to the hypoxia chamber and later again at the end of the experiment at 18 h. Again, the migration of the hypoxic cells was slower than the normoxic cells (Figure 39-b).

The increase of surface area after hypoxia incubation compared to normoxia was significant ($P < 0.05$ and $P < 0.01$) for 10% FBS and CCL21 groups respectively as shown in (Figure 40-b). This means that whilst the migration under hypoxia was lower than normoxia, it was not related to CCR7/CCL21 axis.

(a)

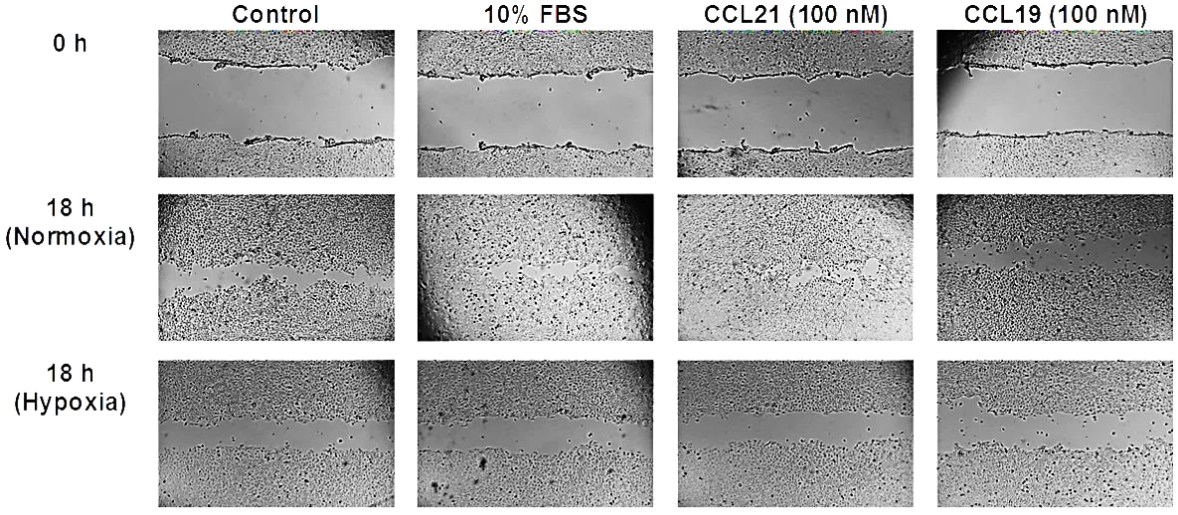

(b)

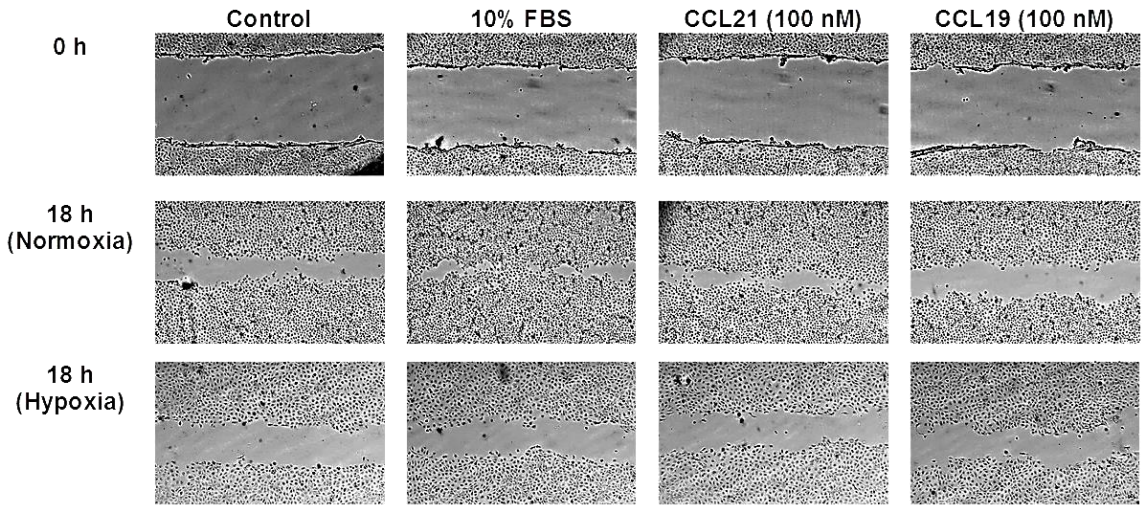

Figure 39: Hypoxia decreased the cell migration of OSC-19 cells after CCL21 treatment compared with cells cultured under normoxia.

(a) Scratches were made on confluent monolayers of OSC-19 cells. Cells were treated with CCL21 or CCL19 at 100 nM or no ligand added (control) in both normoxic and hypoxic cells. Free surface area was measured after the migration of cells on 2 fields per well and averaged and normalized to free surface area at 0 h. Hypoxia decreased the cell migration of OSC-19 cells after CCL21 treatment. (b) Scratches were made inside the hypoxia chamber on confluent monolayers of OSC-19 cells after 24 h of incubating cells in hypoxia chamber. Later Cells were treated with CCL21 or CCL19 at 100 nM or no ligand added (control) in both normoxic and hypoxic cells. Free surface area was measured after the migration of cells on 2 fields per well and averaged and normalized to free surface area at 0 h. Hypoxia decreased the cell migration of OSC-19 cells after CCL21 treatment.

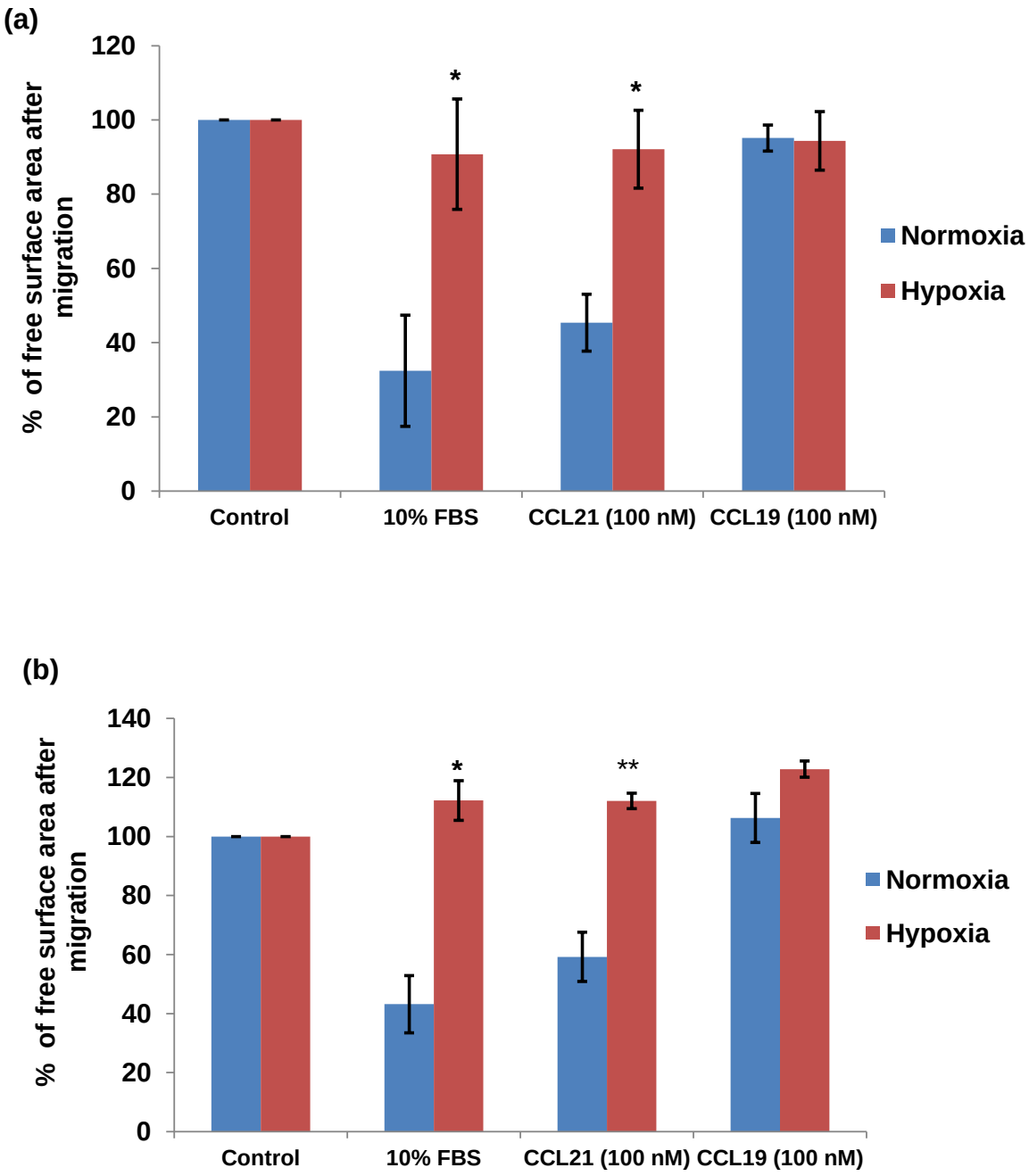

Figure 40: % of free surface area both under normxia and hypoxia after migration.

Data expressed as % of free surface area after migration under hypoxia and normoxia for 18 (a) or after 18 of migration after incubating cells for 24 h under hypoxia (b). Smaller bars indicate more migration. Error bars represent SD of 3 independent experiments. *P < 0.05 and **P < 0.01 for cells cultured under hypoxia compared with normoxic cells for each treatment group.

2.3.12 Effect of $CoCl_2$ on cell Migration

As was the case in hypoxia, the effect of $CoCl_2$ on cell migration has been shown to be controversial (Han et al., 2015, Jeong et al., 2016). Our results showed that $CoCl_2$ increased CCR7 expression, but caused a reduction on the ROS level. Although one could expect that an increase of CCR7 can cause an increase in cell migration, we could not be certain if this effect on migration due to the increase in CCR7 will be observed because of the ROS reduction caused by $CoCl_2$ treatment. The increase in ROS levels have been shown by others to be important for cell migration (Liou and Storz, 2010). Therefore, we looked for the effect of a ROS inducer (H_2O_2 at 200 µM) and a ROS reducer ($CoCl_2$ 100 and 200 µM), on the cell migration aptitude of OSC-19 cells. Our results showed that H_2O_2 increased the cell migration by 40% compared with control (no treatment) decreased the free surface area after migration (Figure 41-a). However, $CoCl_2$ treatment did not increase the migration, 200 µM $CoCl_2$ did not decrease the free surface area compared with control, 135% *vs* 100% respectively for $CoCl_2$ at 200 µM *vs* control. $CoCl_2$ at 100 µM also did not result in any significant increase of cell migration compared with control (the free surface area was 88.6% vs 100% respectively for $CoCl_2$ at 100 µM vs control). The addition of CCL21 (10 nM) to $CoCl_2$ (200 or 100 µM) facilitates migration, decreasing the free surface area after migration compared with $CoCl_2$ (200 or 100 µM) with no CCL21. The migration level resulting from the addition of CCL21 (10 nM) to $CoCl_2$ (200 or 100 µM) was increased significantly by 44% and 37% compared with no CCL21 addition with $P < 0.05$ or P

< 0.01 respectively for $CoCl_2$ at 200 or 100 µM. The % of free surface is shown below in Figure 41-b.

(a)

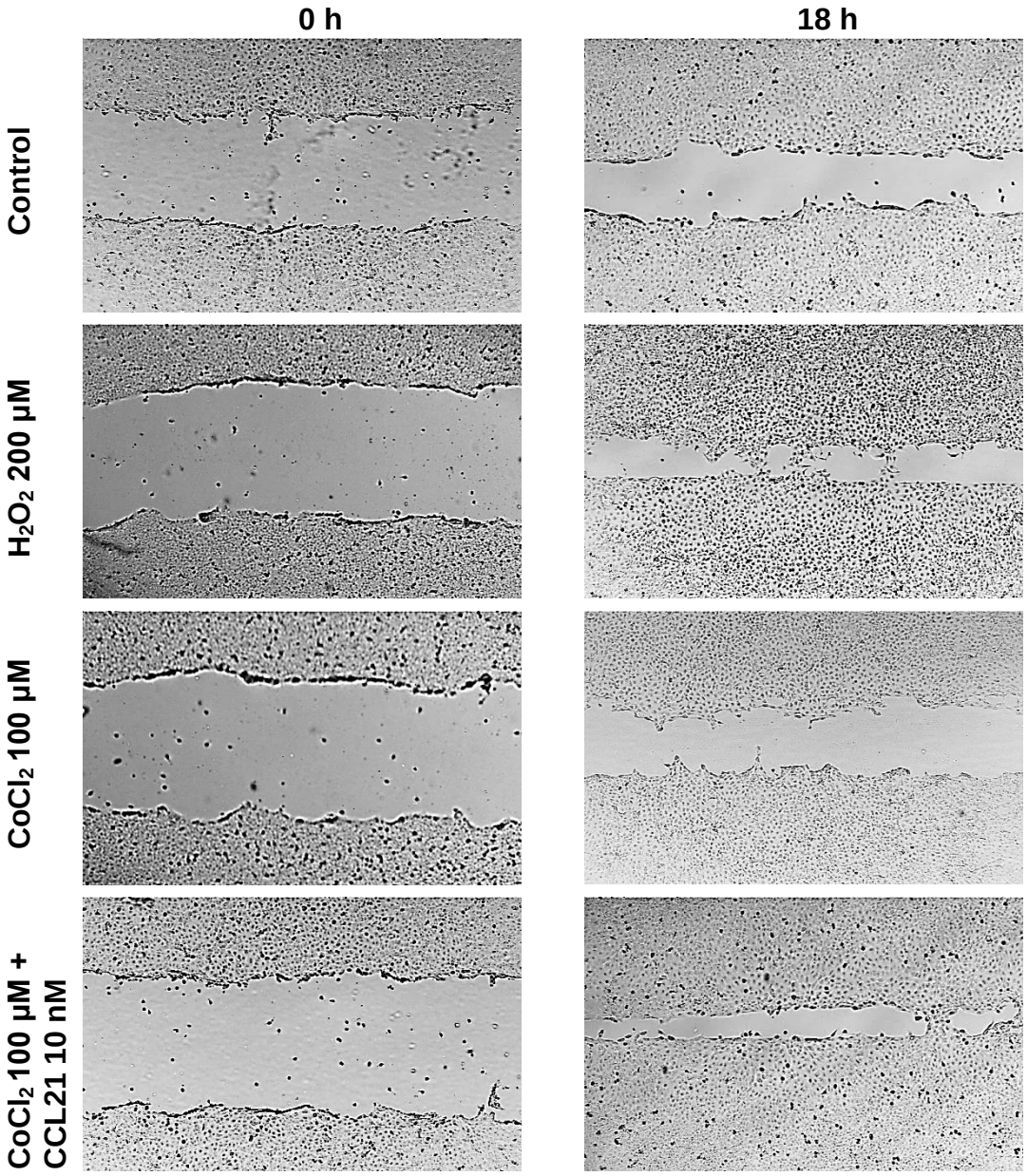

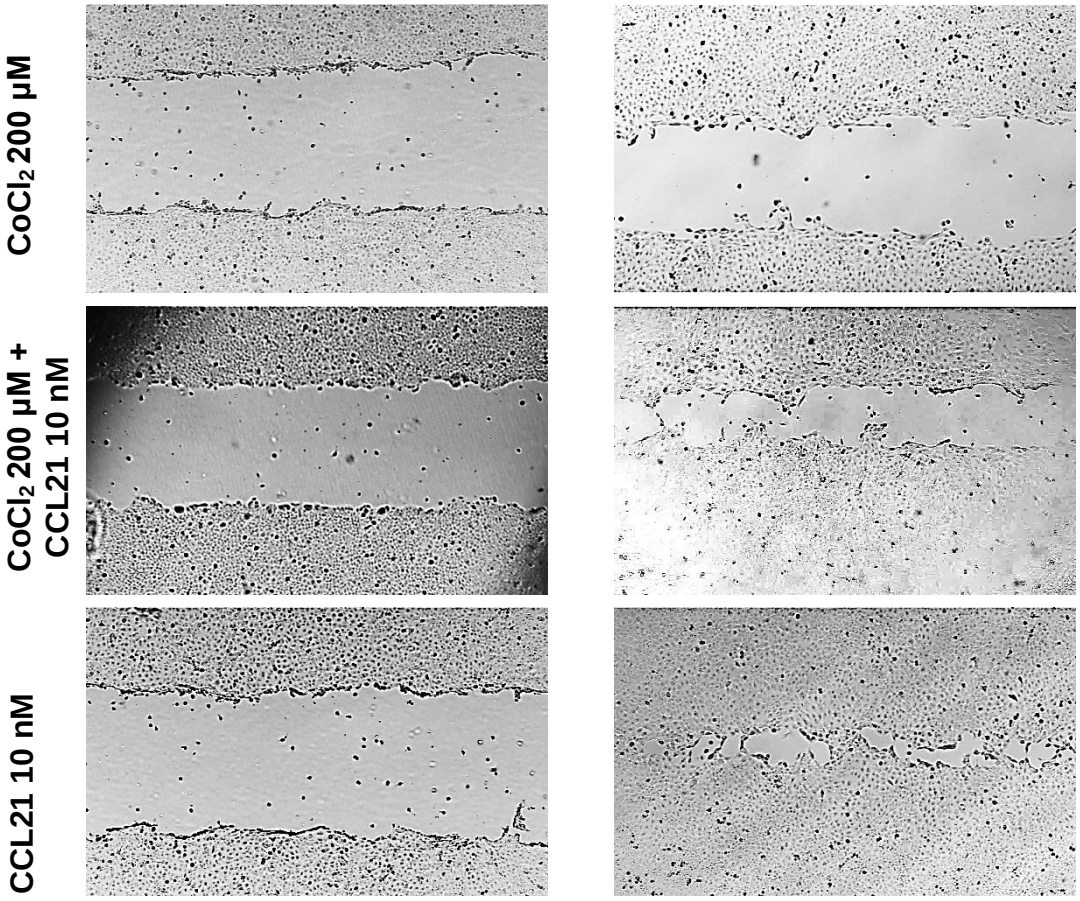
$CoCl_2$ 200 µM
$CoCl_2$ 200 µM + CCL21 10 nM
CCL21 10 nM

(b)

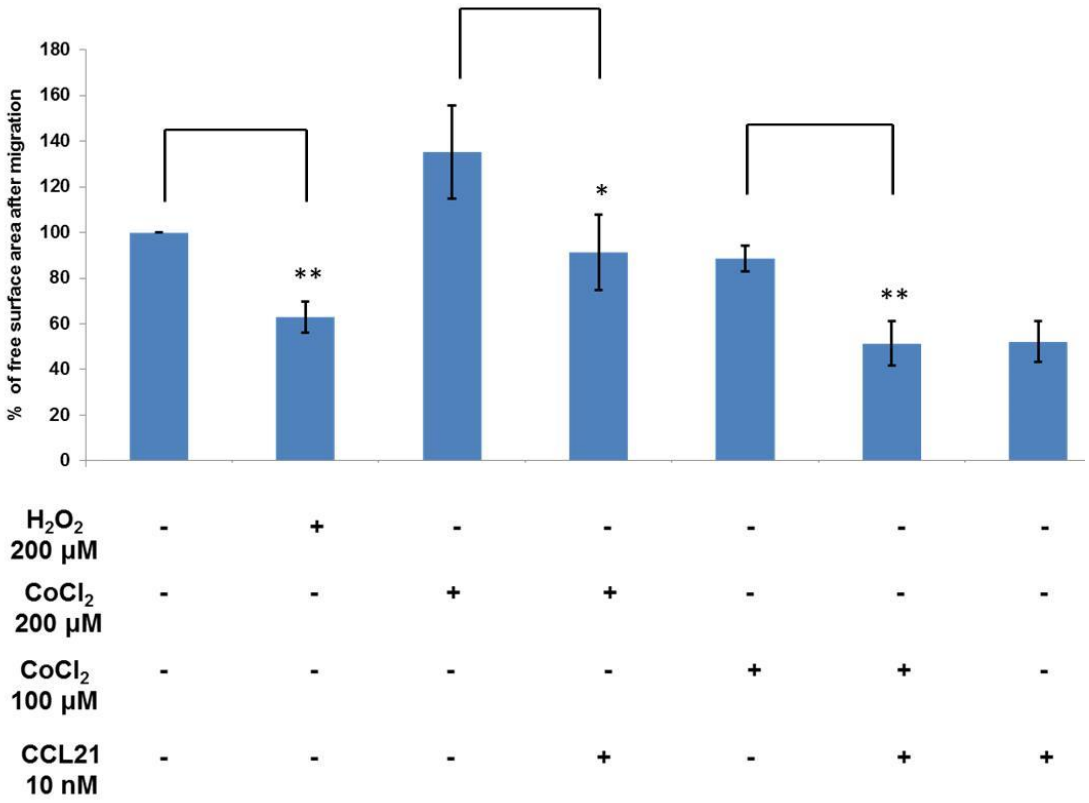

Figure 41: Effect of $CoCl_2$ on cell migration.

(a) $CoCl_2$ with or without CCL21 did not cause increase of cell migration compared with CCL21 10 nM group. However, H_2O_2 decreased the free surface area after migration compared with no H_2O_2 cells. CCL21 increased wound healing in $CoCl_2$ treated cells compared with $CoCl_2$ treated cells with no CCL21. Scratches were made on confluent monolayers of OSC-19 cells. Free surface area was measured after 18 h on 2 fields per well and averaged and normalized to free surface area at 0 h. (b) Data expressed as % of free surface area after migration. Error bars represent SD of 3 independent experiments. **P < 0.01 *P < 0.05 for each comparison shown in the graph.

2.3.13 Proliferation of OSC-19 cells under hypoxia

Hypoxia results in a number of cellular changes but overall, is known to cause a reduction in cell proliferation in most cell types (Hubbi and Semenza, 2015). We have shown previously that CCL21 had no effect on cell proliferation under normoxia in 2 cell lines; FaDu and OSC-19 see section 2.3.3

Therefore, we investigated if CCL21 would equally not affect proliferation under hypoxia. Cells were cultured under normoxia and hypoxia for 24 h before adding CCL21 100 nM for another 72 h and then MTT solution was added for 4 h as described in section 2.2.12.2. Similar to the results we have seen under normoxia, CCL21 did not cause any increase of cell proliferation as shown in Figure 42.

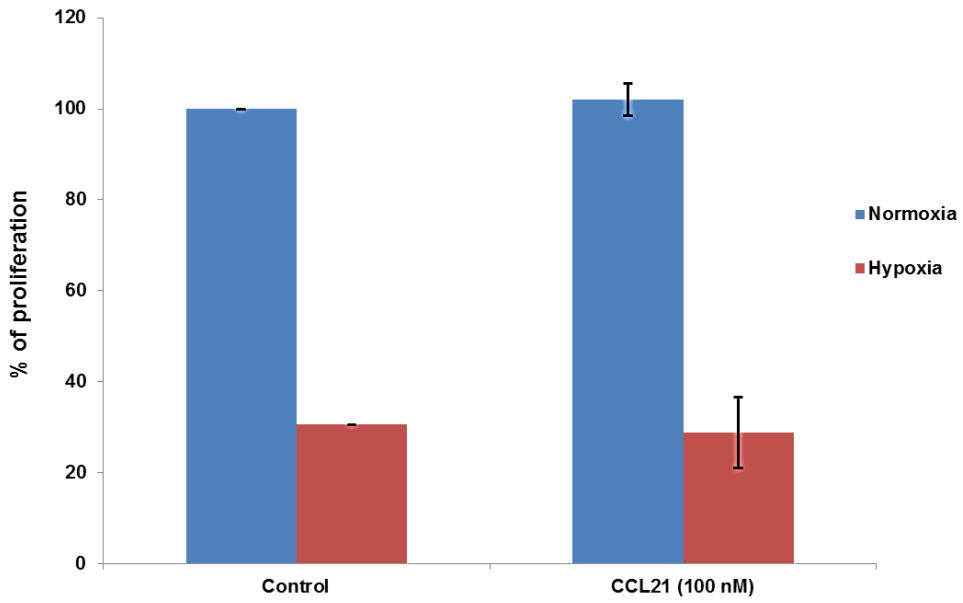

Figure 42: CCL21 did not cause any increase of cell proliferation under hypoxia. Error bars represent SD of 3 independent experiments.

2.3.14 Correlation between hypoxia, CCR7 and Ki-67 in spheroids model

So far, the investigations we had carried out were all in 2D cultured cells. As discussed in chapter 1, 3D *in vitro* model are better representatives of tumours as the intracellular cellular contacts and interactions more closely resembles that in real life tumours. Therefore we decided to investigate the relationship between hypoxia and CCR7 first in multicellular spheroids, and then xenografts and clinical tissues. For the photos of head and neck cell lines grown as spheroids see appendix IV.

2.3.14.1 *Growth curve of OSC-19 and SCC-4 spheroids*

We initially cultured two cell lines OSC-19 and SCC-4 as spheroids, First growth of OSC-19 and SCC-4 spheroids with different cell seeding concentrations; the diameter, solidity and circularity were investigated. Figure 43 shows representative images of OSC-19 and SCC-4 spheroids with different cell seeding concentrations (2000 and 10000) for OSC-19 and 2000 cells for SCC-4 per well. The morphological changes during spheroid formation are different in the two cell lines investigated. In the initial stage, OSC-19 and SCC-4 form spontaneously compact spheroids or cell aggregates in each well, respectively. Afterwards, the OSC-19 spheroids start to form a more solid structure with smooth and continuous surfaces.

Although the SCC-4 spheroids were growing, they were not as solid as the OSC-19 spheroids (day1-day3). After day4, there was no apparent change in the SCC-4 spheroids morphology. Figure 44 shows the change of mean spheroid diameter in

the OSC-19 and SCC-4 spheroids. The spheroid diameter of all spheroids increased sequentially after an initial slight decrease. After a while, the diameter reached a plateau. Nevertheless, the plateau phase appeared earlier in OSC-19 of larger sizes spheroid (day5), and the growth rate of smaller spheroids was higher than that of larger ones.

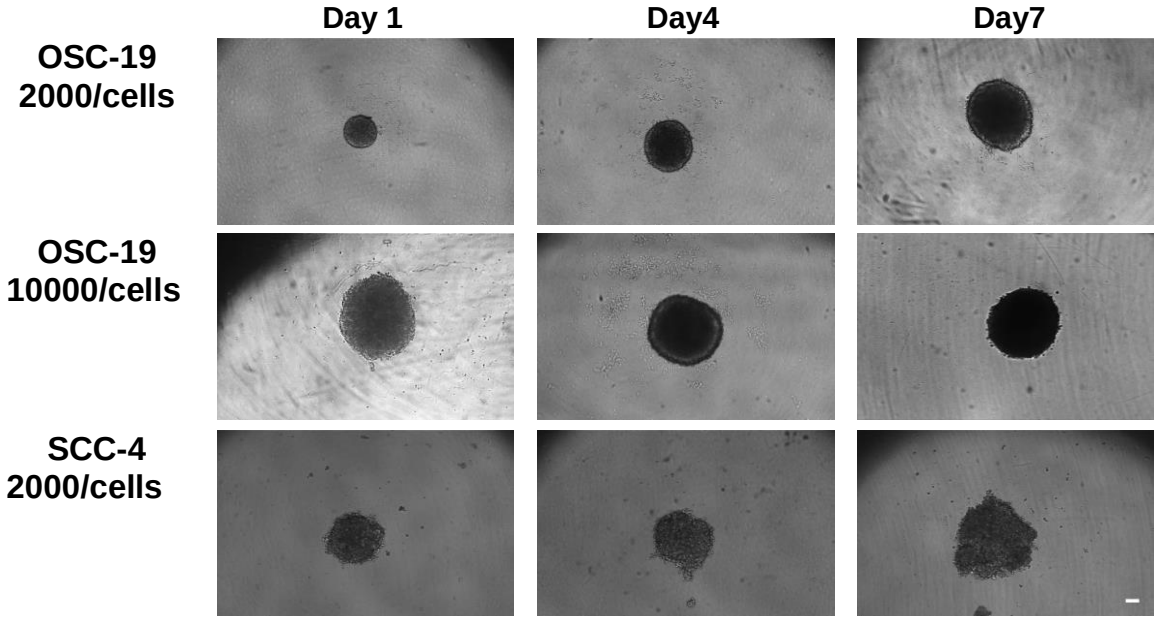

Figure 43: OSC-19 and SCC-4 spheroids cultured over a period of 7 days.

The scale bar = 100 um at 10x objective lens.

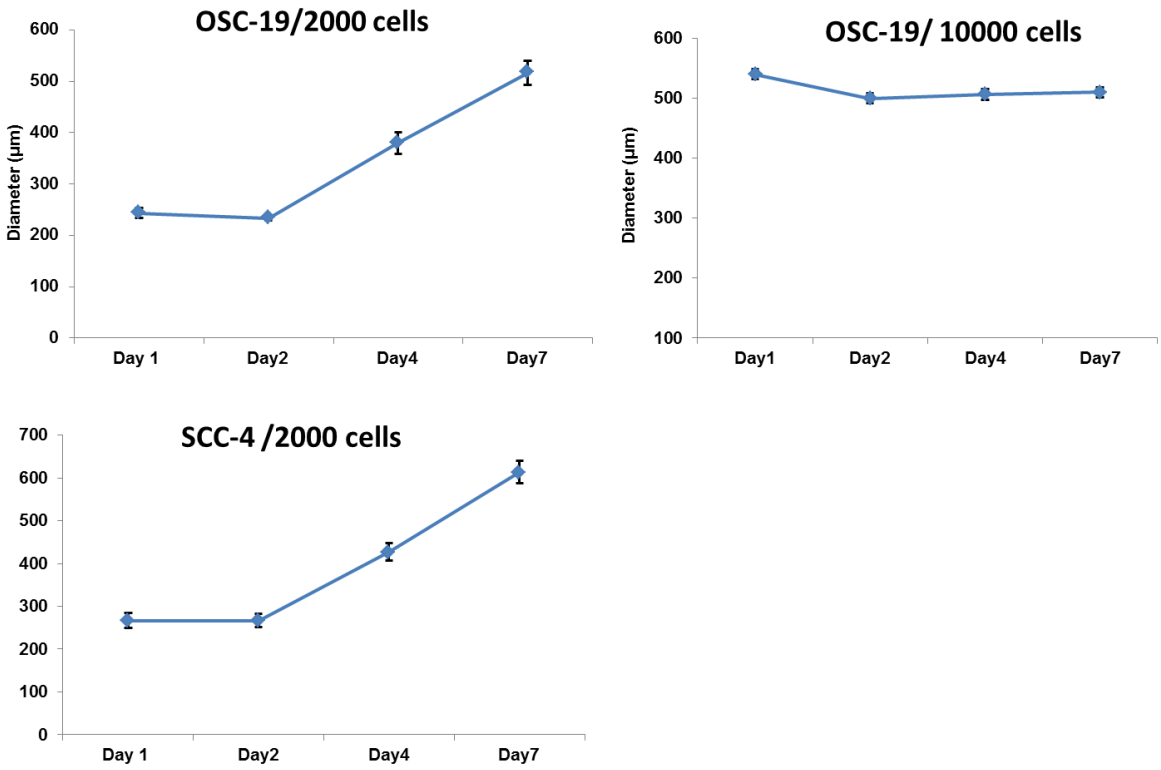

Figure 44: Growth curve of OSC-19 SCC-4 spheroids.

The diameter of OSC-19 and SCC-4 spheroids was measured using calibrated graticule fixed to the light microscope at 10 × objective lens. Error bars represent SD of 3 independent experiments.

2.3.14.2 *CCR7 is upregulated in the hypoxic core of OSC-19 spheroids*

Therefore, we decided to use the OSC-19 spheroids as they were more spherical and compact, compared with SCC-4 spheroids which appeared as an aggregate mass. We harvested OSC-19 spheroids from day1 and day7 from the cultured 2000 cells spheroids to stain for CCR7 (Figure 45). Our results showed uniform expression of CCR7 spheroids of day1 (Figure 45-b) in which there's no hypoxic core developed due to the small size of the spheroids ~230 µm. The maximum

diffusion limit of O_2 is ~200 µm and because of the small size of the spheroids, there was no lack of oxygen or nutrients at day1. On the other hand, CCR7 expression was differential between the spheroid layers with brighter intense staining towards the hypoxic core in ~500 µm at the day7 spheroids (Figure 45-a). To demonstrate that we have an increase of fluorescence intensity in the core of ~500 µm compared to the rim and that the fluorescence intensity was uniform in ~230 µm spheroids, we used Image J to record the fluorescence intensity along a central strip of the Tritc staining of the spheroid see (Figure 45-c).

Due to the differences in CCR7 staining between smaller and bigger spheroids and to confirm the presence of hypoxic areas in the larger spheroids ~500 µm, we stained with pimonidazole for hypoxia and Ki-67 for proliferation. Pimonidazole, is a well-used hypoxia marker and forms adducts with hypoxic cells by binding to thiol group present in the hypoxic cells as it becomes activated after reduction under low O_2 level. These adducts can be detected by IF, IHC and flow cytometry (Varia et al., 1998). The pimonidazole adducts were detected in the hypoxic core and were not present on the periphery of the spheroids (Figure 45-d). Furthermore, Ki-67 straining was higher at the periphery from the rest of the spheroid indicating the progressive decrease of the proportion of proliferative cells from the surface to the center of the spheroid (Figure 45-d). The expression of CCR7 was higher towards the core of the spheroid in comparison with the most outward layer, thus, we have seen an upregulation of CCR7 in the hypoxic core (Figure 45-d).

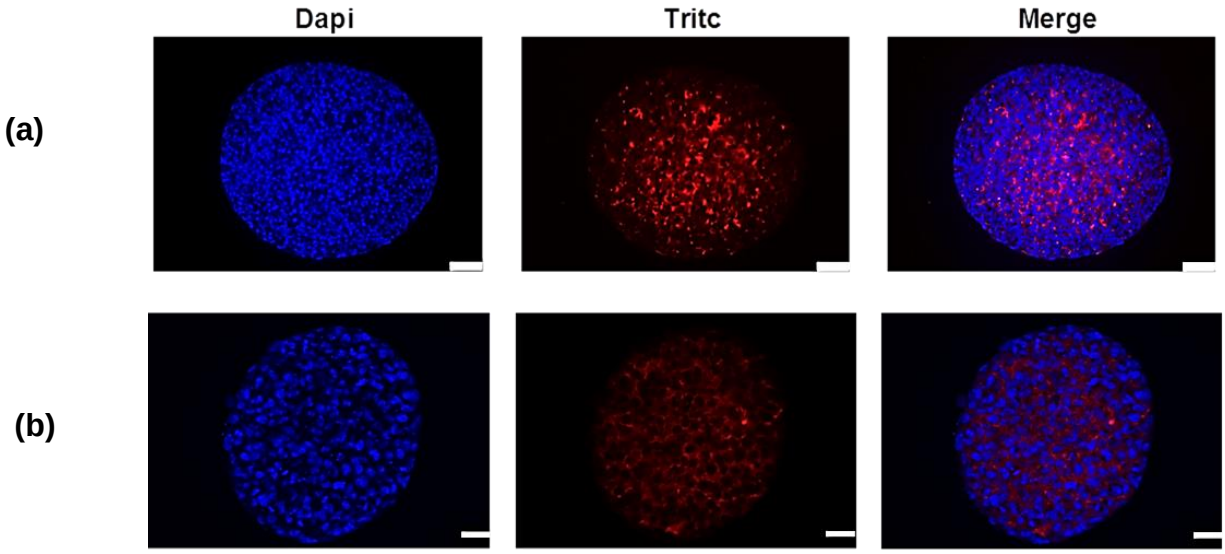
(a)
Dapi
Tritc
Merge
(b)

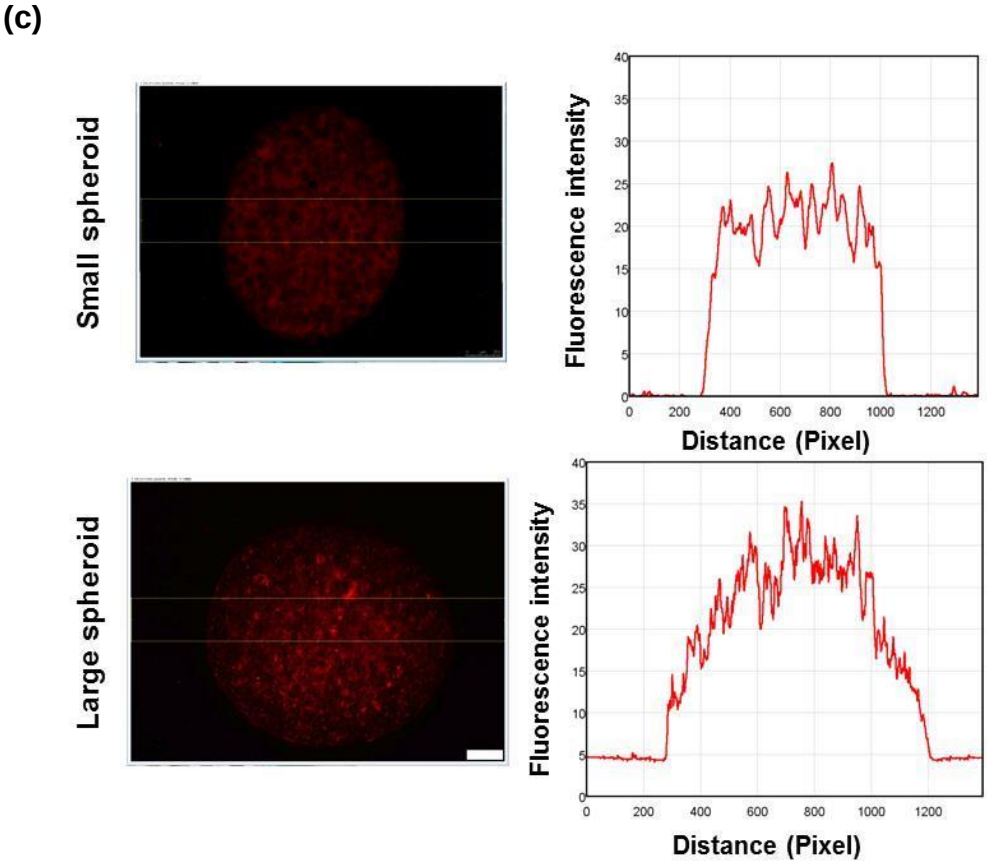
(c)
Small spheroid
Fluorescence intensity
Distance (Pixel)
Large spheroid
Fluorescence intensity
Distance (Pixel)

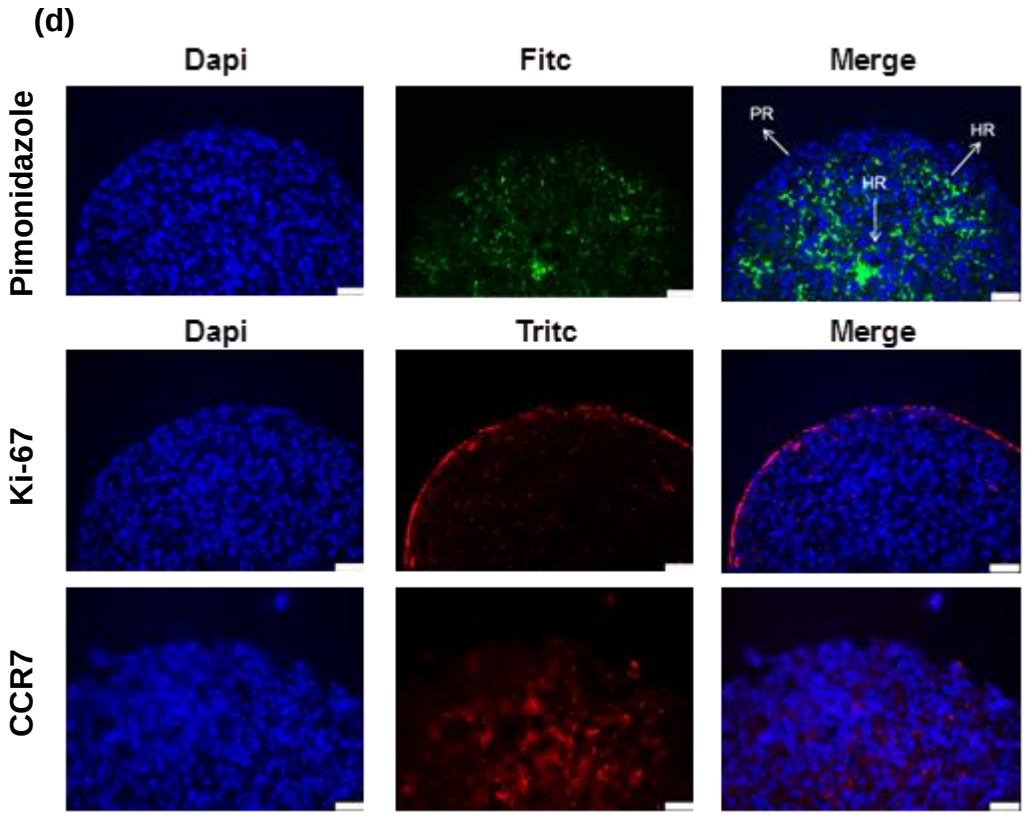

Figure 45: Detection of CCR7 in OSC-19 spheroids by IF technique.

(a) Differential expression of CCR7 is observed in ~500 µm with intense expression towards the core at 20x objective lens with scale bar 25 µm. (b) Homogenous expression of CCR7 in ~ 230 µm at 40x objective lens with scale bar 50 µm.(c) Fluorescence intensity along a central strip of Tritc staining in ~ 230 and 500 µm spheroids (d) In ~500 µm OSC-19 spheroids, hypoxia was detected by pimonidazole (green) staining in the core of the spheroid with no staining at the proliferating rim that was detected by Ki-67 (red).The staining of CCR7 (red) was upregulated towards the core of OSC-19 spheroid at 40x objective lens with scale bar 50 µm. Periphery region (PR) and hypoxic region HR (HR).

2.3.15 Evaluation of CCR7, HIF-1α and Ki-67 expression in xenografts

Tumours grown as xenografts provide a further degree of sophistication to cell-matrix and cell-cell interactions observed in multicellular spheroids. To see if our observations in monolayer cultured cells and multicellular spheroids also extends to xenograft tissue; we evaluated the expression of Ki-67 and HIF-1α in head and neck xenografts that already showed high expression of CCR7 as we saw in section 2.3.1.4. This investigation is also important later on, as it allows us to choose a good xenograft model for testing of our in house synthesized CCR7 antagonist molecules compounds *in vivo.* We stained for HIF-1α because it is expressed in low oxygen environments, and its expression has been associated with resistance to chemo/radiotherapy, increased angiogenesis and poor patient prognosis, Ki-67 staining was chosen to differentiate between hypoxic and non-hypoxic regions. Hypoxic cells will show low Ki-67 staining compared with non-hypoxic cells (Couture et al., 2002).

We anticipate that a good model for testing CCR7 compounds would be one that represents the situation from patients in which chemotherapy and radiotherapy effects are compromised. In sequential sections, it is difficult to identify tumour cells that preferentially express HIF-1α, CCR7 and/or Ki-67 by individual immunostaining procedures. However, we can still see a pattern of expression as described below. Xenograft of OSC-19, A-253 and Detroit 562 are known to exhibit high levels of differentiation, compared with the poor levels of differentiation of FaDu (Vaughan et al., 2010, Bhattacharya et al., 2004, Kawahara et al., 1993, Caamano et al., 1993). OSC-19, Detroit 562 and A-253 xenografts contain well/

moderately differentiated areas, without (OSC-19) or with little micro-vessels (A-253 and Detroit 562) compared with FaDu that contains a high amount of micro-vessels. Tumour cells in these highly to moderate differentiated xenografts were strongly positive for CCR7 (mainly membrane bound localization). In addition, at these regions, HIF-1α staining was predominant with very little Ki-67 staining (Figure 46). However Ki-67 was predominant in areas that were less or poorly differentiated.

For instance, in OSC-19 cells, we can detect keratin pearls; which is a well-known histological observation that is seen in well-differentiated cells. We can see that the cells around these keratin structures highly express membrane bound CCR7 and HIF-1α, but not Ki-67 (Figure 46). On the other hand, the poorly differentiated FaDu cell line showed CCR7 expression that was mainly cytoplasmic, with no HIF-1α staining, with Ki-67 being expressed in all of the cells intracellularly in the nucleus (Figure 46).

OSC-19	CCR7	HIF-1α	Ki-67
10x	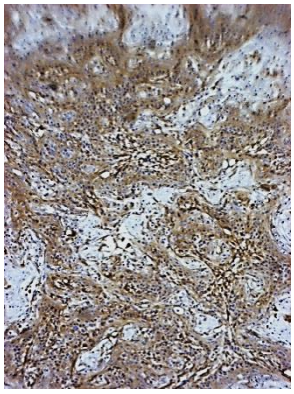	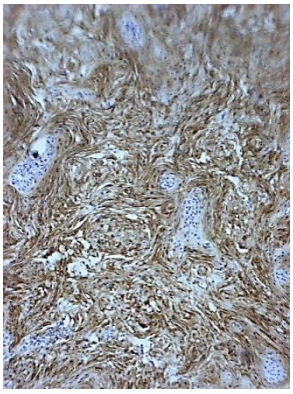	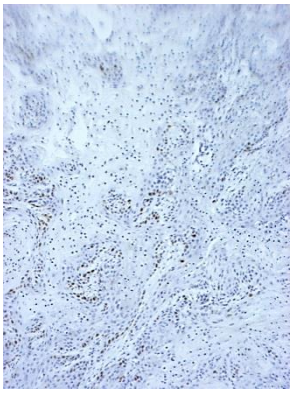
20x	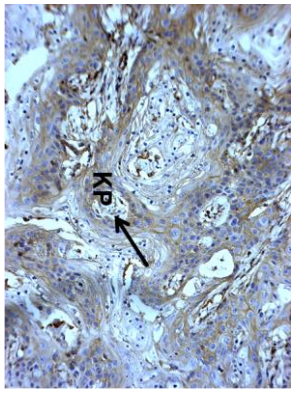	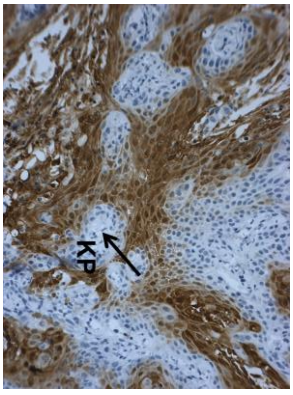	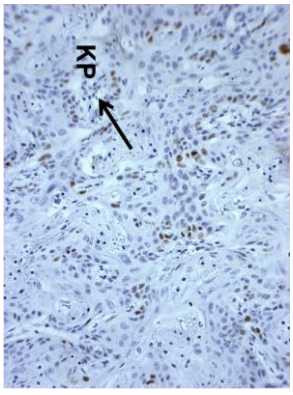
40x	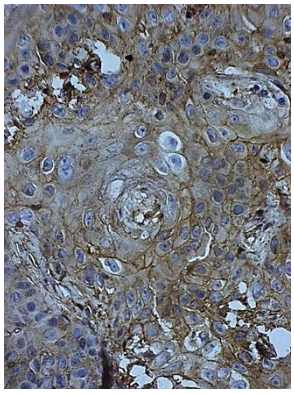	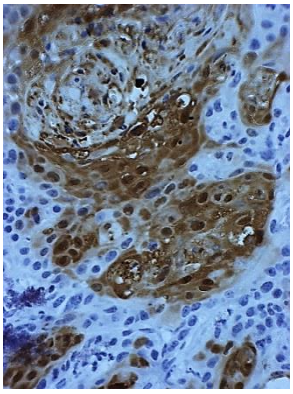	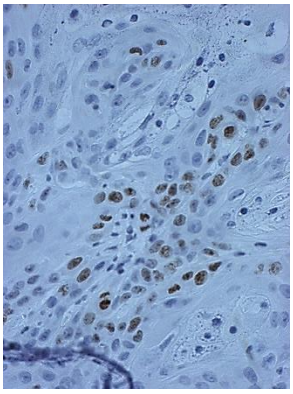

Ki-67	HIF-1α	CCR7	FaDu
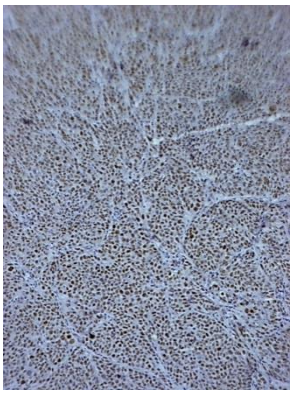	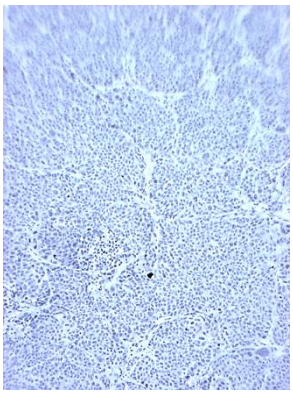	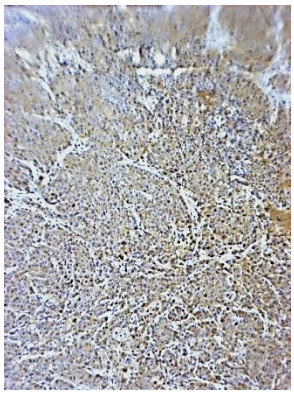	10x
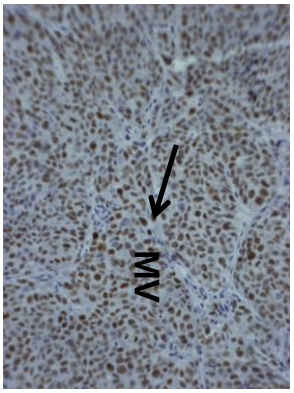	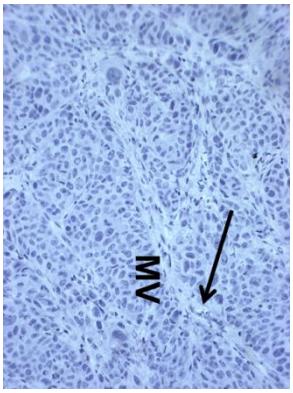	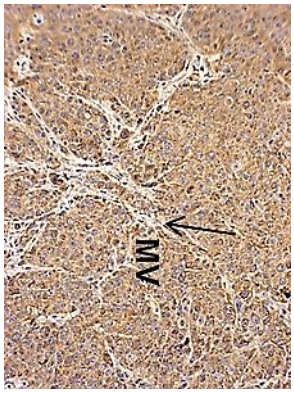	20x
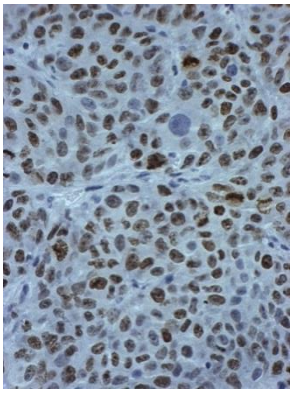	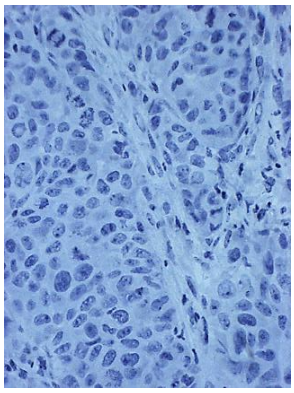	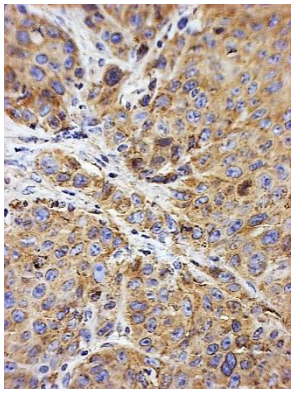	40x

Ki-67	HIF-1α	CCR7	Detroit 256
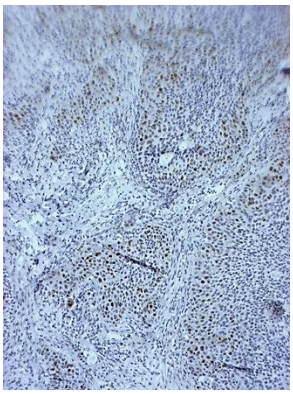	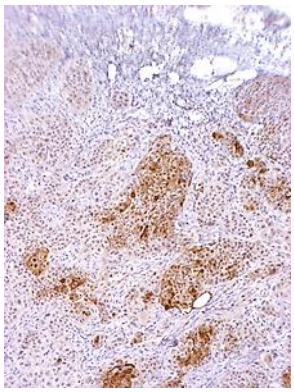	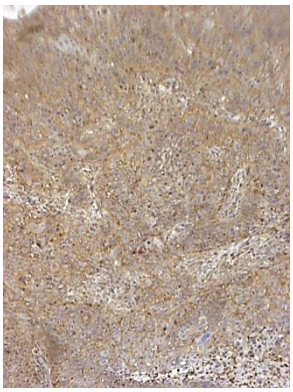	10x
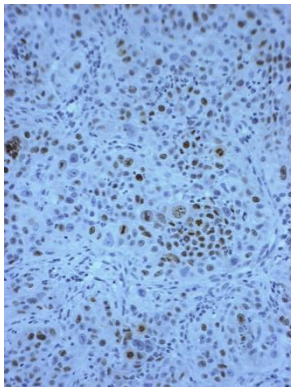	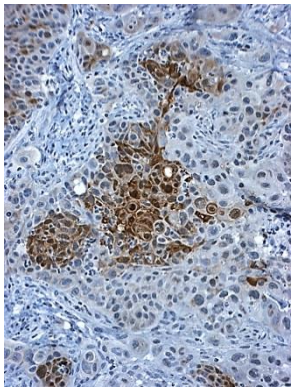	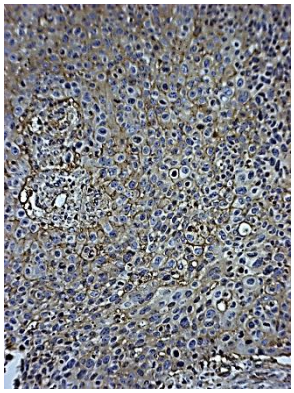	20x
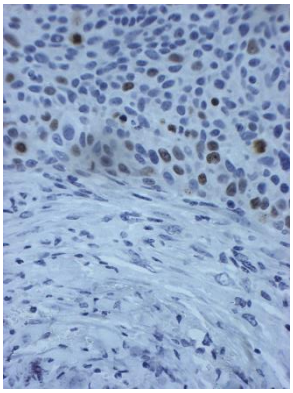	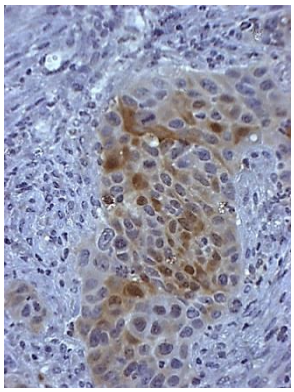	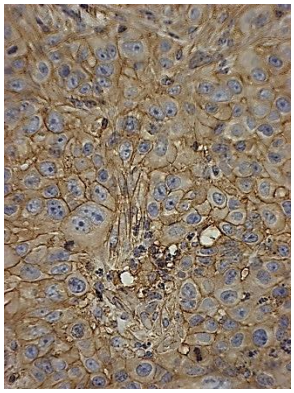	40x

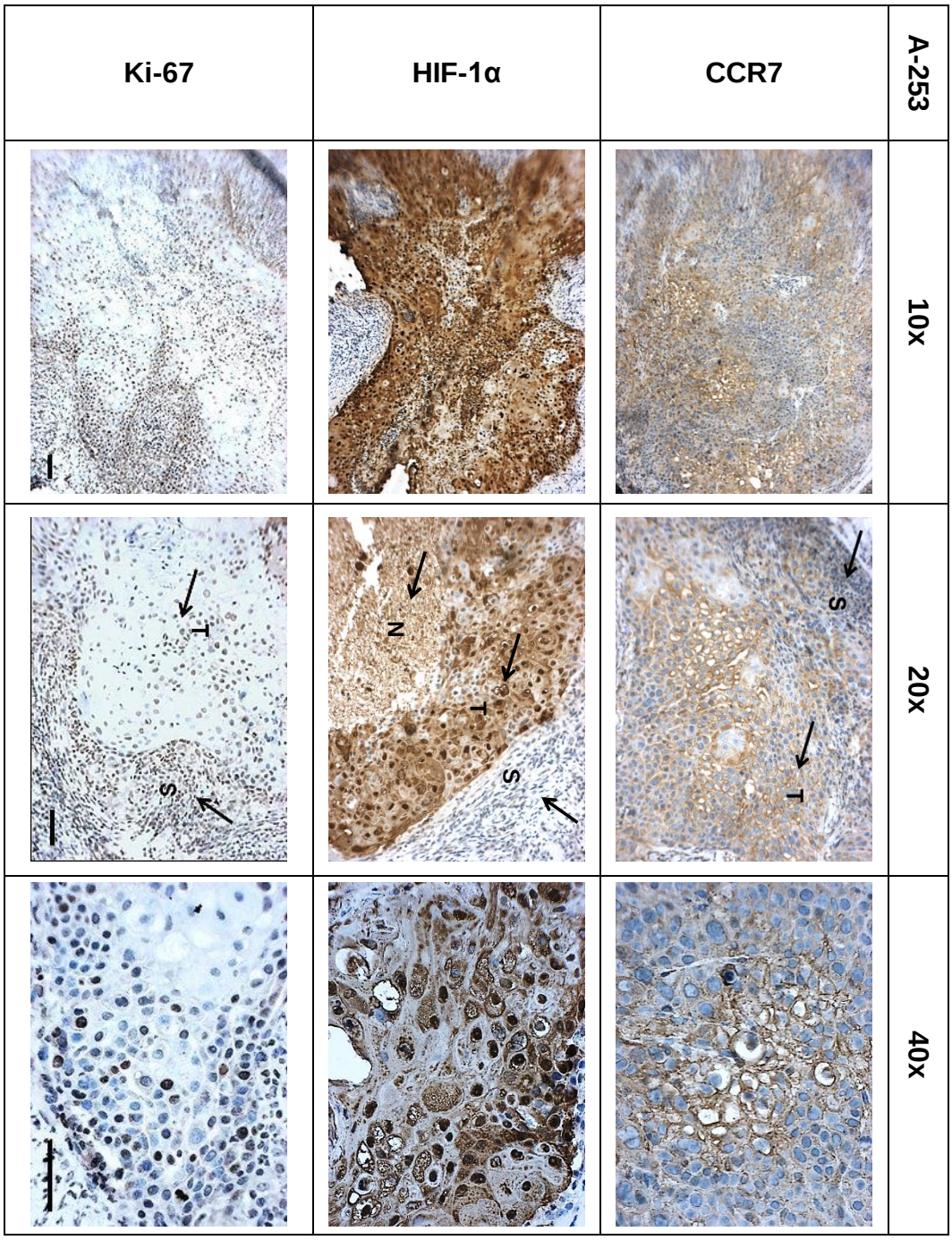

Figure 46: Expression of CCR7, HIF-1α and Ki-67 in head and neck cancer xenografts.

Representative bright field images are shown for the immunohistochemical staining (brown) for CCR7, HIF-1α and Ki-67 in head and neck cancer cell lines. Scale bars indicate 100 µm at 10x, 20x and 40x magnification lens. KP "keratin pearls", MV " Micro-vessles".T "Tumour cells" and S " Stromal cells".

2.3.16 Evaluation of CCR7 and HIF-1α in head and neck clinical samples

So far we have seen that CCR7 expression is upregulated under hypoxia in different head and neck cell lines. Furthermore in our chosen model, OSC-19 cell line, we observed that CCR7 is upregulated by ROS induction, serum deprivation and $CoCl_2$ treatment that mimic hypoxia in cell culture. Since $CoCl_2$ is used to stabilize HIF-1α, we can infer that the increase of CCR7 expression is regulated by HIF-1α. Furthermore, our staining in xenografts of head and neck cell lines showed a trend of HIF-1α and membrane bound CCR7 expression where low Ki-67 expression is present in (OSC-19, Detroit 256 and A-253) xenografts compared to FaDu xenograft that showed cytoplasmic CCR7 with no HIF-1α staining compared to high levels of Ki-67.

These *in vitro* studies were sufficiently encouraging for us to extend our investigation to correlation between HIF-1α and CCR7 in cancer patients at different stages of the disease. We used head and neck microarrays with n=80 patients' sample that were scored independently by two head and neck pathologists using the H-score system. For representative photos of CCR7 and HIF-1α staining see (Figure 47 and Figure 48) respectively. First we evaluated if CCR7 or HIF-1α expression is different in cancer samples from normal tissue samples using Mann-Whitney U test Figure 49. The increase of CCR7 expression was significantly different from normal patients with $P < 0.01$. We did observe a decrease of HIF-1α expression however, that was shown to be not significant with $P = 0.16$. Next, we set to evaluate if high expression of CCR7 or HIF-1α (H-score > 150) is associated with cancer clinical stages and histological grades compared to

normal tissues. Table 11 shows number of tissues expressing high or low level of CCR7 or HIF-1α. Our results showed that high expression of CCR7 is associated with cancer in stage 1 and stage 4 compared to normal (See Table 12). However, high expression of HIF-1α was not associated with cancer in any clinical stages compared to normal (See Table 12). Furthermore both the high expression of CCR7 and HIF-1α was associated with cancer in grade 1 compared with normal with P = 0.0001 and 0.018, respectively for CCR7 and HIF-1α (Table 13). Finally a correlation between CCR7 and HIF-1α was evaluated in each stage and grade. An increase in correlation (R) between CCR7 and HIF-1α was observed with increase in clinical stage (Figure 50). Similarly, expression of CCR7 was highly correlated with HIF-1α in lymph node metastases (Figure 50). Furthermore, there was a correlation between CCR7 and HIF-1α in all grades with the highest correlation observed in grade 1 (R=0.68, P=0.004) Figure 51.

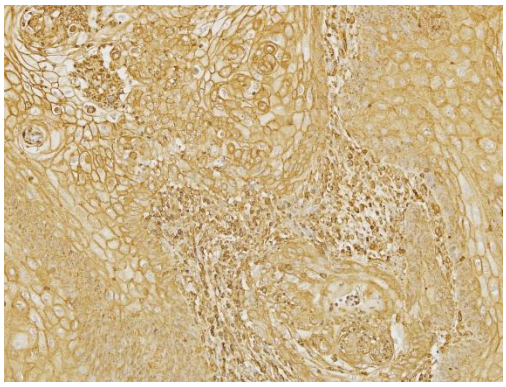

Strong intensity (3)

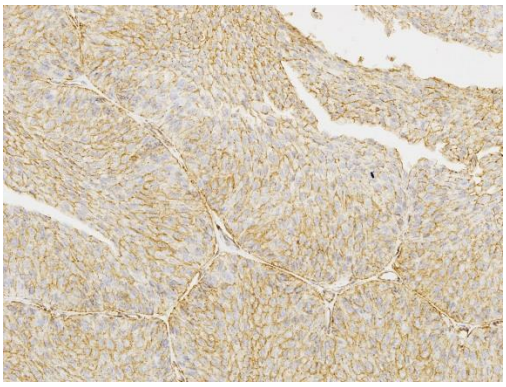

Moderate intensity (2)

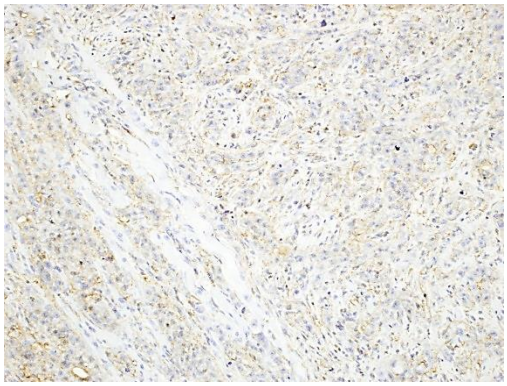

Weak intensity (0)

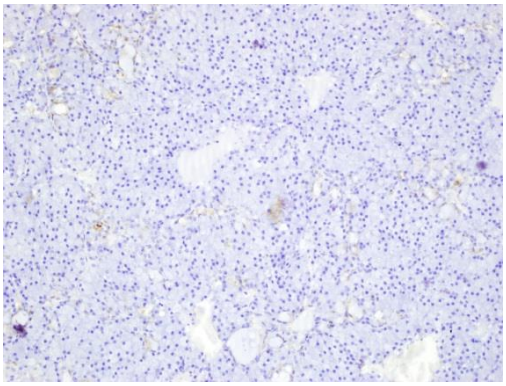

-ve

Figure 47: Expression level of CCR7 in tissue microarrays. The CCR7 expression was membrane bound and cytoplasmic in tumour cells.

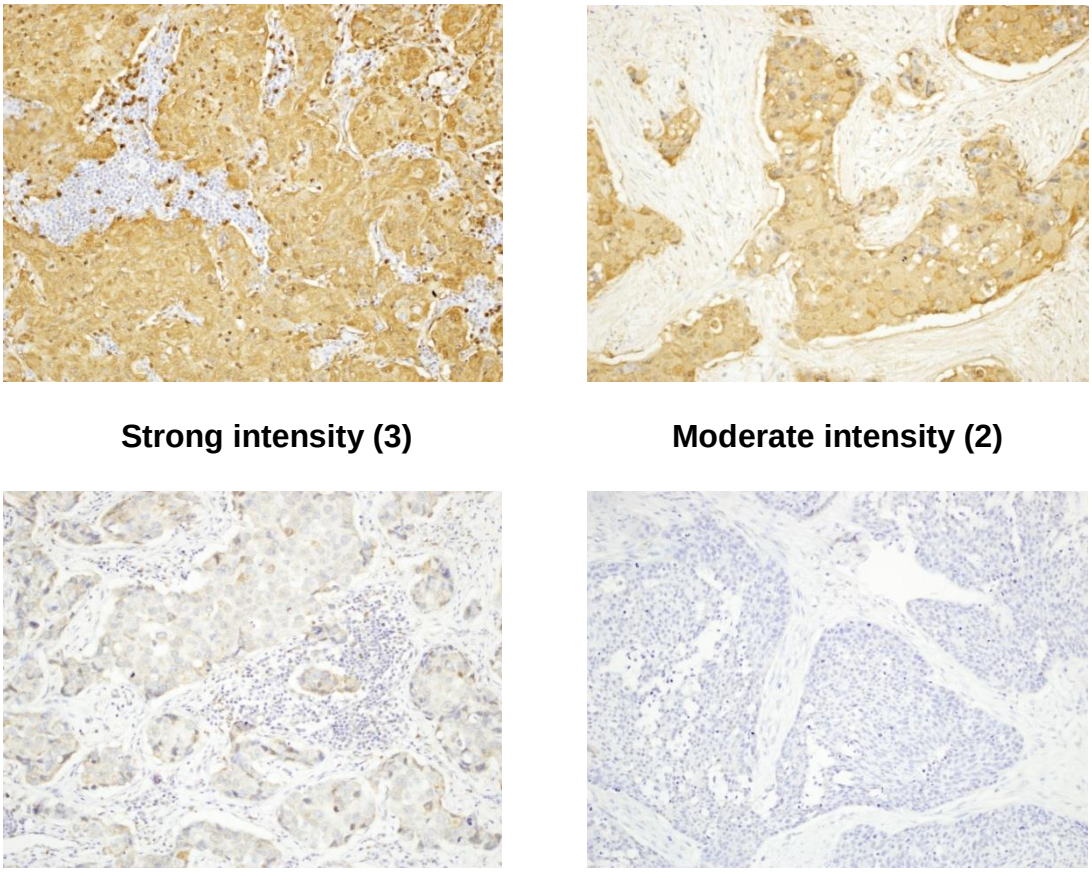

Figure 48: Expression level of HIF-1α in tissue microarrays. The HIF-1α expression was found in the nucleus and the cytoplasm of tumour cells.

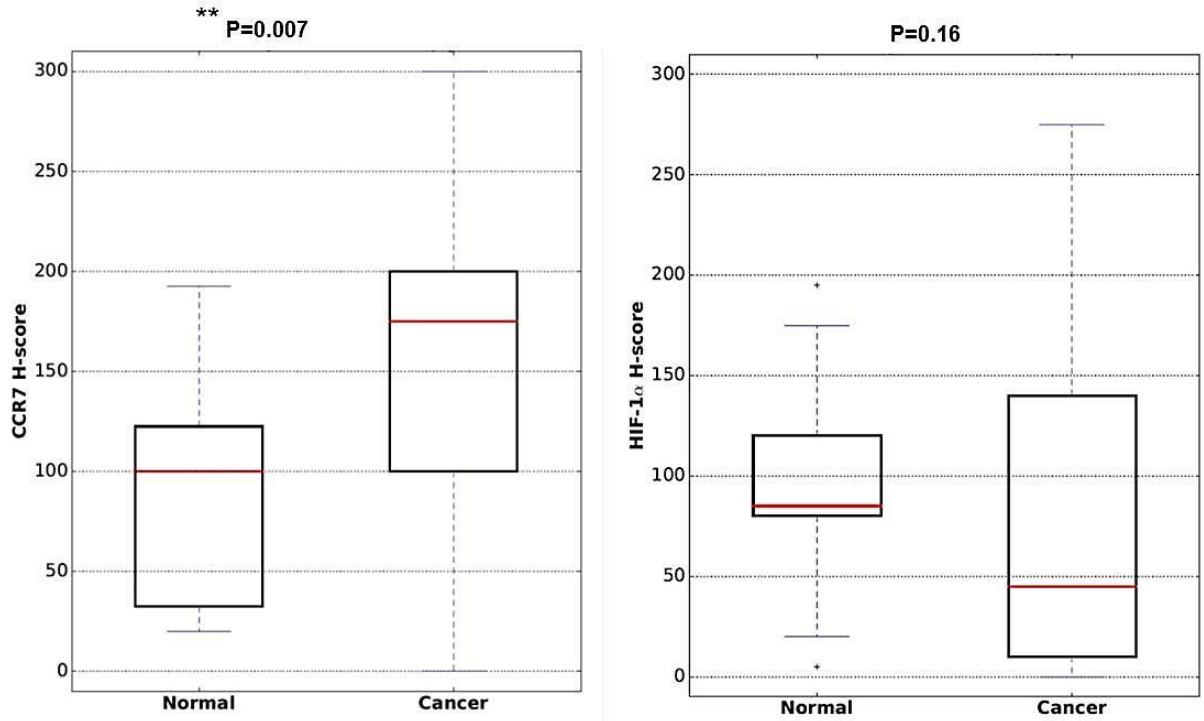

Figure 49: Difference of expression for CCR7 and HIF-1α between normal and cancer patients. P- values were calculated using Mann-Whitney U test.

Table 11: Number of patients expressing high and low of CCR7 and HIF-1α

	CCR7		HIF-1α	
	Low (n)	High (n)	Low (n)	High (n)
Normal	9	2	9	2
Malignant	28	41	53	16

Table 12: Association of high expression of CCR7 or HIF-1α with cancer in different stages of cancer. (LN) = lymph nodes

	CCR7			HIF-1α		
	Low (n)	High (n)	P	Low (n)	High (n)	P
Normal	9	2		9	2	
Stage 1	0	6	P=0.002**	2	4	P=0.1
Stage 2	12	11	P=0.14	18	5	P=1
Stage 3	8	11	P=0.06	17	2	P=0.6
Stage 4	5	8	P=0.05*	10	3	P=1
LN metastasis	3	5	P=0.07	6	2	P=1

Table 13: Association of high expression of CCR7 or HIF-1α with cancer in different histological grades of cancer. (LN) = lymph nodes.

Grade	CCR7			HIF-1α		
	Low (n)	High (n)	P	Low (n)	High (n)	P
Normal	9	2		9	2	
Grade 1	1	15	P=0.0001**	5	11	P=0.018*
Grade 2	11	15	P=0.26	23	3	P=0.6
Grade 3	9	7	P=0.23	16	0	P=0.16

Stage I
R= 0.22 P= 0.67

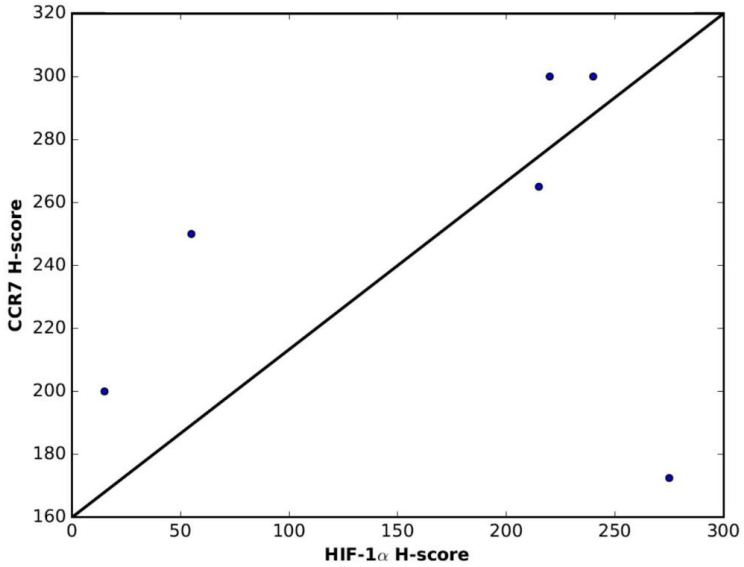

Stage II
R= 0.47 P= 0.03

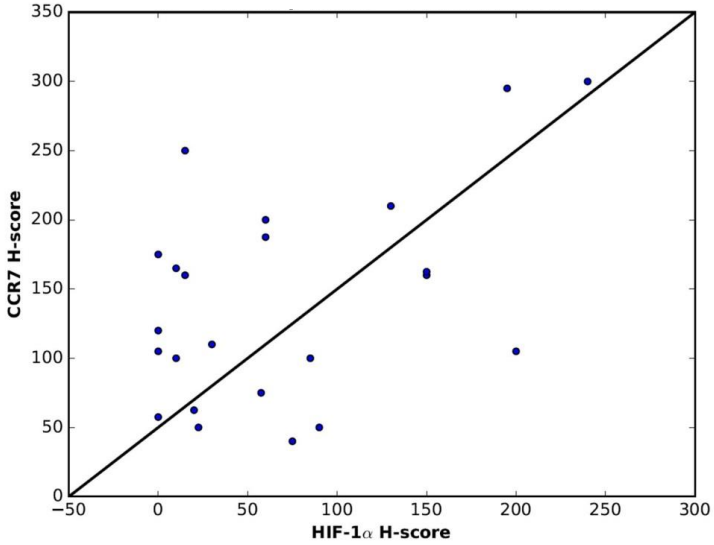

Stage III
R= 0.62 P= 0.005

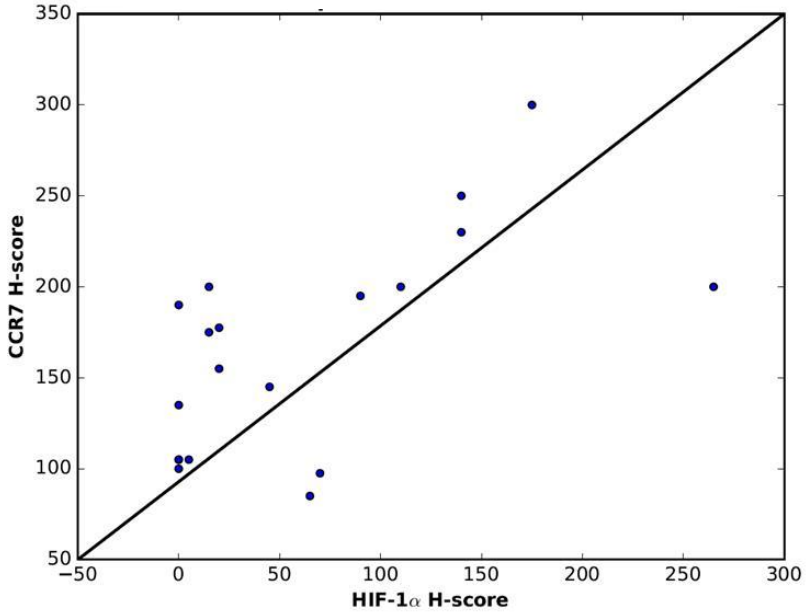

Stage IV
R=0.79 P=0.001

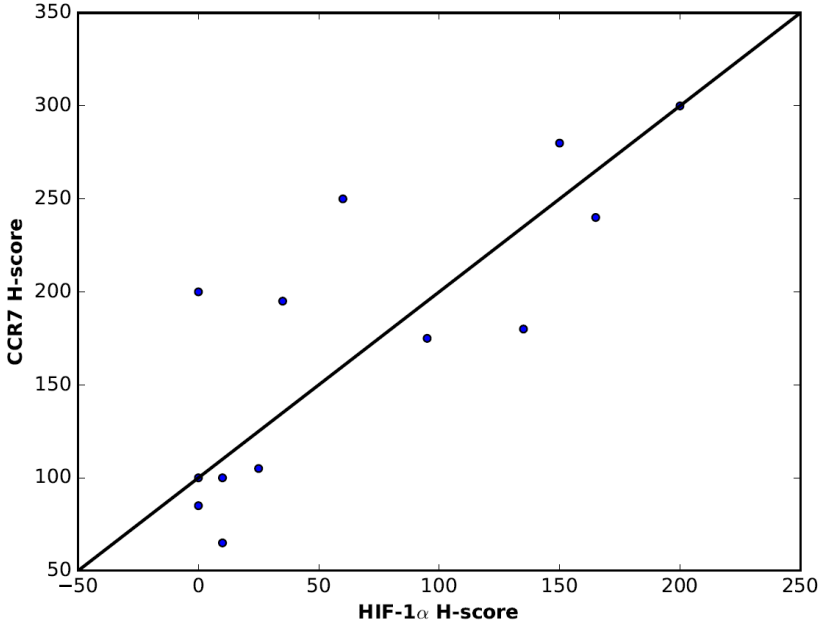

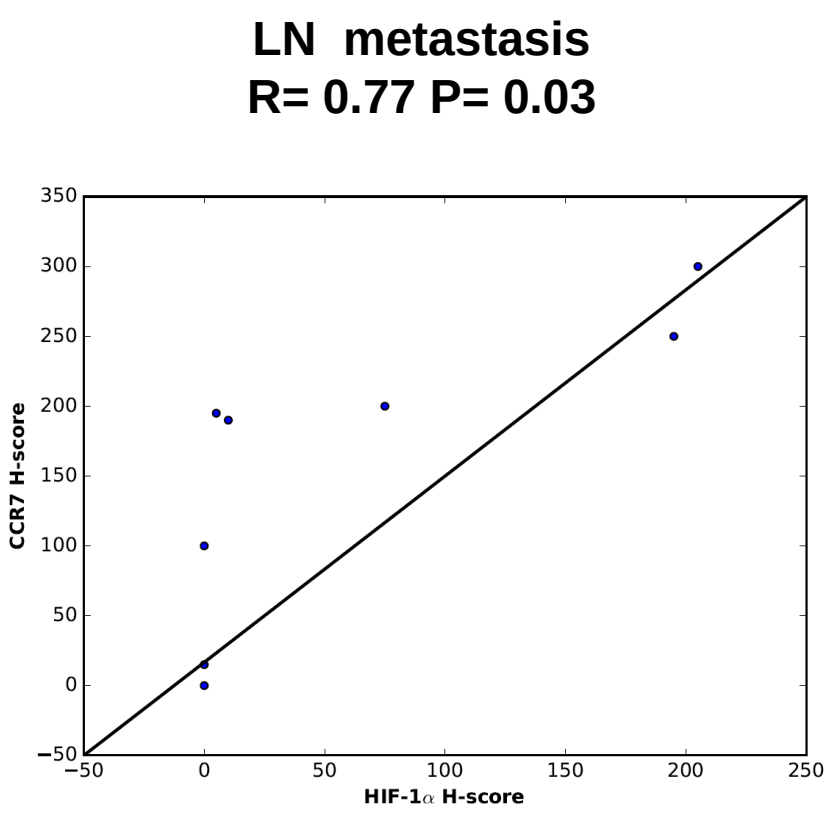

Figure 50: Correlation between CCR7 and HIF-1α in different clinical cancer stages. The correlation is increased with the increase of the stage. Correlation (R) and P-values are calculated using Pearson test.

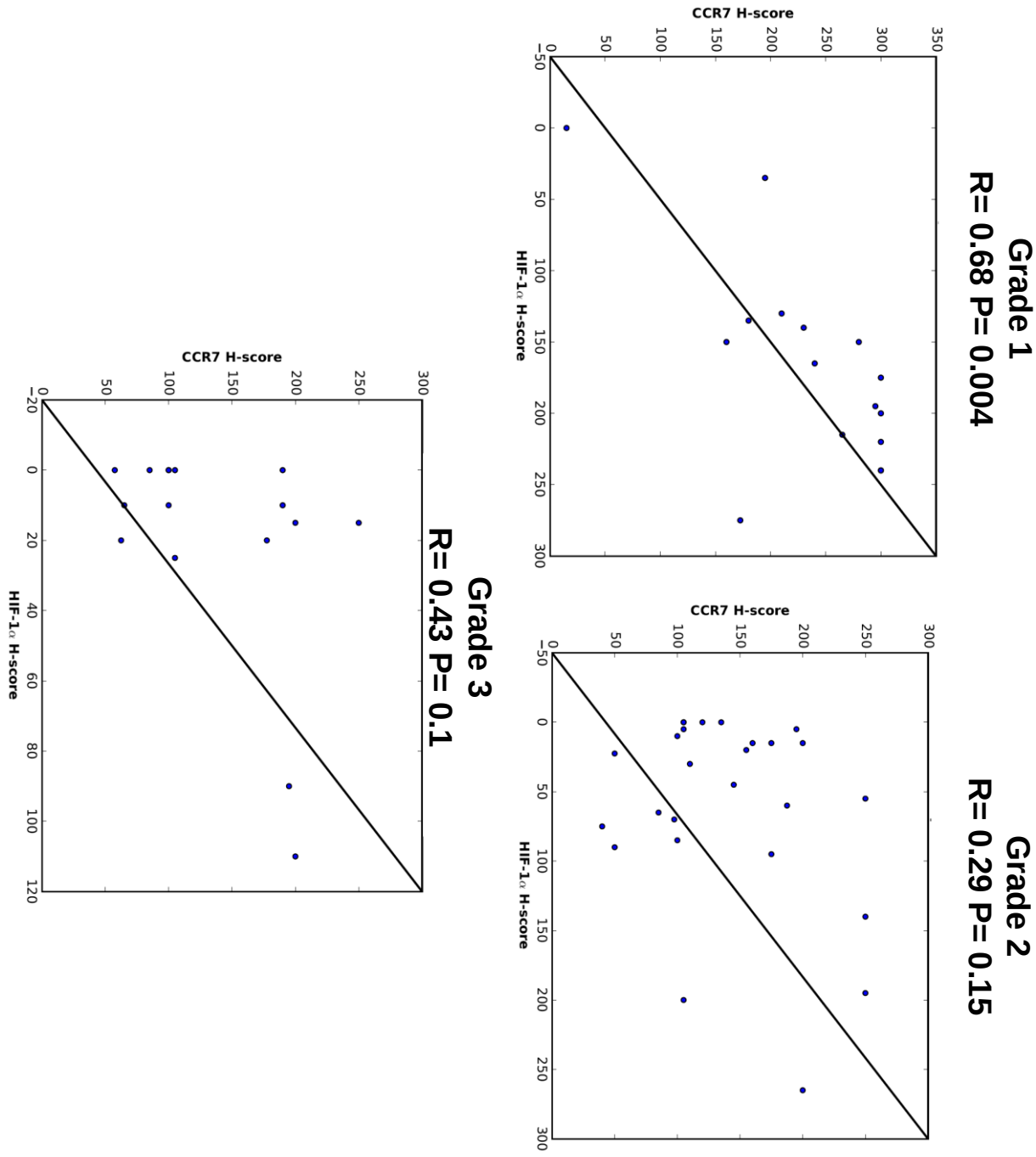

Figure 51: Correlation between CCR7 and HIF-1α in different histological grades. The correlation is only observed in grade 1 with **P < 0.01. Correlation (R) and P-values are calculated using Pearson test.

2.4 Discussion

The involvement of the chemokine receptors in the metastatic process is well demonstrated in the literature (chapter 1). In particular, the expression of CCR7 on cancer cells facilitate their homing to the lymphatic system, at which CCL21 is abundantly expressed whilst CXCR4 expression assists metastasis to brain, lungs, liver and bones where CXCL12 is abundant (Muller et al., 2001).

The present investigation was aimed at studying the expression levels of CCR7 in different cancer cell lines, 3D models and clinical tissue; and about how the level of expression changes upon stress, mainly hypoxic stress; and the CCR7 mediated functional changes in cells as a result of those stress factors. Here the discussion of this chapter is divided in subsections in order to make it easier to follow for the reader.

2.4.1 Expression of CCR7

We used three techniques to assess expression of CCR7 in a number of cancer cell lines including; breast (MCF-7 and MDA-MB-231), head and neck (SCC-4, OSC-19, FaDu, Detroit 265 and A-253), pancreatic (PANC-1), glioma (U-87 MG), prostate (PC-3 and DU-145) and colon (SW-480, COLO-205, DLD-1 and HT-29). Immunofluorescence (IF) is a readily available staining technique that allows us to detect the expression of proteins by visualising a protein in the cell, and to determine if it is present in the cell membrane, the cytoplasm or/ and nucleus. CCR7 is a cell surface receptor but is synthesised and “recycled” through mechanisms that take it into cytoplasm. In our method, cells were permeabilized

after fixing. This allows antibodies to cross into the cytoplasm and interact not only with any protein which is membrane bound, but also in the cytoplasm. Our results, indicate that CCR7 was present in all the investigated cell lines, except for SW-480, HT-29, and that its expression was confined to the membrane or/and the cytoplasm. As chemokine receptors are GPCRs 7TM receptors, it is expected that the protein is mostly found on the membrane. However, some cytoplasmic expression is also expected resulting from the *de novo* synthesis of CCR7, or internalised receptor. Failure to see a relatively larger membrane bound expression compared with cytoplasmic expression, as was the case with U-87 MG and DU-145 cells can be the result of receptor internalization, protein translocation, degradation or a defect in the signal peptide domain that results in membrane bound translocation failure as proposed by (Na et al., 2008). Indeed in the previous study, the CCR7 protein expression was only detected in the cytoplasm and not on the cell membrane in 15 colorectal cell lines including COLO-205, SW-480 and HT-29, suggesting that this is not uncommon for CCR7.

We used IF at first to give us a hint in which cell lines we should expect expression in order to eventually find a good model for *in vitro* studies. Whilst IF provides an easy visual means of detecting CCR7, it does so selectively for those cells within a field of view under a microscope and is qualitative. Therefore, to confirm and validate these IF results, we quantified membrane bound CCR7 expression using a qualitative technique (flow cytometry) in the same cell lines. In this experiment, cells were fixed but not permeablised. Hence, only the expression on the cell surface is detected.

We showed that the expression of CCR7 was highest in pancreatic and head and neck cancer cell lines and lowest in the colon cell lines. These results were in agreement with previous studies. Pancreatic cell lines were shown to be expressing CCR7 and functionally respond to CCL19 and CCL21 in 2D and 3D cell migration models (Sperveslage et al., 2012). Similarly, it has been shown that CCR7 is highly expressed on human tongue cell line SCC-4 and contributes to migration and invasion *in vitro* (Xia et al., 2014).

Another chemokine receptor that is often co-expressed along with CCR7 in cancers, including breast, melanoma, pancreatic and head and neck cancer, is CXCR4 (Pinto et al., 2014, Guo et al., 2013, Ueda et al., 2010, Su et al., 2014); and in addition the high expression of both correlates to poorer prognosis than high expression of either of them alone. Thus, both CCR7 and CXCR4 presence can be utilised as a biomarker for metastasis, we can therefore infer that developing antagonists that target either or both receptors might potentially have better therapeutic benefits, reducing LN metastasis and increasing patient survival

It has been reported that whilst CCR7 mRNA was expressed in 9 HNSCC (head and neck squamous cell carcinoma) cell lines whereas only 3 of them expressed CXCR4 (Ueda et al., 2010). The expression of CCR7 on patient derived tissues correlates highly with lymph node metastasis in pancreatic and head and neck cancers (Ueda et al., 2010, Guo et al., 2013, Nakata et al., 2008).

Our results showed a correlation between CCR7 and CXCR4 expression in many of the cell lines. Notably however, CCR7 expression was higher in all of the cell

lines apart from the prostate cell lines DU-145, PC-3 and the head and neck FaDu, in which CXCR4 expression was higher than CCR7. We note that the expression of CXCR4 in DU-145 and PC-3 has been shown also by some others to be high (Sun et al., 2003, Taichman et al., 2002, Dehghani et al., 2014, Arya et al., 2004). Even though Engl et al (Engl et al., 2006) reported low expression of CXCR4 on DU-145; they nonetheless showed CXCR4 functional responses on DU-145 cells. Our results showing no CXCR4 expression on HT-29 is in agreement with previous literature data (Nimmagadda, 2012, De Silva et al., 2011).

Also in agreement with previous studies (Na et al., 2008, Kawada et al., 2007), our results indicate that the membrane bound expression of CCR7 on colon cell lines was the lowest among the panel of the cell lines tested and that 2 cell lines, namely COLO-205 and SW-480 showed no expression at all.

Western blot data confirm the pattern of expression results from IF and flow cytometry; showed that CCR7 is expressed on the COLO-205 and SW-480 colon cell lines, but as the method we used is only semiquantitative, the differences in CCR7 expression levels among the cell lines was not seen to the same degree as was in the flow cytometry. Western blots were carried out on cell lysate and hence, unlike flow cytometry, total protein content of the cell is analysed.

Whilst, generally speaking, the data from the three different techniques used to determine CCR7 protein expression were in agreement, there were some discrepancies. These discrepancies in expression observed in some cases could be attributed to the different experimental techniques between the different

methods used to detect CCR7 expression, for instance, in the western blot method; the intracellular and membrane bound expression of CCR7 was detected whereas in flow cytometry only membrane bound expression was shown since cells were not permeabilised. In addition, the underlying reason for some of the discrepancies may have to do with localisation of the CCR7 and the inability of the cells to translocate it from the cytoplasm to the membrane.

This is exemplified by the following observation from the literature. Western blot had been used as a detection method for the expression of CCR7 on colon cell lines (Li et al., 2011, Yu et al., 2008). However, a more recent investigation by Na et al has shown that CCR7 is expressed intracellularly but not on cell membrane on colon cell lines (CaCo2, COLO-205, COLO-206F, COLO-320, Cx2, Cx94, DLD-1, HCT116, HT-29, LS174T, SW-403, SW-480, SW620, SW948, SW1116). In this case, because of defects in the signal peptide domain that are responsible for translocation of CCR7 to the cell membrane, there is no significant membrane bound CCR7 (Na et al., 2008). In addition, the authors examined the migratory ability of two cell lines; COLO-205 and COLO-320, and showed that in spite of CCR7 whole cell expression they observed, the cells were not responsive to CCL21 or CCL19 in migratory assay, an observation which is similar to our result with SW-480 and DLD-1. From our results and published data, it is unclear why colon cell lines produce relatively high amounts of intracellular CCR7, hence it's been speculated by Na et al., that if CCR7 ligands are produced within these cell lines that could feed in autocrine loop activation of CCR7 proliferation/ survival. Another possibility is that these defects cause CCR7 to remain within the

cytoplasm, having completely different functions from the membrane bound variant, as proteins that undergo structural changes could either retain their known physiological functions or have different functions (Lee et al., 2003, Lasagni et al., 2003).

Following on from determination of CCR7 expression in cultured monolayered cells, we turned out attention to the expression on the same cells when grown as xenografts. The tumour microenvironment consists of tumour cells and non-malignant cells within a matrix that communicate and interact with the cancer cells. This cross-talk between malignant and non-malignant cells may alter the expression of different proteins (Balkwill et al., 2012). Furthermore, it is known that cancer cells growing *in vivo* face stress conditions very different to the one's encountered in monolayerd cultures, such as hypoxia and lack of nutrients, they also avoid immune responses, and in order to do so, may alter protein expression (Kawada et al., 2007) (However, please note that our xenografts were grown in immunedeficient mice). For example, in melanoma cells, the expression of the chemokine receptor CXCR4 is decreased and the expression of CCR7 is increased, after xenotransplantation (Pinto et al., 2014). Therefore, it becomes critical to confirm CCR7 expression in the tumours after transplantation, as is important to realise that the expression may change *in vivo*.

Using immunohistochemistry, we have demonstrated that in fact, cell lines retained CCR7 expression in xenografts. There were some differences however. Earlier we showed membrane bound expression of CCR7 in cultured FaDu cell line. After

transplantation, although CCR7 expression was detectable in the membrane, it appears to be mostly present in the cytoplasm.

In xenografts, the colon cell lines (DLD-1, HT-29) showed membrane bound and cytoplasmic expression of CCR7 that was lower than the other cell lines grown as xenografts. COLO-205 showed very little cytoplasmic expression of CCR7 compared with the other cell lines. From the literature, we found no investigation of the expression of CCR7 in xenoplanted colon cancer cells; however, data from colon clinical samples is somewhat contradictory. Some authors have shown that the expression of CCR7 on colon tissues was lower than for other chemokines receptors, namely CXCR3 and CXCR4, and that there was no correlation with lymph node metastasis (Kawada and Taketo, 2011). However, others have shown that CCR7 expression on colon clinical samples is strongly correlated with LN metastasis (Gunther et al., 2005). This contradiction could be related to different cellular distribution of CCR7 rather than level of CCR7 expression.The former study used flow cytometry as the detection method while the latter one used IHC. In summary, regarding CCR7 expression data, the head and neck cell lines (OSC-19, Detroit 562) showed the highest membrane bound expression xenografts which agree with the data from flow cytometry.

It is very important to use the correct technique to look for the membrane bound expression of CCR7, as some techniques can show high expression of only intracellular protein and that could be misleading, assuming that this will also correlate to membrane bound expression. It is sometimes difficult to precisely differentiate between membrane bound and cytoplasmic expression of CCR7 in

IHC/IF staining. Therefore, the expression of membrane bound CCR7 cannot be judged only by immunohistochemical studies especially when choosing models to study the functional role of the receptor, as this can lead to false negative results.

In regard to our expression studies of CCR7 in clinical samples, our results showed that the difference of CCR7 expression in head and neck cancer patients compared to normal patients was significant and its high expression in primary tumours was correlated with the clinical stage 1 and 4, grade 1 and lymph node metastasis. Our results are in agreement with CCR7 clinical studies in breast (Liu et al., 2010), tongue carcinoma (Xia et al., 2014), lung (Takanami, 2003), colon and pancreatic (Nakata et al., 2008). Of note, scoring was performed blind to patient clinical characteristics by two pathologists independently.

Finally, all of the expression results in head and neck cancer were encouraging to start functional studies and learn more about CCR7 regulation in cancer in attempt to find a good model for evaluating CCR7 antagonists.

2.4.2 Effect of CCL21/CCL19 on CCR7 activation

Activation of chemokine receptors by its ligands can stimulate chemotaxis, cell growth, migration and invasion (Balkwill, 2012) through activation of a number of intracellular signalling cascades (see chapter 1). However, the presence of the CCR7 receptor on the surface of a cell, does not necessarily guarantee that the cell can respond to CCR7 signalling. There can be a number of reasons that the binding of the chemokine ligand would not initiate a G-protein mediated intracellular signalling cascade. Therefore, it is important to establish that any

receptors which are expressed on the cell surface are “functionally active” meaning that the binding of the chemokine results in a measurable pharmacological response, such as growth, migration and invasion. For this reason, we also assessed functional response of CCR7 expressing cells to chemokines CCL19 and CCL21.

We found increased migration (compared to control) of OSC-19, PC-3, SCC-4 and FaDu cells but not of SW-480 and DLD-1 upon addition of CCL21 in a scratch assay. The inability of SW-480 to migrate was consistent with the lack of membrane bound expression of CCR7. However, DLD-1 cells did not show increased migration, despite the fact that they do express CCR7. As mentioned earlier colon cell lines including DLD-1 have defects in the signal peptide domain resulting in a truncated variant of CCR7 that is unable to be translocated at the cell membrane and are therefore unresponsive to external ligands. This supports the speculation that in colon cell lines loss of function variant or post translational defects of CCR7 might be translocated to the cell membrane. Further studies will be necessary to determine whether this is the reason behind unresponsive membrane bound CCR7 in colon cell lines.

The CCL21/CCR7 axis in cancer has been shown to play a significant role of migration *in vitro*. In a recent study, Xia et al., SCC-4 head and neck cell line showed increased migration in a wound healing assay in SCC-4 expressing CCR7 compared with siCCR7 SCC-4 cells (Xia et al., 2014). Furthermore, SCC-4 failed to migrate to the same extent in CCR7 knockdown cells, upon addition of CCL21.

These findings are consistent with our findings in head and neck SCC-4, OSC-19 and FaDu cells.

Our results also showed a difference between cell migration upon addition of CCL21 (100 nM) and CCL19 (100 nM). OSC-19 cells migrated more readily upon CCL21 addition but not with CCL19 addition.

This difference between CCL19 and CCL21 has been previously mentioned in the literature regarding dendritic cell migration. DCs migrate towards CCL21, but not CCL19 at concentration higher than 20 nM (Steen et al., 2014, Ricart et al., 2011, Nandagopal et al., 2011). Furthermore, Catusse et al., have shown that migration of leukaemia cells towards CCL19 is dependent on the expression of the atypical chemokine “decoy” receptor CRAM (more commonly known as CCRL2) but not CCR7 (Catusse et al., 2010). Whereas, the migration towards CCL21 was not affected by CRAM expression. Therefore, studies on the expression of CRAM in cells which are unresponsive for CCL19 are important.

Regarding CCL19/CCR7 axis, only a few studies have been reported on the role of this interaction in the migration of cancer cells. The only previous report of migration towards CCL19 in a wound healing assay in head and neck cancer was an increase the migration of metastatic PCI-4B and PCI-37B cell lines, (*i.e.* decreased the free surface area) after migration (Liu et al., 2014). Therefore, CCL19 can enhance migration in some cell lines. However, in none of the five cell lines we assessed, was an increase in migration was detectable upon addition of CCL19. The observed difference between our results and those of Liu et al results

can be either due to different cell lines (PCI-4B and PCI-37B are derived from the metastatic lymph nodes of head and neck patients) behaving differently but further investigation may be warranted.

Regarding the wound healing assay, a key point to be answered is if the cells movement is a result of proliferation, migration or both. To clarify this, we stained the cells with proliferation marker Ki-67 using the immunofluorescence technique. The expression of Ki-67 protein is associated with cell proliferation (Scholzen and Gerdes, 2000). Ki-67 is expressed in the nucleus, mainly in the nucleoli during the interphase of cell cycle (Pathmanathan and Balleine, 2013). Our Ki-67 staining in the wound healing assay revealed that the OSC-19 cells did not express Ki-67; hence, the cells are not proliferating during the wound healing experiment. The migrating cells do express CCR7; indicating its role in cancer cells migration.

In order to clarify that CCR7 is activated by both ligands and that the effect seen in migration is related to differential roles of the ligands depending on cell type or/and differential binding to other receptors that eventually might lead to internalization and degradation. We used the Ca^{2+} flux as an indication of receptor activation in OSC-19 cells. Both ligands resulted in CCR7 activation with the response induced by CCL21 being higher than that induced by CCL19. This difference in receptor activation can be due to the different binding affinity of CCL19 and CCL21(Yoshida et al., 1998). We had previously shown that EC_{50} for CCL19 and CCL21 in Ca^{2+} flux mobilisation is 28 and 13.5 nM respectively (AHMED, 2016).

It is clear from our results that the CCR7/CCL21 axis is important for cell migration and also might indicate a different role for CCL19 and CCL21 in the migration of tumour cells. Of note, it has also been reported that lymph nodes express CCL21 to a significantly higher level than CCL19 (Muller et al., 2001). It could be inferred from our *in vitro* results that CCR7 expressing tumour cells may migrate to the lymph nodes where CCL21 is highly expressed.

2.4.3 Evaluation of CCR7 role in proliferation and tumour growth

The data regarding the role of chemokines CCL19 and CCL21 and CCR7 on cell proliferation is contradictory. It has been reported that CCL21 induced cell growth in bladder and lung cancer cell lines (Mo et al., 2015, Xu et al., 2011). Similarly, in thyroid carcinoma it was observed that the proliferation rate was higher with cells cultured with CCL21 than cells cultured without CCL21 in free serum (Sancho et al., 2006). However, a recently published study in another head and neck cell line, SCC-4 (Xia et al., 2014), in which CCR7 knockdown had no significant effect on cell proliferation.

We examined the effects of CCR7 activation on the proliferation in OSC-19 and FaDu cells. We choose these cell lines because of their contrasting Ki-67 staining in xenografts. The Ki-67 expression was very low in OSC-19 in comparison with FaDu (See section 2.3.14). We found that neither CCL21 nor CCL19 increased cell growth after 72 h treatment in either cell lines. Furthermore, differential effect of exogenous and endogenous CCL21 has been described in melanoma cell lines (Shields et al., 2010). In this publication, shRNA was used to knockdown CCL21 or overexpress CCL21 endogenously within the melanoma cell lines. Interestingly,

high CCL21 expressing cells grew significantly larger than low CCL21 expressing cells. However, the addition of exogenous CCL21 had the same effect on the growth of both high and low expressing CCL21 cell lines. Altogether, our results indicate that activation of CCR7 has no or little effect on the proliferation of head and neck cancer cells, in comparison with other cancer types like thyroid and bladder, this might be related to differential effects of exogenous and endogenous activation of CCR7 as shown by (Shields et al., 2010) or different effect of CCL21 in different cancer.

2.4.4 Increase of CCR7 expression and production of CCL21 under stress

As mentioned above, stress conditions may alter the expression of chemokine receptors and their response to their cognate ligands. Accordingly, we examined the effect of serum deprivation on the expression of CCR7 on OSC-19 cells. Our results indicate an increase by 24% significant change in expression; thus, it is possible to assume that the increase in CCR7 expression helps the cells to survive under stress by autocrine activation. Sancho et al., have also shown that CCR7 expression is increased upon serum starvation for 72 h by 53% in thyroid carcinoma (Sancho et al., 2006).

Chemokines and their receptors are major players in cancer related inflammation (Allavena et al., 2011). A variety of chemokines have been detected in tumour cells. For instance, the increased expression of CCL2, CCL5 and CCL17 by tumour and stromal cells was correlated with recruitment of monocytes, leukocytes and lymphocytes that eventually promote tumour progression and immune evasion (Allavena et al., 2011). Therefore, to stress cell mechanically, we wounded the

cells several times and incubated them in low serum conditions. The OSC-19 cells were able to generate statistically significant amounts of CCL21, compared with no wounded control, indicating the importance of CCL21 in the cellular stress process and its role in supporting tumour progression. It was reported that cells of head and neck cancer secrete CCL19 after serum starvation that was detected by Elisa which leads to the activation of CCR7 and promotes tumour growth and progression (Wang et al., 2008). Furthermore, endogenously expressed CCL21 can increase tumour growth and recruitment of host immune cells that support tumour progression by immune evasion in melanoma (Shields et al., 2010). A substantial amount of clinical data in cancer has indicated that infiltration of certain immune cells is correlated with poor prognosis (Kitamura et al., 2015, Yaguchi et al., 2011). Furthermore, we have observed that head and neck xenografts express CCL21. The expression of CCL21 in tumour cells was reported in breast cell lines (Tutunea-Fatan et al., 2015) and head and neck cell lines and clinical samples(Wang et al., 2008).

The expression of CCL21 has shown to be involved in recruiting T regulatory cells that suppress the immune respones that eventually support tumour progression (Shields et al., 2010). Therefore, secretion of CCL21 under stress will provide survival and progression cues for the tumour growth.

2.4.5 Role of hypoxia in the regulation of CCR7

We have mentioned earlier that tumours growing in a body encounter different conditions to cells cultured *in vitro* (Herrmann et al., 2014, Nyga et al., 2011). One of the key differences is that solid tumours usually develop a hypoxic centre that

accounts for major component of the tumour mass. When tumours grow beyond 200 μm, they have reduced blood supply, resulting in oxygen and nutrient deprivation. Clearly, understanding how hypoxia can influence cancer cells is highly relevant to development of new therapeutics. However, because it is difficult to analyse cells in the tumour microenvireonmnet, we have to rely on simpler 2D and 3D models and artificial conditions that can mimic the intratumoural environment. So we first looked at the expression of CCR7 on head and neck cancer cell lines under low oxygen (hypoxia) conditions.

Our results under hypoxia showed that CCR7 was upregulated significantly in the head and neck cell lines we tested (OSC-19, FaDu and Detroit 562). Our observations are consistent with studies on CCR7 upregulation under hypoxia in lung and breast cancer (Li et al., 2009, Wilson et al., 2006). However, in SCC-4 cell lines, which showed the highest expression under normoxia, there was no significant increase of CCR7 expression under hypoxia. Reasons for this are unknown but it could be because the expression of CCR7 under normoxia was already very high to start with.

Growing cell lines as 3D multicellular spheroids mimics the tumour in terms of oxygen and nutrient diffusion better than monolayer culturing. However, as there is no blood supply in spheroids, xenografts would still be a better model to study the behaviour of cells *in vivo*, and to gain a better understanding of how efficient our therapeutic agents can be in reducing cancer progression.

We grew OSC-19 spheroids of about 500 µm diameter. As stated before, 200 µm is the limit of oxygen diffusion, so we did expect the cells in the core of the spheroids to experience hypoxia. We observed that the regionalization of pimonidazole staining matches with the proliferation parameters Ki-67. Furthermore, the CCR7 expression was more intense in the hypoxic core compared with the outermost layer. To our knowledge, the only other study of CCR7 in spheroids was conducted in pancreatic cell lines, in which it has been shown that CCR7 expression was upregulated when the pancreatic cell lines were grown as spheroids (Sperveslage et al., 2012). Although the authors have not looked for the reason of the CCR7 upregulation in the spheroids, they assumed that because the CCR7 gene bears a hypoxia response element that HIFs can bind to it, therefore the CCR7 upregulation could be potentially hypoxia related.

Our results in 2D and 3D showed that CCR7 expression was upregulated under hypoxia. The effect of hypoxia is characterized by changes in the expression of a large number of genes, many of which are regulated directly or indirectly by HIFs. HIFs are α/β heterodimeric DNA binding complexes that direct extensive transcriptional responses, involving the induction of genes with important roles in several aspects of tumor biology, such as angiogenesis, metabolic reprogramming, growth, survival and metastasis. The HIF system is regulated by the activity and abundance of HIF-α subunits (see section 2.1.2). To date, the best characterized known HIFs are HIF-1α and HIF-2α.

In order to identify whether the CCR7 upregulation under hypoxia is controlled by HIF-1α, we treated OSC-19 with $CoCl_2$. It is known that $CoCl_2$, directly hinders the

interaction between pVHL and hydroxylated HIF-1 causing the stabilization of HIF-1α even in the presence of oxygen. Thus, HIF-1α escapes degradation and subsequently heterodimerises with HIF-1β leading to the active HIF-1 transcription factor binding to the hypoxic response element of the promoter region of many target genes. Hence, $CoCl_2$ is used to mimic HIF-1α dependent transcription changes seen during hypoxia.

We showed that $CoCl_2$ caused significant induction of HIF-1α at 200 μM as well as CCR7 upregulation compared with cells untreated with $CoCl_2$. This confirms that HIF-1α is involved in the upregulation of CCR7.

However, this increase of CCR7 expression caused by hypoxia and $CoCl_2$, did not increase the cell migration in response to CCL21 compared with cells treated only with CCL21. On the contrary, hypoxic or $CoCl_2$ treated cells has higher free surface area after migration upon CCL21 addition compared with cells treated with CCL21 alone. These contradictory effects of hypoxia and $CoCl_2$ might be related to a reduction of ROS caused by $CoCl_2$ or hypoxia.

Since the role of ROS in cell migration is well known in the literature (Hurd et al., 2012, Panieri and Santoro, 2016), we decided to investigate this more. Cancer cells exhibit increased levels of ROS production compared with normal cells. The ROS in cancer cells serves different functions. At low concentration ROS may lead to stimulation of cellular pathways for proliferation, cell migration and invasion (Ma et al., 2013). For instance, it has been reported that the increase in ROS level resulted in increase of cell migration in prostate and breast cancer (Ma et al., 2013,

Polytarchou et al., 2005). The exact mechanisms how ROS are involved in tumorigenesis are unclear. It has been shown that ROS can activate the PI3K/Akt/mTOR survival pathway as well as promoting tumour cell survival through the activation of NF-κB and NRF2, transcription factors that increase the expression of antioxidants to avoid ROS-dependent mechanism of cell death (Zablocka and Janusz, 2008). The best characterized mechanism of ROS induced tumour progression and metastasis is HIF-1α stabilization (Sullivan and Chandel, 2014). Furthermore, the increased ROS levels lead to proteases and MMPS activation that are involved in the recognition and degradation of basement membranes as well as in the formation of invadopodia (Tafani et al., 2016). Moreover, ROS also triggers the recruitment of a series of actin-associated proteins such as cofilin and fascin as well as integrins and signalling proteins such as c-Src tyrosine kinases that also assemble together to form the invadopodia (Tafani et al., 2016). These findings suggest that an increase in ROS levels below the threshold for cell death is involved in causing structural changes and adaptive responses in tumour cells to stimulate cell migration and invasion Figure 52. Moreover, tumour cells also express increased levels of antioxidant proteins such as glutathione and superoxide dismutase to help to detoxify from ROS to keep ROS at the required level for cancer progression rather than cell death (Poljsak et al., 2013, Liou and Storz, 2010).

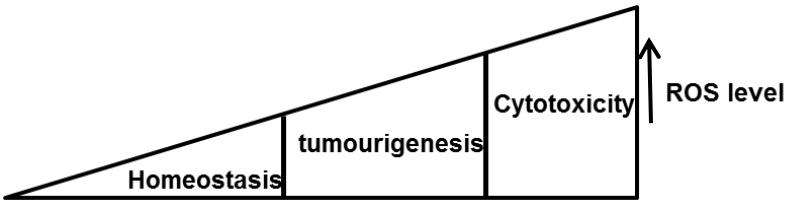

Figure 52: Effect of ROS level on cells.

Our data showed that $CoCl_2$ and hypoxia caused a reduction in ROS levels in OSC-19 cells. This reduction was observed in spite of the upregulation of HIF-1α detected directly in $CoCl_2$ experiment and indirectly in hypoxia (0.1% O_2 related experiments). Therefore, we can speculate that in OSC-19 model system, the cell migration was decreased despite the stabilization of HIF-1α and the accompanying CCR7 upregulation, presumably perhaps through a ROS-associated mechanism. We have not carried out any experiments to shed light on this mechanism, but we can speculate that one reason can be either a strong feedback loop from HIF-1α or directly through HIF-1α mediated decrease in ROS levels. We note that the decrease of cell migration caused by $CoCl_2$ was shown by others in HSC-3 and SCC-4 cells (Han et al., 2015) indicating that the reduction of migration caused by $CoCl_2$ in OSC-19 cells might not be cell line specific. Further investigation using SCC-4 to explore whether a reduction of ROS is observed after $CoCl_2$ treatment is warranted.

In contrast, $CoCl_2$ in HT-29 colorectal cancer cell line, are reported to cause an increase in cell migration through an increase in the intercellular level of ROS and by HIF-1α stabilization (Jeong et al., 2016). This could mean that the relationship between hypoxia, HIF and ROS levels may not necessarily be the same in different cell lines and models. Collectively, the effect of $CoCl_2$ on cell migration might depend on the net outcome between ROS production and HIF-1α stabilization; which could be cell type dependent.

Similarly to the $CoCl_2$ results, our data under hypoxia (0.1% O_2) has shown reduction of ROS level that resulted in deceased cell migration of OSC-19 cells, compared to cells cultured under normoxia. This effect of decrease ROS production under hypoxia may be expected from the low level of O_2 (Lopez-Barneo et al., 2001, Archer et al., 1993, Fan et al., 2007, Fan et al., 2008, Vaux et al., 2001, Fandrey et al., 1994). Others however, have found that ROS can be increased under hypoxia (Kondoh et al., 2013, Bell et al., 2007, Guzy et al., 2005). Even though the precise mechanism through which hypoxia increases ROS is still a matter of debate, it seems that ROS is possibly increased through release by the mitochondria electron transport (Qutub and Popel, 2008).

Mirroring the paradoxical effect of hypoxia on ROS production, the migration under hypoxia seems nearly as conflicting. While some groups have demonstrated increased level of migration under hypoxia, for example in glioblastoma and breast cancer (Nagelkerke et al., 2013, Joseph et al., 2015), others have shown decreased or no increase of migration ability of cells under hypoxia (Raheja et al., 2011, Turner et al., 1999, Qu et al., 2005, Dai et al., 2011). Our data in OSC-19 cells showed a decrease in cell migration in hypoxic cells, compared to normoxic cells despite the significant increase of CCR7. This might be due to reduction of ROS levels as described earlier, changes in the cellular metabolism that can supress cell migration or/and through downregulation of migration-related genes, such as matrix metalloproteinases (MMPs) as previously reported in other studies (Riches et al., 2009, Zhao et al., 2005). Moreover, it has been shown in bladder

cancer that migration of cells under hypoxia was ROS dependent (Shin et al., 2015).

As mentioned above, depending on the ROS level produced, NFκB and HIF-1α can be activated and stabilized respectively. Furthermore, ROS can also affect chemokine and chemokine receptor expressions (Tafani et al., 2016). Our results showed a significant induction of CCR7 expression in OSC-19 after induction of ROS by treating the cells with H_2O_2. Our result on the relationship between ROS and CCR7 is novel and has not been observed before both in cancer and normal cells; thereby further investigations are needed to understand the underlying mechanism in which ROS can affect the expression of CCR7. To our knowledge, we are first in describing a link between ROS and CCR7 in cancer, which may suggest a potential mechanism of how cells may acquire increased CCR7 and a metastatic phenotype. It has been reported that ROS increases expression of CXCR4 in cancer and immune cells (Tafani et al., 2016, Lee et al., 2007, Chetram et al., 2011). Furthermore, ROS increased prostate cancer cell migration and invasion through CXCR4, which was abolished with CXCR4 antagonist AMD3100 (Chetram et al., 2011). Our data in migration showed a decrease of free surface area after H_2O_2 treatment in which CCR7 and ROS levels were elevated, compared to cells untreated with H_2O_2. Therefore, we can assume that this increase of migration upon H_2O_2 treatment is CCR7 dependent. Future studies are needed to confirm the link between oxidative stress and CCR7 on cell migration by inducing ROS in cells in which CCR7 is blocked by CCR7 antibodies or small molecule antagonists and observe changes in cell migration.

Our evaluation of the expression of CCR7, HIF-1α and Ki-67 in xenografts also informs on the choice of suitable *in vivo* model for testing potential therapeutic agents. It is well documented that human tumours generally show significant phenotypic and genotypic heterogeneity (stage, various level of differentiation, chaotic neo-vasculature, differences in expression of genes, etc). It is generally agreed that using preclinical animal xenograft tumour models is useful for modeling the growth and spread of disease, acquiring information about the mechanisms of action and therapeutic efficacy of new anti-tumour agents. Our results showed that differentiated cells of OSC-19, A-253 and Detroit 562 xenograft express higher level of membrane bound CCR7, but not the poorly differentiated FaDu that expressed predominantly cytoplasmic CCR7. Previously, Bhattacharya et al., reported that CD31, a marker for micro-vessels showed no staining in A-253 but showed positive staining in FaDu xenografts (Bhattacharya et al., 2004). This finding is consistent with the fact that normal squamous epithelium also lacks microvessels. Because A-253 originates from the squamous epithelium, it is not surprising that well-differentiated tumour regions share this aspect of the normal differentiation process that was not seen in the poorly differentiated xenograft FaDu. Furthermore, A-253 showed positive staining of hypoxic marker (carbonic annhydrase IX and pimonidazole) at the well-differentiated regions in A-253 and the lack of hypoxia marker staining almost in the entire FaDu tumour (Bhattacharya et al., 2004, Vaughan et al., 2010). Hypoxic tumour cells are expected to be positive for HIF-1α. It was found that most of the less differentiated tumours, namely FaDu express high Ki-67 staining, but not HIF-1α. Our results in FaDu and

A-253 showed the same pattern of HIF-1α expression as shown by (Vaughan et al., 2010). Therefore *in vivo*, the FaDu model may not be a good representative of oropharyngeal cancers, and OSC-19, A-253 and Detroit 562 may make better *in vivo* models to represent the heterogeneity of human tumours. We do of course note that this was a limited study with low specimen numbers of xenografts and therefore did not allow on definitive correlation between HIF-1α and CCR7. In addition, we can postulate that there is a possible correlation of membrane bound CCR7 expression with HIF-1α encouraging enough to investigate if this correlation is present in patient tissue samples.

As expected, our evaluation on CCR7/ HIF-1α correlation in head and neck patients' samples was shown to be significant and increase with the stage level and in lymph node metastasis. Of note, this correlation was highly significant in grade 1 tumour samples indicating that the level of differentiation of tumours play a role in the CCR7/HIF-1α cycle. Our results agree with lung cancer studies in which the CCR7 expression correlated with HIF-1α expression.(Li et al., 2009), our study demonstrates that Hypoxia-HIF-1α/CCR7 is likely to regulate the invasion and migration of head and neck cancer cells under hypoxic microenvironments. CCR7 activation might play a role in promoting a more malignant phenotype of head and neck cancer and represents a therapeutic target.

In summary, CCR7 was expressed in different cancer cell lines, xenografts and clinical head and neck patients. Furthermore, conditions to mimic tumour growth *in vivo;* hypoxia, serum deprivation, cell damage stress, ROS production and 3D growth as spheroids and xenografts, highly supports the increase of CCR7 or

CCL21 in the cell lines where examined. The increase of CCR7 under hypoxia was suggested to be HIF-1α related. The activation of CCR7 by its ligands results in Ca^{2+} mobilization. The addition of exogenous CCL21, but no CCL19, caused increased in migration in different head and neck and prostate cell lines. In this context, the interaction between CCR7 and ECM to facilitate cancer cells invasion and migration is important more specifically binding to GAGs such as heparan sulfate which will induce the localization of CCL21 and activation of CCR7 receptor to start the metastatic cascade (for more information on GAGs binding see chapter 1). Furthermore, both ligands had no effect on cell proliferation implying differential effects of endogenous or exogenous ligands, autocrine/paracrine activation or cell type activation.

Accordingly, the CCR7/CCL21/CCL19 in OSC-19 cells was also further studied in knockdown studies to confirm the role of CCR7 in cell migration (chapter 3), and we investigated the role of CCL21/CCL19 in cell invasion in 2D and 3D assays (chapter 4) and finally, we evaluated the ability of CCR7 small molecule antagonists to reduce CCR7/CCL21 induced cell migration and invasion (chapter 4).

❖ **The main findings of this chapter are:-**

- CCR7 is highly expressed in different cancer cell lines, xenografts and head and neck clinical tissues.

- CCR7 was found to be upregulated under hypoxia in head and neck cell lines. Its expression was also elevated at the hypoxic core of OSC-19 spheroids. Furthermore, the expression of CCR7 and HIF-1α was positively correlated with clinical stages and histological grade 1.

- CCR7 was upregulated after serum deprivation and CCL21 was detected after cell damage in 2D cells or in head and neck xenografts.

- CCR7 was shown for the first time, to the best of our knowledge, to be upregulated in cancer, after ROS induction.

- CCR7/CCL21 binding results in receptor activation that translates into increased cell migration.

Chapter 3:

Effects of CCR7 knockdown using siRNA transfection method

3.1 Introduction

We showed in the previous chapter that CCR7 is expressed in different cancer cell lines, particularly head and neck cancer cell lines, both in cultured cells and in 3D spheroids and xenografts, as well as in clinical tissue; and that the activation of CCR7 by CCL21 contributes to cell migration in prostate and head and neck cancer cell lines. Moreover, we showed that the expression of CCR7 is upregulated under conditions of serum deprivation, hypoxia and ROS increase, potentially through induction of HIF-1α. However, we observed that the increase in CCR7 expression under hypoxia did not necessarily result in increased cell migration compared with cells cultured under normoxia in our model system of OSC-19. We hypothesized that the effects on migration might be triggered by, or connected to a reduction in reactive oxygen species (ROS) under hypoxia in this cell line (see chapter 2). We note that this reduction in ROS under low oxygen atmosphere may not be a general feature of tumours, because it has long been suggested that under physiological conditions, cancer cells continuously promote production of ROS even under hypoxia, or indeed as a consequence of hypoxia (Panieri and Santoro, 2016).

Nevertheless, taken our data in chapter 2 together with literature findings, we felt encouraged to further our investigations to examine the following aspects:- **(1)** Our data so far also showed no significant change in the proliferation rate of head and neck cancer cell lines, in contrast with some reports available in the literature of such effects in other cancer types, for example prostate and bladder cancer (Peng et al., 2015, Mo et al., 2015). This discrepancy might be

due to different experimental settings, but may also be associated with different autocrine/paracrine roles in the activation of CCR7 receptor, as discussed in the previous chapter and later in the discussion section of this chapter. Based on this observation and intrigued by other studies that suggested a role for CCR7 signaling in anti-apoptotic mechanisms in lung and bladder carcinoma cell lines (Xu et al., 2012, Mo et al., 2015); we set out to study if CCR7 mediates survival through anti-apoptotic pathways, rather than by promoting proliferation. **(2)** It's been suggested that chemokines can induce chemo-resistance (Park et al., 2014). Chemotherapy using platinum containing complexes has been shown to eventually induce resistance in head and neck cancers. It has also been demonstrated that this resistance may be mediated through CCR7/CCL21 interaction (Wang et al., 2008). Likewise, colon cancer cell lines treated with CCL21 are more resistant to doxorubicin and 5-fluorouracil, compared with non CCL21 treated cells (Park et al., 2014, Lu et al., 2016). Therefore, we hypothesized that silencing CCR7 in OSC-19 cells may result in increasing cisplatin sensitivity in OSC-19 cells. **(3)** To evaluate whether the knockdown of CCR7 expression would result in reducing the movement of cells and hence influence the disease progression in OSC-19 head and neck cancer cells, as a suitable *in vitro* model for studying the effect of small molecules antagonist ICT13069 targeting CCR7. To our knowledge no prior CCR7 small molecule antagonist has been investigated as a modulator of the metastatic process, despite the substantial evidence that CCR7 expression is associated with lower patient survival and poor prognosis (Irino et al., 2014,

Xia et al., 2014). Our data suggested that the hypoxic upregulation of CCR7 did not increase the migration of cells compared to cells cultured under normoxic conditions. On the contrary, OSC-19 cells moved at a slower rate under hypoxia. Therefore, it is vital to study the effect of silencing CCR7 on the cell migration rate under hypoxia.

Therefore, we decided to knockdown *CCR7* to disrupt its gene expression and study the resulting cells' phenotype (Mittal, 2004, Boettcher and McManus, 2015). The discovery of the RNA interference to reduce the expression of a specific gene was a spectacular achievement and after its discovery nearly two decades ago, has become a method of choice for target validation. Since then, many methods have been developed to reduce (knockdown) or completely silence (knockout) gene expression.

There are 2 main categories for manipulating the gene expression :- (1) The knockdown RNAi method by siRNA or shRNA or (2) the more recent knockout methods, that include the zinc finger nucleases, transcription activator–like effector nucleases and the more recent CRISPR/Cas method.

The choice of the suitable strategy to disrupt the gene expression depends on the experimental goals. Since our ultimate goal is to eventually develop antagonists against CCR7 to stop the metastatic process, we concluded that a transient knockdown by RNAi would better mimic the inhibitory effects of an antagonist than the knockouts strategies.

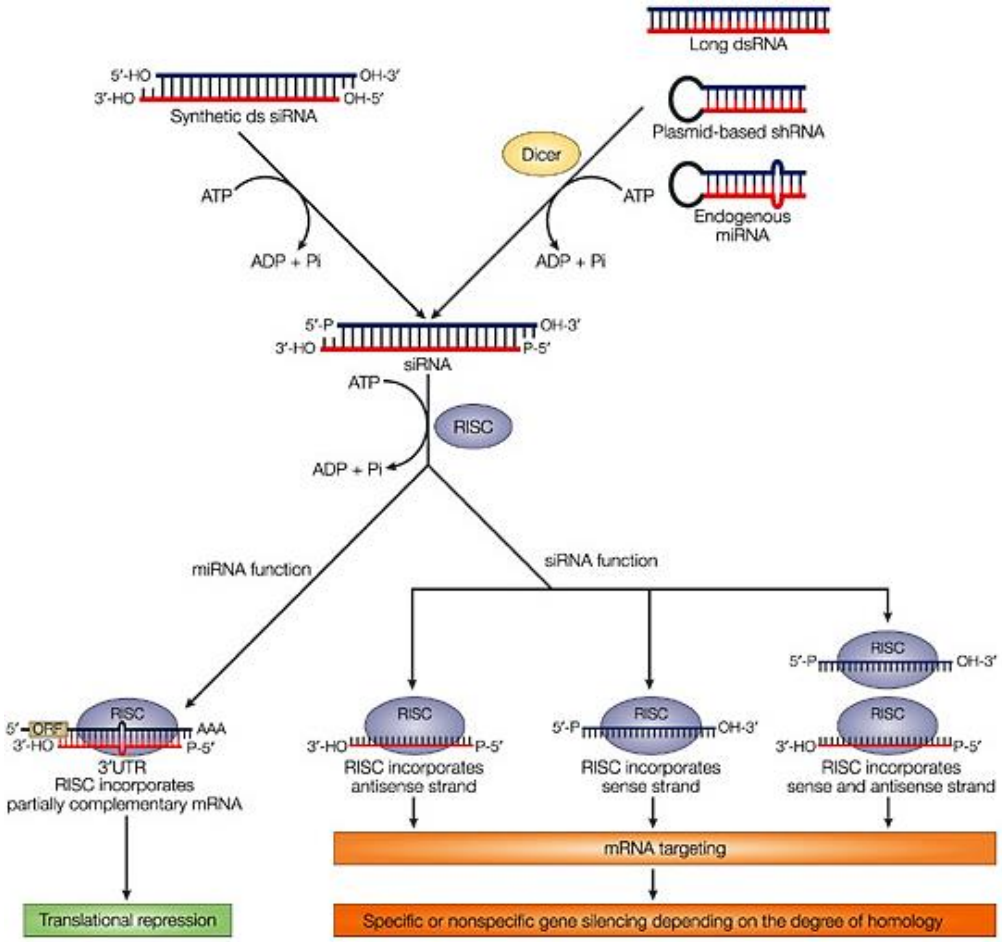

Figure 53: RNAi mechanism for siRNA and shRNA.

shRNA transcripts are transferred into the cytoplasm to be loaded onto the Dicer and processed to siRNA. Both synthetic and endogenously produced siRNA are then loaded onto RISC that eventually lead to mRNA degradation or translational inhibition. From (Mittal, 2004).

There are two types of RNAi; (1) the short interfering siRNA or (2) the short hairpin RNA shRNA. Initially the introduced siRNA with 21 base duplexes or the longer shRNA hairpin transcripts that are synthesized endogenously in the nucleus will be transported to the cytoplasm and then loaded into RNA-induced silencing complex (RISC) that eventually promotes the mRNA degradation

Figure 53 (Mittal, 2004). RNAi is a straightforward technique to produce a knockdown in a very short time with less costly tools compared to other techniques. In addition, there is no need for prior genetic manipulation, because RNAi exploits the natural silencing machinery that exists in every mammalian cell. In this chapter, we utilised siRNA to silence CCR7 and used scramble siRNA as control. The siScramble has the same nucleotide composition, but with a different sequence that is achieved either by randomizing the siRNA of the target gene or reversing it.

3.1.1 Aims and objectives

The expression of CCR7 on cancer cells can promote growth, invasion and migration that lead to the development of secondary metastases particularly to the lymph nodes **(chapter 1 and chapter 2).**

- **The main aims and objectives of this Chapter were:**

- To carry out siRNA knockdown studies on OSC-19 cells and evaluate its efficacy at gene and protein level under normoxic and hypoxic conditions.
- To evaluate the effect of CCR7 knockdown on the: proliferation, apoptosis, migration, ROS generation and cisplatin sensitivity.

3.2 Materials and methods

3.2.1 Preparation of siRNA

siRNA of *CCR7* and non-silencer control RNA scramble were pre-designed and validated by Fisher Scientific with sequences specifically targeted to *CCR7.* The oligonucleotide sequence of *CCR7* and Scramble siRNA were:

- *CCR7* sense, 5'-GCGUCAACCCUUUCUUGUATT-3'
- *CCR7* antisense 5'-UACAAGAAAGGGUUGACGCAG-3'
- Scramble sense 5'UUCUCCGAACGUGUCACGUTT-3'
- Scramble antisense 5'-ACGUGACACGUUCGGAGAATT-3'

The CCR7 and the scrambled oligonucleotide (20nmol) were dissolved in 1 ml of 1x Dharmacon siRNA resuspension buffer to produce a 20 µM or 5 µM solution of siCCR7 or siScramble respectively. Solutions were shaken for 1 h to ensure complete, homogenous solution. The stock solutions were kept at -80˚C. On the day of transfection, further working solutions of 2 µM were also prepared, aliquoted and kept at -80˚C.

3.2.2 Cell seeding

Early passage (2-5) of OSC-19 cells were seeded at a density of 2.1×10^5 cells per 25 cm^2 flask in 5 ml complete RPMI medium or at 1.6×10^4 cells/ well, or 8.0×10^4 cells/well in 24 or 6 well plates respectively. Cells were incubated at 37˚C and 5% CO_2 for 24 h.

3.2.3 Transfection

On the day of transfection, cells were examined under the microscope to ensure that they are evenly distributed in the flasks and have a confluency of

30%-40%. This level of confluency is important to maximize the efficiency of siRNA transfection. Next, solutions of 2 μM of siRNA were brought to R.T. and for each transfection sample, 30 μl of siCCR7 or siScramble were added to 525 μl of Opti-MEM reduced serum medium (Fisher scientific). Solutions were mixed very well by up and down pipetting. Afterwards, the transfection reagent oligofectamine (Fisher scientific) was first homogenised by up and down pipetting, and then diluted into Opti-MEM at a ratio of 1:5, mixed gently and incubated for 30 min at R.T. After incubation, the diluted oligofectamine should turn cloudy. 45 μl of this mixture was combined with the diluted siCCR7 or siScramble and mixed by gentle pipetting 30 times and incubated for 45 min at R.T. The volumes used ensure that (the concentration of oligofectamine should always be 7.5%v/v). Meanwhile, medium was removed from samples to be transfected and 5, 2 or 1 ml of Opti-MEM was added to 25cm^2 flasks, 6 wells and 24 wells plates, respectively. Cells were washed twice with opti-MEM to ensure complete removal of any 10%FBS RPMI medium. Then, 2 ml, 800 μl or 160 μl Opti-MEM was added to each 25cm^2 flasks, 6 wells and 24 wells plates respectively. After 45 min, 500, 200, 40 μl of (siRNA/oligofectamine) was mixed 20 times and added to the 25cm^2 flasks, 6 wells and 24 wells plates, respectively. Cells were incubated at 37˚C and 5% CO_2 for 4 h. After incubation, 2.5 ml, 1 ml, 200 μl of RPMI medium that contains 20%FBS, was added to each flask/well in the 25cm^2 flasks, 6 wells and 24 wells plates, respectively, without removing the transfection mix. Finally, cells were incubated at 37˚C and 5% CO_2 for 24 h, 48 h, 72 h or 96 h before harvesting

cells for CCR7 gene and protein expression as well as other transfection related assays. For transfection assays under hypoxic conditions, the transfection was carried out outside the hypoxic chamber for 72 h. Afterwards, cells were incubated for another 24h in the hypoxic chamber (0.1% O_2) for gene and protein expression or other transfection related assays.

3.2.4 Cell harvesting

At each time point, images were taken to compare siScramble and siCCR7 for any phenotypic changes. Next, the medium was collected into 25 ml universal tubes to ensure collection of any floating cells and then cells were washed twice with 5 ml PBS, trypsinised, combined with the floating cells into the 25 ml tube and centrifuged at 1,000 rcf for 5 min. Then, medium was removed (any residual medium was removed with a Gilson pipette), next cells were re-suspended into 5 ml PBS and centrifuged for 5 min at 1000 rcf. Finally, another PBS wash was carried out and the dry cell pellet with no PBS was kept at -80˚C for gene and protein expression, to confirm the knockdown at gene and protein levels.

3.2.5 CCR7 gene expression after knockdown

3.2.5.1 *RNA extraction and quantification*

Cell pellets that were transfected with siCCR7 or siScramble were taken out from -80˚C and kept on ice for total RNA isolation using RNeasy Mini Kit (Qiagen) following the manufacturer's instruction. Cells were loosened by flicking the tube and the cells were lysed by adding 350 µl of RLT lysis buffer

and vortexed. Cells were then homogenized by pipetting the cell lysate into a QIAshredder spin column (Qiagen) and placed into a 2 ml collection tube and centrifuged for 2 min at 8,000 rcf. Next, 1 volume (350 µl) of 70% ethanol was added to the homogenized cell lysate and mixed well by up and down pipetting. The cell lysate was added to an RNeasy spin column (Qiagen), placed in a 2 ml collection tube (Qiagen) and centrifuged for 15 s at 8,000 rcf. The flow through was discarded and 350 µl RW1 buffer was added to the RNeasy spin column and centrifuged for 15 s at 8,000 ruff. Again, the flow through was discarded and the 80 µl of DNase I mix (10 µl of DNase I stock (Qiagen) with 70 µl of RDD buffer (Qiagen) added to RNeasy spin column and incubated for 15 min at R.T. Afterwards, another 350 µl of RW1 were added to RNeasy spin column and centrifuged for 15 s at 8,000 rcf. The flow through was discarded and 500 µl of RPE buffer was added to the RNeasy spin column and centrifuged for 15 s at 8,000 rcf. Again, another 500 µl of RPE buffer was added and centrifuged for 2 min at 8,000 rcf, after discarding the flow through, the RNeasy spin column was placed into a fresh 2 ml collection tube and centrifuged for 1 min at 8,000 rcf to ensure that no ethanol was carried over. Finally, 40 µl of RNase-free water was added to elute RNA into 1.5 ml collection tube after centrifugation for 1 min at 8,000 rcf. The amount of the eluted RNA was measured by NanoDrop^{TM} 100 spectrophotometer (Thermo Scientific). Total RNA was then used to synthesize single-stranded cDNA and RNA samples were stored at -80˚C.

3.2.5.2 *Complementary DNA synthesis*

Single-stranded cDNA was synthesized using high capacity cDNA reverse transcription Kit (fisher scientific). Kit components were allowed to thaw on ice to prepare the 2x reverse transcription (RT) master mix by mixing kit components (table 1). Then, 2 µg of total RNA in 10 µl nuclease-free H_2O were added to another 10 µl 2X RT master and mixed 2 times by pipetting to produce a 20 µl reaction per Eppendorf. Tubes were then loaded to MJ Research PTC-200 Peltier thermal cycler. The samples were run in the thermal cycler following conditions suitable with high capacity cDNA reverse transcription Kit. Samples were run at 25˚C, 37˚C, 85˚C and 4˚C for 10 min, 120 min, 5 min and infinity, respectively. Finally, cDNA RT samples were stored for short term storage 24h before use at 4˚C or long term at -80˚C.

Table 14: reverse transcription (RT) master mix components

Component	Volume/reaction (µl)
10X RT buffer	2
25X dNTP Mix	0.8
10X RT random primers	2
MultiScribe™ reverse transcriptase	1
RNase inhibitor	1
Nuclease-free H2O	3.2
Total volume	10

3.2.5.3 *Real-time quantitative PCR*

Real-time quantitative PCR (qPCR) was performed using pre-designed primers (Fischer scientific) of 20X TaqMan® probe with an Applied Biosystems™ CCR7 FAM™/MGB probe (Hs01013469_m1) and 20X TaqMan® probe with an Applied Biosystems™ Human ACTB (beta actin) Endogenous Control FAM™ ⁄ MGB Probe, Non-Primer Limited. For a single reaction 12.5 µl of CCR7 or ACTB primer mixed with 1.25 µl of 2X Taqman Universal PCR Master Mix (Fischer scientific) was added to QRT-PCR 96-well plate (MicroAmpTM) in triplicate for each gene of interest in a UV- irradiated hood on 7500 RT-PCR System (Applied Biosystem). 11.25 µl of 40 ng cDNA was added to the PCR mix (cDNA 2 µg was diluted using RNase-free H_2O). Water only and no reverse transcriptase were included as negative control.

The PCR conditions were as follows: Pre-denaturation at 50°C for 2 min and then at 95°C for 10 min, followed by 40 cycles of denaturation at 95°C for 15 s and annealing/extension at 60°C for 1 min.

3.2.5.4 *Data analysis*

The amplified genes by qPCR are measured by producing fluorescence as they are amplified. The fluorescence intensity that is produced from cycles 3-15 is usually not significant and is referred to as a baseline. As more templates are amplified, the fluorescence intensity will increase significant above the baseline at a point called Ct. The method that is used for analyzing qPCR results is comparative quantification ΔΔCt. Therefore to evaluate the efficiency of siCCR7, the following calculations were followed:-

- ΔCt= (Ct of siCCR7 or siScramble sample) – (Ct of β-actin sample) (The higher the ΔCt the lower the expression of CCR7)
- ΔΔCt = (ΔCt of siCCR7) – (ΔCt of siScramble) (ΔΔCt is used to calculate the fold change FC or RQ)
- $RQ = 2^{-\Delta\Delta Ct}$
- % of expression = RQ * 100%

3.2.6 Expression of CCR7 protein after siRNA

To evaluate the efficacy of siRNA at the protein level western blot and flow cytometry were used. Briefly, the protein expression of OSC-19 cells after siRNA was carried out using flow cytometry as described in (section 2.2.8) for

all time points after transfection (24 h, 48 h, 72 h, and 96 h). At each time point the relative fluorescence intensity of siCCR7 was compared to siScramble. Samples after 24h and 72h of transfection were chosen for further analysis using western blot technique. Protein extraction, Bradford assay and western blot were performed as previously described in (section 2.2.9).

3.2.7 Cell proliferation and viability

3.2.7.1 *Trypan blue assay*

To evaluate the role of CCR7 in proliferation, cells were seeded in 6 well plate and transfected with siCCR7 or siScramble as described in (section 3.2.2 and 3.2.3). 24 h later CCL21 (10 nM) was added to appropriate wells for 72 h. Afterwards, cells were washed with PBS, trypsinised and centrifuged. Media was discarded and cells were resuspended in 1 ml of RPMI media, and vortexed. Finally 100 µl of the cell suspension was added to 100 µl of 0.4 % trypan blue solution (Fisher scientific). Trypan blue stains non-viable cells with blue color and leaving the viable cells colourless. Live cells were counted under bright field microscope.

3.2.7.2 *Annexin V –FITC Apoptosis detection assay*

In order to investigate the effect of CCL21/CCR7 interaction on apoptosis of OSC-19 cells after transfection, annexin V–FITC apoptosis assay was conducted. During early apoptosis, phosphatidylserine (PS) residues are usually translocated from the cytoplasmic side of plasma membrane to cell surface side. In late apoptosis, the integrity of plasma membrane is lost due to

apoptotic or necrotic cell death. annexin V-FITC and propidium iodide (PI) are typically used to detect these events, Annexin-V has a high binding affinity to PS residues at the cell surface and thus reflecting the amount of apoptotic cells, while PI binds to DNA and is only able to penetrate the cell after loss of the cell membrane integrity. Therefore, viable cells are negative for both annexin-V and PI, early apoptotic cells are only positive for annexin-V and late apoptotic cells are positive for both annexin-V and PI.

After 24 h of transfection, media containing transfection reagents was removed and OSC-19 cells (siCCR7 and siScramble) were incubated with fresh media with or without CCL21 (10 nM) for 72 h. Then, media was collected in 25 ml tubes and cells were washed with PBS and trypsinised. Trypsinised cells were combined with the collected media and spinned down at 1000 rcf for 5 min. Media was discarded and cell pellet was resuspended in 1 ml of PBS and 0.5 x 10^6 cells were centrifuged and re-suspended in 100 µl of binding buffer (Abcam). Next, 5 µl of annexin V-FITIC and 2 µl of PI were added for 15 min at R.T. in the dark. Finally, another 400 µl of binding buffer were added to each tube before analysing the samples using flow cytometry. The percentage of apoptosis was analyzed using CellQuest analysis software.

3.2.7.3 *Data analysis*

Samples were analysed by flow cytometry, (annexin V-FITC binding by flow cytometry (excitation/emission): ~488/530 nm using FITC signal dectector FL1H and PI staining by the phycoerythrin signal detector FL2H (excitation/ emission): ~535/617 nm.

The cell populations were separated into 4 groups: Live cells with no staining - lower left, early apoptotic with annexin V-FITC staining -lower right, late apoptotic with annexin V-FITC and PI staining - upper right and dead cells with PI staining - upper left, as shown in Figure 54.

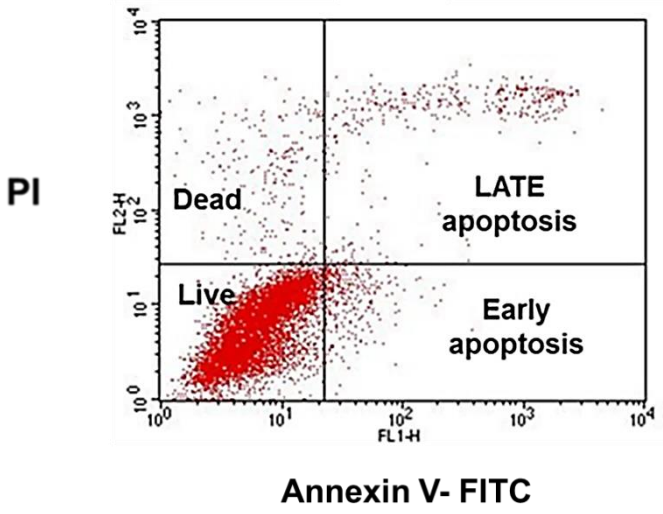

Figure 54: Annexin V-FITC apoptosis Quadrants.

3.2.8 Detection of reactive oxygen species (ROS)

As mentioned above, ROS play important roles in many cellular signaling pathways, including cell migration. OSC-19 cells were seeded in phenol red free RPMI medium (Gibco) in 25 cm^2 flasks and transfected with CCR7 and Scramble siRNAs as described previously (section 3.2.3) using Opti-MEM phenol red free medium (Gibco). After 24 h of transfection, cells were treated with or without CCL21 (10 nM) for another 72 h. The medium of 1 flask was replaced with new medium containing H_2O_2 (200 µM) for another 24 h. H_2O_2 is known to cause increase of ROS levels and therefore is used as positive

control. On the following day, any floating cells were collected into 20 ml universal tubes and adherent cells were washed with 5 ml PBS, trypsinized, neutralised with phenol red free medium and combined with the floating cells, and centrifuged at 1,000 rcf for 3 min. The medium was discarded and cells were washed with 5 ml of PBS and centrifuged again at 1,000 rcf for 3 min. Afterwards, the cell pellets were re-suspended into 2 ml of phenol red free RPMI medium containing 5 µM of 6-carboxy-2',7'-dichlorodihydrofluorescein diacetate (carboxy-H2DCFDA, Fisher scientific). In the presence of ROS, the carboxy-H2DCFDA (a non-fluorescent compound), is converted into a green fluorescent dye and the fluorescence intensity could by measured using flow cytometry. Cells were mixed well, transferred to 6 well plates and incubated with carboxy-H2DCFDA for 30 min at 37°C with gentle shaking to prevent cell adhesion to the well surface. Finally, cells were collected, spinned down, washed in 5 ml PBS, spinned again and re-suspended in 500 µl of PBS and analysed using flow cytometry through signal detector FL1H at excitation/emission: ~ 488/530 nm.

3.2.9 Scratch assay under normoxia

We have demonstrated that the presence of 10 nM CCL21 increased the migration of OSC-19 cells in a number of migration (chapter 2) and invasion (chapter 4) assays; however whether the absence of CCR7 would stop the migration of cells was not considered. Therefore, the knockdown of CCR7 can provide valuable information on the relevance of developing antagonists against CCR7 and eventually increase patient survival.

Briefly, OSC-19 cells were seeded and transfected in 24 well plates as described in (section 3.2.3). After 72 h of transfection, a confluent monolayer of OSC-19 cells was obtained and scratched with a p200 pipet tip as described before in section 2.2.13 Finally, the cell free surface area (at t = 0 and 18 h) was measured and % of cell free surface area was calculated as before in section 2.2.13.

3.2.10 Scratch assay under hypoxia

We have observed in the previous chapter that CCR7 expression was up-regulated under hypoxia, in comparison with cells cultured under normoxia. However, this upregulation did not translate to increase in migration. Therefore, to clarify if this reduction of migration under hypoxia is or not related with the CCR7 expression, OSC-19 cells were transfected to knockdown CCR7 for 72 h under normoxia, scratched and photos were taken before transferring to the hypoxia chamber (t = 0 h for scratch assay). In the hypoxia chamber, siCCR7 or siScramble cells were washed with pre-hypoxic (kept in the hypoxia chamber) BPS and then pre-hypoxic 2% FBS media with or without CCL21 (10 nM) was added and incubated for 18 h 37^{o}C, 0.1% O_2, CO_2 before capturing images and calculating the % of free surface area as described before in 2.2.13.

3.2.11 Effect of siCCR7 on cisplatin sensitivity

The IC_{50} of cisplatin was measured by using MTT assay as described before in section 2.2.12. Briefly, OSC-19 were seeded at 2000 cells/ well in 96 well plate, after 24 h of seeding, Cisplatin (Sigma) was dissolved in water to

produce a stock solution of 3.415 mM. This stock was further diluted with RPMI medium to give final concentrations of 50, 25, 12.5, 6.25, 3.125, 1.562, 0.781 and 0.391 μM in the wells. Finally, 96 h after seeding, MTT solution was added, incubated and the blue-purple formazan colour read by using a colorimetric plate reader at 540 nm.

In order to see if CCR7 is involved in cisplatin resistance, siRNA was performed to see whether knockdown CCR7 will increase cisplatin sensitivity i.e. increase cell death. To detect the level of apoptosis, OSC-19 cells were seeded in 6 well plates and after 24 h cells were transfected with siRNAs as described in (section 3.2.3). After 24 h of transfection, cells were washed with 1 ml of BPS and then treated with or without cisplatin at IC_{50} ~ 1.5 μM for another 72 h.

3.2.12 Statistical data analysis

The significance of the results was assessed through a comparison of means using two-tailed student t-test. Results were expressed as the mean ± standard deviation. P values were calculated to determine statistical significance of the results. ***P < 0.05 and **P < 0.01**.

3.3 Results:

3.3.1 OSC-19 cells retain their morphological appearance after siRNA transfection.

Cell images were taken 24 h, 48 h, 72 h and 96 h after transfection with siCCR7 and siScramble. Images showed no morphological changes between siCCR7 and siScramble cells Figure 55. Knockdown of siCCR7 did not cause any change to OSC-19 polygonal shaped cobblestone pattern compared to the siScramble negative control.

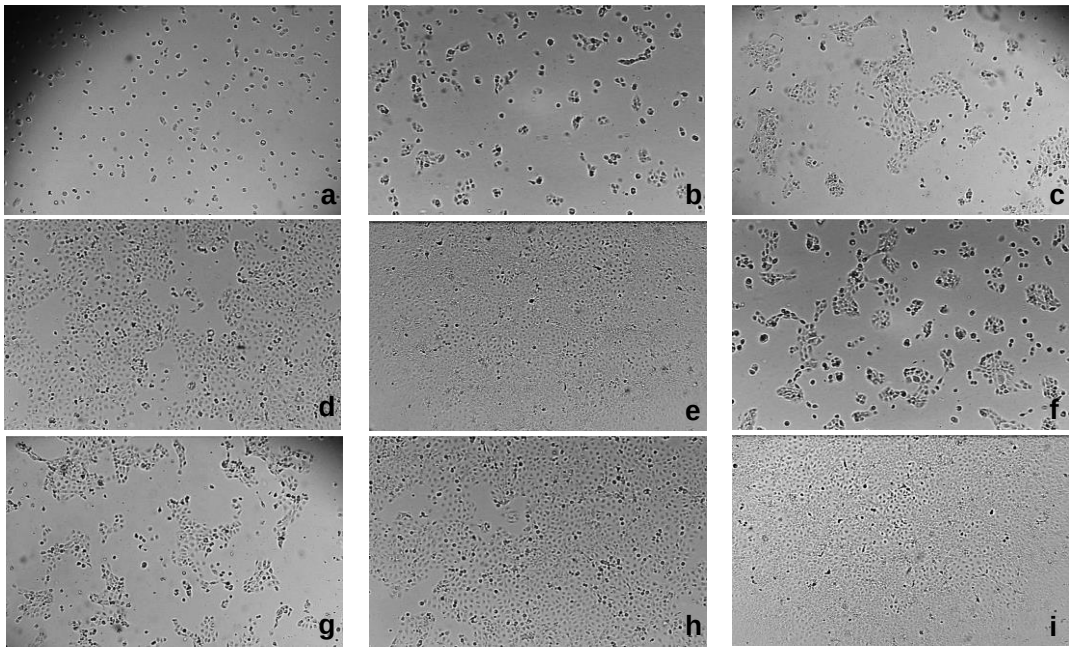

Figure 55: Representative images of OSC-19 after transfection

Cells maintain their normal phenotype after siRNA of CCR7. (a) Cells density before 24h of transfection. (b-e) Phenotypic appearance of OCS-19 cells after 24 h, 48 h, 72 h and 96 h of siCCR7 transfection. (f-j) Phenotypic appearance of OCS-19 cells after 24 h, 48 h, 72 h and 96 h of siScramble transfection. Cell were examined at 10x (photos shown) and 20x and 40x objective magnification lens but were not photographed

3.3.2 Downregulation of CCR7 mRNA by siCCR7 reduces cell surface protein levels of CCR7

Following transfection with siCCR7 and siScramble for 24 h, 48 h, 72 h and 96 h, cells were harvested and analysed by qPCR to evaluate CCR7 mRNA level. CCR7 expression was significantly down-regulated in OSC-19 cells transfected with siCCR7, in comparison with the cells transfected with siScramble. There was significant degradation of CCR7 mRNA by siRNA by 60 %, 72%, 85% and 88% after 24 h, 48 h, 72 h and 96 h, respectively (Figure 56). The effect of siCCR7 on protein expression was assessed by flow cytometry. As shown in (Figure 57-a, b), the results demonstrated that siCCR7 significantly downregulated the protein level in comparison to the control siScramble. The fold change of the mean fluorescence intensity after normalization to siScramble was 0.42, 0.39, 0.32, and 0.21 for 24 h, 48 h, 72 h and 96 h, respectively. In addition, the protein expression was also confirmed at two time points 24 h and 72 h by western blot analysis (Figure 57-c). The band density that corresponds to the siCCR7 cells was reduced compared with that of the siScramble cells at both time points.

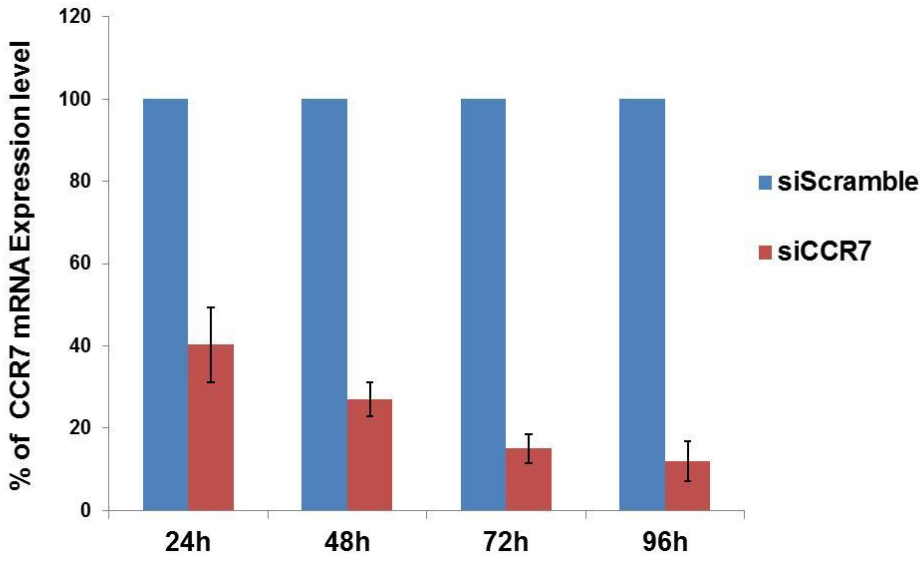

Figure 56: Knockdown of CCR7 at mRNA.

After transfection, the efficiency of siCCR7 at gene level was evaluated by qPCR. CCR7 expression was decreased and maintained up to 96 h. Results represent 3 independent experiments and error bars represent SD.

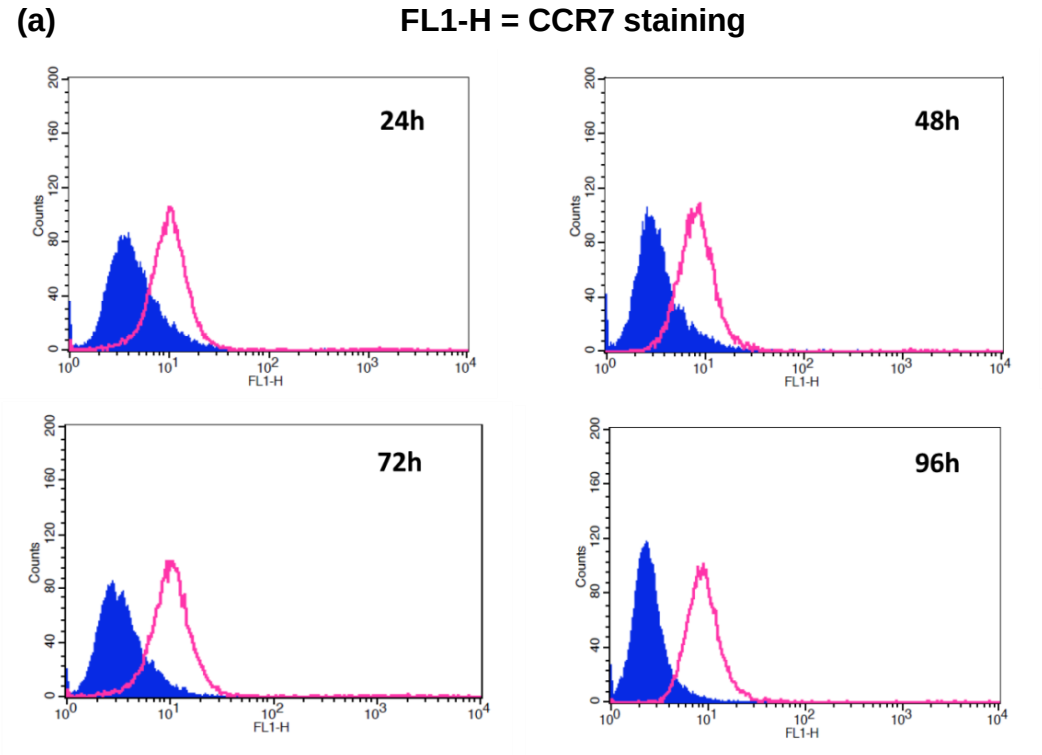

(b)

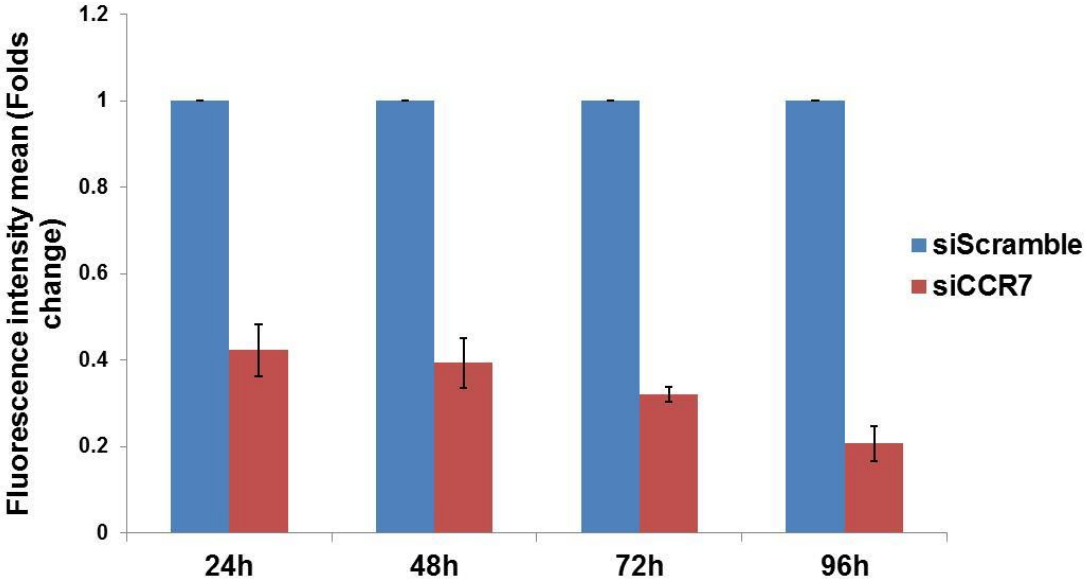

(c)

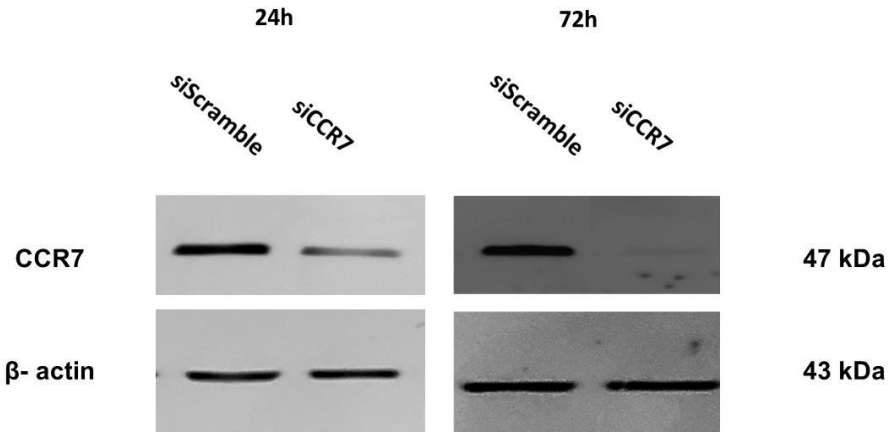

Figure 57: The downregulation of the protein level of CCR7.

The efficiency of the siRNA at protein level was evaluated by flow cytometry at 24 h, 48 h, 72 h, and 96 h. (a) siCCR7 (the blue filled curve) was shifted to the left of the siScramble (the unfilled pink curve) indicating decrease in expression. (b) Analysis of flow cytometry data using mean fluorescence intensity, siCCR7 samples were normalized to siScramble samples and represented as fold change. (c) Western blot evaluation of siCCR7 at 24h and 72h showed decrease in expression in siCCR7 compared with siScramble. Results represent 3 independent experiments and error bars represent SD.

3.3.3 Downregulation of CCR7 mRNA and protein level by siCCR7 is maintained under Hypoxia

Before we can examine whether the presence of CCR7 is important for cell migration, we ought to confirm that the level of knockdown is maintained under hypoxia. We showed in Chapter 2 that under hypoxia, the expression of CCR7 protein is increased. So it is important for us to demonstrate that mechanisms that increase CCR7 expression under hypoxia cannot override the knockdown. Transfection was performed under normoxia and 72 h later cells were transferred to the hypoxia chamber for another 24 h (this time point was chosen because we have seen an increase in CCR7 expression under hypoxia at this particular time point, for results see chapter 2 section 2.3.8) and checked for gene and protein level of CCR7. The CCR7 was downregulated by 72% and 78% at mRNA and protein level, respectively (Figure 58).

(a)

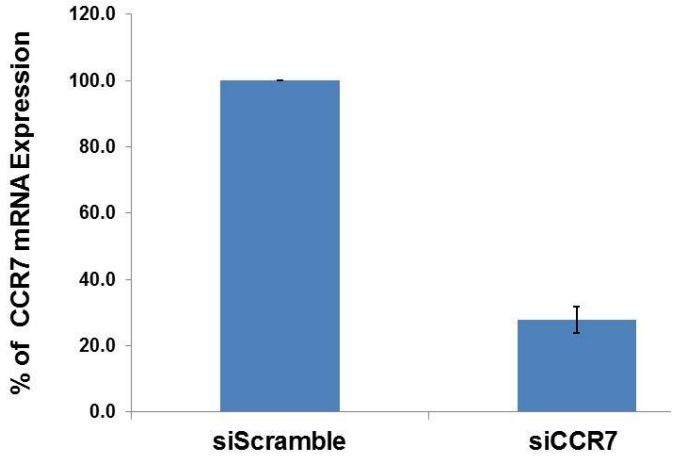

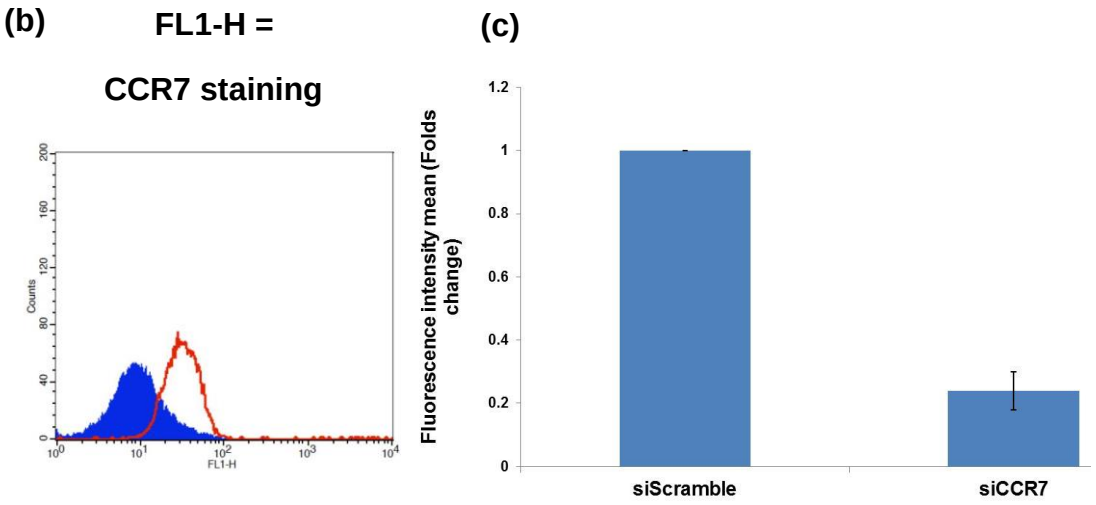

Figure 58: The knockdown of CCR7 using siCCR7 was maintained under hypoxia.

Silencing of CCR7 mRNA decreased the expression level of CCR7 in OSC-19 cells at the gene level. (b) The protein level of CCR7 after transfection was assessed by flow cytometry. The siCCR7 (blue filled curve) was shifted to left compared with siScramble (red unfilled curve (c) analysis of flow cytometry data using mean fluorescence intensity, siCCR7 samples were normalized to siScramble samples and represented as fold change Results represent 3 in dependent experiments and error bars represent SD.

3.3.4 Downregulation of CCR7 expression inhibits cell migration both under normoxia and hypoxia

We recall from Chapter 2 that the migration level of OSC-19 cell was increased upon CCL21 addition under normoxia compared to control, but not under hypoxia. We studied cell migration under normoxic and hypoxic conditions with and without CCL21 in siCCR7 and siScramble cells, to clarify whether CCR7 plays a role in of cell migration under hypoxia or not.

Figure 59-b shows the cell migration under normoxia and the % of free surface area is represented in Figure 59-a. The % of free surface area of siCCR7 group after CCL21 addition was similar to the control group in which no CCL21

was added (101% vs 100%). However, the siScramble group with CCL21 has significantly less % of free surface area compared with its control (39% vs 105%), respectively. Furthermore, the % of the free surface area was significantly higher in the siCCR7 added group (101%) compared with siScramble group (39%) after the addition of 10 nM CCL21 ($P < 0.01$). On the other hand, the addition of 10 nM CCL19 did not cause any significant difference in the % of free surface area of OSC-19 between siCCR7 or siScramble groups, 93 % versus 102% respectively ($P > 0.05$).

The effect of siCCR7 on OSC-19 cells was also studied under 10% FBS without the addition of CCL21, the migration of OSC-19 cells was reduced by 58% under the knockdown of CCR7.

Under hypoxia however, the % of free surface area of siCCR7 group is 115% vs 89% for the siScramble Figure 60. This 26% difference was significant with a $P < 0.05$. This indicates the significance of CCR7 expression both under normoxia and hypoxia Figure 60.

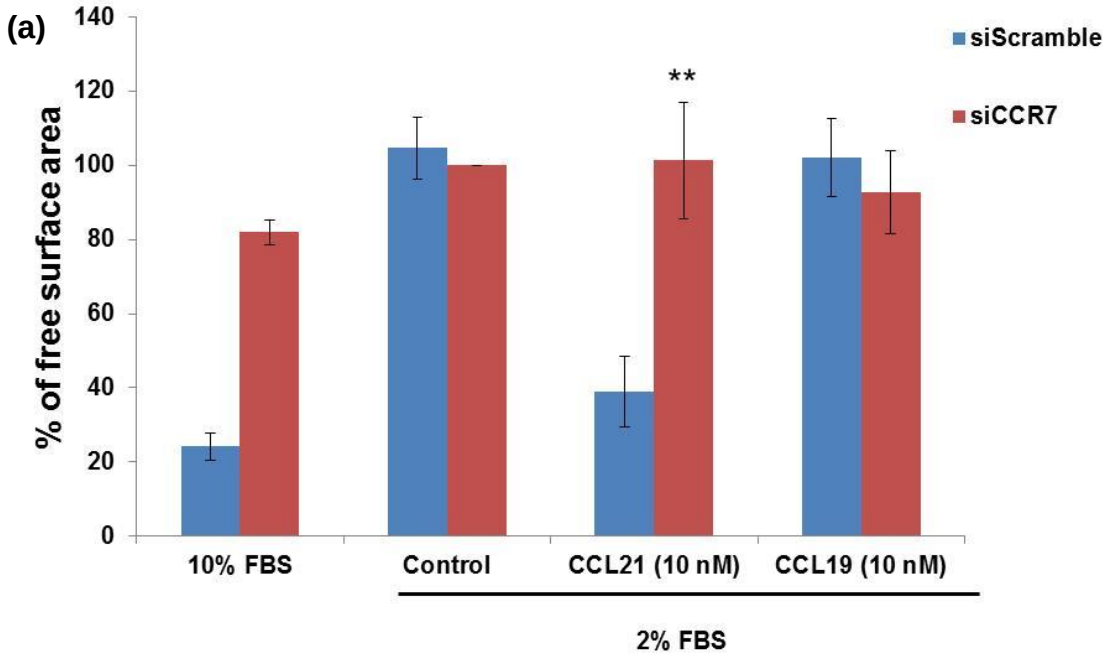

Figure 59: Migration of OSC-19 cells after the knockdown of CCR7 under normoxia.

Free surface area was measured after 18 h on 2 fields per well and averaged and normalized to free surface area at 0h. Cells were treated with CCL21 at 10 nM, CCL19 at 10 nM or no ligand added (control). (a) Data expressed as the mean of % of free surface area after migration. Scale bar represents 100 µm and **P < 0.01 compared with siScramble-CCL21 group. Results represent 3 in dependent experiments and error bars represent SD. (b) Representative images of OSC-19 cell before (0h) and after (18h) migration.

(b)

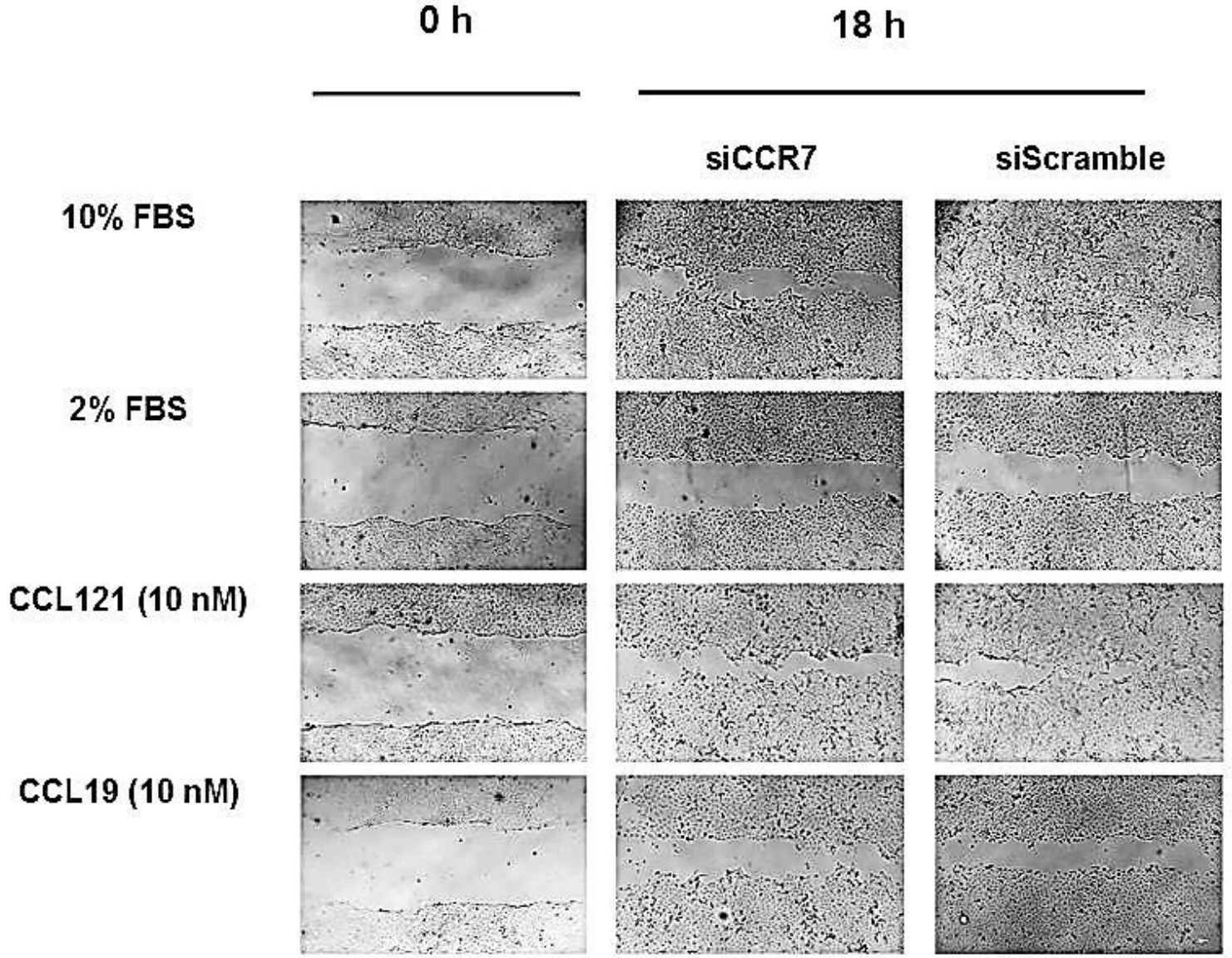

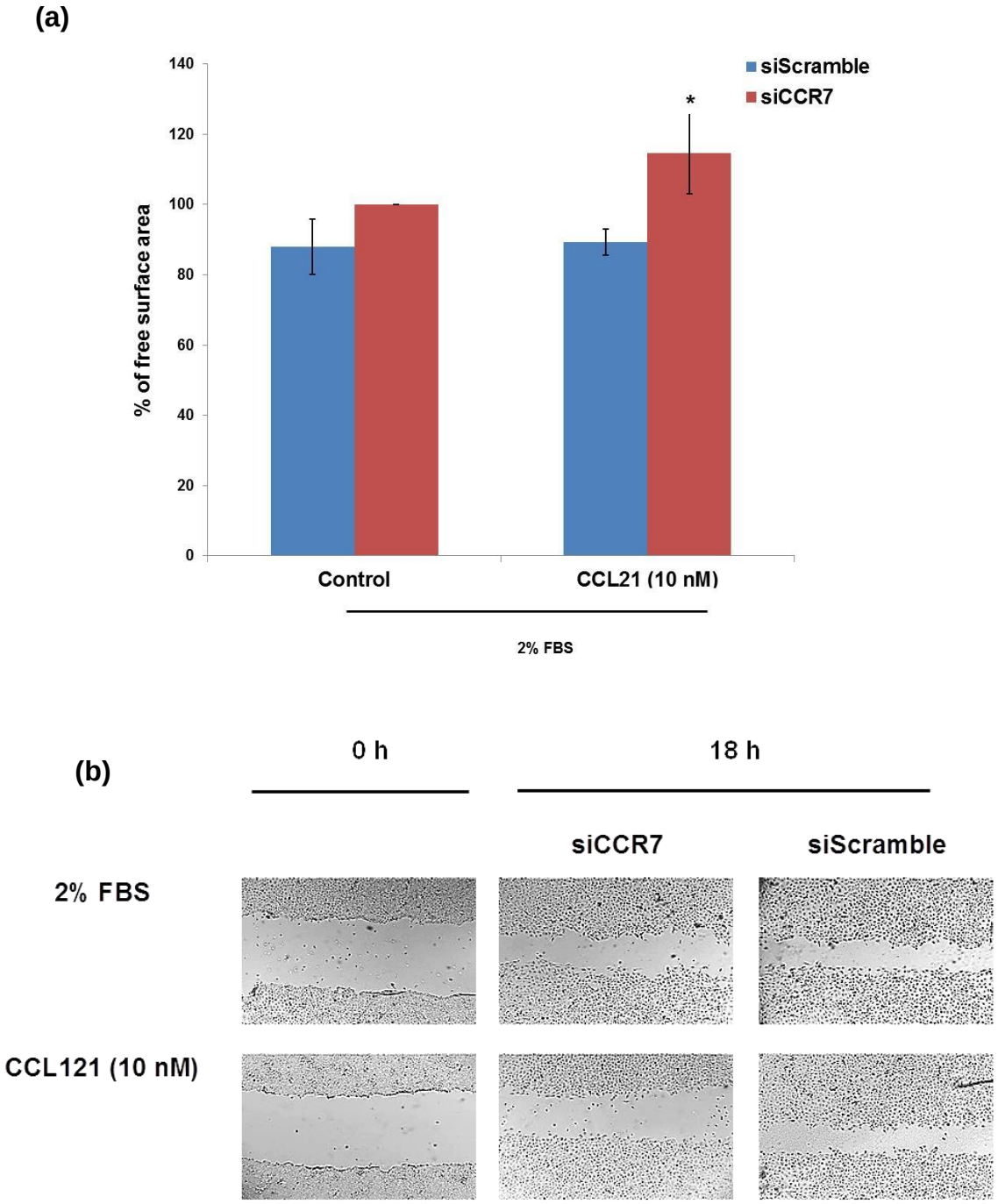

Figure 60: Migration of OSC-19 cells after the knockdown of CCR7 under hypoxia.

Free surface area was measured after 18 h on 2 fields per well and averaged and normalized to free surface area at 0h. Cells were treated with CCL21 at 10 nM or no ligand added 2% FBS (control). (a) Data expressed as the mean of % of free surface area after migration. Results represent 3 in dependent experiments and error bars represent SD. *P < 0.05 compared with siScramble-CCL21 group. (b) Representative images of OSC-19 cell before (0 h) and after (18 h) migration.

3.3.5 Effect of CCR7 downregulation on cell proliferation and apoptosis

It has been shown that CCR7/CCL21 is involved in cell survival and proliferation in different types of cancers (see chapter 1). However, in wildtype OSC-19 cells we could not see a significant increase in cell proliferation as determined by MTT assay (section 2.3.3 and 2.3.13). Whilst MTT assay is a robust and reliable method for the determining the number of metabolically active cells, it does not provide any information on the fate of cells or mechanisms by which cell numbers are suppressed. Therefore we wondered if using another type of assay would provide us with information about the mechanisms by which CCR7 axis is involved in controlling cell proliferation. To investigate the effect of proliferation on cells transfected with siCCR7 and un-transfected cells, the trypan blue exclusion assay was performed as described previously in section 3.2.7.1. Our results showed that knockdown of CCR7 caused no significant difference of total live cells number compared to the siScramble cells ($p > .05$) Figure 61 Moreover, the addition of CCL21 (10 nM) on siCCR7 transfected and un-transfected cells had no significant increase on cell proliferation rate with P values = 0.79 and 0.54, respectively Figure 61. This agrees with our result in MTT assay (chapter 2) in which CCL21 had no effect on proliferation in OSC-19 wild type cells.

Trypan blue exclusion assay provides information on cell viability, as did our MTT assay results on proliferation rate, but does not give any information on the mechanisms of cell death. Therefore, we decided to use an annexin V-FITC assay to look for the effect of CCL21 on apoptosis and to investigate if

CCL21 would decrease or have the same % of apoptotic cells compared to the cells with no CCL21 Figure 61-b,c).

To ensure the annexin V-FITC assay was working properly and able to detect apoptosis, we first treated one siScramble OSC-19 cells flask with H_2O_2 and observed a 19.1% increase in apoptosis (Figure 61-c). We then tested the treated siScramble and siCCR7 transfected cells with CCL21. CCL21 did not change the % of apoptosis in siCCR7 or siScramble cells. The % of apoptotic cells was 11.2% and 10% for siCCR7 transfected OSC-19 cells with or without CCL21, respectively (Figure 61-c). Moreover, addition of CCL21 had no effect on the % of apoptosis in siScramble cells (9.1% for siScramble and 9.3% siScramble/CCL21 group (Figure 61-c).

(a)

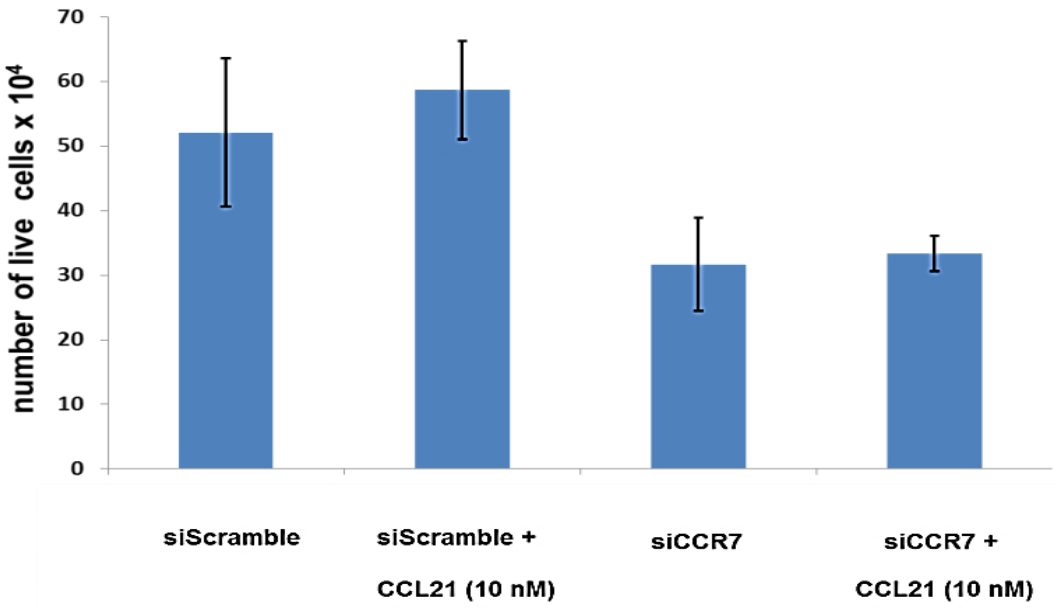

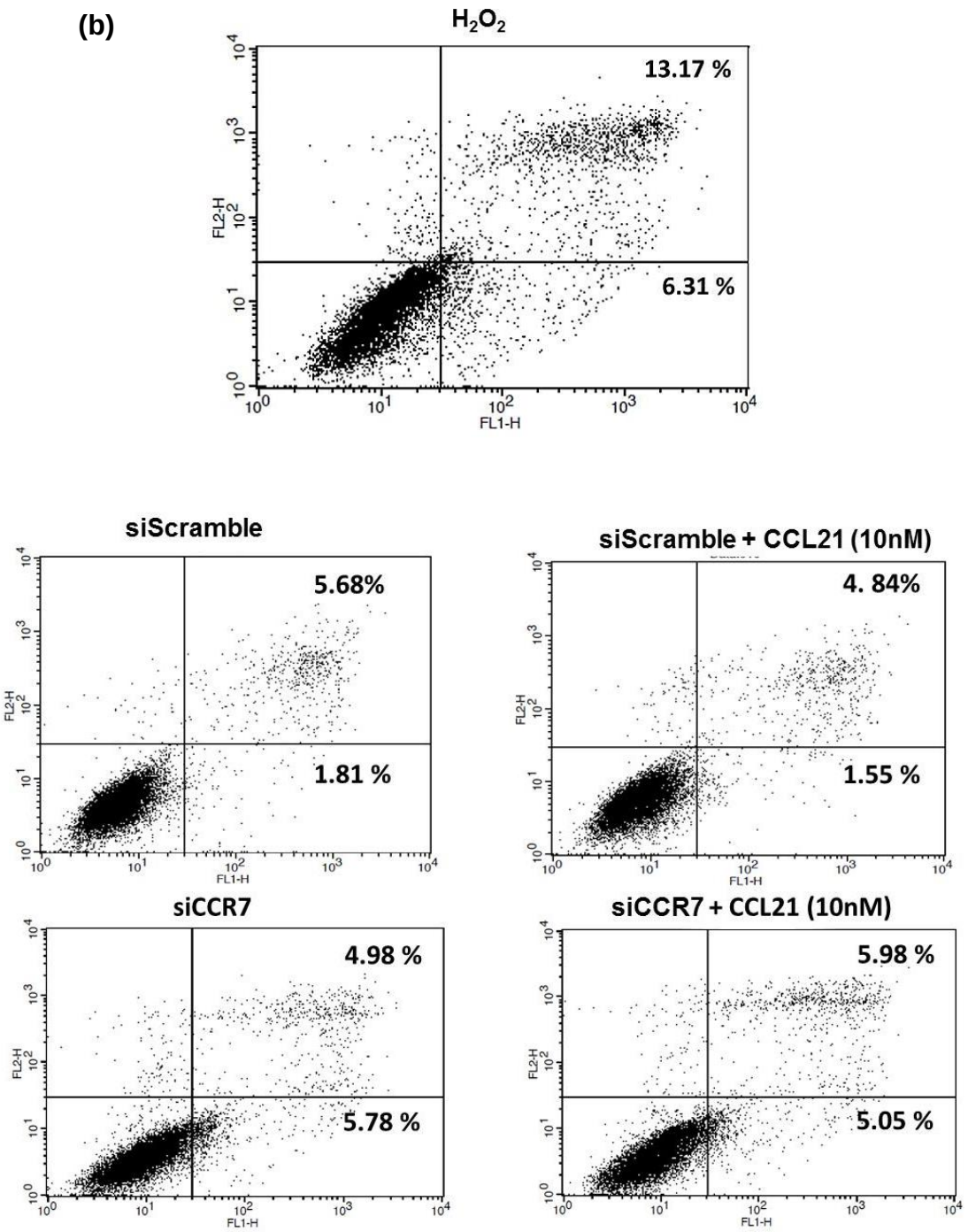
(b)
H_2O_2
13.17 %
6.31 %
FL2-H
FL1-H
siScramble
5.68%
1.81 %
siScramble + CCL21 (10nM)
4. 84%
1.55 %
siCCR7
4.98 %
5.78 %
siCCR7 + CCL21 (10nM)
5.98 %
5.05 %

(c)

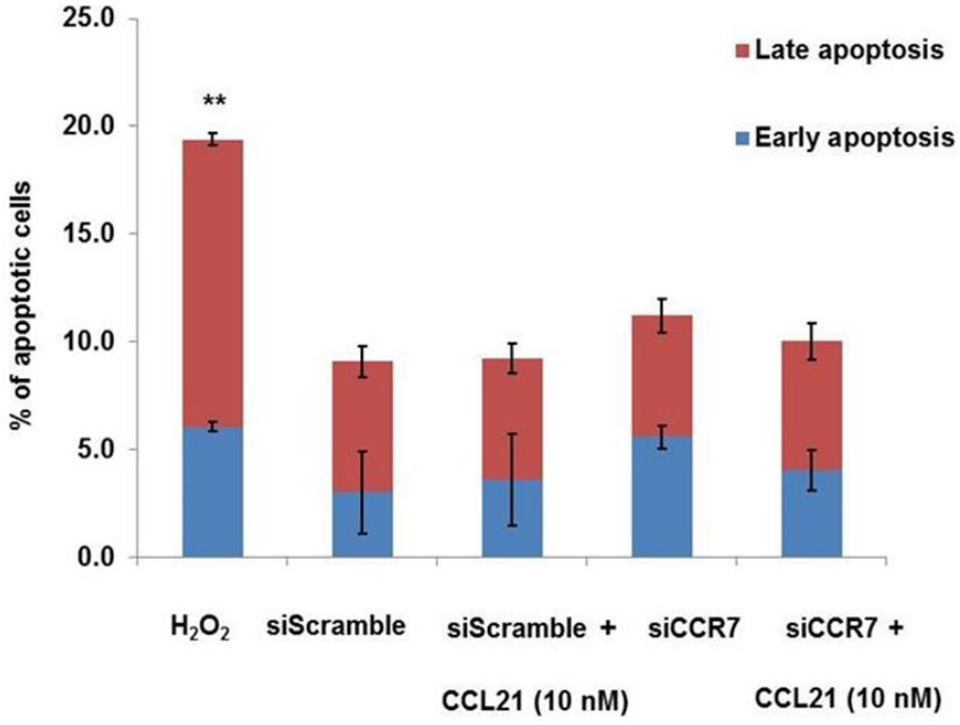

Figure 61: Effect of siCCR7 on cell proliferation and apoptosis.

Number of live cells after siCCR7 with or without CCL21 using trypan blue assay. Values are the mean of 3 independent experiments and error bars are SD (b) Representative images of apoptosis level after treating cells with or without CCL21 10 nM. OSC-19 cells were treated with CCL21, 24 h after transfection. After treatment with CCL21 for 72 h, apoptosis was measured using annexin V staining. (c) Values are representing the % of early and late apoptotic cells of the mean of 3 independent experiments and error bars are SD. *P < 0.05 compared with siScramble group.

It has been suggested by others that CCR7 activation can provide anti-apoptotic cues in lung cancer cells (Xu et al., 2012), however, based on our data, we must conclude that CCL21/CCR7 axis has no such effect in OSC-19 cells. However, this result ought to be revisited as it has been suggested that the activation of survival pathways is observed either by autocrine activation of

the chemokine receptors (Balkwill, 2012) or as a result of the loss of cell attachment (Xu et al., 2012).

3.3.6 Effect of siCCR7 and CCL21 on ROS level

We saw in the previous chapter (section 2.3.10) that addition of H_2O_2 (ROS inducer) in OSC-19 cells resulted in CCR7 upregulation. Furthermore, ROS can have a complex and often contradictory effects on cancer cells, for instance either increasing cell apoptosis or survival (Zablocka and Janusz, 2008).

Hence the link between ROS and chemokines, we decided to investigate whether the lack of anti-apoptotic effects of CCL21 (10 nM) is in itself associated with an increase in ROS that counteract the CCL21 effect on cell proliferation/survival. We performed siRNA transfection to look for the effect of CCR7 downregulation on ROS production upon CCL21 addition. Again, addition of H_2O_2 was used as a positive control for ROS production and caused a 0.45 fold increase of mean fluorescence intensity compared with siScramble group, $P < 0.01$ (Figure 62).

In fact, we observed that the knockdown of CCR7 had no significant effect on the baseline ROS levels in cells, compared with siScramble group, $P = 0.75$ (Figure 62). Furthermore, the addition of CCL21 to siScramble or siCCR7 groups did not cause any changes on the ROS levels with $P = 0.34$, 0.83 compared with siScramble and siCCR7 groups with no CCL21 added, respectively. We can therefore conclude that whilst an increase in ROS results

in an upregulation of CCR7 expression, the activation of CCR7 by CCL21 or the knockdown of CCR7 had no effect on ROS production.

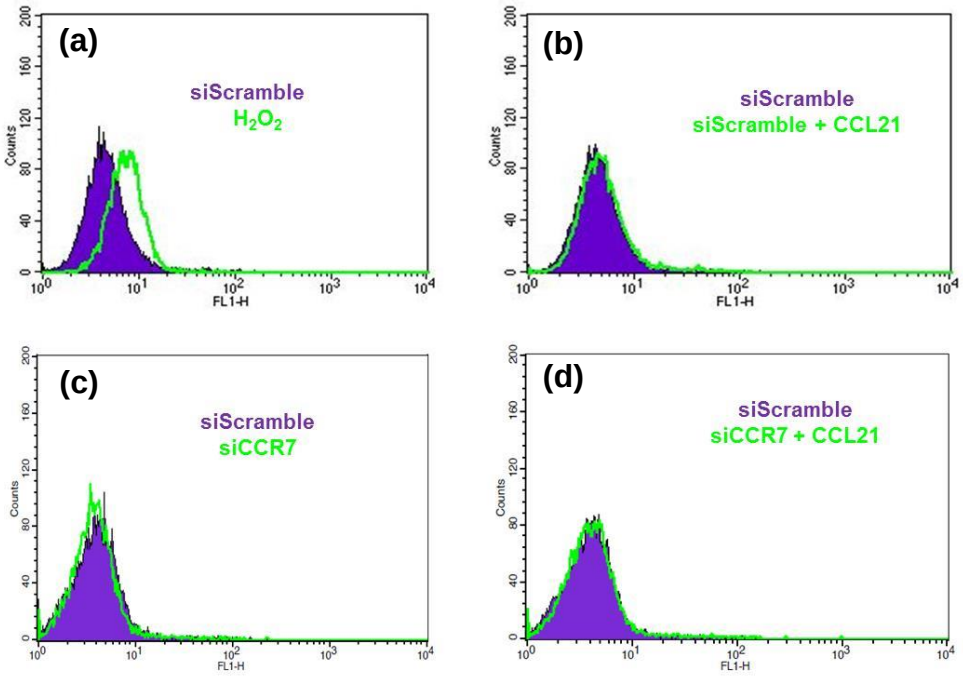

(e)

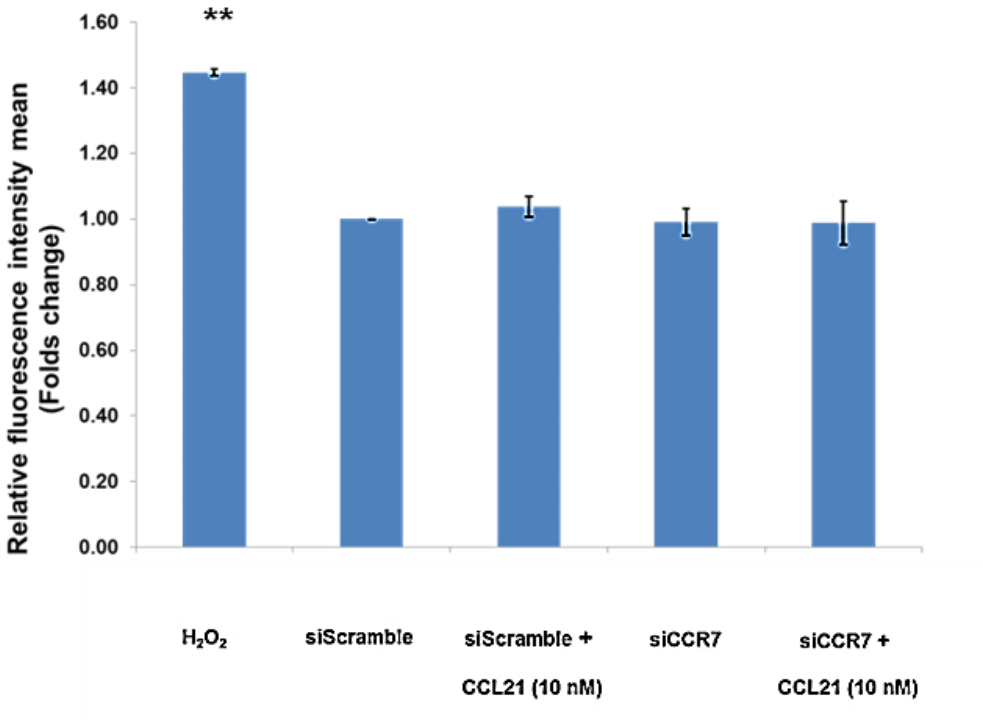

Figure 62: Detection of the ROS level after the knockdown of CCR7.

siScramble and siCCR7 were treated with or without CCL21 10 nM for another 72h after transfection. (a-d) Images represent the change of ROS level (green unfilled curve) in H_2O_2, siScramble with CCL21, siCCR7 or siCCR7 with CCL21 compared to siScramble (purple filled curve). (e) Analysis of flow cytometry data using mean fluorescence intensity Values are the mean of 3 independent experiments and error bars are SD.

3.3.7 Impact of CCR7 expression on Cisplatin sensitivity

Chemotherapy resistance either by intrinsic or acquired mechanism typically leads to tumour relapse and decrease the overall survival (Lippert et al., 2008). In addition, acquired resistance might develop as a result of inducing genetic and/or epigenetic mutations or through other mechanisms after continuous exposure to radiotherapy and chemotherapeutics agents. Hence, chemokines and their receptor might play a vital role in chemotherapy resistance by activating anti-apoptotic pathways and blocking pro-apoptotic pathways (Sarvaiya et al., 2013). For instance, the increased expression of CXCR4 was associated with higher chemo-resistance in pancreatic, ovarian and prostate cancer that lead to poorer progression-free survival and a lower overall survival (Zhang et al., 2015, Domanska et al., 2012, Li et al., 2014).

There is direct and indirect evidence to suggest that the CCR7 can contribute to resistance in head and neck cancers. In addition, the expression of CCR7 on metastatic head and neck cell lines contributed to cisplatin resistance through Akt activation.

Therefore, we decided to study the effect of CCR7 activation in head and neck cell lines on cisplatin sensitivity and particularly, apoptosis. First, we chose 2 cell lines FaDu and OSC-19 and determined the IC_{50} of cisplatin in each by MTT assay as 4±1 and 1.5±1 μM, respectively (Figure 63). We then compared changes in the apoptosis level by flow cytometry after treating the siCCR7 and ScrambleCCR7 cells with cisplatin for 72 h. Our results, showed increase of apoptosis after cisplatin treatment both in siCCR7 and siScramble groups

(Figure 64-a). The % of apoptosis was increased from 10% to 45% for siScramble group and from 12% to 39%) for siCCR7 group. The difference of % of apoptotic cells between siCCR7 and siScramble (Figure 64-a) was not significant after cisplatin treatment with P > 0.05 as shown in (Figure 64-b). It appears based on our results from OSC-19, and the data from others on SCC-4 (Xia et al., 2014),that CCR7 axis is probably not involved in survival at least of these two cell lines.

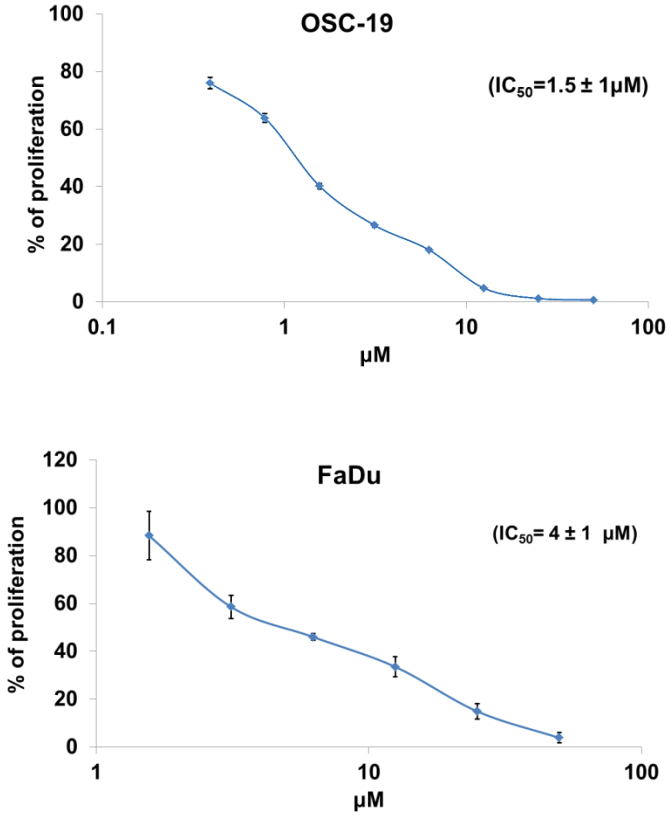

Figure 63: Determination of cisplatin IC_{50} in OSC-19 and FADU.

Cells were seeded at 1 x 10^4 cells/ml in 96 well plate, 24 h later cells were treated with cisplatin for another 72 h. After 96 h, MTT solution was added and 4 h later media was removed and the formazan crystals were dissolved with DMSO. The absorbance was read at 540 nm. OSC-19 error bars are average from n= 3 independent experiments and FaDu n =2.

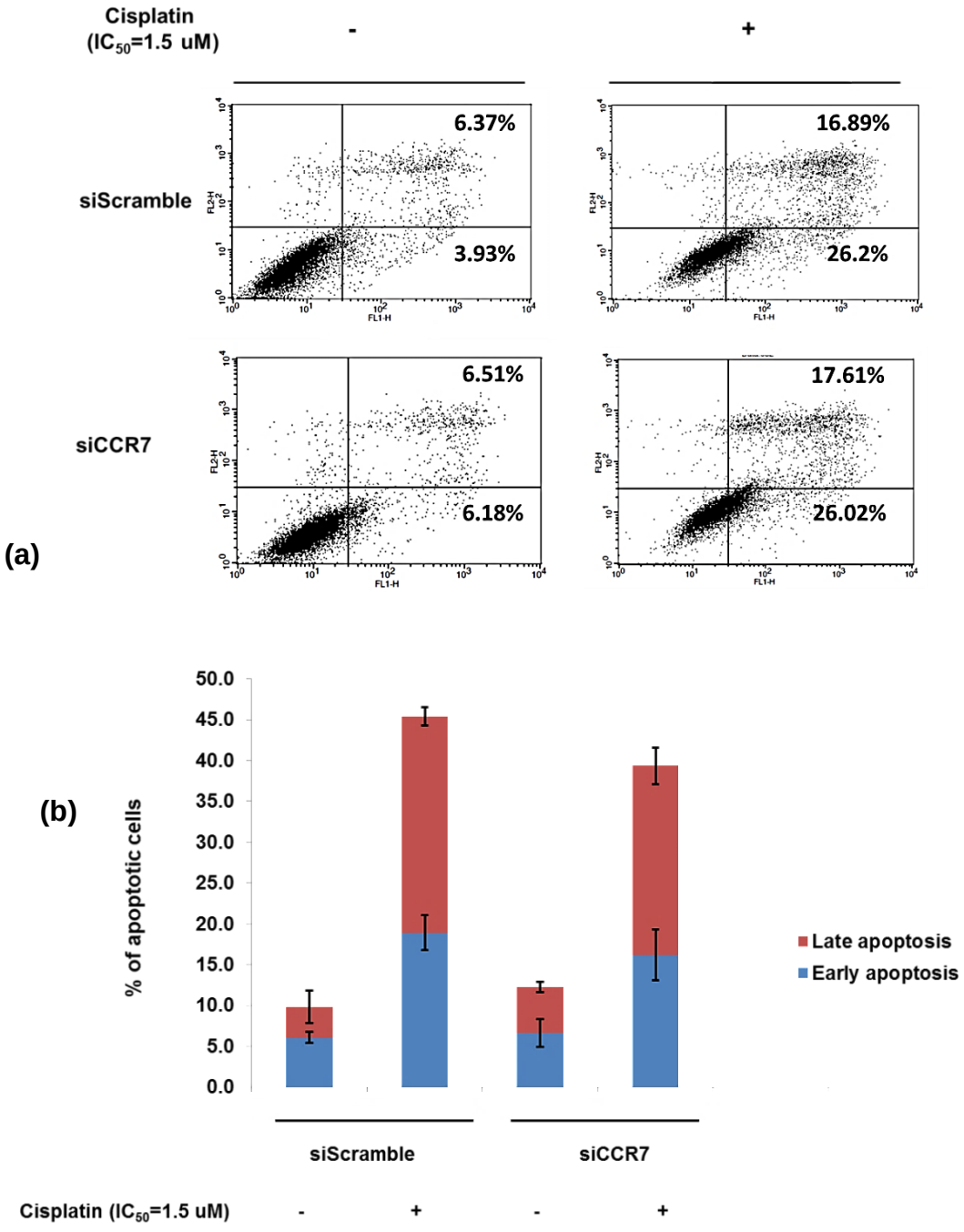

Figure 64: Effect of CCR7 downregulation on cisplatin sensitivity.

Cells were treated with cisplatin for 72h after transfection (a) Images represent the % of apoptosis I siCCR7 and siScramble cells with and without cisplatin. (b) Values are representing the % of early and late apoptotic cells of the mean of 3 independent experiments and error bars are SD.

3.4 Discussion:

The main challenge to increase patient survival is mainly from the complications related to the metastatic process. Thankfully, many aspects of the process and the main key players are being elucidated. For example, in different cancer cell lines and tissues, the significance of CCR7 expression to cancer progression and its role in the metastatic process has been shown (Zhou et al., 2013, Sancho et al., 2006, Hong et al., 2016, Li et al., 2014, Hirakawa et al., 2007, Nardone et al., 2016, Cunningham et al., 2010, Chen et al., 2015, Maekawa et al., 2008, Zhao et al., 2011).

Our findings in the previous chapter indicated the importance of CCR7 expression in head and neck and prostate cell lines in cell migration. Altogether, these findings encourage the development of agents which tackle the spread of cancer cells through prevention of the CCR7 receptor. One of the many strategies to further confirm the importance of CCR7 as a valid target to initiate small molecules design program against it, is the siRNA technology. Indeed, several studies have used the knockdown of CCR7 (Mo et al., 2015, Xu et al., 2011, Chen et al., 2015).

The use of siRNA technique to knock down CCR7 in our OSC-19 cell line was successful at the gene and protein level and maintained during all the experimental time points under normoxia. Furthermore, despite the upregulation of CCR7 under hypoxia in siCCR7 and siScramble cells, the level of knockdown in the siCCR7 cells was maintained. In this chapter, we confirmed that the increase of cell migration was through CCL21/CCR7 interaction in OSC-19 cells and siCCR7

significantly abrogated the effect of CCL21. In addition, cells in which CCR7 was knocked down had reduced migration compared to scrambled control in 10% FBS. Our observation is consistent with other publications on prostate and tongue carcinoma (Xia et al., 2014, Chen et al., 2015). We found that the difference was not significant in 2% FBS media, but that is probably because migration of cells is much reduced in low serum conditions anyway. This suggests that expression of CCR7 may have a wider role in the cell migration, perhaps through cross talk with other axes.

Furthermore, we have observed in chapter 2 that the migration of OSC-19 cells under hypoxia was lower than cells cultured under normoxia despite the increase of CCR7 expression. This is despite our results showing that the migration of siCCR7 cells under hypoxia was less than siScramble. This suggests that whilst CCR7 clearly does play a role in migration of OSC-19 cells, reduction of ROS under hypoxia can effectively oppose that role.

Several studies have suggested that expression of CCR7 on cancer cells is pivotal for proliferation and survival on bladder, lung, prostate, thyroid, pancreatic and breast cancer cell lines (Mo et al., 2015, Xu et al., 2011, Peng et al., 2015, Sancho et al., 2006, Zhang et al., 2016b, Boyle et al., 2016). However, our results from chapter 2 and 3 have shown that although there is a small trend of CCL21 in increasing proliferation (MTT assay and trypan blue results), we observed no statistically significant increase of proliferation by adding exogenous CCL21 or CCL19. Furthermore, our transfection results showed also that silencing CCR7 by siRNA had no significant effect on proliferation. Despite the discrepancy with other

cancer types, our data is consistent with Xia et al study on tongue carcinoma cell line, where they report no significant increase on proliferation of SCC-4 after CCL21 addition (Xia et al., 2014). Furthermore, many studies examined the regulatory mechanism of the CCL21/CCR7 interaction on proliferation and survival. It has been reported P-ERK and P-Akt are involved in increasing cell proliferation in lung and esophageal cancers respectively (Xu et al., 2012, Ye et al., 2011).Xia et al reported no increase in P-Akt after treating the SCC-4 cell line with CCL21. Therefore, it is possible that the effect of CCL21 or CCL19 on CCR7 in regard to cell proliferation and survival might be head and neck cell line specific.

To determine whether the expression of CCR7 has any anti-apoptotic effects on OSC-19 cells despite its insignificant effect on proliferation, the % of apoptotic cells were measured using the flow cytometry after the activation of CCR7 by CCL21 on siCCR7 and siScramble cells. Our preliminary results showed no effect on apoptosis in response to CCL21/CCR7 interaction in contrast to the anti-apoptotic effect observed in other cancers (Xu et al., 2012). In addition, silencing CCR7 had no significant effect on apoptosis with or without CCL21. In contrast to our findings, others have shown anti-apoptotic response to CCL21 in bladder and non-small cell lung cancer cells (Mo et al., 2015, Xu et al., 2012). CCL21/CCR7 had anti-apoptotic in these cell models by up-regulating Bcl-2 and downregulating Bax possibly via ERK activation.

However, in study by Ziegler et al., CCL19 did not affect T cells and HUT78 lymphoma cell line proliferation at concentrations up to 100 nM but they did report an apoptotic effect at concentrations higher than 500 nM of CCL19 (Ziegler et al.,

2007). The physiologic concentrations of a chemokine in normal tissue or tumour are hard to determine precisely. Ziegler's apoptotic effect could be only valid for the physiological environment within lymph nodes in which high chemokine concentrations are present. However, it is likely that it will not be observed in tumour tissues because such very high concentrations of chemokines are probably not present in tumour microenvironment.

Recently, there is emerging evidence linking the chemokine system to ROS (Sozzani et al., 2005, Chetram and Hinton, 2013). Furthermore, depending on the level of ROS produced within the tissue, cytotoxic level of ROS can increase the cell kill (Ozben, 2007). For instance, anthracyclines and epipodophyllotoxins, are used to induce cell death by increasing ROS production. Therefore, we speculated that CCL21/CCR7 survival cues might be counteracted by ROS dependent mechanism. Our results showed that CCL21 did not increase the ROS level in siScramble or siCCR7 transfected OSC-19 cells. Moreover, silencing CCR7 had no effect on ROS production. Therefore ROS might be excluded as the underlying mechanism to conceal the survival signal triggered by CCL21. Alternatively, we could hypothesise that in OSC-19 cells no anti-apoptotic signalling is activated by CCL21/CCR7 interaction.

From this work, it is not clear whether results of our investigation of OSC-19 can be more generally applicable. However, considering the limited role of CCL21 in increasing survival in SCC-4 (Xia et al., 2014) along with our OSC-19 results, we might conclude, at least for head and neck cell lines originating from tongue that CCL21 does not increase tumour survival.

Another likely interpretation for the compromised role of CCL21 in OSC-19 cells can be drawn from CXCR4 studies (Wendt et al., 2008, Wendt et al., 2006). Wendt et al., has shown that autocrine activation of CXCL12 on CXCR4 by stable re-expression of CXCL12 in mammary carcinoma cells inhibited cell migration but increased proliferation (Wendt et al., 2008). Furthermore, after re-expression of CXCL12 in breast cell line MDA-MB-231, the cell responded very poorly to the exogenous CXCL12 in Ca^{2+} flux and transwell chemotaxis assays. Authors propose that the epigenetically silenced CXCL12 in mammary carcinoma cells by hypermethylation might give a selective advantage for the paracrine signal to promote cell migration and metastasis (Wendt et al., 2008). Furthermore, silencing of endogenously expressed CXCL12 in colorectal cell lines promoted their metastatic behavior (Wendt et al., 2006).

Taken together, our apoptosis and proliferation results in OSC-19 supported by (Xia et al., 2014) study on SCC-4, the expression of CCL21 in head and neck xenografts (chapter 2) and the differential effect of autocrine/paracrine activation of CXCR4, we can suggest that exogenous/paracrine or endogenous/autocrine activation of CCR7 might result in different effects in head and neck cell lines depending on the type of the signalling loop. Therefore, further investigation on the effect of autocrine stimulation of CCR7 in head and neck cancer cells on proliferation and apoptosis is warranted.

The conventional standard therapy for head and neck cancer is surgery and/or radiotherapy as a primary treatment for non-metastasized cancer, in addition, platinum based chemotherapy in combination with radiation is the current standard

for surgically inaccessible and metastasized head and neck cancer tumours (Vokes and Athanasiadis, 1996, Kelland, 2007). However, patients often gain resistance for the platinum chemotherapeutic agents; and therefore only 50%-60% of the head and neck patients are cured of the cancer (Sano et al., 2011).

Platinum resistance is often acquired after many cycles of therapy or in some cases, tumours were intrinsically resistant. Therefore identifying the underlying mechanism of chemo-resistance is highly important to increase patient survival. Two main mechanisms have been demonstrated to be responsible for platinum resistance; insufficient DNA binding or recovery after DNA binding by increased survival signalling or increased removal from DNA by excision repair (Kelland, 2007).

Cisplatin is one of the most used cytotoxic drugs used to improve patient survival; however, chemo-resistance is a major hurdle to its clinical use. Li et al., has reported that the expression of CXCR4 is higher in cisplatin resistant ovarian cell line A2780/cis compared with A2780 in vitro (Li et al., 2014). In addition, Li et al demonstrated that the cisplatin chemo-resistance was reduced in cells transfected with siCXCR4 both in parental and resistant ovarian cell lines.

In regard to CCR7, it has been shown that activation of CCR7 leads to increased survival signaling in metastatic PCI-4B or PCI-15B head and neck cancer cell lines after treatment with cisplatin, and that the mechanism is through Akt activation (Wang et al., 2008). Conversely, our findings showed that siCCR7 had no effect on

cisplatin sensitivity of OSC-19 cells suggesting that CCR7 is not involved in the chemo-resistance of cisplatin in this cell line.

Of course, our study on the correlation of CCR7 and cisplatin has several limitations. (1) We designed our experiment based on the results of siCXCR4 on parental ovarian A2780 cell line, which showed that siCXCR4 increased the cisplatin chemo-sensitivity. Hence we only studied the effect of siCCR7 on parental OSC-19 cells without developing an OSC-19 resistant cell line to compare with the parental cell line. (2) Assuming a differential effect of autocrine and paracrine activation of CCR7, a study on the effect of autocrine activation of CCR7 on cisplatin sensitivity is necessary.

In summary, the data generated in this chapter confirmed that importance of CCR7/CCL21 in cell migration both under normoxic and hypoxic conditions encouraging the development of anti-metastatic compounds to see whether similar effect will be achieved using small molecules. In addition, the presence of CCR7 by exogenous ligands showed no increase in proliferation or decrease of apoptosis.

Hence, in order to further study the effect of blocking CCL21/CCR7 axis using small molecules developed in house, pharmacological experiments will be carried out using OSC-19 as a model for evaluating CCR7 antagonists **(chapter 4)**.

❖ **The main findings of this Chapter were:**

- Significant and specific knockdown of CCR7 was achieved at gene and protein level.

- CCR7 is involved in increased cell migration of OSC-19 cells under normoxic and hypoxic conditions.

- CCR7 is not involved in increasing cell survival and proliferation or providing anti-apoptotic signal in OSC-19 by exogenous CCL21.

Chapter 4:

Identification and Pharmacological evaluation of small molecule CCR7 antagonists

4.1 Introduction

4.1.1 Therapeutic implications of targeting CCR7

The role of chemokines and their receptors in cancer is well established and has been discussed in the preceding chapters. In particular, it is known that their expression on tumour cells facilities the metastatic process at different stages (Sarvaiya et al., 2013). Once the metastatic spread of cancer cells to the secondary sites has occurred, treatment options become very limited. Therefore, preventing chemokine induced migration provides a good opportunity to develop new treatments for cancer.

The association between CCR7 upregulation by tumour cells and lymph node metastasis has been validated in different types of cancers (Zhao et al., 2011, Zhou et al., 2013). Indeed, CCR7 has been suggested to be used as a biomarker to increase reliability of computed tomography to assess the lymph node metastasis status in bladder cancer (Chen et al., 2016), and in conjunction with CXCR4 as a biomarker for axillary lymph node metastasis in T1 breast cancer (Cabioglu et al., 2005). So far, several lines of evidence, including knockout, knockdown, anti-sense studies and the use of neutralizing antibodies, have supported the validity of CCR7 as an anti-metastatic therapeutic target. Despite this evidence, investigating the effect of inhibiting CCR7 in tumours using small molecule antagonists has not received much attention probably for a number of reasons, namely:- (1) There are small molecule antagonists that target other chemokine receptors important in cancer as well as diseases such as acquired

immune deficiency syndrome (AIDS) and asthma (Wells et al., 2006). However, there are currently no small molecule CCR7 antagonists available that can be used as a biological tool, or as a lead in a drug discovery programme (Lazennec and Richmond, 2010). The lack of any CCR7 antagonists is unusual. CCR7 belongs to the GPCR family of receptors. This makes it an attractive therapeutic target, as GPCRs are considered a highly druggable receptor class, indeed 40% of drugs currently in the market target GPCRs (Wu et al., 2009). In fact, it appears that our group is the only one with access to a CCR7 antagonist (AHMED, 2016) (2) CCR7 has a well- documented role in adaptive immunity (Comerford et al., 2013). Thus, it could be argued that inhibiting the receptor might raise the risk of developing autoimmune diseases as an undesired side effect. However, knockout studies in mice have demonstrated that the animals remain healthy and show no autoimmune disease symptoms within their life span period (Comerford et al., 2013). In addition, there are now a number of chemokine antagonists have been successfully registered by the FDA: Plerixafor, which targets CXCR4 and has shown anti-metastatic activity in animal models. It is being evaluated in clinical trials for ovarian cancer, osteogenic sarcoma and acute myeloid leukaemia (Lanza et al., 2014, Zlotnik et al., 2011); Maraviroc, which is indicated for HIV infection by blocking CCR5 (Xu et al., 2014); and Mogamulizumab, a monoclonal antibody against CCR4 that is indicated for T lymphoma and some allergic diseases (Ogura et al., 2014). All of them have completed initial clinical trials with no toxicity or adverse immune response effects observed in healthy adults (Giles and Loberg,

2006). Altogether, this is a very encouraging motivation for the development of CCR7 inhibitors.

Recently, there has been a resurgence and renewed interest in looking at the beneficial effects of targeting CCR7 in preventing lymph node metastasis in cancer. Silencing CCR7 in mice or loss of CCL21 by the natural mutation paucity of lymph node T cells (plt) resulted in impaired migration of lymphocytes and DCs to the lymph nodes (Legler et al., 2014). We know that tumour cells hijack the normal mechanisms by which DCs travel to the lymph node following chemotaxis gradients. Therefore, it is reasonable to investigate if the inhibition of CCR7 would have an anti-metastatic and anti-migratory effect, and to determine if this effect can mirror what has been observed with DCs. (Legler et al., 2014).

The evidence so far is encouraging. For example, Shuyi et al. have investigated the use of double-stranded short interfering RNA (siRNA) to target CCR7 mRNA in colon cancer cells both *in vitro* and *in vivo*. Silencing CCR7 mRNA by siRNA transfection was found to decrease cytoplasmic Ca^{2+} mobilization and strongly inhibit chemotaxis and invasion *in vitro*. Furthermore, blocking the expression of CCR7 on tumour cells in animal models correlated with less lymph node metastasis (Shuyi et al., 2008).

Inhibiting CCR7 using neutralizing antibodies has been shown to block the activation of pro-survival signals in head and neck cancer (Kruizinga et al., 2009). Recently, inhibiting CCR7 expression using synthetic microRNA, Let-7a, has been shown to decrease the invasion and migration of breast cancer cells (Kim et al., 2012). Furthermore, using anti-CCL21 antibodies blocked metastasis of murine

melanoma cells completely (Wiley et al., 2001). Chemotrap-1, an engineered soluble receptor utilizing an endogenous human protein sequence that binds to CCL21 also blocked the lymphatic metastasis of murine melanoma cells (Lanati et al., 2010).

Of course, whilst antibody and microRNA therapies are more selective, they involve high costs of production, and are associated with the potential risk of developing immunogenicity (Wu et al., 2009). Similarly, the use of soluble receptors as antagonists has some drawbacks; the short half- life and the high doses required to achieve good binding (Jones and Rose-John, 2002), Therefore, synthesising and developing small molecules to antagonize CCR7 can provide a more economical and safer option to prevent metastasis and improve the efficacy of treatment and significantly benefit patients.

4.1.2 Development of CCR7 antagonists

Taken together, our own results and the published evidence on the role of CCR7 in cancer progression encouraged us to identify and develop a series of novel CCR7 antagonists. Currently, our group at the ICT at University of Bradford is actively involved in this line of research and a brief background to our discoveries is outlined below. ICT5189 (Figure 65) was discovered by our group as a weak CCR7 antagonist (AHMED, 2016) and tested in our Ca^{2+} flux assay. A derivative compound, namely ICT5888 lacking the 4- propyl 1,3 oxazole moiety was also synthesized. Both compounds showed similar efficacy in the Ca^{2+} flux assay. We decided to carry on with ICT5888, which has a simpler structure, as our lead compound and starting point for the medicinal chemistry program.

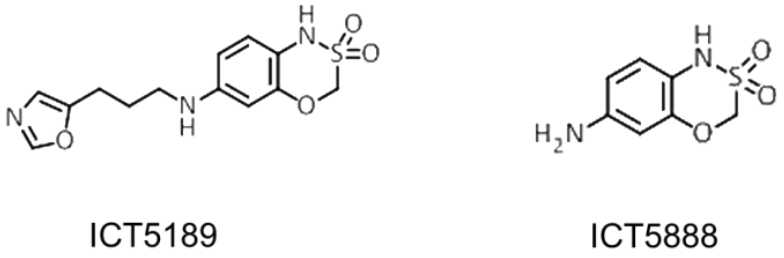

ICT5189 ICT5888

Figure 65: Compound ICT5189 and ICT5888.

Both compounds reduced the Ca^{2+} flux induced by CCL21 and therefore identified as hit molecules; see Figure 69 for Ca^{2+} flux IC_{50}.

4.1.3 Drug Design of Analogues

As mentioned before, ICT5888 was shown to be active by Ca^{2+} flux assay. The next step was to build up a library of ICT5888 analogues in order to identify which parts of the molecule are responsible for its biological activity. Our screening cascade is outlined in Figure 66. The Ca^{2+} flux assay was used to determine relative potency of compounds and thus determine what effect structural modifications have on the biological activity. Next, active compounds are tested for cytotoxicity (MTT assay) to confirm that the observed effect is not due to cytotoxicity rather than true antagonism. When compounds are not cytotoxic and are active in the Ca^{2+} assay, further biological analysis is performed, to determine whether any of the compounds can stop the CCR7 functional effects on cell migration and invasion. The cycle of chemical synthesis and biological evaluation is repeated in a reiterative fashion in order to discover more potent and drug-like compounds. Accordingly, many analogous were prepared to study the ICT5888 structure activity relationship (SAR) and to find a more potent compound to be

used in subsequent studies. All of the analogues synthesis was performed by Dr. Mohanned Ahmed (ICT) and MSc students (Anwar Salem and Taher Shalabi). Furthermore, The IC_{50s} of compounds from the Ca^{2+} flux assay were generated by Dr. Victoria Vinader and Dr. Mohanned Ahmed. For Ca^{2+} flux data see Figure 69.

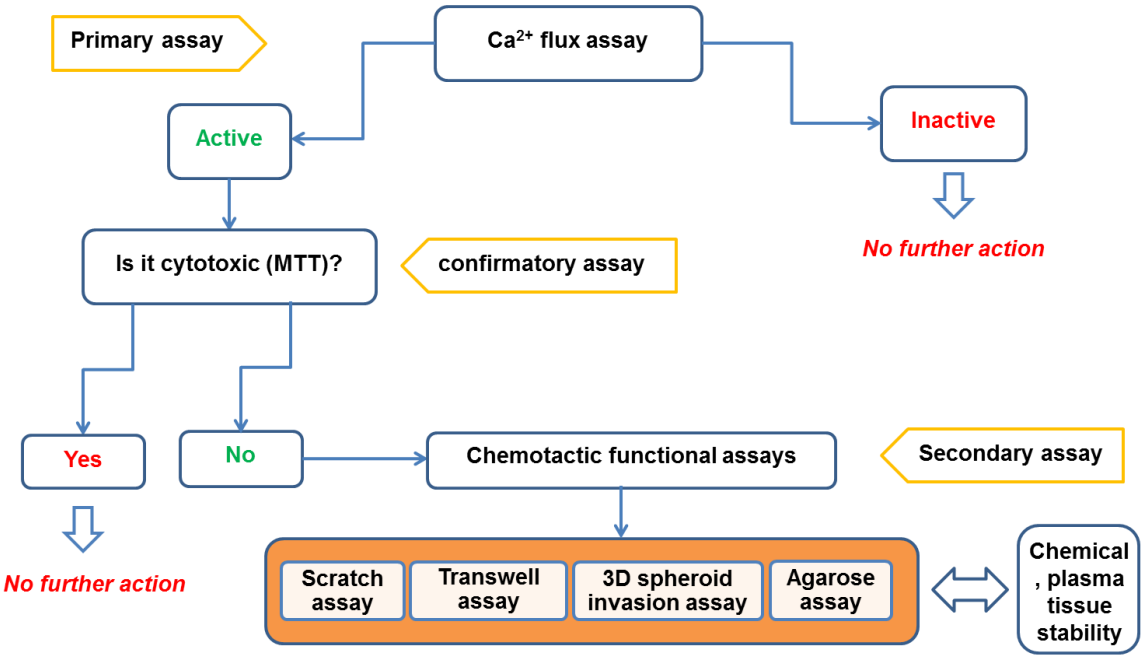

Figure 66: Screening cascade of biological assays in the process of drug discovery of CCR7 antagonists. Figure courtesy of Dr. Victoria Vinader.

4.1.4 Aims and objectives

CCR7 expression in head and neck cancer cell lines (OSC-19) affected cells migration (chapter 2) and invasion in 2D and 3D assays (see sections 4.3.44.3.5). Therefore, developing small molecule antagonists against CCR7 will enhance our understanding of its role in cancer and potentially disrupt migration and invasion which will have a strong impact on the survival rate of patients.

❖ **The main aims and objectives of this chapter are:**

- To evaluate the effect of CCR7/CCL21/CCL19 axis in 2D and 3D invasion assays.
- To evaluate the effect of CCR7 antagonists on cell proliferation, migration and invasion

4.2 Materials and methods

4.2.1 Materials

Tissue culture materials and reagents were all obtained from (Sigma-Aldrich) unless otherwise specified.

4.2.2 Cell culture

OSC-19 cells were obtained from as described earlier in chapter 2. Cells were cultured at 37°C and maintained at 5% CO_2 and 100% humidity. Cells were cultured in complete RPMI 1640 medium supplemented with 10% FBS and L-glutamine (2 mM) and Sodium pyruvate solution (1 mM). Cells were passaged when reach 75% confluency as described earlier in section 2.2.5.

4.2.3 Synthesis of CCR7 compounds

Small molecule CCR7 antagonists were synthesized in house by the medicinal chemistry team at ICT by Dr Victoria Vinader, Dr. Mohanned Ahmed and Msc students (Anwar Salem and Taher Shalabi).

4.2.4 Ca^{2+} flux assay

Testing of compounds for ranking by Ca^{2+} flux assay was done by Dr. Victoria Vinader and Dr. Mohanned Ahmed. Briefly, OSC-19 cells were seeded in a 96-well black tissue culture treated plate at $1x10^5$ cells/well and left to attach overnight in the incubator. The following day, medium was removed and cells were washed with 100 µl of the assay buffer twice. Quickly but carefully 100 µl of the loading dye (Molecular Probes™ Fluo-4 NW, Invitrogen) was added to each well and incubated for 30 min at 37°C. Serial dilutions of the antagonists were prepared and 20 µl

were added to the appropriate wells and incubated for another 30 min. Fluorescence intensity was then measured in response to 20 µl of 100 nM of CCL21 added using Thermo scientific Flourskan Ascent FL at excitation wavelength 485 nm and emission wavelength 538 nm at 37°C

4.2.5 Cytotoxicity assay using MTT

The cytotoxicity of CCR7 antagonists was determined by MTT assay. Toxic concentrations will cause cell death, leading to a reduction in the colour purple color produced by the presence of formazan crystals and consequently less absorbance readings. Similarly to the proliferation assay, OSC-19 cells were seeded in a 96-well plate at a density of 1 x 10^4 cells/ ml and were incubated for 24 h. On the following day, 20 µl of different serial dilutions were added to the appropriate wells to achieve the desired concentration in wells of **ICT5888** (1mM, 0.75 mM, 0.5mM, 0.25 mM, 0.1 mM, 10µM, 1µM, 0.1µM), **ICT13069** (250µM, 100µM, 10µM, 1µM), **ICT13124** (200 µM, 100 µM, 10 µM, 1uM). (250 µM, 100 µM, 10 µM, 1 µM) **ICT13122** (500 µM, 250 µM, 100 µM, 10 µM, 1µM, 0.1µM) (250 µM, 100 µM, 10 µM, 1uM), **ICT13070** (250 µM, 150 µM, 100 µM, 10 µM, 1 µM), **ICT13072**, (250 µM, 150 µM, 100 µM, 10 µM, 1 µM), **ICT13301**, **ICT13303**, **ICT13309**, **ICT13310**, **ICT13311**, **ICT13312**, **ICT13313**, **ICT1325** (250 µM, 150 µM, 100 µM, 10 µM, 1 µM). Following compound treatment, cells were incubated for another 72 h. Then, 20 µl of 5 mg/ ml MTT stock solution (for preparation of MTT stock solution see appendix II) was added to the cells and incubated for 4 h. After 4 h, the medium was removed and 150 µl of DMSO was added to each well, to dissolve the purple-blue formazan crystals produced. Absorbance was then

recorded at 540 nm using a colorimetric plate reader (Thermo scientific). The % of cell viability was determined using the following equation:-

$$Proliferation(\%) = \frac{A - B}{C - B} * 100$$

Where A is the absorbance of treated cells with specific concertation of each compound, B is the absorbance of blank and C is the absorbance of untreated cells.

4.2.6 Wound healing assay

The non-cytotoxic and active compounds in MTT and Ca^{2+} flux assays, respectively, were tested in a wound healing assay to determine if they are able to stop the migration of cells. We chose the wound healing assay because it is relatively fast, easy and inexpensive to perform to compare among compounds for stopping the migration of cells and can be modified, to incorporate the addition of CCR7 ligands. The assay was performed as described earlier in section 2.2.13 with the adjustment of the addition of compounds. Briefly, OSC-19 cells were seeded at a density of 8.5 x 10^5 cells/well in 24 well tissue culture treated plates and allowed to attach overnight and reach confluency. On the following day, the supernatant was removed and the wells were washed with PBS. A wound was scratched using the tip of a p200 pipette tip. Afterwards, the cells were washed twice with PBS and treated with CCR7 antibody or antagonists for 2 h, before the addition of CCL21 (10 nM final concentration). We used CCR7 antibody (monoclonal anti-human CCR7 antibody, R&D systems) to confirm that blocking the CCR7 receptor indeed results in a reduction of the migration ability of cells and

that the CCR7 small molecule antagonist can exert a similar effect. The antibody at different final concentrations (100, 10, 1, 0.1 µg/ml) was also added to OSC-19 cells 2 h before adding the CCL21 (10 nM final concentration). We studied the effect of different compounds in blocking the migration, namely, ICT5888 and its analogues (ICT5888, ICT13069, ICT13070, ICT13072) at a top concentration of 100 µM for 2 h (note that this at least a IC_{10} concentration, as determined by MTT). Afterwards, CCL21 (10 nM final concentration) or medium was added to wells and left in the incubator at 37°C, 5% CO_2 and 100% humidity for another 16 h. Compound ICT13069 was the most effective at this top concertation and therefore, further investigation was taken at different concentrations (100µM, 1µM, 1µM, 100nM, 10nM, 1nM). Later analogues of ICT13069 were tested at 1µM, along with ICT13069 to decide which compound had similar or better activity than ICT13069. Images of the scratches were taken using a lumascope 488 microscope at 0 and 18 h. Image J software was used to determine the free surface area of the wound at 0 h and at 18 h, as described earlier in section 2.2.13. Each experiment was repeated at least 3 times in independent occasions.

4.2.7 Transwell invasion assay:

The transwell inserts (pore size 8 µm, Corning) were coated with 100 µl of 50 µg/ml collagen I (collagen type 1 rat tail, Corning) and incubated at 37°C overnight. The following day, the remaining collagen was aspirated, and the inserts were washed well with a free serum medium. OSC-19 cell suspension (150 µl) treated with serial dilutions of compound ICT13069 (100 µM, 10 µM, 100 nM, 10 nM) was added at a density of 6.7 x 10^5 cells/ml to the top compartment of the inserts. The top inserts contained no serum or chemoattractant, whereas the medium in the lower wells contained 0, 10 or 100 nM of CCL21 or CCL19 respectively. After 48 h of incubation at 37°C, 5% CO_2, the cell suspension was removed from the top inserts and the cells attached to the upper side of the membrane were wiped off with a cotton swab. Cells on the lower side of the membrane were fixed with 70% ethanol for 2 min at R.T. and left for air dry. The membrane was carefully cut off using a scalpel and placed onto a microscope slide using mounting medium containing DAPI (Fischer scientific) to facilitate nuclear staining. Images of the invaded cells using 4 representative fields for each membrane were taken using a Leica fluorescence microscope at 200x magnification power (Figure 67-a). Invaded cells were counted using Image J software as follows: images were opened through Image J, the blue channel was selected and converted to binary (Figure 67-b) and counted (Figure 67-c). Mean number of cells was calculated from at least 3 independent experiments.

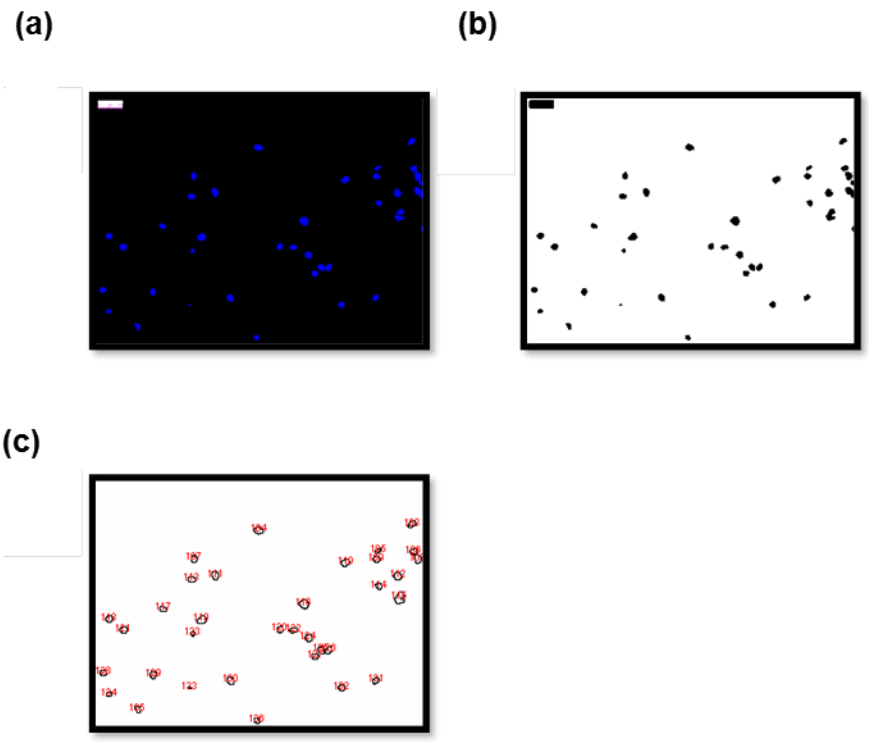

Figure 67: Data analysis of cells able to invade through the collagen coated transwell membrane using Image J

(a) Cells stained with DAPI were analyzed through Image J. (b) Images converted to binary for Image J recognition. (c) Cells were counted through Image J.

4.2.8 Forming spheroids using the hanging drop method

First, a cell suspension of OSC-19 cells at a density of 6.7 x 10^4 cells/ml was prepared. The cell suspension was prepared with or without 20% methylcellulose (For the preparation of 20% methylcellulose see appendix III). 30 µl of cell suspension was taken using a multichannel pipette and seeded onto the lid of a 60 mm petri dish, 0. 5 ml of PBS was added to the bottom of the dish to prevent the dehydration of the drops. The lid was then carefully inverted and placed on top of the PBS filled dish and incubated at 37°C and 5% CO_2 overnight.

4.2.9 Detection of CCR7 in OSC-19 spheroids

In order to confirm that the OSC-19 spheroids that will be used in the invasion assay, do express CCR7, we stained them for CCR7 expression. Briefly, spheroids of 200 µm diameter were transferred to a 20 ml universal tube and allowed to sediment down slowly and treated with Bouin's solution as described earlier in section 2.2.21.3 All the later fixation steps until embedding spheroids in paraffin were followed exactly as described before in section 2.2.21. After sectioning of 5 µm thick sections, the staining by IHC means for detection of CCR7 expression was followed as described in section 2.2.10.

4.2.10 Spheroid invasion assay

Collagen I (1.5mg/ml, 3ml) was prepared by mixing 600 µl of 5x PBS, 23 µl of 1N NaOH ,1455 µl of distilled water and 922 µl of collagen 4.88mg/ml (collagen type 1 rat tail, Corning). 75 l of this mixture was added to each well of flat bottomed 96 well plate and incubated for 30 min at 37°C, then 1 spheroid in 2 µl of medium was placed onto the collagen bed in each well and overlaid with another 75 µl of collagen mixture and incubated for another 30 min at 37^{o}C. Afterwards, serial dilutions of compound ICT13069 in 150 µl of 1% FBS medium with or without CCL21 or CCL19 at (100 nM) were added to each well. The plate was incubated for 20 h. Spheroid invasion was visualized by microscopy. Images were taken at 0 and 20 h on a lumascope 488 microscope. Data analysis was performed by utilising Image J and represented as % area of invasion (Figure 68). The % Area of invasion was calculated using the following equation:

$$\%\ area\ of\ invasion = (B - A) * 100\%$$

Where A is the % area before invasion and B is the % area after invasion.

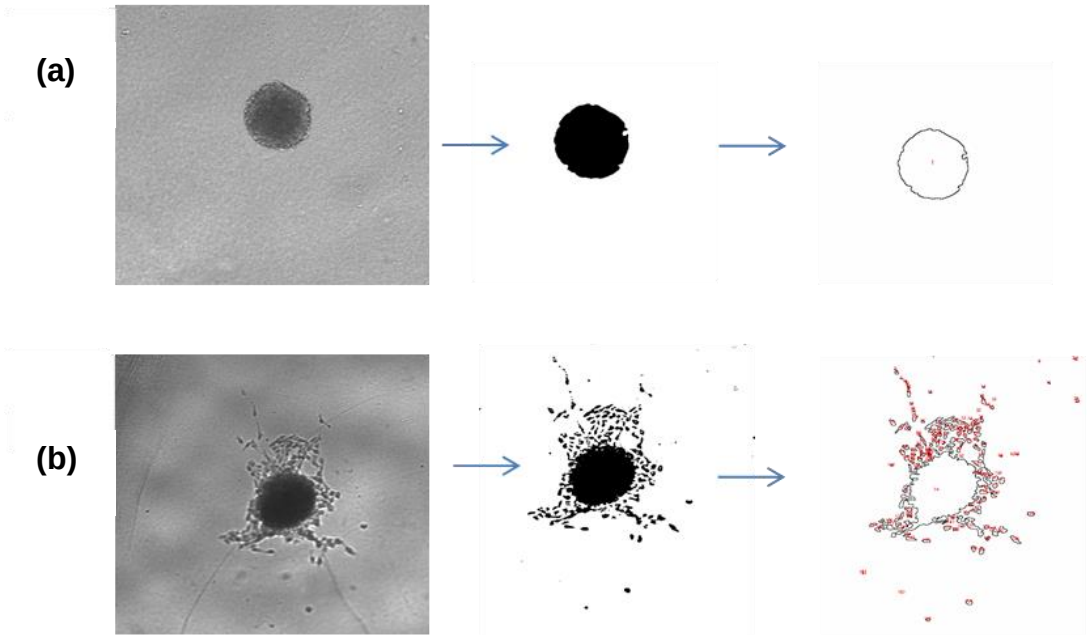

Figure 68: Data analysis of spheroid invasion assay using Image J.

(a) Spheroids at 0 h were captured using lumascope 488 microscope, converted with image J to binary picture of black and white and % area was determined. (b) Invading spheroids after 20 h were captured through lumascope 488 and converted to binary picture of black and white with Image J and the % area determined.

4.2.11 Spheroid viability assay

We performed a spheroid viability assay to confirm that our spheroids were viable during the invasion assay experimental set-up. Calcein (1 µg/ml) was used to stain the viable cells and PI (200 µg/ml) to stain dead cells; since PI does not enter intact membranes in viable cells it will only stain dead cells. A mixture was prepared by adding 1 µl of calcein solution and 4 µl of PI to 995 µl of PBS, 100 µl of this solution was added to the wells that contain embedded spheroids and images were taken using the time-lapse confocal fluorescent microscope Nikon eclipse TE2000e.

4.2.12 Statistical data analysis

The significance of results was assessed through a comparison of means using two-tailed student t-test. Results were expressed as the mean ± standard deviation. P values were calculated to determine statistical significance of the results. ***P < 0.05 and **P < 0.01.**

4.3 Results

4.3.1 Determination of IC_{50} from MTT assay

Before confirming any *in vitro* data from assays, it is important to determine whether the compounds are having their effect at non-cytotoxic concentrations. If any compound was exerting its effect in reducing Ca^{2+} flux at concentration above IC_{10} obtained from MTT assay, the compound would be excluded from further analysis. We use the MTT assay to determine the cytotoxicity of our compounds. The cytotoxic effect was determined by testing a range of different concentrations for compounds (ICT5888, ICT13069, ICT13070, ICT13072, ICT13122, ICT13124, ICT13301, ICT13303, ICT13309, ICT13310, ICT13311, ICT13312, ICT13313 and ICT13325). Cytotoxicity is expressed as $IC_{50,}$ which is the concentration of the compound that caused 50% reduction of the optical density measured at 540 nm (Figure 69-a). IC_{50} were calculated from graphs and represented in the following table (Figure 69-b). All compounds inhibited cell proliferation in a dose dependent manner. In most cases, cytotoxicity is only observed at very high concentrations. For all further assays, compounds were used at estimated IC_{10} or below.

Ca^{2+} flux data were produced by Dr. Victoria Vinader and Dr. Mohanned Ahmed. IC_{50} for Ca^{2+} flux is the concentration of the compound that caused 50% reduction of the fluorescence intensity caused by CCL21 (Figure 69-b). If IC_{50} is not available (NA), the compound was tested in Ca^{2+} flux assay at the IC_{10} or lower concentration obtained from MTT. If active at this particular concentration,

compound will be evaluated in scratch assay. Our team is currently testing these compounds in Ca^{2+} flux assay to have IC_{50} values.

(a)

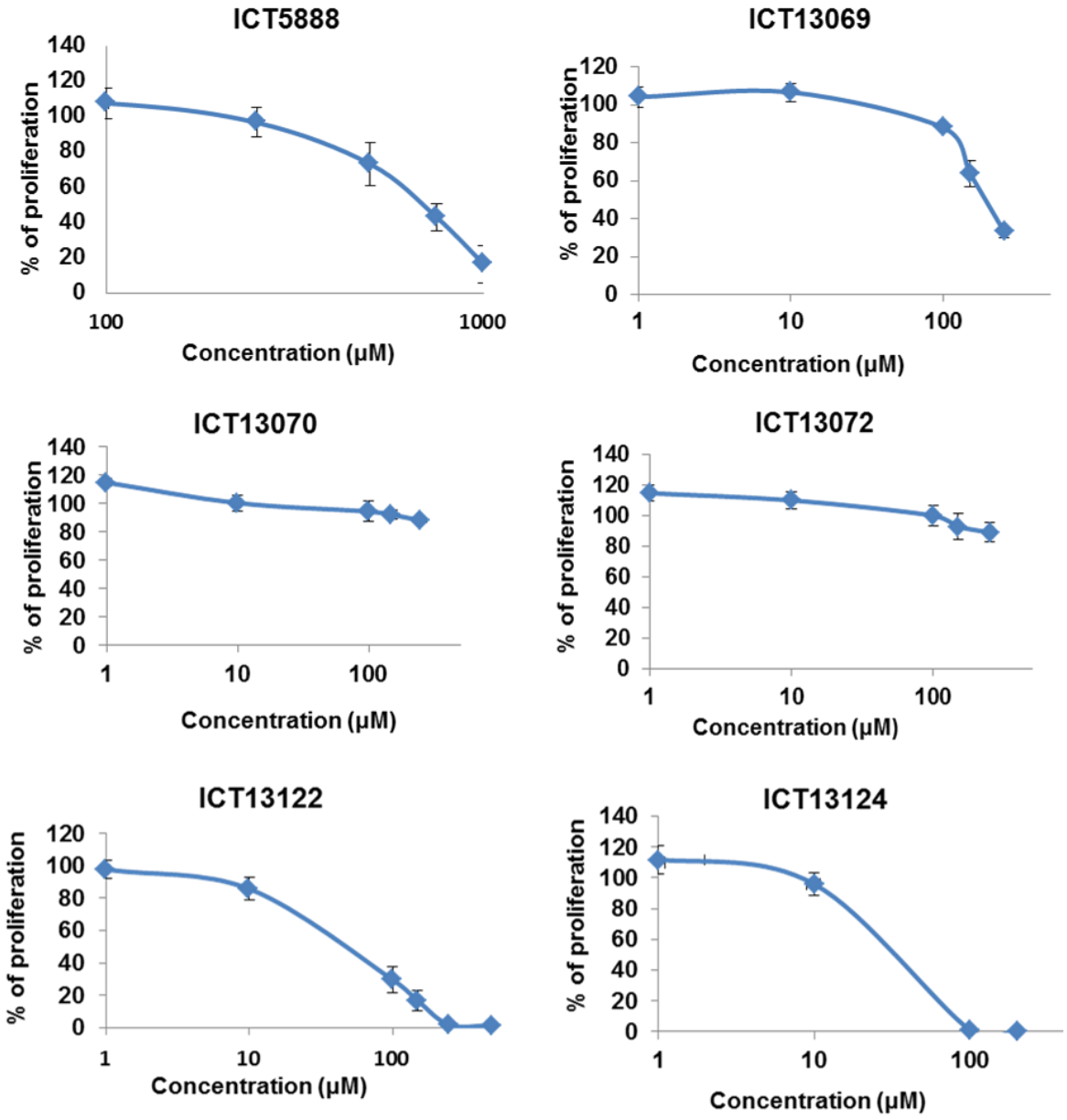

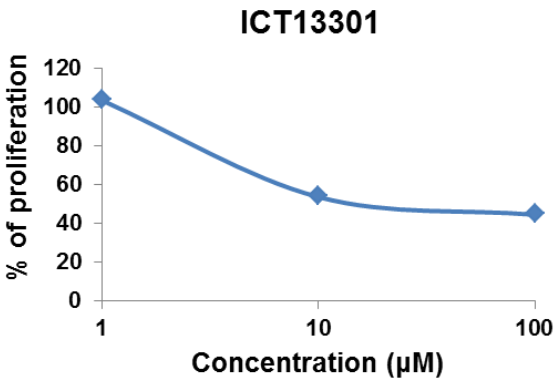
ICT13301
% of proliferation
120
100
80
60
40
20
0
1
10
100
Concentration (μM)

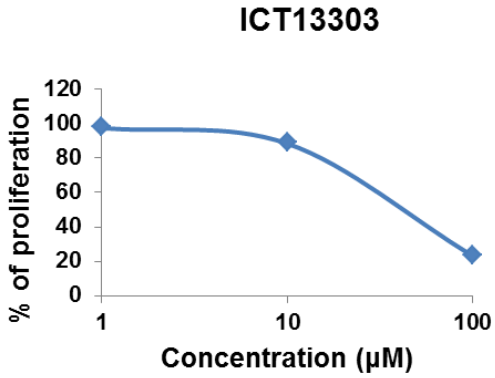
ICT13303
% of proliferation
120
100
80
60
40
20
0
1
10
100
Concentration (μM)

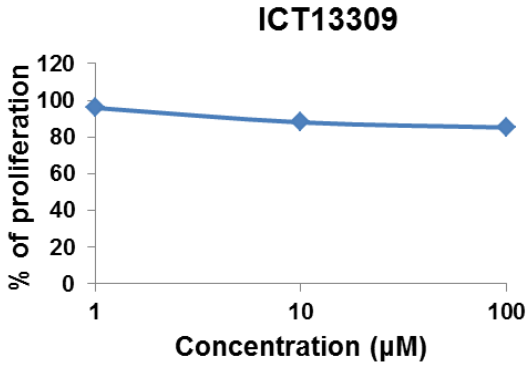
ICT13309
% of proliferation
120
100
80
60
40
20
0
1
10
100
Concentration (μM)

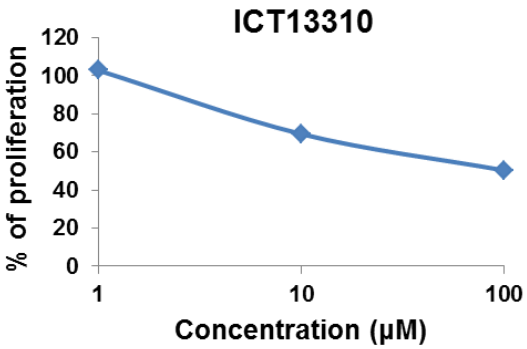
ICT13310
% of proliferation
120
100
80
60
40
20
0
1
10
100
Concentration (μM)

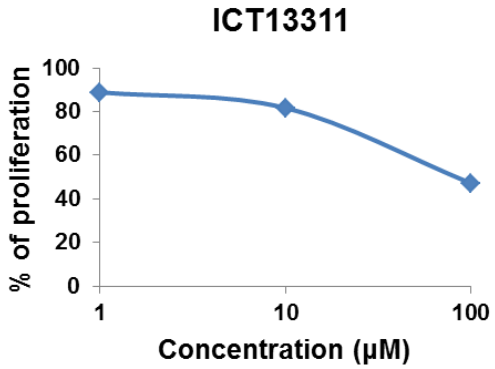
ICT13311
% of proliferation
100
80
60
40
20
0
1
10
100
Concentration (μM)

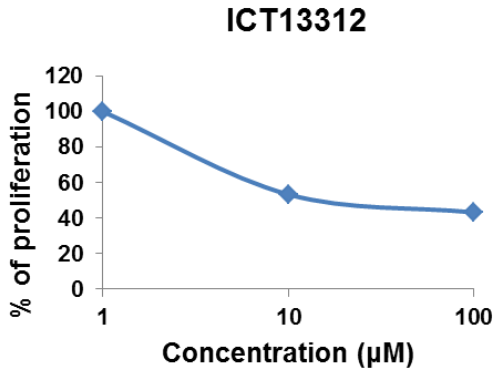
ICT13312
% of proliferation
120
100
80
60
40
20
0
1
10
100
Concentration (μM)

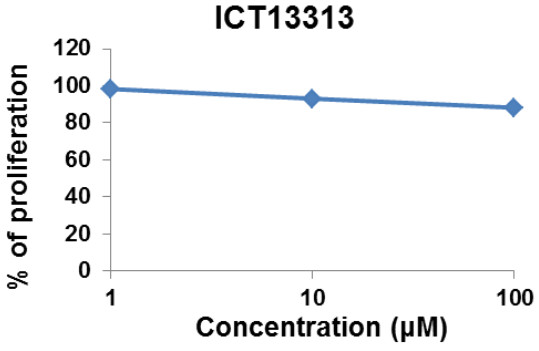
ICT13313
% of proliferation
120
100
80
60
40
20
0
1
10
100
Concentration (μM)

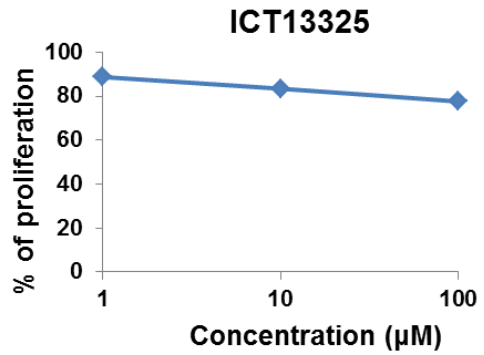
ICT13325
% of proliferation
100
80
60
40
20
0
1
10
100
Concentration (μM)

(b)

Compound	$IC_{50}(\mu M)$	
	MTT	Ca^{2+} flux
ICT5888	680 ± 20	10 ± 0.19
ICT13069	190 ± 20	0.19 ± 0.2
ICT13070	> 250	5.7 ± 1.3
ICT13072	> 250	6.8 ± 2.7
ICT13122	45 ± 5	1.0 ± 0.9
ICT13124	35 ± 5	0.10 ± 0.3
ICT13301	15 ± 5	NA
ICT13303	40 ± 5	NA
ICT13309	> 250	NA
ICT13310	120 ± 20	NA
ICT13311	80 ± 20	NA
ICT13312	15 ± 5	NA
ICT13313	> 250	NA
1CT13325	> 250	NA

Figure 69: Effect of CCR7 antagonists on cell viability and Ca^{2+}flux data

(a) OSC-19 cells were seeded in 96-well plate and treated with a range of concentrations for 72 h. (b) Compounds were ordered according to IC_{50} from higher to lower. Each value expressed is the average calculated from 3 independent experiments however for the newest generation of compounds only n = 1 was generated. Ca^{2+} flux data was generated by Dr. Victoria Vinader and Dr. Mohanned Ahmed. NA = Not available.*Cytotoxicity and Ca^{2+} flux release inhibition is expressed as IC_{50} which is the concentration of the compound that caused 50% reduction of response. Absorption or fluorescence intensity is proportional to cell viability. Error bars represent SD.

4.3.2 Effect of CCR7 antagonists on cell migration in wound healing assay

We have shown in chapter 2 that CCL21 increased the cell migration but that there was no significant difference between using 100 nM and 10 nM of this chemokine in wound closure. We also showed that CCL19 had no effect on cell migration compared with control at the concentrations we used. Next, we sought to determine whether the induced cell migration caused by CCL21 could be blocked by a CCR7 antibody. Cells migrated significantly more in response to CCL21 than control (2%FBS medium without CCL21) This effect was abrogated in the presence of CCR7 selective antibody (Figure 70-a).

CCR7 neutralizing antibody blocked CCL21 induced cell migration in a dose dependent manner. The effect of CCL21 was abrogated significantly at 100 µg/ml, 10 µg/ml and 1µg/ml (Figure 70-b).

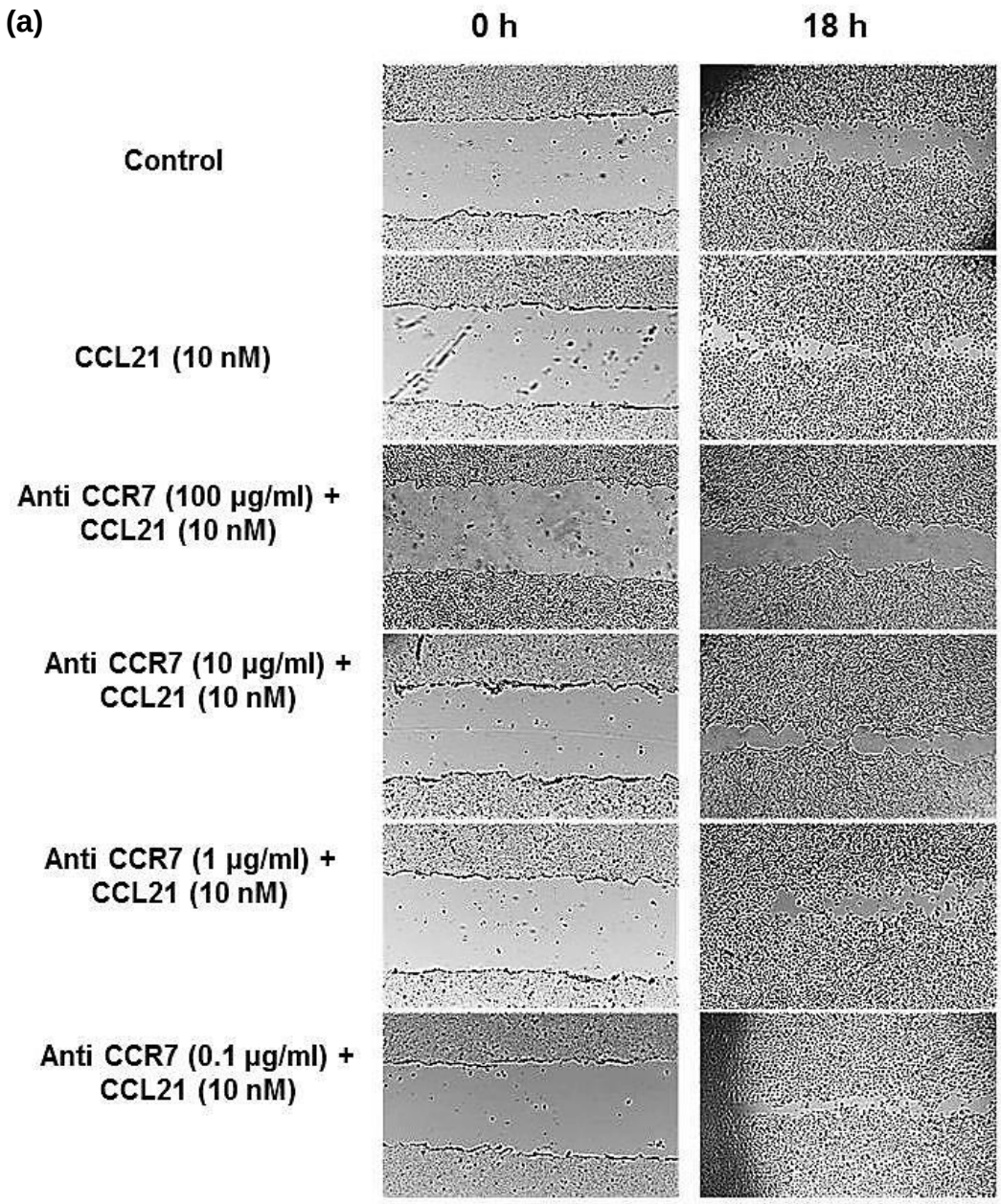
(a)
0 h
18 h
Control
CCL21 (10 nM)
Anti CCR7 (100 µg/ml) + CCL21 (10 nM)
Anti CCR7 (10 µg/ml) + CCL21 (10 nM)
Anti CCR7 (1 µg/ml) + CCL21 (10 nM)
Anti CCR7 (0.1 µg/ml) + CCL21 (10 nM)

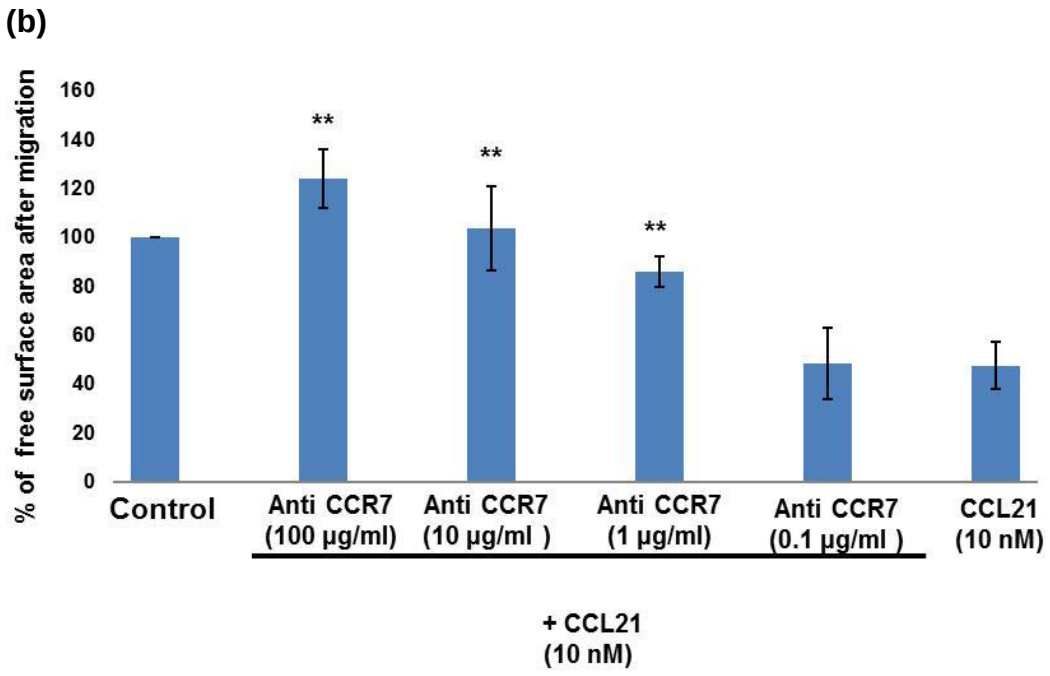

Figure 70: Effect of blocking CCR7 in wound healing assay.

(a) 52% increase of cell migration was observed after 18 h in the presence of CCL21 compared with control. This effect was abrogated by a CCR7-neutralizing antibody in a dose dependent manner. (b) Data expressed as percentage of free surface area after migration. Error bars represent SD. **P < 0.01 compared with CCL21 10 nM group.

Compounds that showed the highest IC_{50} in the MTT assay and were the most active in the Ca^{2+} flux assay were selected to investigate for their ability to block cell migration and/or invasion. The wound healing assay was chosen for initial screening Figure 71. Our results show that CCR7 antagonists ICT5888, ICT13069, ICT13070 and ICT13072 can block the migration induced by CCL21 10 nM by 57%, 88%, 49% and 27%, respectively. This is in agreement with the Ca^{2+} flux results in which ICT13069 showed one of the highest activity (For Ca^{2+} flux data see figure 69). The free surface area after migration was the highest with

compound ICT13069 compared with control. ICT13072 showed similar activity to ICT5888, ICT13070 showed the lowest activity in blocking the migration.

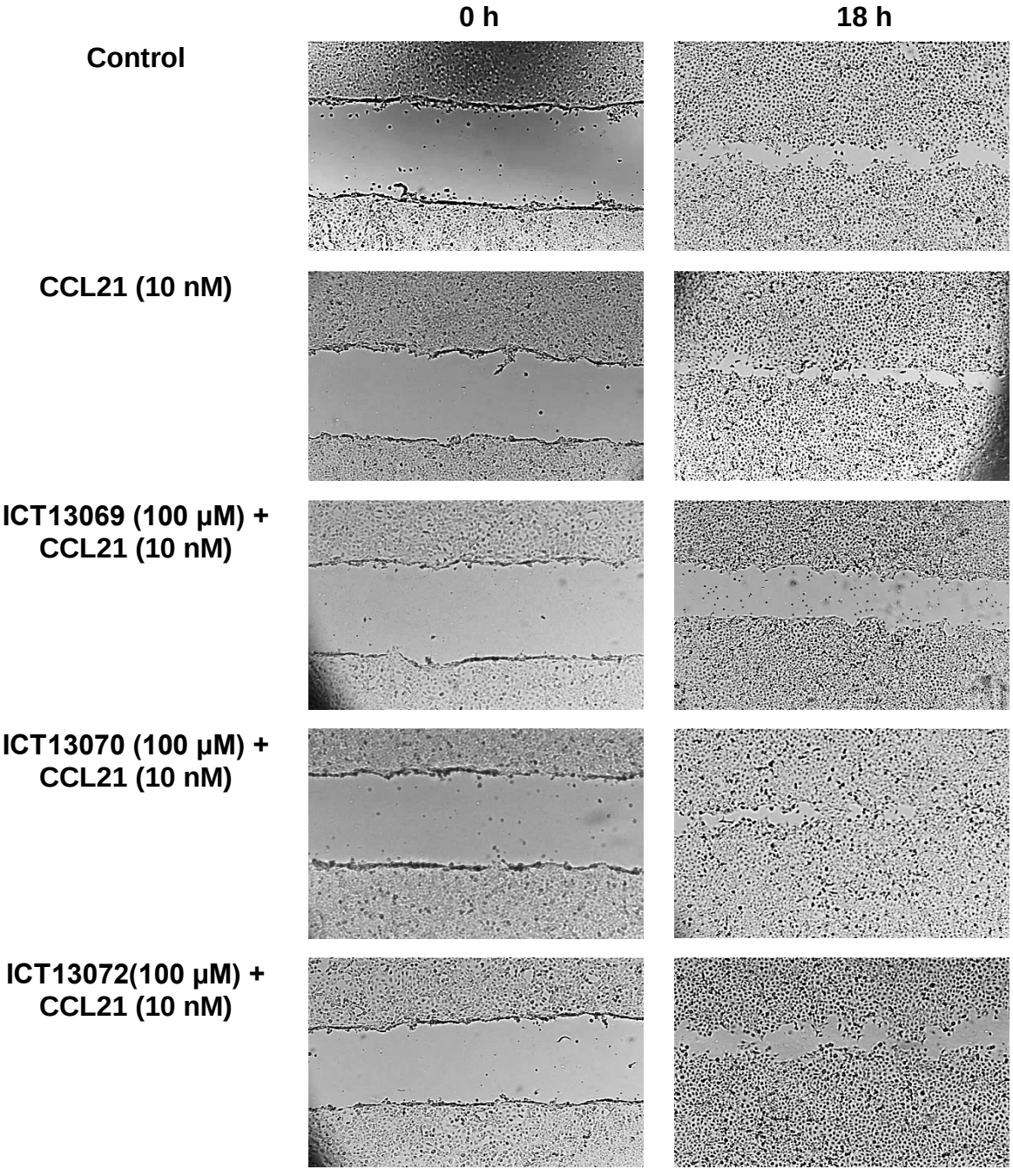

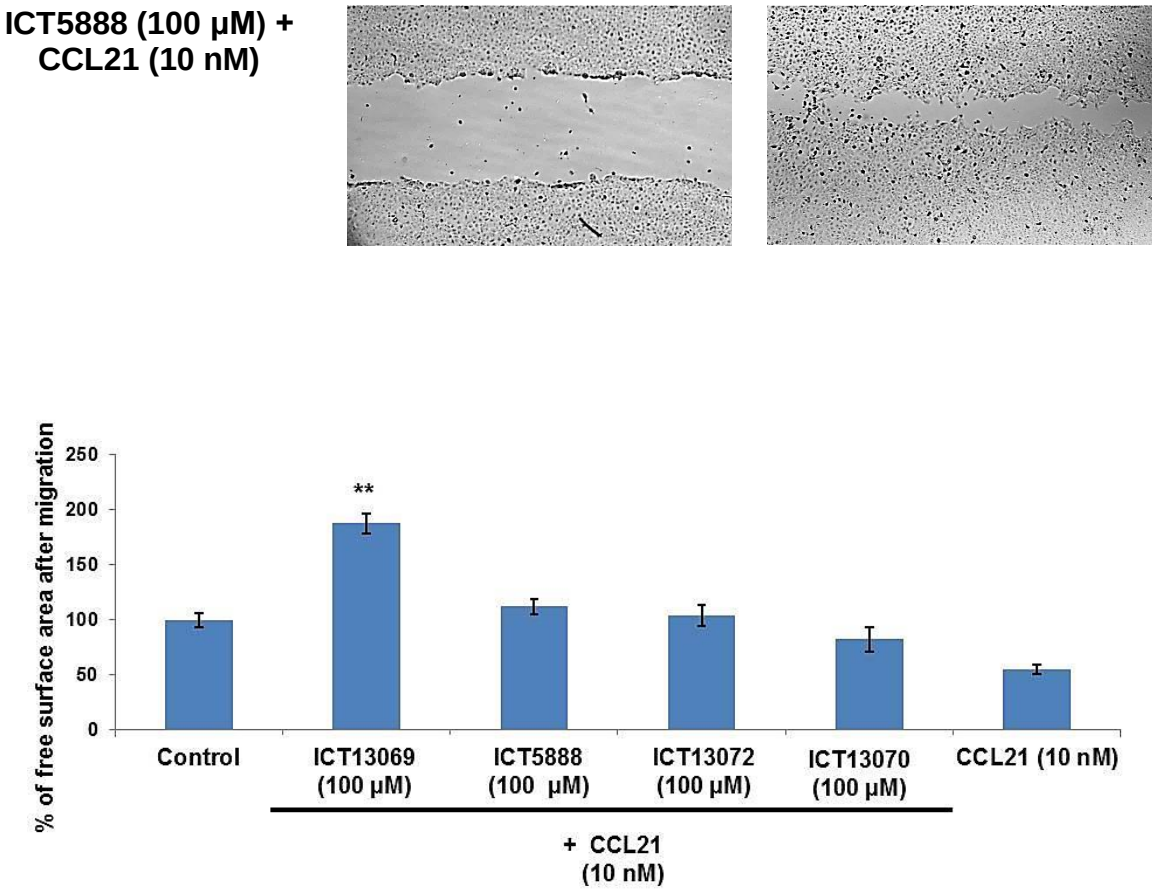

Figure 71: Comparison of CCR7 antagonists for blocking cell migration in wound healing assay.

(a) CCL21 increased cell migration compared with control. ICT5888, ICT13069, ICT13070, ICT13072 blocked the migration induced by CCL21. The scale bar represents 100 µm (b) The free surface area after migration was highest with ICT13069 followed by ICT5888, ICT13070 and ICT13072. Error bars represent SD from 3 independent experiments. **P < 0.01 compared with CCL21 10 nM group.

4.3.3 ICT13069 modulates cell migration in wound healing assay

ICT13069 showed the highest activity in blocking cell migration compared with the other analogues (see the previous section). Therefore we decided to investigate ICT13069 further over a concentration range to establish that the effect is dose dependent; and in other migration/invasion assays. ICT13069 impeded the

migration of OSC-19 cells induced by CCL21 in wound healing assay in a dose dependent manner Figure 72. The % of free surface area is represented in (Figure 72-b).

(a)

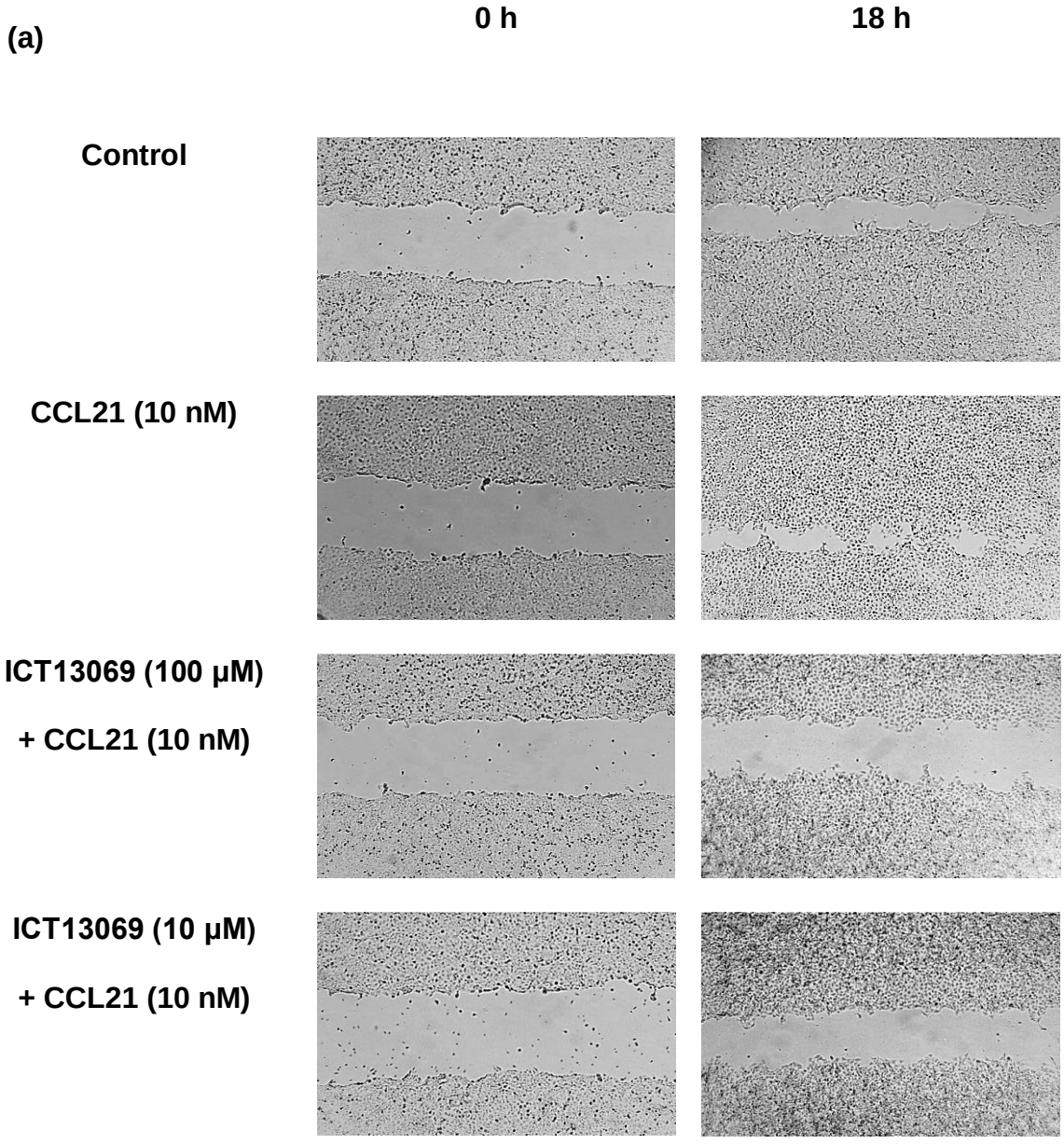

ICT13069 (1 μM)

+ CCL21 (10 nM)

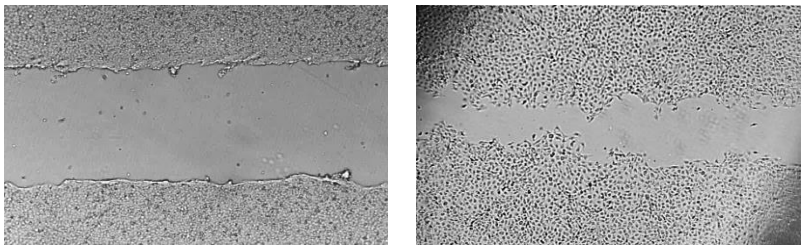

ICT13069 (100 nM)

+ CCL21 (10 nM)

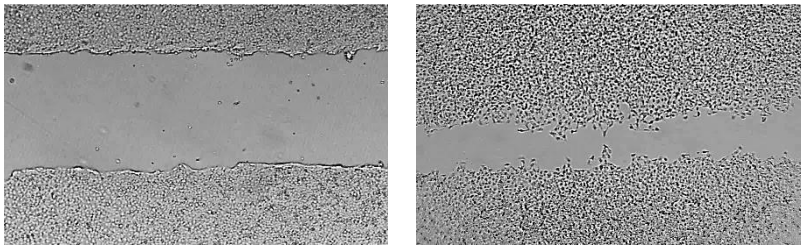

ICT13069 (10 nM)

+ CCL21 (10 nM)

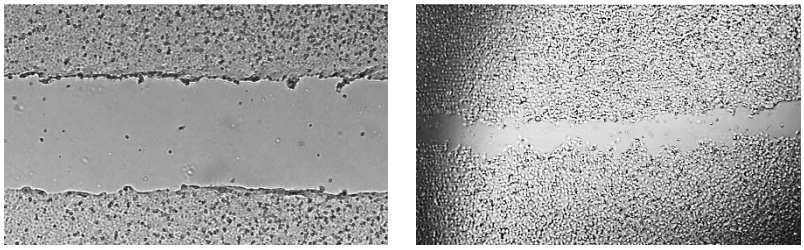

ICT13069 (1 nM)

+ CCL21 (10 nM)

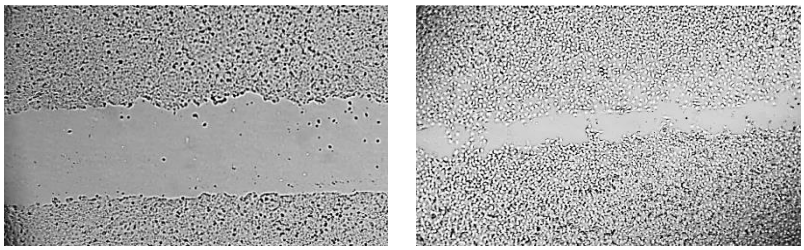

(b)

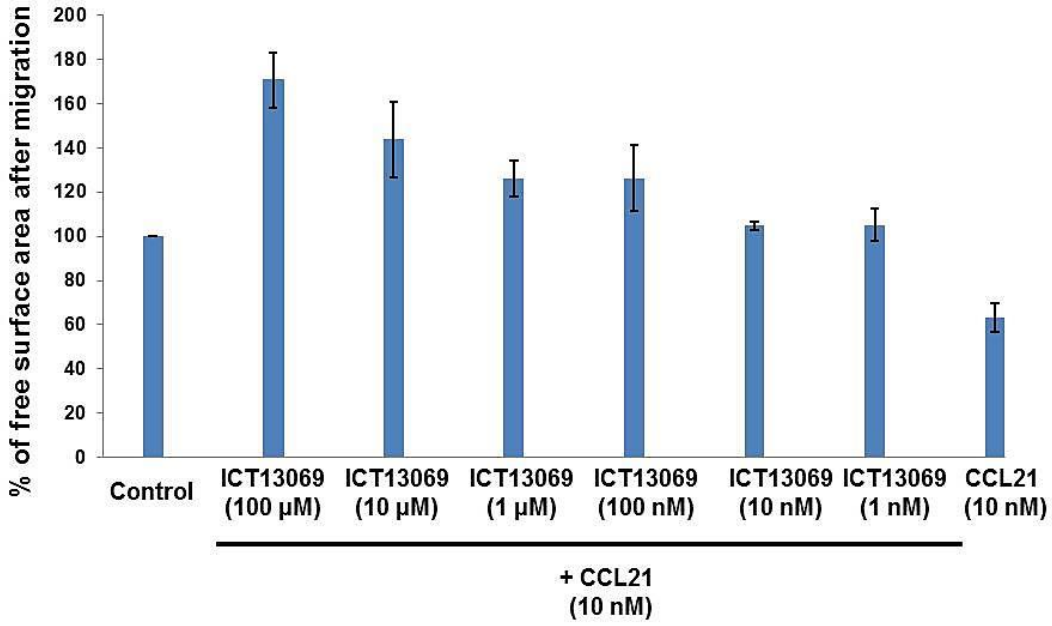

Figure 72: ICT13069 inhibits cell migration in a dose dependent manner.

OSC-19 cells were treated with ICT13069 at different concentrations for 2 h before adding CCL21 (10 nM). Images were taken before and after migration. (b) Free surface area was measured after 18 h and expressed as percentage compared to control with no ligand added. Error bars represent SD from 3 independent experiments.

4.3.4 ICT13069 modulates cell invasion in transwell assay

In order to analyse the effect of ICT13069 on cell invasion, we first determined whether CCL21 and CCL19 would have any effect on cell invasion. Our data showed that CCL21 and CCL19 significantly enhanced the invasion ability of OSC-19 cells through a collagen coated transwell membrane in a dose dependent manner, compared to control with free serum (Figure 73-a) medium and no ligand added to the lower chamber. Numbers of invading cells were highest at 100 nM of CCL21 or CCL19 (Figure 73-b).

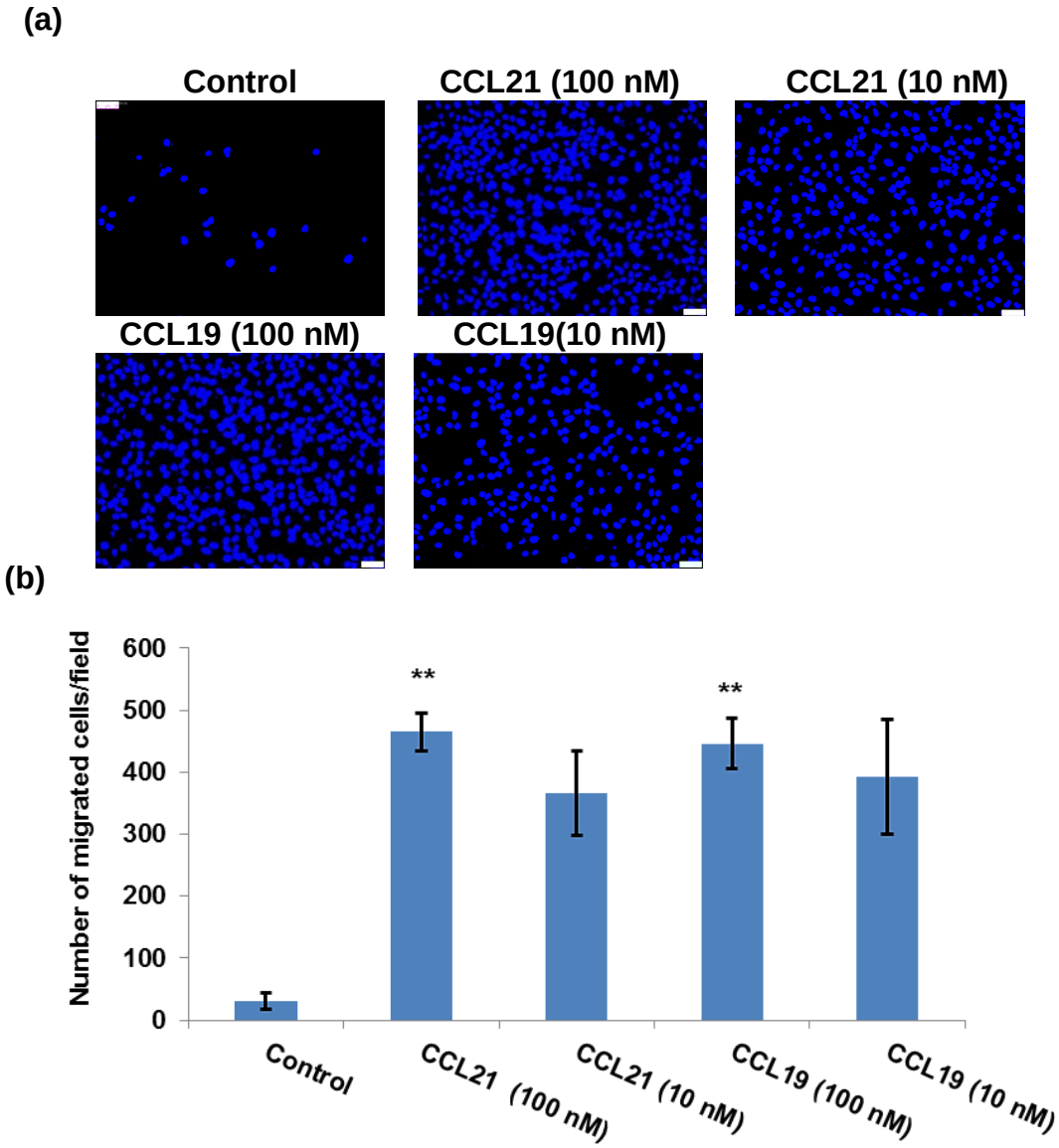

Figure 73: CCL21 and CCL19 induce OSC-19 invasion.

OSC-19 cells were seeded at on transwell and left for 48 h to invade from the upper membrane towards the lower chamber. (a) Cells that had invaded through collagen and face the lower chamber were captured using Leica DM 2000 microscope with scale bar 50 µm. CCL21 and CCL19 induced the migration of cells compared with the control group. (b) Number of migrated cells was counted and averaged using Image J. Error bars represent SD from 3 independent experiments. **P < 0.01 compared with control group.

We tested ICT13069 at different concentrations against CCL21 (at 100 nM). ICT13069 inhibited cells invasion towards CCL21 (100 nM) in a transwell assay also in a dose dependent manner (Figure 74-a). ICT13069 at 100 μM caused significant inhibition of cells invasion towards the lower chamber where CCL21 (100 nM) was added. The number of migrated cells is presented in (Figure 74-b).

(a)

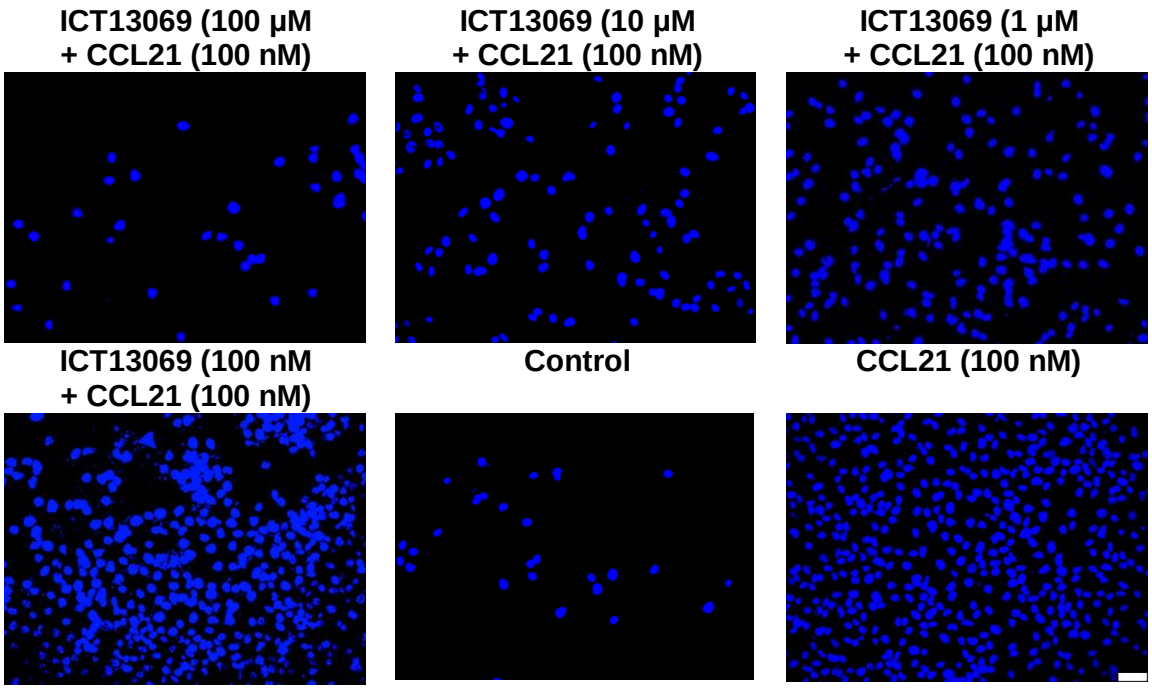

(b)

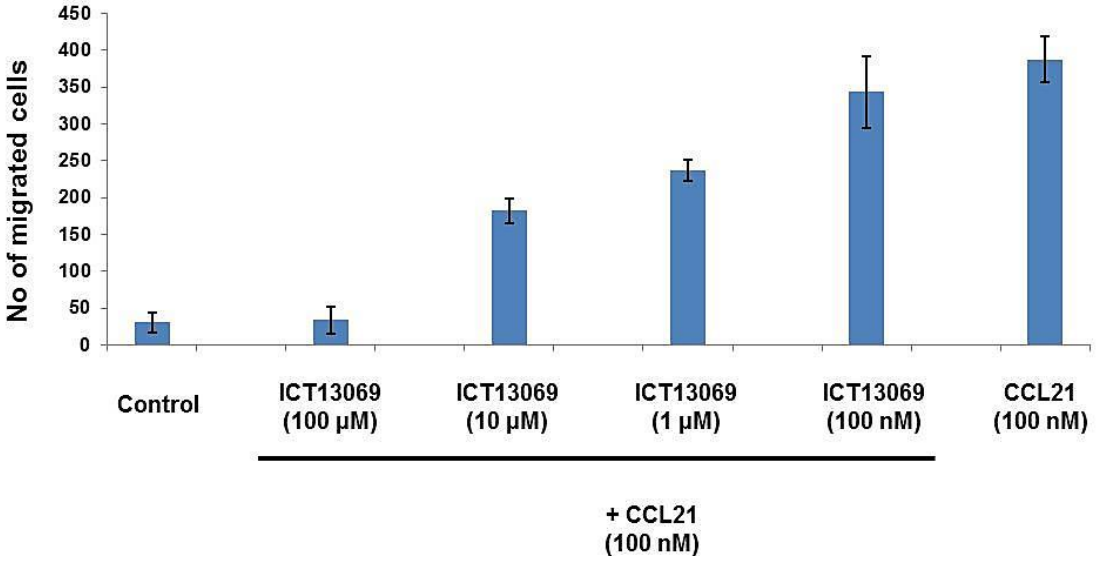

Figure 74: ICT13069 inhibits cell invasion in transwell assay.

OSC-19 cells were treated with or without ICT13069 and seeded on the upper chamber and left to migrate towards CCL21 (100 nM) in the lower chamber for 48 h. OSC-19 cells were treated with ICT13069 (100 µM), ICT13069 (10 µM), ICT13069 (1 µM) and ICT13069 (100 nM). (a) Images of migrated cells that were fixed with 70% ethanol and stained with DAPI, were captured after 48 h. ICT13069 inhibited cell invasion in a dose dependent manner. (b) Number of migrated cells were counted using Image J. Error bars represent SD from 3 independent experiments.

4.3.5 ICT13069 modulates cell invasion in 3D spheroid invasion assay

OSC-19 spheroids (200 μm diameter) form tight round spheroids by the hanging drop method using methylcellulose (Figure 75-a, b). To confirm that CCR7 is still expressed after growing OSC-19 as spheroids, IHC staining for CCR7 was performed on OSC-19 spheroids (Figure 75). OSC-19 spheroids show +ve (brown) stain on the cell membrane indicating CCR7 expression (Figure 75-c). -ve controls showed no staining of CCR7 (Figure 75-d). Spheroids formed from the hanging drop method were transferred and embedded into collagen which was then immersed in medium.

We initially attempted the assay using chemoattractants CCL21 and CCL19 in medium containing 10%FBS, however, the migration was so fast that the effect of CCL21 on invasion was not clear compared with control (10%FBS). This is because 10%FBS itself acts as a chemoattractant and can cause a strong invasion in the spheroids on its own. Next, we intended to use 0% FBS to dilute the ligands in which we would be able to see the effect of CCL21 compared to control (0%FBS in this case), however, the lack of any serum caused the spheroids to lose their ability to invade in the presence of CCL21. This is presumably because serum is a requirement in matrix invasion experiments so the cells can use the plasminogen that is present within the FBS to break through and invade through the matrix. Therefore, we decided to conduct the experiments in medium containing 1%FBS.

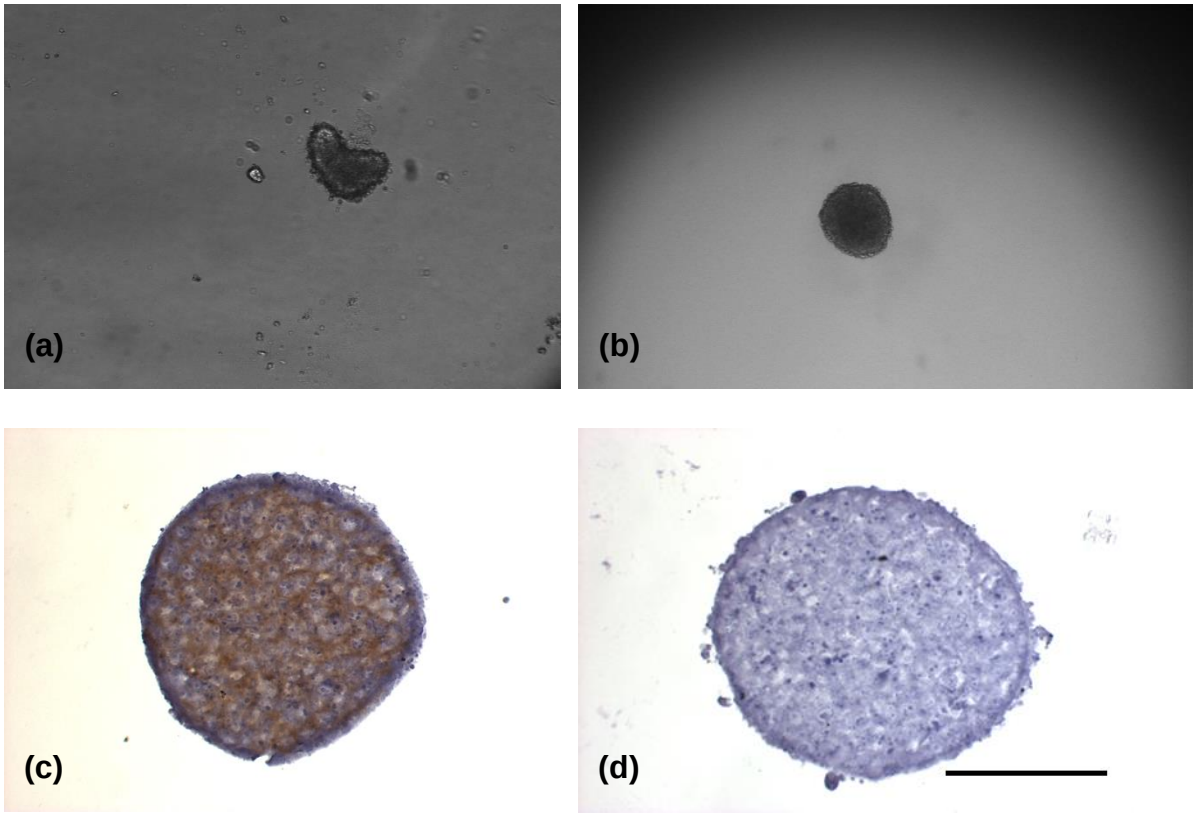

Figure 75: OSC-19 spheroids formed by the hanging drop method.

Seeding 2000 cells in each drop formed tight unrounded spheroids without methyl cellulose added to the cell suspension (a). Adding methylcellulose to the cell suspension induced the forming of tight round spheroids (b). (c) IHC staining of OSC-19 spheroids confirms that OSC-19 spheroids sustain CCR7 expression after growing as 3D. (d) Negative control of IHC. Scale bar 125 µm at 10x objective lens.

Next, we sought to determine if OSC-19 were viable after embedding in collagen and during the invasion assay. Figure 76 shows that OSC-19 were mainly viable (green) after 24 h of invasion for 1% FBS (a), 10% FBS (b) and CCL21 100 nM in 1% FBS (d) with very few dead cells (red) in the middle of the spheroid. However, 0% FBS (c) resulted in significant cell death all over the spheroid.

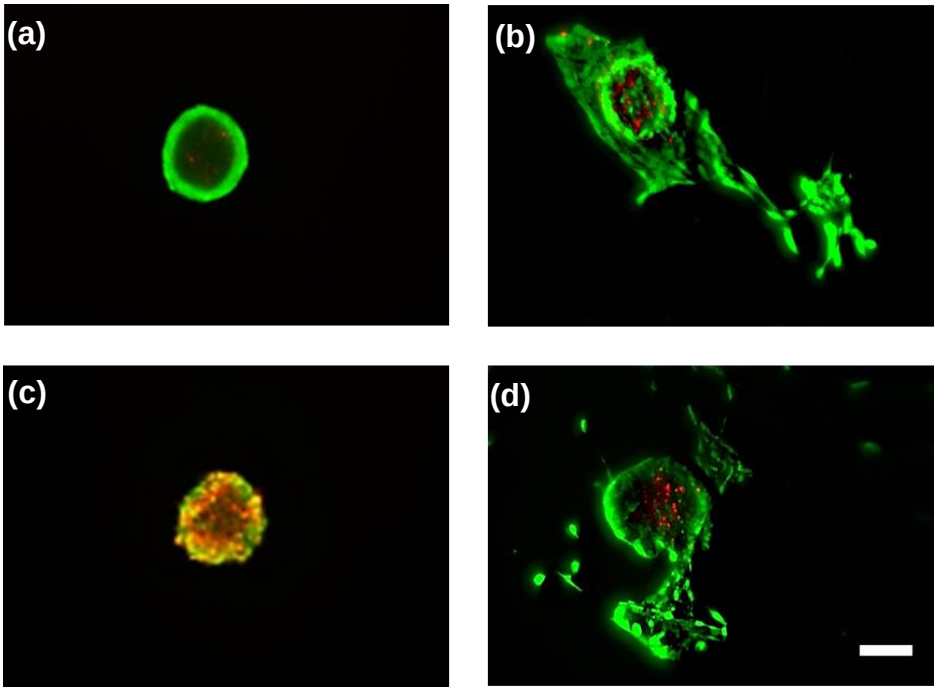

Figure 76: Display images of OSC-19 spheroids embedded in collagen for 24 h with calcein or PI.

To confirm the viability of OSC-19 spheroids during the invasion assay, OSC-19 spheroids were stained with calcein (green) indicating viable cells and PI (red) indicating red cells after 24 h of embedding them into collagen. Spheroid in 1%FBS (a), 10%FBS (b), CCL21 100 nM in 1% FBS (d) were largely viable with few dead cells (red) in the core of the spheroid. However, spheroids left in 0%FBS (c) into collagen were mostly dead. Scale bar represents 100 µm. Images were captured using time-lapse confocal microscopy.

The experiments were conducted using 100 nM CCL21 and CCL19 in 1%FBS and both showed an increase in the percentage of invasion after 20 h compared with control of 1% FBS medium with no ligand added (Figure 77-a). The % area of invasion is calculated as described earlier in section 4.2.10 and represented in (Figure 77-b).

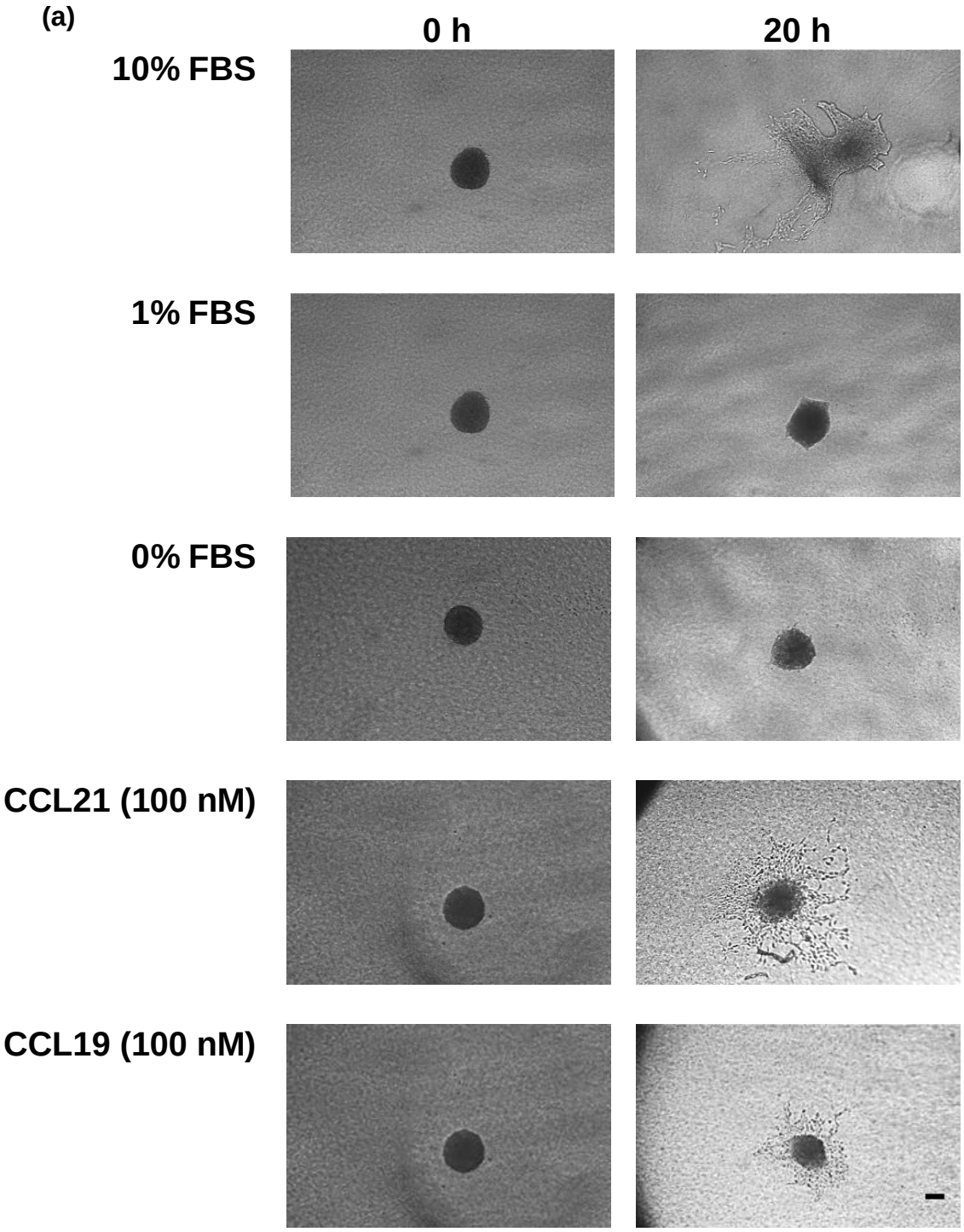
(a)
0 h
20 h
10% FBS
1% FBS
0% FBS
CCL21 (100 nM)
CCL19 (100 nM)

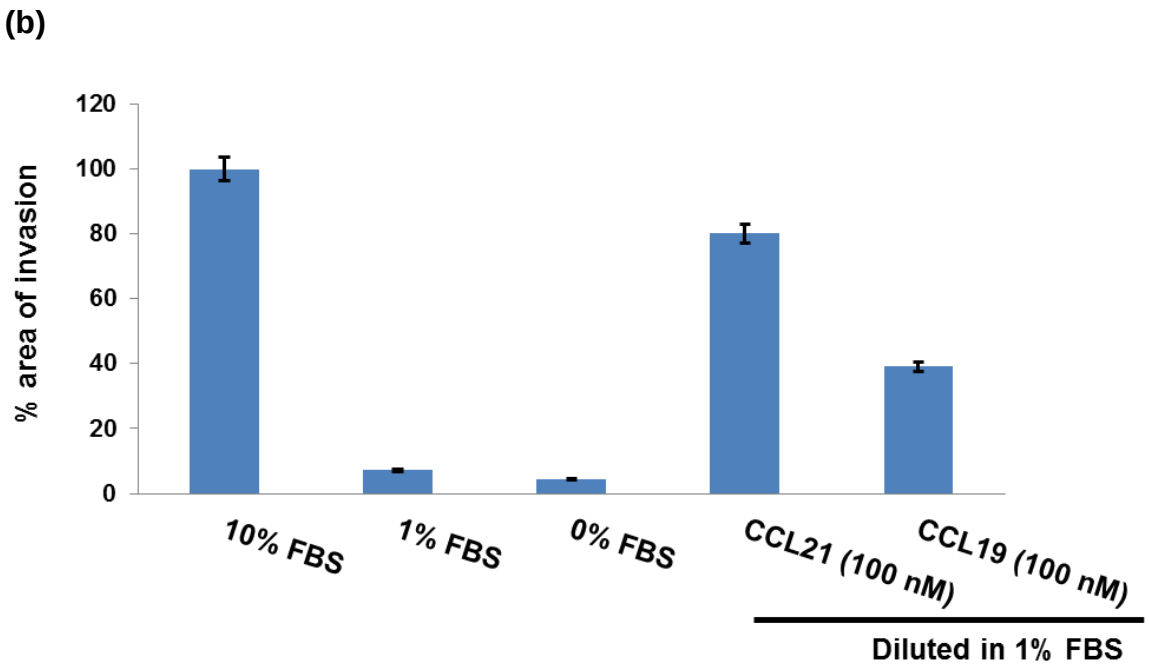

Figure 77: CCL21 and CCL19 induced invasion of OSC-19 spheroids embedded in collagen.

(a) Both CCL21 and CCL19 induced OSC-19 invasion compared with control 1% FBS no ligand added. OSC-19 spheroids invaded the collagen in response to 10%FBS, but no invasion was observed with 1% or no FBS. Scale bar represents 100 µm at 10x objective lens. Upon adding CCL21 (100 nM) and CCL19 (100nM) in 1% FBS medium resulted in increased invasion capability of OSC-19 spheroids. In addition, OSC-19 spheroids invaded through collagen to higher level when stimulated with CCL21, compared with CCL19. (b) Data expressed as percentage area of invasion. Error bars represent SD from 3 independent experiments.

The importance of testing compounds in a 3D spheroid model has been highlighted in the literature (Abbott, 2003, Friedrich et al., 2009, Mehta et al., 2012). In particular, screening compounds in 3D models can be more predictive for cells that are more resistant to chemotherapy and radiation compared to 2D models. Therefore, we investigated the effect of ICT13069 in blocking OSC-19 invasion in a 3D spheroid model. ICT13069 inhibited the spheroids invasion in a dose dependent manner (Figure 78). ICT13069 at 100 µM showed complete inhibition of

cell invasion induced by CCL21 (100 nM). Comparing cell invasion and migration inhibition at 10 µM in 2D and 3D indicates that 2D OSC-19 cells showed higher sensitivity for ICT13069, compared with OSC-19 spheroids. The % of area of invasion is represented in (Figure 78-b).

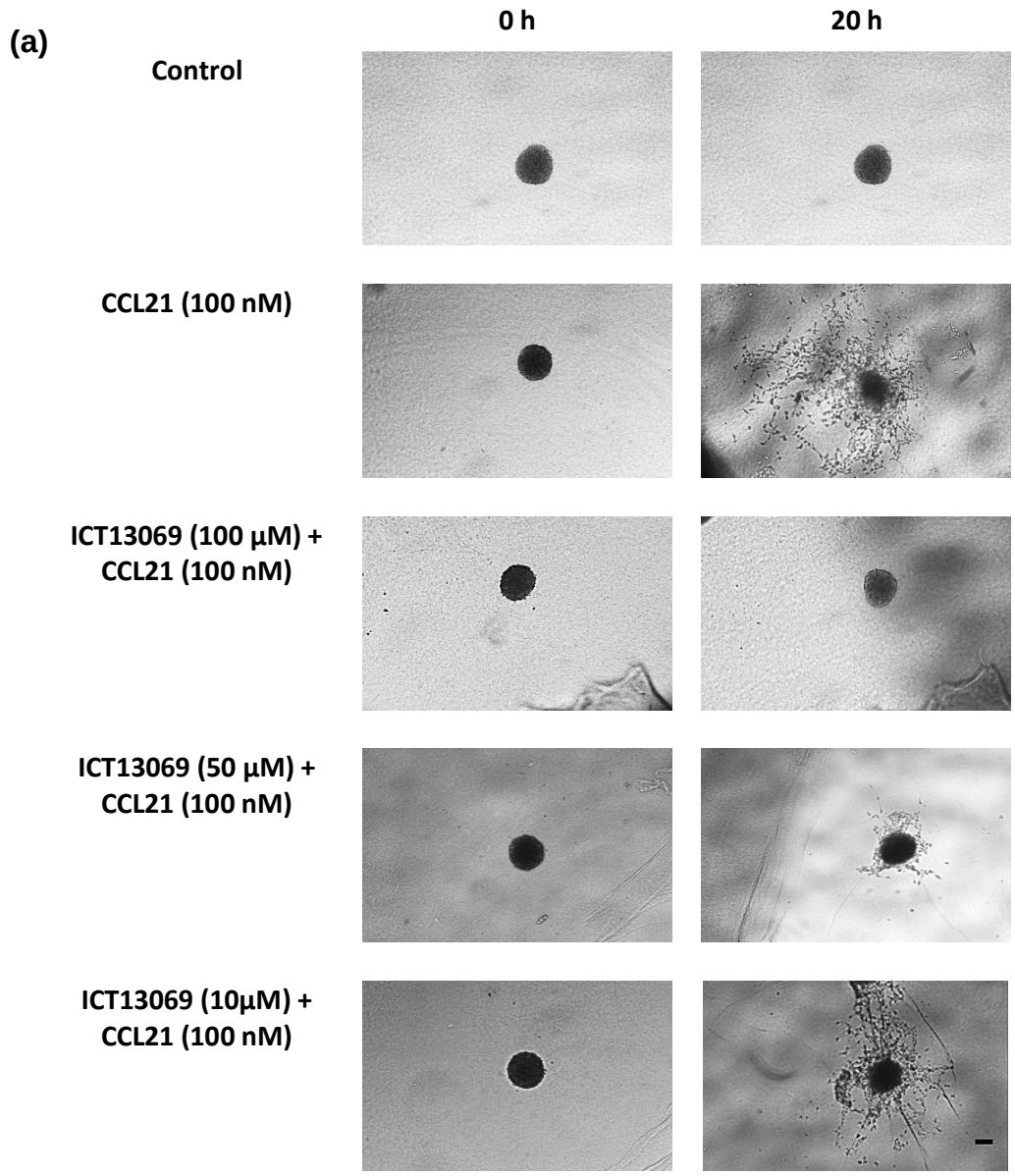

(b)

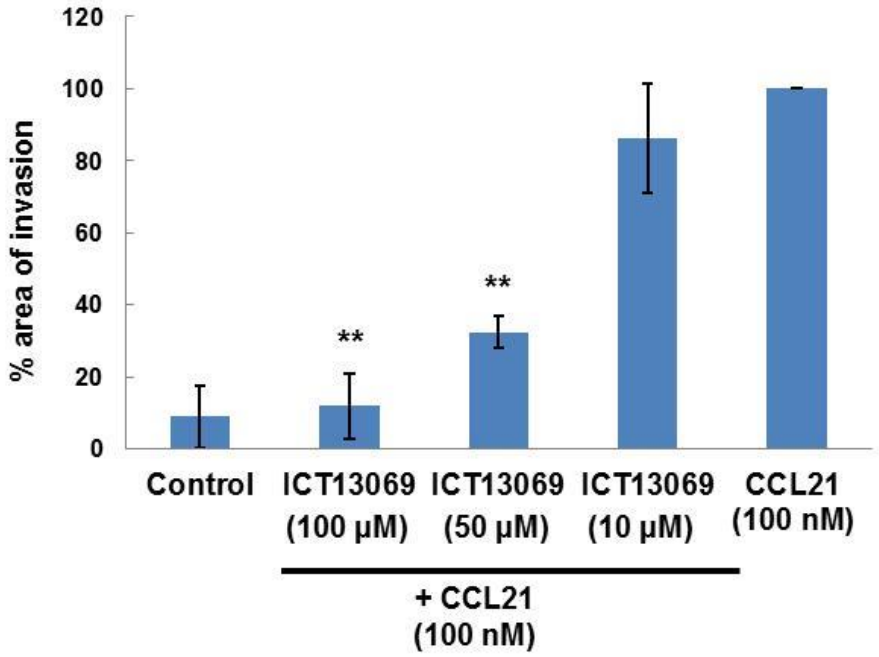

Figure 78: ICT13069 inhibits OSC-19 spheroids invasion in 3D invasion assay.

(a) OSC-19 spheroids embedded into collagen were left to invade through after adding CCL21 (100 nM) with or without ICT13069. ICT13069 inhibited cell invasion induced by CCL21 (100 nM) in a dose dependent manner after 20 h. (b) Data expressed as % area of invasion normalized to area invaded by CCL21 (100 nM). Error bars represent SD of 3 independent experiments. **P < 0.01 compared with CCL21 group.

4.3.6 Analogues of ICT13069

ICT13069 was shown to be effective in wound healing, transwell and 3D spheroid invasion assays. To understand the SAR better and develop a more potent compound, synthesis of ICT13069 analogues was undertaken. All the analogues along with ICT13069 were tested in the scratch assay at 1 µM. We choose the 1 µM to allow for direct comparison and because the majority of the analogues showed no significant toxicity at this concentration in the MTT assay. Analogues that showed similar or higher activity than ICT13069 were to be tested at serial

dilutions in order to obtain IC_{50} and confirm the efficacy of the more potent analogues, which will direct the medicinal chemistry team in synthesizing more potent and drug-like compounds. The effect of analogues at 1 μM in reducing CCL21 induced migration is shown in Figure 79. Compounds ICT13311, ICT13309, ICT13325 showed similar activity to ICT13069. Furthermore, ICT13312 showed better activity than ICT13069 ($P < 0.05$). The % of free surface area of all analogues is presented in (Figure 79-b).

(a)

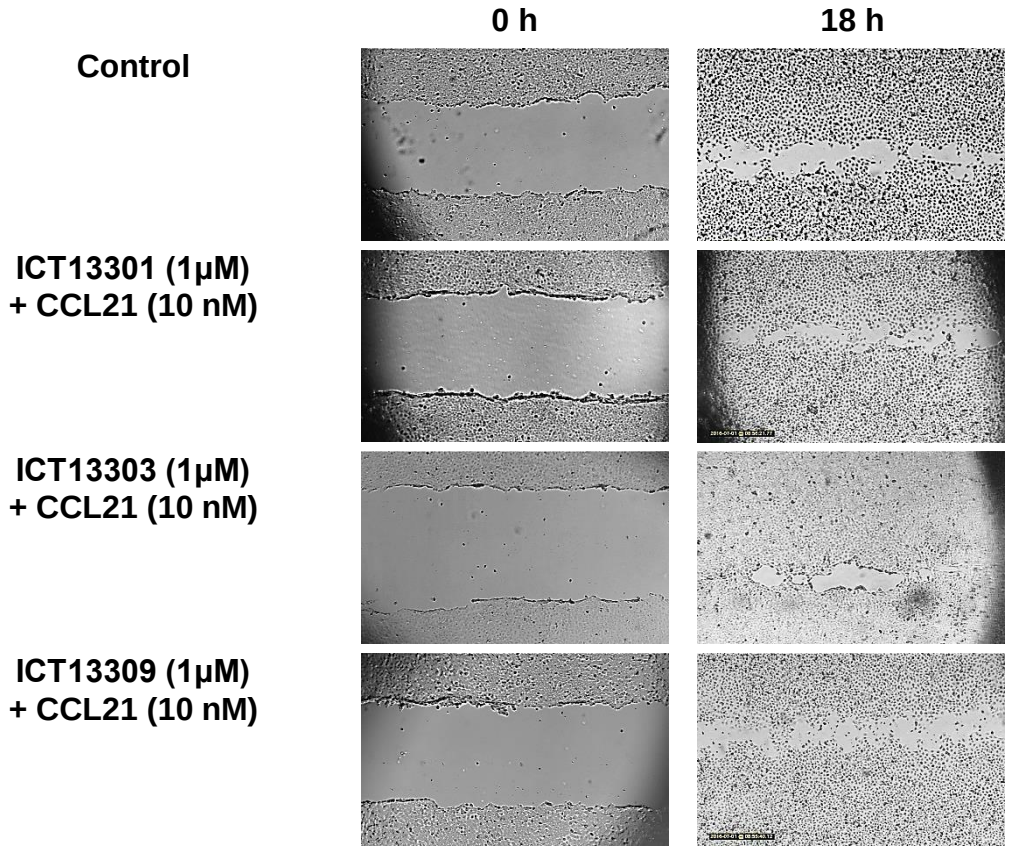

ICT13310 (1μM) + CCL21 (10 nM)

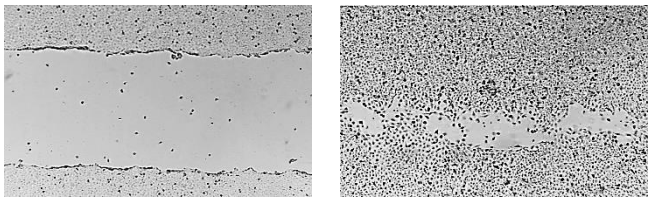

ICT13311 (1μM) + CCL21 (10 nM)

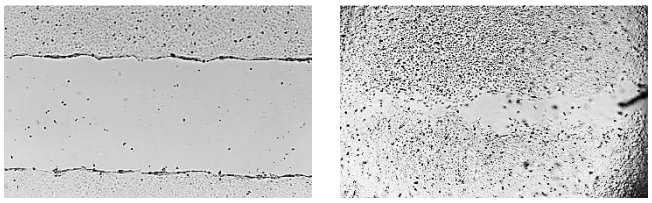

ICT13312 (1μM) + CCL21 (10 nM)

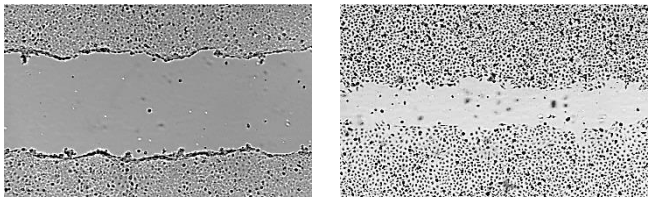

ICT13313 (1μM) + CCL21 (10 nM)

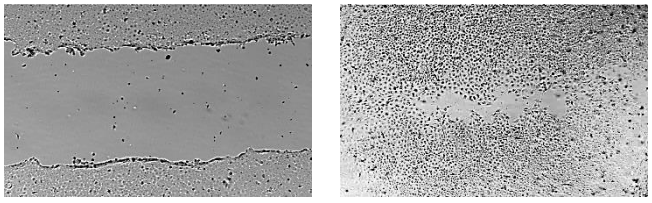

ICT13069 (1μM) + CCL21 (10 nM)

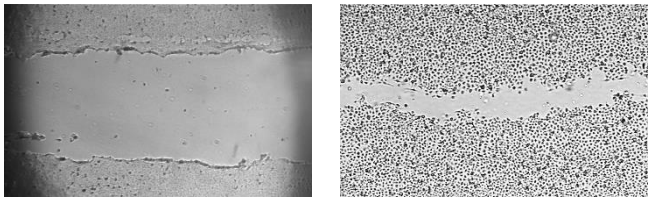

ICT13325 (1μM) + CCL21 (10 nM)

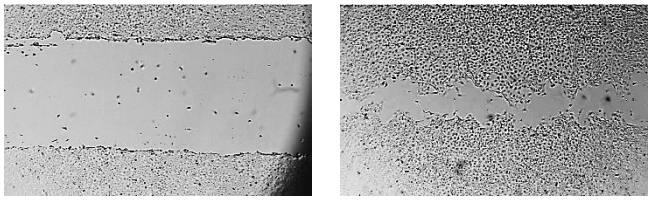

CCL21 (10 nM)

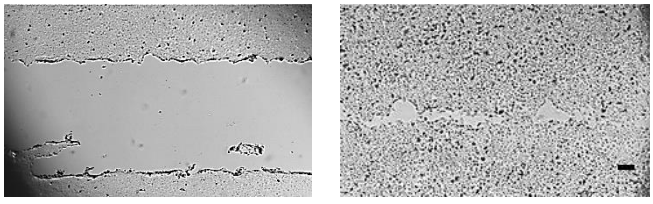

(b)

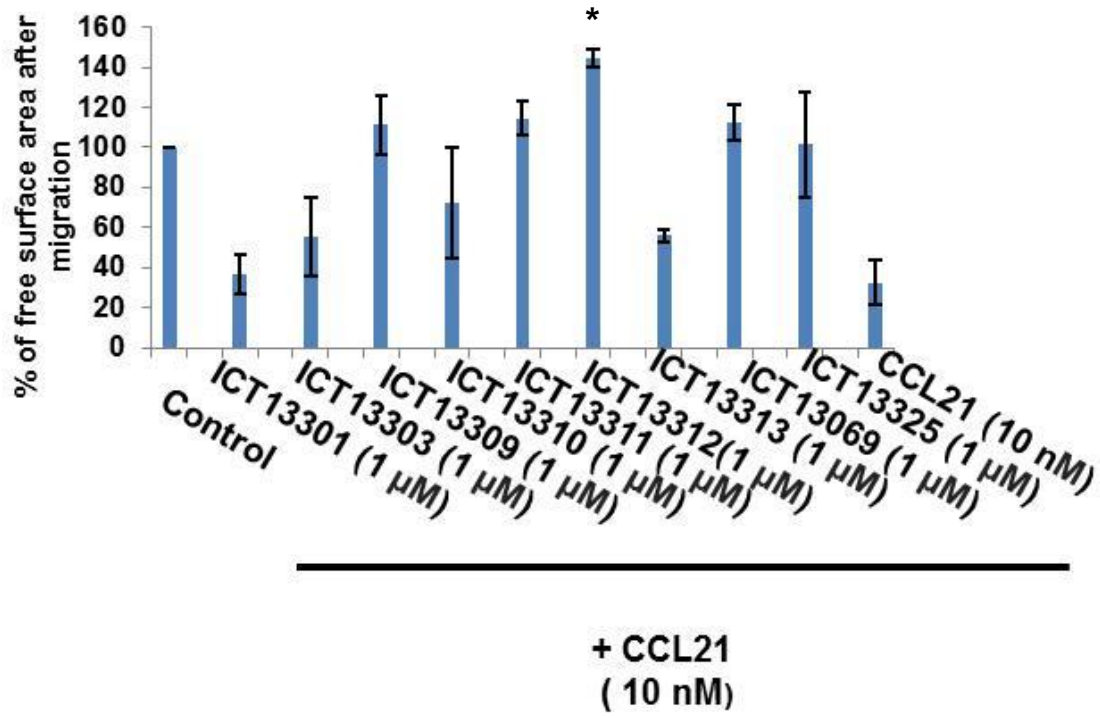

Figure 79: Comparison among ICT13069 analogues in blocking cell migration in wound healing assay.

(a) CCL21 increased cell migration compared with control. Compounds ICT13311, ICT13325, ICT13309 and ICT13312 blocked the migration induced by CCL21 similarly or better than ICT3069. The scale bar represent 100 µm (b) The free surface area after migration was highest with ICT13312. Error bars represent SD from 3 independent experiments. *P < 0.05 compared with ICT13069.

4.4 Discussion

Currently, a number of options are available for cancer treatment including surgery, cytotoxic chemotherapy, radiotherapy, immunotherapy, and targeted therapy. Cytotoxic chemotherapy continues to be the mainstay for many patients; however, recently the focus of cancer treatment is shifting towards targeted therapies because they aim to act specifically on cancer cells with nearly no effect on normal cells, thus reducing side effects. The addition, of newer agents has shown to increase the survival rate of patients in some cancers (Tan et al., 2017). Chemokine receptor antagonists are amongst one of the most exciting of new targeted therapeutics.

The overexpression of chemokine receptors on cancer cells is detectable on many cancer types compared with their normal counterparts (Slettenaar and Wilson, 2006). These receptors have shown to be involved in increase cell survival, proliferation, adhesion, or/and migration as well as direct metastasis to form secondary metastases on tissues or organs in which their cognate ligands are present (Vela et al., 2015). Since the most common reason of cancer related death is metastasis in which chemokine receptors play a significant role, they are considered highly relevant targets for the development of potential new anti-metastatic drugs. As a result, much effort has focused on the development of small molecules which inhibit the activation of chemokine receptors. We have seen in chapter 3 that knock down of CCR7 using RNA interference technology (siRNA), decreased the migration of head and neck cancer cells both under normoxia and hypoxia. Our results, along with other successful anti chemokine receptor

strategies, such as anti-CXCR4 agents, encouraged us to develop small molecule antagonists against CCR7. Our group has committed significant effort to the development of small molecule antagonists of chemokine receptors, in particular, CCR7 antagonist, particularly since to date, no small molecules CCR7 have been described in the literature.

The role of CCL21/CCR7 axis in cell migration is well documented in different types of cancer; our data from chapter 2 has shown that this axis is important in cell migration of head and neck and prostate cancer cell lines. In this chapter, we look into the effect of CCR7/CCL21/CCL19 in invasion in 2D and 3D before testing our in house synthesized CCR7 antagonists.

To assess the role of CCL21/CCL19 in invasion, we used a Boyden chamber transwell assay that requires the cells to travel through collagen to reach the other side of the inserts. Our findings indicate significant differences between cell movement towards CCL21 and CCL19 compared to control (no ligands added), in a dose dependent manner. Our results in OSC-19 cells are consistent with other reports in bladder, oesophageal and head and neck cancer cell lines (Xia et al., 2014, Cheng et al., 2014, Mo et al., 2015, Shi et al., 2015). In all the reported studies, tumour cells invade towards CCL21 in a dose dependent manner. In addition, CCR7 knockdown or inhibition using CCR7 antibodies, reduces cell invasion towards CCL21. Regarding the CCL19 axis, it has been reported in head and neck cancer metastatic cell lines such as PCI-4B, that CCL19 induced significant cell invasion in a transwell assay *in vitro* compared to medium lacking CCL19 (Wang et al., 2005).

As previously discussed, cells grown in a 3D environment represent more closely the normal cellular function in the tumour (Achilli et al., 2012). Furthermore, spheroids are used as a “negative selection” tool to reduce testing drugs in animal models and for “positive selection” of compounds for further drug development (Katt et al., 2016). Therefore the more we learn from *in vitro* models that mimic tumours *in vivo* for drug screening, the higher chance to succeed *in vivo*.

The effect of CCL21/CCL19 in 3D spheroid models of the head and neck cancer has not been published before, so we investigated the effect of CCR7 ligands on the invasion ability of OSC-19 spheroids. The hanging drop method allows the production of tight OSC-19 cells spheroids of controlled sizes, this method was chosen because of its simplicity and reliability (Achilli et al., 2012).

Although we had confirmed the expression of the receptor on single cells by flow cytometry, we stained the OSC-19 spheroids for CCR7 as well, to confirm its expression on 3D OSC-19 cells before performing our invasion assays. After growing them for 24 h by the hanging drop method, spheroids were transferred and embedded in collagen and immersed under medium (containing 1% FBS) with or without CCR7 ligands (CCL19 and CCL21), after 20 h incubation, we observed a clear increase of invasion in response to both ligands. The choice of 1% serum medium is critical in this assay. Initially, we observed no invasion of OSC-19 spheroids upon adding CCL21 or CCL19 in serum free medium. In contrast, OSC-19 spheroids invaded the collagen towards 10% FBS even in the absence of CCL19 or CCL21. In 1% FBS we saw no significant invasion in our 3D model invasion assay, making it a good control. Therefore, we decided to dissolve CCL21

and CCL19 in 1% FBS in this assay. We speculated that one reason embedded spheroids do not invade collagen is perhaps because they do not survive in 0% FBS medium. This is in agreement with our viability results. In contrast, we showed that embedded OSC-19 spheroids into collagen and topped up with 1% FBS medium were largely viable, as demonstrated by the calcein and PI labelling. Hence these spheroids could invade after the addition of CCL21 or CCL19. Indeed, viable OSC-19 spheroids invasion through collagen increased significantly, following CCL21 or CCL19 addition in 1% FBS medium (compared with our control 1% FBS with no ligand added). Our results demonstrate that OSC-19 spheroids are quite sensitive to the serum levels, more so than monolayer cultures. However, this is not surprising; cells or spheroids invading through basement membranes are in need of a source of plasminogen to breach through such matrix. However, the lack of nutrients in tumours grown *in vivo,* along with other stress factors will on the contrary to *in vitro* OSC-19 spheroids, stimulate the cell invasion and migration since proteases including plasminogen are present within the tumour microenvironment.

It is clear from our results that the CCR7/CCL21 axis is important for cell migration and invasion in 2D and 3D models. Our results also point towards a different role for CCL19 and CCL21 in the migration of tumour cells. We have observed that CCL21 has also a stronger stimulating effect in inducing Ca^{2+} flux mobilisation (chapter 2) and cells invasion in 2D and 3D than CCL19 in OSC-19 cells. Of note, it has also been reported that lymph nodes express CCL21 to a significantly higher level than CCL19 (Muller et al., 2001). It could be inferred from our *in vitro* results

that CCR7 expressing tumour cells may migrate to the lymph nodes where CCL21 is highly expressed.

Due to the strong association that we observed between CCR7 and CCL21 in migration and invasion in OSC-19 cells, we decided to investigate whether the modulation of CCR7 in these cells would abrogate the observed effects.

Initially, we used a CCR7 monoclonal antibody in our wound healing assay. CCR7 monoclonal antibody showed complete abrogation of CCL21 induced migration at 100 µg/ml and 10 µg/ml concentration. The CCR7 antibody inhibited the effects of CCL21 in a dose dependent manner. This encouraged us to use the small molecule CCR7 antagonists which are prepared by the medicinal chemists in our team at ICT. Our screening cascade to evaluate these compounds starts by determining if they are able to abrogate the Ca^{2+} flux triggered by CCL21 addition to the cells. If positive, to confirm if the activity observed is related to CCR7 inhibition or just cytotoxicity, compounds are evaluated in an MTT assay. This is a necessary step, as cytotoxic compounds cause cell death and therefore would reduce the fluorescence response in the Ca^{2+} flux assay leading to false positives.

The Ca^{2+} flux data, together with the MTT cytotoxicity information, allows the selection of CCR7 antagonist compounds that are effectively non-cytotoxic. For the selected compounds, the cytotoxicity IC_{50s} from the MTT assay were in most cases at least 20 times higher than the IC_{50s} from the Ca^{2+} flux assay.

Ca^{2+} flux is a functional assay, but it does not show if the antagonist compounds have the desired effects on cellular functions like migration or invasion. Therefore,

our next step was to evaluate if these compounds would reduce migration and invasion of OSC-19 cells. We chose the scratch assay as our first secondary functional assay, because its advantages in terms of cost and ease of experimental design. Initial lead compound ICT5888 produces inhibition of CCL21-induced activity of the OSC-19 cell line in Ca^{2+} flux assay and completely abrogates CCL21 induced migration at 100 µM in the wound healing assay.

In order to identify more potent compounds and to understand the SAR better, we extended the study to follow up compounds by testing at a single concentration (100 µM), non-cytotoxic in the MTT assay. We eliminate ICT13122 and ICT13124 from our study because they expressed the lowest IC_{50} from the MTT assay and were least soluble in medium and therefore lacked the desired drug-like properties. Our results indicate that ICT13072 had similar activity to ICT5888 in blocking cell migration. ICT13070 resulted in less free surface area after migration compared to ICT5888. ICT13070 had relatively lower free surface area compared with ICT13072. Notably, ICT13069 showed enhanced inhibition of migration, 66% difference in free surface area between ICT13069 and ICT5888. The information gained from these results were used to establish a SAR for this class of CCR7 inhibitors by other members of our lab, but since that is not discussed here as it is beyond the scope of this dissertation.

Next, we tested ICT13069 at different concentrations to obtain a dose response curve. ICT13069 inhibited the migration induced by CCL21 (10 nM) even at 1 nM concentration. Our results indicate that ICT13069 reduced CCL21 induced cell migration not only back to control level but even greater than the control. The

reason for this is not known. It has been reported that chemokines are secreted after wounding cells in wound healing assay (Behm et al., 2012, Ghosh et al., 2012). Ghosh et al., confirmed the secretion of CXCL12 after creating a wound in the cell monolayer, and we have seen increase of CCL21 secretion after wounding the OSC-19 monolayer (chapter 2). Although the concentration of secreted CCL21 was fairly low, other chemoattractants and molecules involved in cells migration could also have been excreted and contributed to migration. Furthermore, by blocking CCR7 we could also prevent any cross talk by CCR7 with other pathways such as transforming growth factor β1 (TGF-β1) (Ma et al., 2015) and integrin (Li et al., 2011) thus further reducing the migratory aptitude of cells. For example, it has been reported in Li et al study that there is a cross talk between CCR7 and αvβ3 integrin in head and neck metastatic cancer cell line (Li et al., 2011). Binding of CCR7 ligands to its receptor causes transactivation of αvβ3 and inhibition of αvβ3 integrin resulting in inhibition of migration of tumour cells. In accordance with our results it has been shown that IS201, αvβ3 inhibitor, blocked the migration of cells in CCL19 added wells with 40% higher inhibition compared to the control where no ligand was added, in a wound healing assay (Li et al., 2011).

As ICT13069 was the most active antagonist in the CCL21 mediated wound healing assay for stopping the migration of OSC-19 cells, we decided to progress it for further investigation in a Boyden chamber transwell migration assay that has an invasion component (the inserts were coated with collagen). In our transwell assay, ICT13069 was able to modulate cell invasion in a dose dependent manner, confirming that ICT13069 not only can block CCL21 induced migration but also

invasion in a head and neck cancer cell line. A similar experiment in bladder cancer, but using a CCR7 monoclonal antibody has been reported in the literature (Mo et al., 2015). ICT13069 was more potent in blocking migration in the wound healing assay than in the transwell invasion, this however can be due to the fact that they are basically two different assays.

We next moved onto the assess potency of ICT13069 in a 3D model. It has been shown that many drugs lose their efficacy in 3D compared to 2D experimental conditions. On the contrary, others have shown the opposite effects (Desoize et al., 1998, Edmondson et al., 2014). The use of CCR7 antagonist molecules in 3D invasion assays has not been reported in the literature. Here we were able to demonstrate that ICT13069 at 100 µM caused complete inhibition of invasion of OSC-19 collagen embedded spheroids induced by CCL21 at 100 nM. This effect is consistent with what was seen in the wound healing and the transwell assays. However, ICT13069 at 10 µM was less effective in blocking the invasion compared with the 2D assays. At 10 µM ICT13069 caused 15% reduction in invasion triggered by 100 nM CCL21.

Next a series of ICT13069 analogues were developed and tested initially in the wound healing assay. Compounds ICT13301, ICT13303, ICT13310 and ICT13013 showed lower activity in the migration assay compared with ICT13069. Compounds; ICT13325, ICT13309, ICT13011 had similar activity as ICT13069 and ICT13312 shower higher activity than ICT13069. Of course, to better elucidate the SAR, we need to perform dose response curves with all the compounds that had similar or higher activity than ICT13069 in order to compare their IC_{50} in reducing

the migration of cells. Compounds showing higher activity than ICT13069 would be further analysed with serial dilutions and in different assays. Of note, some compounds have exhibit an increase of free surface, higher than 100% (control) level, while the particular reasons are currently unknown, we can speculate that this effect could be attributed to cross talk between CCR7 and other pathways (see above) or that the compounds are able to block other chemokine receptors or GPCRs. Therefore, cross talk as well as selectivity studies in OSC-19 cells are warranted.

In conclusion, we demonstrated that functional CCR7 is expressed on OSC-19 squamous carcinoma cells, and its ligands CCL21 or CCL19 caused an increase in cell migration and invasion *in vitro*. Neutralizing CCR7 by using a commercially available monoclonal antibody and CCR7 small molecule antagonists developed in house results in decreased cell migration and invasion induced by its ligands. Of note, ICT13069 resulted in significant inhibition of cell migration and invasion. So far, our investigations suggest that ICT13069 effects are caused by blocking CCR7. Taken together, these findings support the use and development of CCR7 antagonists for the potential treatment of lymph node metastasis to increase patient survival.

❖ **The main findings of this chapter:-**

- CCL21 and CCL19 increased the cell invasion in transwell assay.

- To the best of our knowledge, this is the first report of CCL21 and CCL19 can increase cell invasion in a 3D assay.

- Blocking CCR7 receptor by ab and small molecules antagonists resulted in reduced CCL21 induced migration and invasion in 2D and 3D in vitro models.

Chapter 5:

General discussion, conclusion and future work

5.1 Discussion

Cancer remains one of the major causes of global mortality (Siegel et al., 2017). Cancerous cells differ from other normal cells with their unlimited replication and proliferation potential, persistent ability to promote angiogenesis, evasion of apoptosis, and invasion of neighboring and/or distant tissues and metastasis (Hanahan and Weinberg, 2000, Hanahan and Weinberg, 2011). Head and neck cancer is the sixth most common cancer type worldwide (Bianchini et al., 2011). Surgery, radiotherapy and chemotherapy, alone or in combination, are the mainstay therapeutic approaches in head and neck cancers. Despite this, survival rates and prognosis have not improved significantly (Bianchini et al., 2011). The majority of patients develop local and/or regional recurrences. Furthermore, distant metastases occur in 20%–30% of head and neck patients (Vermorken and Specenier, 2010). Metastasis accounts for the majority of cancer related deaths including head and neck cancer (Mehlen and Puisieux, 2006).

Cancer metastasis is a complex multistep process. It has been proposed that cancer cells are able to “hijack” the molecular mechanisms of directional migration of leukocytes by chemokines, to direct themselves to specific organs (Balkwill, 2012). Chemokines and their receptors, facilitate tumor growth, promote EMT and increase angiogenesis. Indeed, the expression of certain chemokine receptors on the surface of cancer cells has be shown as a key for the promotion of metastasis and particularly, organ specific metastasis (Steeg, 2016).

Two chemokine receptors, CXCR4 and CCR7, have been shown to be highly involved in the metastatic process (Balakin et al., 2008). Cancer cells expressing

CCR7 receptors on their surface, home to the lymphatic system, where its ligand CCL21 is abundantly expressed (Muller et al., 2001). Often when the spread of cancer cells to the sentinel lymph nodes has occurred, lymph node removal is the primacy choice for treatment. Therefore, CCR7 expression has been suggested as a diagnostic marker to predict the metastatic spread status (Chen et al., 2016, Cabioglu et al., 2005). For example, if CCR7 is not upregulated, surgery could be avoided and a treatment of chemotherapy or targeted- drugs can be prioritised.

A number of studies have shown that blocking CCR7 using antibodies or knocking down CCR7 results in decreased invasion and migration of cancer cells *in vitro* (Xia et al., 2014, Sperveslage et al., 2012). Furthermore, knocking down CCR7 *in vivo* has been correlated with less lymph node metastases in animal models (Xia et al., 2014, Tutunea-Fatan et al., 2015, Mashino et al., 2002, Cunningham et al., 2010).

Therefore this project was initiated to investigate the expression of CCR7 receptor in different cancer cell lines, xenografts and clinical samples to determine its presence in cancer and to determine how it may affect cancer progression, how we may simulate clinical situations (e.g. hypoxia) and to evaluate the efficacy of developing small molecules CCR7 antagonists.

Notably, CCR7 expression was detected in most of the cancer cell lines examined (chapter 2) and particularly in head and neck cancer cell lines. Furthermore, the head and neck cell lines (SCC-4, OSC-19, FaDu, Detroit 562 and A-253) were exposed to hypoxia (0.1% O_2), under these conditions, upregulation of CCR7 in

OSC-19, FaDu, and Detroit 562 cells was observed. Furthermore, we also observed CCR7 upregulation in the hypoxic core of OSC-19 spheroids.

We propose that the hypoxic upregulation of CCR7 can be potentially mediated by HIF-1α. Researches have analysed the CCR7 gene, and showed the presence of HREs binding sites of HIFs; therefore we assumed that binding of HIF-1α to HRE will induce the transcription of CCR7 (Li et al., 2009).

In addition to cells and spheroids, we have also shown that CCR7 is highly expressed in xenograft and clinical tissues. The expression of CCR7 in head and neck xenografts showed a potential correlation with HIF-1α expression and cell differentiation. This correlation between hypoxia and differentiation is precedent, as it has been shown that hypoxia and hypoxia mimicking agents can cause cell differentiation in leukemia cells (Huang et al., 2003). Our clinical patient's samples confirmed the previous observed correlation in xenografts between CCR7 and HIF-1α. This correlation was increased accordingly with clinical stages and lymph node metastasis. In regard to the histological status of the patient samples the highest correlation between CCR7 and HIF-1α was observed in grade 1 in which cells are mostly differentiated. We hence postulate that developing drugs that target CCR7 (antagonize the receptor), will be beneficial to target not only undifferentiated cells that could be damaged by chemotherapy and radio-therapy, but also, such strategy may have the advantage to target the less proliferating differentiated cells that remain unaffected by conventional chemotherapy. This is particularly important when considering tumour recurrence, after conventional therapy, because these well differentiated cells will still have proliferating cells at the rim that are

responsible for tumour re-growth and metastasis (Bhattacharya et al., 2004). Furthermore, it has been shown that differentiated cells can undergo dedifferentiation to cancer stem cells which are responsible for tumour heterogeneity and tumour recurrence after treatment (Friedmann-Morvinski and Verma, 2014).

Our results showed that CCL21 induces cell migration and invasion in wound healing migration, transwell invasion and spheroid invasion assays under normoxia. Although we demonstrated upregulation of CCR7 expression in OSC-19 under hypoxia, our migration (scratch assay) results indicate that migration is reduced in comparison to the same experiments carried out under normoxia. To clarify if such effects are govern by CCR7, we performed knockdown studies (chapter 3) and shown that CCR7 presence enhances the migration of OSC-19 under hypoxia when compared with knockdown CCR7 cells. Our preliminary results suggest that the reduction in migration under hypoxic conditions could be mediated through other factors, such as the downregulation of ROS under hypoxia. We studied ROS levels and showed a decrease not only when cells were cultured in the hypoxia chamber, but also when subjected to $CoCl_{2.}$ This decrease in ROS paralleled the reduced migratory ability of OSC-19 cells.

Studies on the ROS effect in regard to cell migration and cell kill in cancer are controversial (Zablocka and Janusz, 2008). Our data indicates that induction of ROS increases cell migration and CCR7 expression. Whether this increased migration is CCR7-dependent has not yet been demonstrated. We believe that ROS concentrations should be carefully evaluated during therapeutic treatments,

since survival mechanisms and metastasis can inadvertently be induced. The current practice in treatment is to elevate the ROS level to increase the cell kill. However, as ROS can also increase the cell survival, future studies should consider neutralizing ROS molecules, instead of increasing concentrations as another therapeutic option.

Recently, our understanding of the significance and differences in CCR7 activation by its two ligands (CCL19 and CCL21) has increased. It has been suggested that CCR7 could have ligand biased signalling pathways leading to different functional effects (Steen et al., 2014). It is believed that CCL21 is mainly involved in migration *in vivo,* while CCL19 could support this role by providing survival signals (Comerford et al., 2013). We have observed that CCL19 has a limited role in migration (chapter 2) compared to CCL21, however it still enhances the invasion of OSC-19 cells in transwell and spheroid invasion assays (chapter 4).

Another important aspect of CCR7 activation by CCL21/CCL19 is the effect on survival, proliferation and apoptosis. We have demonstrated that CCL21 and CCL19 treatment does not resulted in increased proliferation in two head and neck (OSC-19 and FaDu) cell lines and other prostate cell lines (PC-3, DU-145, data not shown but currently under investigation in our group). Furthermore, CCL21 did not decrease the apoptotic cell death in OSC-19 cells.

This could be explained by different autocrine/paracrine loops activation of CCR7 (Wendt et al., 2008) or endogenous/ exogenous activation of CCR7 as seen in melanoma (Shields et al., 2010) breast (Wendt et al., 2008) cell lines (see discussion in chapter 2 and 3). Furthermore, secretion of CCL21 as detected in

OSC-19 cell line supernatant after mechanical stress and head and neck tumour xenografts might suggest the presence of autocrine activation of CCR7 to support tumour proliferation and growth after stress.

It also appears that the different signalling pathways that are triggered by CCR7 activation could differ from cell to cell type and/or whether CCL19 or CCL21 is the activating ligand (see discussion chapter 1). This biased signalling suggestion could be associated to the theory of “functional selectivity”. Different ligands can prompt different receptor conformations resulting in the activation of specific signalling pathways and certain agonists can induce one or more multifaceted conformations that are able to activate multiple G proteins, while others induce only a conformation able to activate a specific subtype of G proteins. This again is an area that requires further investigation, in particular, to understand the interaction between signalling pathways and CCR7 activation.

Furthermore, Mei-Lin Su et al, have reported that the sialylation of CCR7 affects its activation by CCL19 (Su et al., 2014). This study showed that CCL19 can activate CCR7 as long as the receptor is sialylated. This recent study, warrants investigating the sialylation of CCR7 in different cancer types and what roles do CCL19 and CCL21 play differentially to support the lymph metastasis. However, CCL19 studies are sparse and therefore, its effects in cancer biology should be evaluated more carefully. It has also been shown that CCL19 is involved in endocytosis and desensitization of the CCR7 receptor (Kohout et al., 2004), while CCL21 has negligible effect on this.

The possibility of inhibiting CCR7 functional activity was also evaluated in order to study its potential as a pharmacological target. The knockdown of CCR7 has shown that CCR7 is important in cell migration and confirmed that the increase of migration seen in chapter 2 is connected to the binding of CCL21 to CCR7.

To follow on from the knockdown studies, our medicinal chemistry team is focused on the development of CCR7 small molecule antagonists, to determine if small molecules CCR7 antagonists could affect cell migration and invasion. Synthesising and developing small molecules to antagonise CCR7 can provide more economical and safer option than antibody and microRNA therapies to prevent metastasis and improve efficacy and patient benefit. Nonetheless, if compounds are going to be generated, developing a good model for evaluating the lymph node metastasis status *in vivo* is paramount, to enable the successful selection and eventually transition to clinical trials (Horuk, 2009); in this context, the following points are key: (1) to determine the most beneficial time of administrating these compounds *in vivo* to explicit the most of its benefits to have a good efficacy and (2) to determine appropriate study end-points are warranted.

Furthermore, Horuk et al, have suggested that a potential failure of chemokine inhibitors in clinical trials could result from the redundancy of the chemokine network (Horuk, 2009). Taking this into consideration, one could also consider the development of dual antagonist that for example can target CCR7 and another chemokine receptor involved in cancer, for example CXCR4.

Dual antagonism is usually not an easy alternative, and could give rise to undesired side effect profiles. However, effective examples of dual antagonisms

already exist in diseases other than cancer such as, schizophrenia and AIDS (Roth et al., 2004, Wermuth, 2004) Furthermore, reparixin, a dual inhibitor of CXCR1 and CXCR2 has been shown to be effective in reducing inflammation in cerebral ischemia (Villa et al., 2007, Horuk, 2009).

Our in house antagonists, namely ICT13069 has been shown to stop cell migration and invasion in 2D and 3D assays. Currently, further work is continuing within the medicinal chemistry team to understand the SAR and to develop more potent drug-like compound such as follow up lead ICT13312. CCR7 antagonism is still a novel therapeutic target with a promising potential therapeutics in cancer and indeed other areas (e.g. inflammation) and to date, no CCR7 small molecule antagonists have been reported in the literature.

5.2 Conclusion:

In summary, the results presented in this thesis show the importance of the CCR7/CCL21 axis in cancer cell migration and invasion, we have also demonstrated that this axis can be modulated by small molecule antagonists. Of note, ICT13069 resulted in significant inhibition of cell migration and invasion. As such effects are triggered by CCL21, our investigations suggest that ICT13069 effects are caused by blocking CCR7, but further investigations remain. Our results also showed that CCR7 expression in cancer can be upregulated by, serum deprivation, hypoxia and increased ROS levels, conditions that resemble those present in tumours growing in clinical settings. We proposed that the induction of CCR7 expression under hypoxia is potentially regulated through HIF-1α, as we also observed it by $CoCl_2$ treatment, head and neck xenografts and clinical samples. Furthermore, a model for *in vitro* testing of compounds in OSC-19 cells, demonstrated that compounds could be predictive of the *in vivo* conditions.

We are still gathering exciting information to support the role of CCR7 in cancer, to understand the chemokine biased signalling in the context of cancer metastasis and progression.

The eventual development of CCR7 antagonist directed therapies may yet offer new hope for addressing cancer metastasis and patient survival. Taken together, these findings support the use and development of CCR7 antagonists for the potential treatment of lymph node metastasis to increase patient survival.

❖ The **novel** findings of this work include:-

- Expression of CCR7 under hypoxia is upregulated in head and neck cell lines and OSC-19 spheroids and its expression is potentially regulated by HIF-1α as shown by $CoCl_2$ treatment, xenografts and clinical samples.

- This is the first time to demonstrate a correlation between CCR7 expression and histological grade 1 in in head and neck clinical tissues.

- This is the first time to show a relationship between ROS and CCR7 in cancer as has been observed in OSC-19 cells, in which ROS has induced the expression of CCR7.

- This is the first to show that CCL21 and CCL19 can increase the invasion of cancer cells in a 3D spheroid model “OSC-19”.

- This is the first time to show that CCL21 induced CCR7 activation can be modulated by small molecules antagonist *in vitro.*

5.3 Future work

Therefore the future work should include:

- Investigation of its correlation between CCR7 and differentiation markers to see whether increased CCR7 expression in hypoxic region influences cell differentiation.

- Regulation of CCR7 by hypoxia expression was a key aspect in this study. For example, the effect of hypoxia on alteration of CCR7 expression was evaluated along with its consequences of cell migration and proliferation and therefore to confirm that this upregulation of CCR7 was through HIF-1α, knockdown studies of HIF-1α under hypoxia should be perform to confirm its effect on CCR7 expression.

- Furthermore, future investigations should focus on the mechanism by which CCR7 expression is altered by ROS and serum deprivation.

- Future investigations should study if different intracellular signalling pathways are activated by CCL21 or CCL19 since we have observed differential effect of their activation of CCR7 in OSC-19 cell migration. For instance, a recent study has shown that CCL19 is associated with increase proliferation, invasion and inhibiting anoikis through ERK and Akt pathways in breast cancer (Su et al., 2014). Of note, this study showed that CCL21, which is proved by us and many published work to have more significant

importance on the downstream effects upon CCR7 activation, did not increase the expression level of either ERK or Akt.

- To understand if there is a different role of CCL21 induced activation by paracrine and autocrine loops, knock in studies of CCL21 should be considered to evaluate the effect of autocrine activation of CCR7 in head and neck cell lines.

- As both CCL19 and CCL21 are the ligands of CCR7 that resulted in increasing cell invasion in 2D and 3D models, further investigations should be performed to determine whether ICT13069 would block the invasion induced with CCL19 or whether that ICT13069 works through CCL21/CCR7 axis only. Although OSC-19 cell line is a satisfactory model for testing compounds, however hence it is a metastatic cell line, further characterization of other primary and metastatic head and neck cancer cell lines is important to determine whether the effect seen in OSC-19 cell line is cell line specific. In addition, studying primary-derived patient cells as well as organoids is important to understand the CCR7 driven metastatic related events in better models.

- Since the chemokine system is a redundant and promiscuous one, studying the effect of CCR7 upregulation or blocking on the expression of other chemokine receptors is warranted.

- Our Study demonstrated the importance of 3D spheroid as a model more closely resembled *in vivo* tumours in drug screening. Accordingly, co-culturing of spheroids with stromal cells would be important to further bring the gap closer between *in vitro* and *in vivo* and to be a better indicator of *in vivo* drug efficacy.

- To test the most potent drug-like compound in tumour xenografts such as OSC-19 to determine if the effects seen *in vitro* can be translated to an *in vivo* setting. In this context, the pharmacokinetic profile of ICT13069 and related molecules is being studied within the team. Furthermore, testing the antagonists against other chemokine receptor is important to determine their selectivity.

Chapter 6:

References

References:

ABBOTT, A. **2003**. Cell culture: biology's new dimension. *Nature,* 424**,** 870-2.

ACHEN, M. G. & STACKER, S. A. **2008**. Molecular control of lymphatic metastasis. *Annals of the New York Academy of Sciences,* 1131**,** 225-34.

ACHILLI, T.-M., MEYER, J. & MORGAN, J. R. **2012**. Advances in the formation, use and understanding of multi-cellular spheroids. *Expert Opinion on Biological Therapy,* 12**,** 1347-1360.

AGALIANOS, C., GOUVAS, N., PAPAPARASKEVA, K. & DERVENIS, C. **2016**. Positive para-aortic lymph nodes following pancreatectomy for pancreatic cancer. Systematic review and meta-analysis of impact on short term survival and association with clinicopathologic features. *HPB (Oxford),* 18**,** 633-41

AHMED, M., BASHEER, H. A., AYUSO, J. M., AHMET, D., MAZZINI, M., PATEL, R., SHNYDER, S. D., VINADER, V. & AFARINKIA, K. **2017**. Agarose Spot as a Comparative Method for in situ Analysis of Simultaneous Chemotactic Responses to Multiple Chemokines. *Scientific Reports,* 7, 1075.

AHMAD, S., AKHTAR, K., SINGH, S. & SIDDIQUI, S. **2011**. FNAB of metastatic lesions with special reference to clinicopathological analysis of primary site in cases of epithelial and non-epithelial tumors. *Journal of Cytology / Indian Academy of Cytologists,* 28**,** 61-65.

AHMED, M. S. A. 2016. *New C-C Chemokine Receptor Type 7 Antagonists.* Doctorate University of Bradford.

ALBERTELLA, M. R., LOADMAN, P. M., JONES, P. H., PHILLIPS, R. M., RAMPLING, R., BURNET, N., ALCOCK, C., ANTHONEY, A., VJATERS, E., DUNK, C. R., HARRIS, P. A., WONG, A., LALANI, A. S. & TWELVES, C. J. **2008**. Hypoxia-selective targeting by the bioreductive prodrug AQ4N in patients with solid tumors: results of a phase I study. *Clinical Cancer Research,* 14**,** 1096-104.

ALLAVENA, P., GERMANO, G., MARCHESI, F. & MANTOVANI, A. **2011**. Chemokines in cancer related inflammation. *Experimental Cell Research,* 317**,** 664-73.

ALLEN, S. J., CROWN, S. E. & HANDEL, T. M. **2007**. Chemokine:Receptor Structure, Interactions, and Antagonism. *Annual Review of Immunology,* 25**,** 787-820.

ARCHER, S. L., HUANG, J., HENRY, T., PETERSON, D. & WEIR, E. K. **1993**. A redox-based O2 sensor in rat pulmonary vasculature. *Circulation Research,* 73**,** 1100-12.

ARANOVICH, D., MEIR, K., LOTEM, M. M., APPELBAUM, L. & MERHAV, H. **2013**. Ocular Melanoma Metastasizing to Intra-Abdominal Lymph Nodes. *Case Reports in Surgery,* 2013**,** 4.

ARYA, M., PATEL, H. R., MCGURK, C., TATOUD, R., KLOCKER, H., MASTERS, J. & WILLIAMSON, M. **2004**. The importance of the CXCL12-CXCR4 chemokine ligand-receptor interaction in prostate cancer metastasis. *Journal of Experimental Therapeutics and Oncology,* 4**,** 291-303.

ATCC. American Type Culture Collection [Online]. [Accessed 2017]

AZAB, A. K., HU, J., QUANG, P., AZAB, F., PITSILLIDES, C., AWWAD, R., THOMPSON, B., MAISO, P., SUN, J. D., HART, C. P., ROCCARO, A. M., SACCO, A., NGO, H. T., LIN, C. P., KUNG, A. L., CARRASCO, R. D., VANDERKERKEN, K. & GHOBRIAL, I. M. **2012**. Hypoxia promotes dissemination of multiple myeloma through acquisition of epithelial to mesenchymal transition-like features. *Blood,* 119**,** 5782-5794.

BALAKIN, K. V., IVANENKOV, Y. A., TKACHENKO, S. E., KISELYOV, A. S. & IVACHTCHENKO, A. V. **2008**. Regulators of chemokine receptor activity as promising anticancer therapeutics. *Current Cancer Drug Targets,* 8**,** 299-340.

BALKWILL, F. R. **2012**. The chemokine system and cancer. *The Journal of Pathology,* 226**,** 148-157.

BEHM, B., BABILAS, P., LANDTHALER, M. & SCHREML, S. **2012**. Cytokines, chemokines and growth factors in wound healing. *Journal of the European Academy of Dermatology and Venereology,* 26**,** 812-20.

BELL, E. L., KLIMOVA, T. A., EISENBART, J., SCHUMACKER, P. T. & CHANDEL, N. S. **2007**. Mitochondrial reactive oxygen species trigger hypoxia-inducible factor-dependent extension of the replicative life span during hypoxia. *Molecular and Cellular Biology,* 27**,** 5737-45.

BENNETT, L. D., FOX, J. M. & SIGNORET, N. **2011**. Mechanisms regulating chemokine receptor activity. *Immunology,* 134**,** 246-256.

BHATTACHARYA, A., TOTH, K., MAZURCHUK, R., SPERNYAK, J. A., SLOCUM, H. K., PENDYALA, L., AZRAK, R., CAO, S., DURRANI, F. A. & RUSTUM, Y. M. **2004**. Lack of microvessels in well-differentiated regions of human head and neck squamous cell carcinoma A253 associated with functional magnetic resonance imaging detectable hypoxia, limited drug delivery, and resistance to irinotecan therapy. *Clinical Cancer Research,* 10**,** 8005-17.

BIANCHINI, C., CIORBA, A., PELUCCHI, S., PIVA, R. & PASTORE, A. **2011**. Targeted therapy in head and neck cancer. *Tumori,* 97**,** 137-41.

BIRKENBACH, M., JOSEFSEN, K., YALAMANCHILI, R., LENOIR, G. & KIEFF, E. **1993**. Epstein-Barr virus-induced genes: first lymphocyte-specific G protein-coupled peptide receptors. *Journal of Virology,* 67**,** 2209-20.

BOETTCHER, M. & MCMANUS, M. T. **2015**. Choosing the Right Tool for the Job: RNAi, TALEN or CRISPR. *Molecular Cell,* 58**,** 575-585.

BONECCHI, R. & GRAHAM, G. J. **2016**. Atypical Chemokine Receptors and Their Roles in the Resolution of the Inflammatory Response. *Frontiers in Immunology,* 7**,** 224.

BOYLE, S. T., INGMAN, W. V., POLTAVETS, V., FAULKNER, J. W., WHITFIELD, R. J., MCCOLL, S. R. & KOCHETKOVA, M. **2016**. The chemokine receptor CCR7 promotes mammary tumorigenesis through amplification of stem-like cells. *Oncogene,* 35**,** 105-115.

BRESLIN, S. & O'DRISCOLL, L. **2013**. Three-dimensional cell culture: the missing link in drug discovery. *Drug Discovery Today,* 18**,** 240-9.

BROWN, J. M. & WILSON, W. R. **2004**. Exploiting tumour hypoxia in cancer treatment. *Nature Reviews: Cancer,* 4**,** 437-447.

BUONAMICI, S. **2009**. CCR7 signalling as an essential regulator of CNS infiltration in T-cell leukaemia. *Nature,* 459**,** 1000-1004.

CAAMANO, J., ZHANG, S. Y., ROSVOLD, E. A., BAUER, B. & KLEIN-SZANTO, A. J. **1993**. p53 alterations in human squamous cell carcinomas and carcinoma cell lines. *American Journal of Pathology,* 142**,** 1131-9.

CABIOGLU, N., YAZICI, M. S., ARUN, B., BROGLIO, K. R., HORTOBAGYI, G. N., PRICE, J. E. & SAHIN, A. **2005**. CCR7 and CXCR4 as novel biomarkers predicting axillary lymph node metastasis in T1 breast cancer. *Clinical Cancer Research,* 11**,** 5686-93.

CAIRNS, R. A. & HILL, R. P. **2004**. Acute Hypoxia Enhances Spontaneous Lymph Node Metastasis in an Orthotopic Murine Model of Human Cervical Carcinoma. *Cancer Research,* 64**,** 2054.

CATUSSE, J., LEICK, M., GROCH, M., CLARK, D. J., BUCHNER, M. V., ZIRLIK, K. & BURGER, M. **2010**. Role of the atypical chemoattractant receptor CRAM in regulating CCL19 induced CCR7 responses in B-cell chronic lymphocytic leukemia. *Molecular Cancer,* 9**,** 297-297.

CANCER RESEARCH UK, 2014. Cancer mortality statistics. [Online]. [Accessed 2017].

CELLOSAURUS EXPASY. Cellosaurus [Online]. [Accessed 2017]

CHAMBERS, A. F., GROOM, A. C. & MACDONALD, I. C. **2002**. Metastasis: Dissemination and growth of cancer cells in metastatic sites. *Nature Reviews: Cancer,* 2**,** 563-572.

CHATTERJEE, S., AZAD, B. B. & NIMMAGADDA, S. **2014**. The Intricate Role of CXCR4 in Cancer. *Advances in Cancer Research,* 124**,** 31-82.

CHEN, J., CUI, Y. U., LIU, L., LI, C., TANG, Y., ZHOU, X. U., QI, L. I. N. & ZU, X. **2016**. CCR7 as a predictive biomarker associated with computed tomography for the diagnosis of lymph node metastasis in bladder carcinoma. *Oncology Letters,* 11**,** 735-740.

CHEN, Y., TIAN, Y., JI, Z., LIU, Z. & SHANG, D. **2015**. CC-chemokine receptor 7 is overexpressed and correlates with growth and metastasis in prostate cancer. *Tumor Biology,* 36**,** 5537-5541.

CHENG, S., HAN, L., GUO, J., YANG, Q., ZHOU, J. & YANG, X. **2014**. The essential roles of CCR7 in epithelial-to-mesenchymal transition induced by hypoxia in epithelial ovarian carcinomas. *Tumour Biol,* 35**,** 12293-8.

CHETRAM, M. A. & HINTON, C. V. **2013**. ROS-mediated regulation of CXCR4 in cancer. *Frontiers in biology,* 8**,** 10.1007/s11515-012-1204-4.

CHETRAM, M. A., ODERO-MARAH, V. & HINTON, C. V. **2011**. Loss of PTEN permits CXCR4-mediated tumorigenesis through ERK1/2 in prostate cancer cells. *Molecular Cancer Research,* 9**,** 90-102.

COMERFORD, I., HARATA-LEE, Y., BUNTING, M. D., GREGOR, C., KARA, E. E. & MCCOLL, S. R. **2013**. A myriad of functions and complex regulation of the CCR7/CCL19/CCL21 chemokine axis in the adaptive immune system. *Cytokine & Growth Factor Reviews,* 24**,** 269-83.

COUSSENS, L. M. & WERB, Z. **2002**. Inflammation and cancer. *Nature,* 420**,** 860-867.

COUTURE, C., RAYBAUD-DIOGENE, H., TETU, B., BAIRATI, I., MURRY, D., ALLARD, J. & FORTIN, A. **2002**. p53 and Ki-67 as markers of radioresistance in head and neck carcinoma. *Cancer,* 94**,** 713-22.

CUI, X., HARTANTO, Y. & ZHANG, H. **2017**. Advances in multicellular spheroids formation. 14.

CUNNINGHAM, H. D., SHANNON, L. A., CALLOWAY, P. A., FASSOLD, B. C., DUNWIDDIE, I., VIELHAUER, G., ZHANG, M. & VINES, C. M. **2010**. Expression of the C-C chemokine receptor 7 mediates metastasis of breast cancer to the lymph nodes in mice. *Translational Oncology,* 3**,** 354-61.

DACHS, G. U. & TOZER, G. M. **2000**. Hypoxia modulated gene expression: angiogenesis, metastasis and therapeutic exploitation. *European Journal of Cancer,* 36**,** 1649-60.

DAI, Y. A. O., BAE, K. & SIEMANN, D. W. **2011**. IMPACT OF HYPOXIA ON THE METASTATIC POTENTIAL OF HUMAN PROSTATE CANCER CELLS. *International Journal of Radiation Oncology, Biology, Physics,* 81**,** 521-528.

DAS, S., SARROU, E., PODGRABINSKA, S., CASSELLA, M., MUNGAMURI, S. K., FEIRT, N., GORDON, R., NAGI, C. S., WANG, Y., ENTENBERG, D., CONDEELIS, J. & SKOBE, M. **2013**. Tumor cell entry into the lymph node is controlled by CCL1 chemokine expressed by lymph node lymphatic sinuses. *Journal of Experimental Medicine,* 210**,** 1509-28.

DE SILVA, R. A., PEYRE, K., PULLAMBHATLA, M., FOX, J. J., POMPER, M. G. & NIMMAGADDA, S. **2011**. Imaging CXCR4 expression in human cancer xenografts: evaluation of monocyclam 64Cu-AMD3465. *Journal of Nuclear Medicine,* 52**,** 986-93.

DECAESTECKER, C., DEBEIR, O., VAN HAM, P. & KISS, R. **2007**. Can anti-migratory drugs be screened in vitro? A review of 2D and 3D assays for the quantitative analysis of cell migration. *Medicinal Research Reviews,* 27**,** 149-76.

DEHGHANI, M., KIANPOUR, S., ZANGENEH, A. & MOSTAFAVI-POUR, Z. **2014**. CXCL12 Modulates Prostate Cancer Cell Adhesion by Altering the Levels or Activities of or Activities of β1-Containing Integrins International Journal of Cell Biology, 2014**,** 11.

DENKO, N. C. **2008**. Hypoxia, HIF1 and glucose metabolism in the solid tumour. *Nature Reviews: Cancer,* 8**,** 705-13.

DESGROSELLIER, J. S. & CHERESH, D. A. **2010**. Integrins in cancer: biological implications and therapeutic opportunities. *Nature reviews. Cancer,* 10**,** 9-22.

DESOIZE, B., GIMONET, D. & JARDILLER, J. C. **1998**. Cell culture as spheroids: an approach to multicellular resistance. *Anticancer Research,* 18**,** 4147-58.

DOMANSKA, U. M., TIMMER-BOSSCHA, H., NAGENGAST, W. B., OUDE MUNNINK, T. H., KRUIZINGA, R. C., ANANIAS, H. J. K., KLIPHUIS, N. M., HULS, G., DE VRIES, E. G. E., DE JONG, I. J. & WALENKAMP, A. M. E. **2012**. CXCR4 Inhibition with AMD3100 Sensitizes Prostate Cancer to Docetaxel Chemotherapy. *Neoplasia (New York, N.Y.),* 14**,** 709-718.

DOWSLAND, M. H., HARVEY, J. R., LENNARD, T. W., KIRBY, J. A. & ALI, S. **2003**. Chemokines and breast cancer: a gateway to revolutionary targeted cancer treatments? *Current Medicinal Chemistry,* 10**,** 579-592.

DVORAK, H. F., FORM, D. M., MANSEAU, E. J. & SMITH, B. D. **1984**. Pathogenesis of desmoplasia. I. Immunofluorescence identification and localization of some structural proteins of line 1 and line 10 guinea pig tumors and of healing wounds. *Journal of the National Cancer Institute,* 73**,** 1195-205.

ECCLES, S. A., BOX, C. & COURT, W. **2005**. Cell migration/invasion assays and their application in cancer drug discovery. *Biotechnology Annual Review,* 11**,** 391-421.
EDMONDSON, R., BROGLIE, J. J., ADCOCK, A. F. & YANG, L. **2014**. Three-Dimensional Cell Culture Systems and Their Applications in Drug Discovery and Cell-Based Biosensors. *Assay and Drug Development Technologies,* 12**,** 207-218.
ELKASHEF, S. M., ALLISON, S. J., SADIQ, M., BASHEER, H. A., RIBEIRO MORAIS, G., LOADMAN, P. M., PORS, K. & FALCONER, R. A. **2016**. Polysialic acid sustains cancer cell survival and migratory capacity in a hypoxic environment. *Scientific Reports,* 6**,** 33026.
ERLER, J. T., BENNEWITH, K. L., NICOLAU, M., DORNHOFER, N., KONG, C., LE, Q.-T., CHI, J.-T. A., JEFFREY, S. S. & GIACCIA, A. J. **2006**. Lysyl oxidase is essential for hypoxia-induced metastasis. *Nature,* 440**,** 1222-1226.
EVANS, S. M., DU, K. L., CHALIAN, A. A., MICK, R., ZHANG, P. J., HAHN, S. M., QUON, H., LUSTIG, R., WEINSTEIN, G. S. & KOCH, C. J. **2007**. Patterns and Levels of Hypoxia in Head and Neck Squamous Cell Carcinomas and their Relationship to Patient Outcome. *International Journal of Radiation Oncology, Biology, Physics,* 69**,** 1024-1031.
FAN, J., CAI, H. & TAN, W. S. **2007**. Role of the plasma membrane ROS-generating NADPH oxidase in CD34+ progenitor cells preservation by hypoxia. *Journal of Biotechnology,* 130**,** 455-62.
FAN, J., CAI, H., YANG, S., YAN, L. & TAN, W. **2008**. Comparison between the effects of normoxia and hypoxia on antioxidant enzymes and glutathione redox state in ex vivo culture of CD34(+) cells. *Comparative Biochemistry and Physiology. Part B: Biochemistry and Molecular Biology,* 151**,** 153-8.
FANDREY, J., FREDE, S. & JELKMANN, W. **1994**. Role of hydrogen peroxide in hypoxia-induced erythropoietin production. *Biochemical Journal,* 303**,** 507.
FERNANDEZ, E. J. & LOLIS, E. **2002**. Structure, function, and inhibition of chemokines. *Annual Review of Pharmacology and Toxicology,* 42**,** 469-99.
FÖRSTER, R., DAVALOS-MISSLITZ, A. C. & ROT, A. **2008**. CCR7 and its ligands: balancing immunity and tolerance. *Nature Reviews: Immunology,* 8**,** 362-71.
FOTY, R. **2011**. A simple hanging drop cell culture protocol for generation of 3D spheroids. *J Vis Exp*.
FRIEDMANN-MORVINSKI, D. & VERMA, I. M. **2014**. Dedifferentiation and reprogramming: origins of cancer stem cells. *EMBO Reports,* 15**,** 244-253.
FRIEDRICH, J., SEIDEL, C., EBNER, R. & KUNZ-SCHUGHART, L. A. **2009**. Spheroid-based drug screen: considerations and practical approach. *Nature Protocols,* 4**,** 309-24.
FUJIWARA, S., NAKAGAWA, K., HARADA, H., NAGATO, S., FURUKAWA, K., TERAOKA, M., SENO, T., OKA, K., IWATA, S. & OHNISHI, T. **2007**. Silencing hypoxia-inducible factor-1alpha inhibits cell migration and invasion under hypoxic environment in malignant gliomas. *International Journal of Oncology,* 30**,** 793-802.
GANGULY, K. K., PAL, S., MOULIK, S. & CHATTERJEE, A. **2013**. Integrins and metastasis. *Cell Adh Migr,* 7**,** 251-61.
GHOSH, M. C., MAKENA, P. S., GORANTLA, V., SINCLAIR, S. E. & WATERS, C. M. **2012**. CXCR4 regulates migration of lung alveolar epithelial cells through activation of Rac1 and matrix metalloproteinase-2. *American Journal of Physiology: Lung Cellular and Molecular Physiology,* 302**,** L846-56.
GIELING, R. G., BABUR, M., MAMNANI, L., BURROWS, N., TELFER, B. A., CARTA, F., WINUM, J. Y., SCOZZAFAVA, A., SUPURAN, C. T. & WILLIAMS, K. J. **2012**. Antimetastatic effect of sulfamate carbonic anhydrase IX inhibitors in breast carcinoma xenografts. *Journal of Medicinal Chemistry,* 55**,** 5591-600.
GILES, R. & LOBERG, R. D. **2006**. Can we target the chemokine network for cancer therapeutics? *Current Cancer Drug Targets,* 6**,** 659-70.
GUISE, C. P., MOWDAY, A. M., ASHOORZADEH, A., YUAN, R., LIN, W.-H., WU, D.-H., SMAILL, J. B., PATTERSON, A. V. & DING, K. **2014**. Bioreductive prodrugs as cancer therapeutics: targeting tumor hypoxia. *Chinese Journal of Cancer,* 33**,** 80-86.

GUO, J., LOU, W., JI, Y. & ZHANG, S. **2013**. Effect of CCR7, CXCR4 and VEGF-C on the lymph node metastasis of human pancreatic ductal adenocarcinoma. *Oncology Letters,* 5**,** 1572-1578.
GUZY, R. D., HOYOS, B., ROBIN, E., CHEN, H., LIU, L., MANSFIELD, K. D., SIMON, M. C., HAMMERLING, U. & SCHUMACKER, P. T. **2005**. Mitochondrial complex III is required for hypoxia-induced ROS production and cellular oxygen sensing. *Cell Metab,* 1**,** 401-8.
HAESSLER, U., PISANO, M., WU, M. & SWARTZ, M. A. **2011**. Dendritic cell chemotaxis in 3D under defined chemokine gradients reveals differential response to ligands CCL21 and CCL19. *Proceedings of the National Academy of Sciences of the United States of America,* 108**,** 5614-9.
HAMEL, D. J., SIELAFF, I., PROUDFOOT, A. E. & HANDEL, T. M. **2009**. Chapter 4. Interactions of chemokines with glycosaminoglycans. *Methods in Enzymology,* 461**,** 71-102.
HAN, S., HAN, W., NI, Y., WANG, Z. & HU, Q. **2015**. [Establishment of CoCl2 induced hypoxic cell model of oral squamous cell carcinoma and a preliminary study on the biological behaviour change]. *Zhonghua Kou Qiang Yi Xue Za Zhi,* 50**,** 173-7.
HANAHAN, D. & WEINBERG, ROBERT A. Hallmarks of Cancer: The Next Generation. *Cell,* 144**,** 646-674.
HANAHAN, D. & WEINBERG, R. A. **2000**. The Hallmarks of Cancer. *Cell,* 100**,** 57-70.
HANAHAN, D. & WEINBERG, ROBERT A. **2011**. Hallmarks of Cancer: The Next Generation. *Cell,* 144**,** 646-674.
HAUSER, M. A. & LEGLER, D. F. **2016**. Common and biased signaling pathways of the chemokine receptor CCR7 elicited by its ligands CCL19 and CCL21 in leukocytes. *Journal of Leukocyte Biology,* 99**,** 869-82.
HERESI, G. A., WANG, J., TAICHMAN, R., CHIRINOS, J. A., REGALADO, J. J., LICHTSTEIN, D. M. & ROSENBLATT, J. D. **2005**. Expression of the chemokine receptor CCR7 in prostate cancer presenting with generalized lymphadenopathy: report of a case, review of the literature, and analysis of chemokine receptor expression. *Urologic Oncology,* 23**,** 261-7.
HILLER, D. & CHU, Q. D. **2011**. CXCR4 and axillary lymph nodes: review of a potential biomarker for breast cancer metastasis. *International Journal of Breast Cancer,* 2011**,** 420981.
HIRAKAWA, S., BROWN, L. F., KODAMA, S., PAAVONEN, K., ALITALO, K. & DETMAR, M. **2007**. VEGF-C-induced lymphangiogenesis in sentinel lymph nodes promotes tumor metastasis to distant sites. *Blood,* 109**,** 1010-7.
HIRSCHHAEUSER, F., MENNE, H., DITTFELD, C., WEST, J., MUELLER-KLIESER, W. & KUNZ-SCHUGHART, L. A. **2010**. Multicellular tumor spheroids: an underestimated tool is catching up again. *Journal of Biotechnology,* 148**,** 3-15.
HOCKEL, M. & VAUPEL, P. **2001**. Tumor hypoxia: definitions and current clinical, biologic, and molecular aspects. *Journal of the National Cancer Institute,* 93**,** 266-76.
HONG, H., HE, C., ZHU, S., ZHANG, Y., WANG, X., SHE, F. & CHEN, Y. **2016**. CCR7 mediates the TNF-alpha-induced lymphatic metastasis of gallbladder cancer through the "ERK1/2 - AP-1" and "JNK - AP-1" pathways. *Journal of Experimental and Clinical Cancer Research,* 35**,** 51.
HORUK, R. **2009**. Chemokine receptor antagonists: overcoming developmental hurdles. *Nature Reviews: Drug Discovery,* 8**,** 23-33.
HU, C. J., WANG, L. Y., CHODOSH, L. A., KEITH, B. & SIMON, M. C. **2003**. Differential roles of hypoxia-inducible factor 1alpha (HIF-1alpha) and HIF-2alpha in hypoxic gene regulation. *Molecular and Cellular Biology,* 23**,** 9361-74.
HU, T. H., YAO, Y., YU, S., HAN, L. L., WANG, W. J., GUO, H., TIAN, T., RUAN, Z. P., KANG, X. M., WANG, J., WANG, S. H. & NAN, K. J. **2014**. SDF-1/CXCR4 promotes epithelial-mesenchymal transition and progression of colorectal cancer by activation of the Wnt/beta-catenin signaling pathway. *Cancer Letters,* 354**,** 417-26.
HUANG, H., SHAH, K., BRADBURY, N. A., LI, C. & WHITE, C. **2014**. Mcl-1 promotes lung cancer cell migration by directly interacting with VDAC to increase mitochondrial Ca2+ uptake and reactive oxygen species generation. *Cell Death & Disease,* 5**,** e1482.
HUANG, X., SU, K., ZHOU, L., SHEN, G., DONG, Q., LOU, Y. & ZHENG, S. **2013**. Hypoxia preconditioning of mesenchymal stromal cells enhances PC3 cell lymphatic metastasis

accompanied by VEGFR-3/CCR7 activation. *Journal of Cellular Biochemistry,* 114**,** 2834-41.

HUANG, Y., DU, K. M., XUE, Z. H., YAN, H., LI, D., LIU, W., CHEN, Z., ZHAO, Q., TONG, J. H., ZHU, Y. S. & CHEN, G. Q. **2003**. Cobalt chloride and low oxygen tension trigger differentiation of acute myeloid leukemic cells: possible mediation of hypoxia-inducible factor-1alpha. *Leukemia,* 17**,** 2065-73.

HUBBI, M. E. & SEMENZA, G. L. **2015**. Regulation of cell proliferation by hypoxia-inducible factors. *American Journal of Physiology: Cell Physiology,* 309**,** C775-82.

HURD, T. R., DEGENNARO, M. & LEHMANN, R. **2012**. Redox regulation of cell migration and adhesion. *Trends in Cell Biology,* 22**,** 107-15.

IRINO, T., TAKEUCHI, H., MATSUDA, S., SAIKAWA, Y., KAWAKUBO, H., WADA, N., TAKAHASHI, T., NAKAMURA, R., FUKUDA, K., OMORI, T. & KITAGAWA, Y. **2014**. CC-Chemokine receptor CCR7: a key molecule for lymph node metastasis in esophageal squamous cell carcinoma. *BMC Cancer,* 14**,** 291.

JEONG, S. H., JEON, Y. J. & PARK, S. J. **2016**. Inhibitory effects of dieckol on hypoxia-induced epithelial-mesenchymal transition of HT29 human colorectal cancer cells. *Mol Med Rep,* 14**,** 5148-5154.

JONES, S. A. & ROSE-JOHN, S. **2002**. The role of soluble receptors in cytokine biology: the agonistic properties of the sIL-6R/IL-6 complex. *Biochimica et Biophysica Acta (BBA) - Bioenergetics,* 1592**,** 251-63.

JOSEPH, J. V., CONROY, S., PAVLOV, K., SONTAKKE, P., TOMAR, T., EGGENS-MEIJER, E., BALASUBRAMANIYAN, V., WAGEMAKERS, M., DEN DUNNEN, W. F. A. & KRUYT, F. A. E. **2015**. Hypoxia enhances migration and invasion in glioblastoma by promoting a mesenchymal shift mediated by the HIF1α–ZEB1 axis. *Cancer Letters,* 359**,** 107-116.

KATT, M. E., PLACONE, A. L., WONG, A. D., XU, Z. S. & SEARSON, P. C. **2016**. In Vitro Tumor Models: Advantages, Disadvantages, Variables, and Selecting the Right Platform. *Frontiers in Bioengineering and Biotechnology,* 4**,** 12.

KAWADA, K., HOSOGI, H., SONOSHITA, M., SAKASHITA, H., MANABE, T., SHIMAHARA, Y., SAKAI, Y., TAKABAYASHI, A., OSHIMA, M. & TAKETO, M. M. **2007**. Chemokine receptor CXCR3 promotes colon cancer metastasis to lymph nodes. *Oncogene,* 26**,** 4679-4688.

KAWADA, K. & TAKETO, M. M. **2011**. Significance and mechanism of lymph node metastasis in cancer progression. *Cancer Research,* 71**,** 1214-8.

KAWAHARA, E., OKADA, Y., NAKANISHI, I., IWATA, K., KOJIMA, S., KUMAGAI, S. & YAMAMOTO, E. **1993**. The expression of invasive behavior of differentiated squamous carcinoma cell line evaluated by an in vitro invasion model. *Japanese Journal of Cancer Research,* 84**,** 409-18.

KAWASHIRI, S., KUMAGAI, S., KOJIMA, K., HARADA, H. & YAMAMOTO, E. **1995**. Development of a new invasion and metastasis model of human oral squamous cell carcinomas. *European Journal of Cancer Part B: Oral Oncology,* 31b**,** 216-21.

KELLAND, L. **2007**. The resurgence of platinum-based cancer chemotherapy. *Nature Reviews: Cancer,* 7**,** 573-584.

KIETZMANN, T., MENNERICH, D. & DIMOVA, E. Y. **2016**. Hypoxia-Inducible Factors (HIFs) and Phosphorylation: Impact on Stability, Localization, and Transactivity. *Frontiers in Cell and Developmental Biology,* 4.

KIM, S. J., SHIN, J. Y., LEE, K. D., BAE, Y. K., SUNG, K. W., NAM, S. J. & CHUN, K. H. **2012**. MicroRNA let-7a suppresses breast cancer cell migration and invasion through downregulation of C-C chemokine receptor type 7. *Breast Cancer Research,* 14**,** R14.

KITAMURA, T., QIAN, B.-Z. & POLLARD, J. W. **2015**. Immune cell promotion of metastasis. *Nature reviews. Immunology,* 15**,** 73-86.

KOCHETKOVA, M., KUMAR, S. & MCCOLL, S. R. **2009**. Chemokine receptors CXCR4 and CCR7 promote metastasis by preventing anoikis in cancer cells. *Cell Death and Differentiation,* 16**,** 664-73.

KOHOUT, T. A., NICHOLAS, S. L., PERRY, S. J., REINHART, G., JUNGER, S. & STRUTHERS, R. S. **2004**. Differential desensitization, receptor phosphorylation, beta-arrestin recruitment,

and ERK1/2 activation by the two endogenous ligands for the CC chemokine receptor 7. *Journal of Biological Chemistry,* 279**,** 23214-22.

KONDOH, M., OHGA, N., AKIYAMA, K., HIDA, Y., MAISHI, N., TOWFIK, A. M., INOUE, N., SHINDOH, M. & HIDA, K. **2013**. Hypoxia-Induced Reactive Oxygen Species Cause Chromosomal Abnormalities in Endothelial Cells in the Tumor Microenvironment. *PloS One,* 8**,** e80349.

KOOPMANN, W. & KRANGEL, M. S. **1997**. Identification of a glycosaminoglycan-binding site in chemokine macrophage inflammatory protein-1alpha. *Journal of Biological Chemistry,* 272**,** 10103-9.

KOTAKE-NARA, E. & SAIDA, K. **2007**. Characterization of CoCl2-induced reactive oxygen species (ROS): Inductions of neurite outgrowth and endothelin-2/vasoactive intestinal contractor in PC12 cells by CoCl2 are ROS dependent, but those by MnCl2 are not. *Neuroscience Letters,* 422**,** 223-7.

KOUKOURAKIS, M. I., GIATROMANOLAKI, A., SIVRIDIS, E., SIMOPOULOS, C., TURLEY, H., TALKS, K., GATTER, K. C. & HARRIS, A. L. **2002**. Hypoxia-inducible factor (HIF1A and HIF2A), angiogenesis, and chemoradiotherapy outcome of squamous cell head-and-neck cancer. *International Journal of Radiation Oncology, Biology, & Physics,* 53**,** 1192-202.

KOWALSKI, L. P. **2001**. Noncervical lymph node metastasis from head and neck cancer. *ORL J Otorhinolaryngol Relat Spec,* 63**,** 252-5.

KRAMER, N., WALZL, A., UNGER, C., ROSNER, M., KRUPITZA, G., HENGSTSCHLÄGER, M. & DOLZNIG, H. **2013**. In vitro cell migration and invasion assays. *Mutation Research/Reviews in Mutation Research,* 752**,** 10-24.

KROCK, B. L., SKULI, N. & SIMON, M. C. **2011**. Hypoxia-Induced Angiogenesis: Good and Evil. *Genes & Cancer,* 2**,** 1117-1133.

KRUIZINGA, R. C., BESTEBROER, J., BERGHUIS, P., DE HAAS, C. J. C., LINKS, T. P., DE VRIES, E. G. E. & WALENKAMP, A. M. E. **2009**. Role of Chemokines and Their Receptors in Cancer. *Current Pharmaceutical Design,* 15**,** 3396-3416.

LALANI, A. S., ALTERS, S. E., WONG, A., ALBERTELLA, M. R., CLELAND, J. L. & HENNER, W. D. **2007**. Selective tumor targeting by the hypoxia-activated prodrug AQ4N blocks tumor growth and metastasis in preclinical models of pancreatic cancer. *Clinical Cancer Research,* 13**,** 2216-25.

LANATI, S., DUNN, D. B., ROUSSIGNE, M., EMMETT, M. S., CARRIERE, V., JULLIEN, D., BUDGE, J., FRYER, J., ERARD, M., CAILLER, F., GIRARD, J. P. & BATES, D. O. **2010**. Chemotrap-1: an engineered soluble receptor that blocks chemokine-induced migration of metastatic cancer cells in vivo. *Cancer Research,* 70**,** 8138-48.

LANZA, F., GARDELLINI, A., LASZLO, D. & MARTINO, M. **2014**. Plerixafor: what we still have to learn. *Expert Opinion on Biological Therapy***,** 1-5.

LASAGNI, L., FRANCALANCI, M., ANNUNZIATO, F., LAZZERI, E., GIANNINI, S., COSMI, L., SAGRINATI, C., MAZZINGHI, B., ORLANDO, C., MAGGI, E., MARRA, F., ROMAGNANI, S., SERIO, M. & ROMAGNANI, P. **2003**. An alternatively spliced variant of CXCR3 mediates the inhibition of endothelial cell growth induced by IP-10, Mig, and I-TAC, and acts as functional receptor for platelet factor 4. *Journal of Experimental Medicine,* 197**,** 1537-49.

LAZENNEC, G. & RICHMOND, A. **2010**. Chemokines and chemokine receptors: new insights into cancer-related inflammation. *Trends in Molecular Medicine,* 16**,** 133-44.

LEE, J. H., SEO, Y. W., PARK, S. R., KIM, Y. J. & KIM, K. K. **2003**. Expression of a splice variant of KAI1, a tumor metastasis suppressor gene, influences tumor invasion and progression. *Cancer Research,* 63**,** 7247-55.

LEE, R. L., WESTENDORF, J. & GOLD, M. R. **2007**. Differential role of reactive oxygen species in the activation of mitogen-activated protein kinases and Akt by key receptors on B-lymphocytes: CD40, the B cell antigen receptor, and CXCR4. *J Cell Commun Signal,* 1**,** 33-43.

LEGLER, D. F., UETZ-VON ALLMEN, E. & HAUSER, M. A. **2014**. CCR7: Roles in cancer cell dissemination, migration and metastasis formation. *International Journal of Biochemistry and Cell Biology,* 54c**,** 78-82.

LI, F., ZOU, Z., SUO, N., ZHANG, Z., WAN, F. & ZHONG, G. **2014**. CCL21/CCR7 axis activating chemotaxis accompanied with epithelial-mesenchymal transition in human breast carcinoma. *Medical Oncology,* 31.

LI, J., JIANG, K., QIU, X., LI, M., HAO, Q., WEI, L., ZHANG, W., CHEN, B. & XIN, X. **2014**. Overexpression of CXCR4 is significantly associated with cisplatin-based chemotherapy resistance and can be a prognostic factor in epithelial ovarian cancer. *BMB Reports,* 47**,** 33-38.

LI, J., SUN, R., TAO, K. & WANG, G. **2011**. The CCL21/CCR7 pathway plays a key role in human colon cancer metastasis through regulation of matrix metalloproteinase-9. *Digestive and Liver Disease,* 43**,** 40-47.

LI, P., LIU, F., SUN, L., ZHAO, Z., DING, X., SHANG, D., XU, Z. & SUN, C. **2011**. Chemokine receptor 7 promotes cell migration and adhesion in metastatic squamous cell carcinoma of the head and neck by activating integrin αvβ3. *International Journal of Molecular Medicine,* 27**,** 679-87.

LI, Y., QIU, X., ZHANG, S., ZHANG, Q. & WANG, E. **2009**. Hypoxia induced CCR7 expression via HIF-1alpha and HIF-2alpha correlates with migration and invasion in lung cancer cells. *Cancer Biology & Therapy,* 8**,** 322-30.

LI, Y., ZHANG, Q., WANG, Y., QIU, X. & WANG, E. **2008**. [Effects of hypoxia on the expression of CCR7 and proliferation, invasiveness of A549 cells.]. *Zhongguo Fei Ai Za Zhi. Chinese Journal of Lung Cancer,* 11**,** 704-6.

LI, Z., HODGKINSON, T., GOTHARD, E. J., BOROUMAND, S., LAMB, R., CUMMINS, I., NARANG, P., SAWTELL, A., COLES, J. & LEONOV, G. **2016**. Epidermal Notch1 recruits RORgamma(+) group 3 innate lymphoid cells to orchestrate normal skin repair. *Nature communications,* 7**,** 11394.

LIN, R. Z. & CHANG, H. Y. **2008**. Recent advances in three-dimensional multicellular spheroid culture for biomedical research. *Biotechnology Journal,* 3**,** 1172-84.

LIOU, G.-Y. & STORZ, P. **2010**. Reactive oxygen species in cancer. *Free Radical Research,* 44**,** 10.3109/10715761003667554.

LIPPERT, T. H., RUOFF, H. J. & VOLM, M. **2008**. Intrinsic and acquired drug resistance in malignant tumors. The main reason for therapeutic failure. *Arzneimittel-Forschung,* 58**,** 261-4.

LIU, F.-Y., SAFDAR, J., LI, Z.-N., FANG, Q.-G., ZHANG, X., XU, Z.-F. & SUN, C.-F. **2014**. CCR7 Regulates Cell Migration and Invasion through JAK2/STAT3 in Metastatic Squamous Cell Carcinoma of the Head and Neck. *BioMed Research International,* 2014**,** 11.

LIU, Q., BERCHNER-PFANNSCHMIDT, U., XF, LLER, U., BRECHT, M., WOTZLAW, C., ACKER, H., JUNGERMANN, K., KIETZMANN, T. & FORSTER, R. E. **2004**. A Fenton Reaction at the Endoplasmic Reticulum Is Involved in the Redox Control of Hypoxia-Inducible Gene Expression. *Proceedings of the National Academy of Sciences of the United States of America,* 101**,** 4302-4307.

LIU, Y., JI, R., LI, J., GU, Q., ZHAO, X., SUN, T., WANG, J., LI, J., DU, Q. & SUN, B. **2010**. Correlation effect of EGFR and CXCR4 and CCR7 chemokine receptors in predicting breast cancer metastasis and prognosis. *Journal of Experimental and Clinical Cancer Research,* 29**,** 16.

LIU, Y. L., YU, J. M., SONG, X. R., WANG, X. W., XING, L. G. & GAO, B. B. **2006**. Regulation of the chemokine receptor CXCR4 and metastasis by hypoxia-inducible factor in non small cell lung cancer cell lines. *Cancer Biology & Therapy,* 5**,** 1320-6.

LOPEZ-BARNEO, J., PARDAL, R. & ORTEGA-SAENZ, P. **2001**. Cellular mechanism of oxygen sensing. *Annual Review of Physiology,* 63**,** 259-87.

LU, L. L., CHEN, X. H., ZHANG, G., LIU, Z. C., WU, N., WANG, H., QI, Y. F., WANG, H. S., CAI, S. H. & DU, J. **2016**. CCL21 Facilitates Chemoresistance and Cancer Stem Cell-Like Properties of Colorectal Cancer Cells through AKT/GSK-3beta/Snail Signals. *Oxidative Medicine and Cellular Longevity,* 2016**,** 5874127.

MA, H., GAO, L., LI, S., QIN, J., CHEN, L., LIU, X., XU, P., WANG, F., XIAO, H., ZHOU, S., GAO, Q., LIU, B., SUN, Y. & LIANG, C. **2015**. CCR7 enhances TGF-β1-induced epithelial-

mesenchymal transition and is associated with lymph node metastasis and poor overall survival in gastric cancer. *Oncotarget,* 6**,** 24348-24360.
MA, J., ZHANG, Q., CHEN, S., FANG, B., YANG, Q., CHEN, C., MIELE, L., SARKAR, F. H., XIA, J. & WANG, Z. **2013**. Mitochondrial Dysfunction Promotes Breast Cancer Cell Migration and Invasion through HIF1α Accumulation via Increased Production of Reactive Oxygen Species. *PloS One,* 8**,** e69485.
MAEKAWA, S., IWASAKI, A., SHIRAKUSA, T., KAWAKAMI, T., YANAGISAWA, J., TANAKA, T., SHIBAGUCHI, H., KINUGASA, T., KUROKI, M. & KUROKI, M. **2008**. Association between the expression of chemokine receptors CCR7 and CXCR3, and lymph node metastatic potential in lung adenocarcinoma. *Oncology Reports,* 19**,** 1461-8.
MAJMUNDAR, A. J., WONG, W. J. & SIMON, M. C. **2010**. Hypoxia-Inducible Factors and the Response to Hypoxic Stress. *Molecular Cell,* 40**,** 294-309.
MASHINO, K. **2002**. Expression of chemokine receptor CCR7 is associated with lymph node metastasis of gastric carcinoma. *Cancer Research,* 62**,** 2937-2941.
MEHLEN, P. & PUISIEUX, A. **2006**. Metastasis: a question of life or death. *Nature Reviews: Cancer,* 6**,** 449-458.
MEHTA, G., HSIAO, A. Y., INGRAM, M., LUKER, G. D. & TAKAYAMA, S. **2012**. Opportunities and challenges for use of tumor spheroids as models to test drug delivery and efficacy. *Journal of Controlled Release,* 164**,** 192-204.
MELLADO, M., RODRÍGUEZ-FRADE, J. M., MAÑES, S. & MARTÍNEZ-A, C. **2001**. CHEMOKINE SIGNALING AND FUNCTIONAL RESPONSES: The Role of Receptor Dimerization and TK Pathway Activation. *Annual Review of Immunology,* 19**,** 397-421.
MITTAL, V. **2004**. Improving the efficiency of RNA interference in mammals. *Nature Reviews: Genetics,* 5**,** 355-365.
MO, M., ZHOU, M., WANG, L., QI, L., ZHOU, K., LIU, L.-F., CHEN, Z. & ZU, X.-B. **2015**. CCL21/CCR7 Enhances the Proliferation, Migration, and Invasion of Human Bladder Cancer T24 Cells. *PloS One,* 10**,** e0119506.
MONTERO, A. J., ESCOBAR, M., LOPES, G., GLÜCK, S. & VOGEL, C. **2012**. Bevacizumab in the Treatment of Metastatic Breast Cancer: Friend or Foe? *Current Oncology Reports,* 14**,** 1-11.
MUELLER, A. & ZLOTNIK, A. 2009. *Methods of inhibiting metastasis*. US patent application.
MULLER, A., HOMEY, B., SOTO, H., GE, N., CATRON, D., BUCHANAN, M. E., MCCLANAHAN, T., MURPHY, E., YUAN, W., WAGNER, S. N., BARRERA, J. L., MOHAR, A., VERASTEGUI, E. & ZLOTNIK, A. **2001**. Involvement of chemokine receptors in breast cancer metastasis. *Nature,* 410**,** 50-6.
MUMPRECHT, V. & DETMAR, M. **2009**. Lymphangiogenesis and cancer metastasis. *Journal of Cellular and Molecular Medicine,* 13**,** 1405-1416.
MURPHY, P. M. **2001**. Chemokines and the Molecular Basis of Cancer Metastasis. *New England Journal of Medicine,* 345**,** 833-835.
MUZ, B., DE LA PUENTE, P., AZAB, F. & AZAB, A. K. **2015**. The role of hypoxia in cancer progression, angiogenesis, metastasis, and resistance to therapy. *Hypoxia,* 3**,** 83-92.
NA, I. K., BUSSE, A., SCHEIBENBOGEN, C., GHADJAR, P., COUPLAND, S. E., LETSCH, A., LODDENKEMPER, C., STROUX, A., BAUER, S., THIEL, E. & KEILHOLZ, U. **2008**. Identification of truncated chemokine receptor 7 in human colorectal cancer unable to localize to the cell surface and unreactive to external ligands. *International Journal of Cancer,* 123**,** 1565-72.
NAGELKERKE, A., BUSSINK, J., MUJCIC, H., WOUTERS, B. G., LEHMANN, S., SWEEP, F. C. G. J. & SPAN, P. N. **2013**. Hypoxia stimulates migration of breast cancer cells via the PERK/ATF4/LAMP3-arm of the unfolded protein response. *Breast Cancer Research : BCR,* 15**,** R2-R2.
NAKATA, B., FUKUNAGA, S., NODA, E., AMANO, R., YAMADA, N. & HIRAKAWA, K. **2008**. Chemokine receptor CCR7 expression correlates with lymph node metastasis in pancreatic cancer. *Oncology,* 74**,** 69-75.
NANDAGOPAL, S., WU, D. & LIN, F. **2011**. Combinatorial Guidance by CCR7 Ligands for T Lymphocytes Migration in Co-Existing Chemokine Fields. *PloS One,* 6**,** e18183.

NARDONE, V., BOTTA, C., CARAGLIA, M., MARTINO, E. C., AMBROSIO, M. R., CARFAGNO, T., TINI, P., SEMERARO, L., MISSO, G., GRIMALDI, A., BOCCELLINO, M., FACCHINI, G., BERRETTA, M., VISCHI, G., ROCCA, B. J., BARONE, A., TASSONE, P., TAGLIAFERRI, P., DEL VECCHIO, M. T., PIRTOLI, L. & CORREALE, P. **2016**. Tumor infiltrating T lymphocytes expressing FoxP3, CCR7 or PD-1 predict the outcome of prostate cancer patients subjected to salvage radiotherapy after biochemical relapse. *Cancer Biology & Therapy***,** 0.

NEPTUNE, E. R. & BOURNE, H. R. **1997**. Receptors induce chemotaxis by releasing the betagamma subunit of Gi, not by activating Gq or Gs. *Proceedings of the National Academy of Sciences,* 94**,** 14489-14494.

NGUYEN, D. X., BOS, P. D. & MASSAGUE, J. **2009**. Metastasis: from dissemination to organ-specific colonization. *Nature Reviews: Cancer,* 9**,** 274-284.

NIMMAGADDA, S. **2012**. Differential expression of chemokine receptors and their role in cancer imaging. *Frontiers in Oncology,* 2.

O'HAYRE, M., SALANGA, C. L., HANDEL, T. M. & ALLEN, S. J. **2008**. Chemokines and cancer: migration, intracellular signalling and intercellular communication in the microenvironment. *Biochemical Journal,* 409**,** 635-49.

OGURA, M., ISHIDA, T., HATAKE, K., TANIWAKI, M., ANDO, K., TOBINAI, K., FUJIMOTO, K., YAMAMOTO, K., MIYAMOTO, T., UIKE, N., TANIMOTO, M., TSUKASAKI, K., ISHIZAWA, K., SUZUMIYA, J., INAGAKI, H., TAMURA, K., AKINAGA, S., TOMONAGA, M. & UEDA, R. **2014**. Multicenter phase II study of mogamulizumab (KW-0761), a defucosylated anti-cc chemokine receptor 4 antibody, in patients with relapsed peripheral T-cell lymphoma and cutaneous T-cell lymphoma. *Journal of Clinical Oncology,* 32**,** 1157-63.

OH, S. W., LEE, Y. M., KIM, S. & CHIN, H. J. **2014**. Cobalt chloride attenuates oxidative stress and inflammation through NF-kappaB inhibition in human renal proximal tubular epithelial cells. 29 Suppl 2**,** S139-45.

OH, Y. S., KIM, H. Y., SONG, I. C., YUN, H. J., JO, D. Y., KIM, S. & LEE, H. J. **2012**. Hypoxia induces CXCR4 expression and biological activity in gastric cancer cells through activation of hypoxia-inducible factor-1alpha. *Oncology Reports,* 28**,** 2239-46.

OLIVEIRA-NETO, H. H., DE SOUZA, P. P., DA SILVA, M. R., MENDONCA, E. F., SILVA, T. A. & BATISTA, A. C. **2013**. The expression of chemokines CCL19, CCL21 and their receptor CCR7 in oral squamous cell carcinoma and its relevance to cervical lymph node metastasis. *Tumour Biology,* 34**,** 65-70.

OTT, T. R., PAHUJA, A., NICKOLLS, S. A., ALLEVA, D. G. & STRUTHERS, R. S. **2004**. Identification of CC chemokine receptor 7 residues important for receptor activation. *Journal of Biological Chemistry,* 279**,** 42383-92.

OZBEN, T. **2007**. Oxidative stress and apoptosis: impact on cancer therapy. *Journal of Pharmaceutical Sciences,* 96**,** 2181-96.

PANIERI, E. & SANTORO, M. M. **2016**. ROS homeostasis and metabolism: a dangerous liason in cancer cells. *Cell Death & Disease,* 7**,** e2253.

PARK, S. Y., HAN, J., KIM, J. B., YANG, M. G., KIM, Y. J., LIM, H. J., AN, S. Y. & KIM, J. H. **2014**. Interleukin-8 is related to poor chemotherapeutic response and tumourigenicity in hepatocellular carcinoma. *European Journal of Cancer,* 50**,** 341-50.

PATHMANATHAN, N. & BALLEINE, R. L. **2013**. Ki67 and proliferation in breast cancer. *Journal of Clinical Pathology,* 66**,** 512-6.

PATRA, B., CHEN, Y. H., PENG, C. C., LIN, S. C., LEE, C. H. & TUNG, Y. C. **2013**. A microfluidic device for uniform-sized cell spheroids formation, culture, harvesting and flow cytometry analysis. *Biomicrofluidics,* 7**,** 54114.

PENG, C., ZHOU, K., AN, S. & YANG, J. **2015**. The effect of CCL19/CCR7 on the proliferation and migration of cell in prostate cancer. *Tumor Biology,* 36**,** 329-335.

PITKIN, L., LUANGDILOK, S., CORBISHLEY, C., WILSON, P. O., DALTON, P., BRAY, D., MADY, S., WILLIAMSON, P., ODUTOYE, T., RHYS EVANS, P., SYRIGOS, K. N., NUTTING, C. M., BARBACHANO, Y., ECCLES, S. & HARRINGTON, K. J. **2007**. Expression of CC chemokine receptor 7 in tonsillar cancer predicts cervical nodal metastasis, systemic relapse and survival. *British Journal of Cancer,* 97**,** 670-7.

POLJSAK, B., SUPUT, D. & MILISAV, I. **2013**. Achieving the balance between ROS and antioxidants: when to use the synthetic antioxidants. *Oxidative Medicine and Cellular Longevity,* 2013**,** 956792.

POLYTARCHOU, C., HATZIAPOSTOLOU, M. & PAPADIMITRIOU, E. **2005**. Hydrogen peroxide stimulates proliferation and migration of human prostate cancer cells through activation of activator protein-1 and up-regulation of the heparin affin regulatory peptide gene. *Journal of Biological Chemistry,* 280**,** 40428-35.

PORCILE, C., BAJETTO, A., BARBIERI, F., BARBERO, S., BONAVIA, R., BIGLIERI, M., PIRANI, P., FLORIO, T. & SCHETTINI, G. **2005**. Stromal cell-derived factor-1alpha (SDF-1alpha/CXCL12) stimulates ovarian cancer cell growth through the EGF receptor transactivation. *Experimental Cell Research,* 308**,** 241-53.

PORE, N. & MAITY, A. **2006**. The chemokine receptor CXCR4: a homing device for hypoxic cancer cells? *Cancer Biology & Therapy,* 5**,** 1563-5.

QU, X., YANG, M. X., KONG, B. H., QI, L., LAM, Q. L., YAN, S., LI, P., ZHANG, M. & LU, L. **2005**. Hypoxia inhibits the migratory capacity of human monocyte-derived dendritic cells. *Immunology and Cell Biology,* 83**,** 668-73.

QUTUB, A. A. & POPEL, A. S. **2008**. Reactive oxygen species regulate hypoxia-inducible factor 1alpha differentially in cancer and ischemia. *Molecular and Cellular Biology,* 28**,** 5106-19.

RAHEJA, L. F., GENETOS, D. C., WONG, A. & YELLOWLEY, C. E. **2011**. Hypoxic regulation of mesenchymal stem cell migration: the role of RhoA and HIF-1alpha. *Cell Biology International,* 35**,** 981-9.

RAMAN, D., SOBOLIK-DELMAIRE, T. & RICHMOND, A. **2011**. Chemokines in health and disease. *Experimental Cell Research,* 317**,** 575-589.

RAN, S., VOLK, L., HALL, K. & FLISTER, M. J. **2010**. Lymphangiogenesis and lymphatic metastasis in breast cancer. *Pathophysiology,* 17**,** 229-51.

RICART, B. G., JOHN, B., LEE, D., HUNTER, C. A. & HAMMER, D. A. **2011**. Dendritic cells distinguish individual chemokine signals through CCR7 and CXCR4. *Journal of Immunology,* 186**,** 53-61.

RICHES, K., MORLEY, M. E., TURNER, N. A., O'REGAN, D. J., BALL, S. G., PEERS, C. & PORTER, K. E. **2009**. Chronic hypoxia inhibits MMP-2 activation and cellular invasion in human cardiac myofibroblasts. *Journal of Molecular and Cellular Cardiology,* 47**,** 391-399.

ROBERTS, A. M., WATSON, I. R., EVANS, A. J., FOSTER, D. A., IRWIN, M. S. & OHH, M. **2009**. SUPPRESSION OF HIF2α RESTORES p53 ACTIVITY VIA HDM2 AND REVERSES CHEMORESISTANCE OF RENAL CARCINOMA CELLS. *Cancer Research,* 69**,** 9056-9064.

ROBINS, K. A. 2006. *Cancer biology,* London, Pearson Prentice Hall.

ROHWER, N., DAME, C., HAUGSTETTER, A., WIEDENMANN, B., DETJEN, K., SCHMITT, C. A. & CRAMER, T. **2010**. Hypoxia-Inducible Factor 1α Determines Gastric Cancer Chemosensitivity via Modulation of p53 and NF-κB. *PloS One,* 5**,** e12038.

ROHWER, N., LOBITZ, S., DASKALOW, K., JÖNS, T., VIETH, M., SCHLAG, P. M., KEMMNER, W., WIEDENMANN, B., CRAMER, T. & HÖCKER, M. **2009**. HIF-1α determines the metastatic potential of gastric cancer cells. *British Journal of Cancer,* 100**,** 772-781.

ROLFO, C., RAEZ, L. E., RUSSO, A., REGUART, N., CAMPELO, R. G., BRONTE, G., PAPADIMITRIOU, K. & SILVESTRIS, F. **2014**. Molecular target therapy for bone metastasis: starting a new era with denosumab, a RANKL inhibitor. *Expert Opinion on Biological Therapy,* 14**,** 15-26.

ROSSI, D. & ZLOTNIK, A. **2000**. The Biology of Chemokines and their Receptors. *Annual Review of Immunology,* 18**,** 217-242.

ROTH, B. L., SHEFFLER, D. J. & KROEZE, W. K. **2004**. Magic shotguns versus magic bullets: selectively non-selective drugs for mood disorders and schizophrenia. *Nature Reviews: Drug Discovery,* 3**,** 353-359.

RUDDON, R. W. 2007. *Cancer biology,* New York, Oxford University Press.

SAMENI, M., DOSESCU, J., YAMADA, K. M., SLOANE, B. F. & CAVALLO-MEDVED, D. **2008**. Functional Live-Cell Imaging Demonstrates that β1-Integrin Promotes Type IV Collagen Degradation by Breast and Prostate Cancer Cells. *Molecular imaging,* 7**,** 199-213.

SANCHO, M., VIEIRA, J. M., CASALOU, C., MESQUITA, M., PEREIRA, T., CAVACO, B. M., DIAS, S. & LEITE, V. **2006**. Expression and function of the chemokine receptor CCR7 in thyroid carcinomas. *Journal of Endocrinology,* 191**,** 229-238.

SANO, D., MATSUMOTO, F., VALDECANAS, D. R., ZHAO, M., MOLKENTINE, D. P., TAKAHASHI, Y., HANNA, E. Y., PAPADIMITRAKOPOULOU, V., HEYMACH, J., MILAS, L. & MYERS, J. N. **2011**. Vandetanib Restores Head and Neck Squamous Cell Carcinoma Cells' Sensitivity to Cisplatin and Radiation *Clinical Cancer Research,* 17**,** 1815.

SARVAIYA, P. J., GUO, D., ULASOV, I., GABIKIAN, P. & LESNIAK, M. S. **2013**. Chemokines in tumor progression and metastasis. *Oncotarget,* 4**,** 2171-2185.

SASAKI, K., NATSUGOE, S., ISHIGAMI, S., MATSUMOTO, M., OKUMURA, H., SETOYAMA, T., UCHIKADO, Y., KITA, Y., TAMOTSU, K., SAKURAI, T., OWAKI, T. & AIKOU, T. **2008**. Expression of CXCL12 and its receptor CXCR4 correlates with lymph node metastasis in submucosal esophageal cancer. *Journal of Surgical Oncology,* 97**,** 433-8.

SCAGLIOTTI, G. V., HIRSH, V., SIENA, S., HENRY, D. H., WOLL, P. J., MANEGOLD, C., SOLAL-CELIGNY, P., RODRIGUEZ, G., KRZAKOWSKI, M., MEHTA, N. D., LIPTON, L., GARCIA-SAENZ, J. A., PEREIRA, J. R., PRABHASH, K., CIULEANU, T. E., KANAREV, V., WANG, H., BALAKUMARAN, A. & JACOBS, I. **2012**. Overall survival improvement in patients with lung cancer and bone metastases treated with denosumab versus zoledronic acid: subgroup analysis from a randomized phase 3 study. *Journal of Thoracic Oncology,* 7**,** 1823-9.

SCARINGI, C., MINNITI, G., CAPORELLO, P. & ENRICI, R. M. **2012**. Integrin inhibitor cilengitide for the treatment of glioblastoma: a brief overview of current clinical results. *Anticancer Research,* 32**,** 4213-23.

SCHAFER, M. & WERNER, S. **2008**. Cancer as an overhealing wound: an old hypothesis revisited. *Nature Reviews: Molecular Cell Biology,* 9**,** 628-638.

SCHIOPPA, T., URANCHIMEG, B., SACCANI, A., BISWAS, S. K., DONI, A., RAPISARDA, A., BERNASCONI, S., SACCANI, S., NEBULONI, M., VAGO, L., MANTOVANI, A., MELILLO, G. & SICA, A. **2003**. Regulation of the Chemokine Receptor CXCR4 by Hypoxia. *The Journal of Experimental Medicine,* 198**,** 1391-1402.

SCHNEIDER, C. A., RASBAND, W. S. & ELICEIRI, K. W. **2012**. NIH Image to ImageJ: 25 years of image analysis. *Nat Meth,* 9**,** 671-675.

SCHOLTEN, D. J., CANALS, M., MAUSSANG, D., ROUMEN, L., SMIT, M. J., WIJTMANS, M., DE GRAAF, C., VISCHER, H. F. & LEURS, R. **2012**. Pharmacological modulation of chemokine receptor function. *British Journal of Pharmacology,* 165**,** 1617-1643.

SCHOLZEN, T. & GERDES, J. **2000**. The Ki-67 protein: from the known and the unknown. *Journal of Cellular Physiology,* 182**,** 311-22.

SCHROEDER, A., HELLER, D. A., WINSLOW, M. M., DAHLMAN, J. E., PRATT, G. W., LANGER, R., JACKS, T. & ANDERSON, D. G. **2012**. Treating metastatic cancer with nanotechnology. *Nature Reviews: Cancer,* 12**,** 39-50.

SEMENZA, G. L. **2001**. Hypoxia-inducible factor 1: oxygen homeostasis and disease pathophysiology. *Trends in Molecular Medicine,* 7**,** 345-50.

SEMENZA, G. L. **2012**. Hypoxia-inducible factors in physiology and medicine. *Cell,* 148**,** 399-408.

SEMENZA, G. L. **2013**. HIF-1 mediates metabolic responses to intratumoral hypoxia and oncogenic mutations. *The Journal of Clinical Investigation,* 123**,** 3664-3671.

SHANG, Z. J., LIU, K. & SHAO, Z. **2009**. Expression of chemokine receptor CCR7 is associated with cervical lymph node metastasis of oral squamous cell carcinoma. *Oral Oncology,* 45**,** 480-5.

SHANNON, L. A., CALLOWAY, P. A., WELCH, T. P. & VINES, C. M. **2010**. CCR7/CCL21 Migration on Fibronectin Is Mediated by Phospholipase Cγ1 and ERK1/2 in Primary T Lymphocytes. *Journal of Biological Chemistry,* 285**,** 38781-38787.

SHI, M., CHEN, D., YANG, D. & LIU, X.-Y. **2015**. CCL21-CCR7 promotes the lymph node metastasis of esophageal squamous cell carcinoma by up-regulating MUC1. *Journal of Experimental and Clinical Cancer Research,* 34**,** 149.

SHIELDS, J. D., KOURTIS, I. C., TOMEI, A. A., ROBERTS, J. M. & SWARTZ, M. A. **2010**. Induction of lymphoidlike stroma and immune escape by tumors that express the chemokine CCL21. *Science,* 328**,** 749-752.

SHIN, D. H., DIER, U., MELENDEZ, J. A. & HEMPEL, N. **2015**. Regulation of MMP-1 expression in response to hypoxia is dependent on the intracellular redox status of metastatic bladder cancer cells. *Biochimica et Biophysica Acta (BBA) - Molecular Basis of Disease,* 1852**,** 2593-2602.

SHUYI, Y., JUPING, D., ZHIQUN, Z., QIONG, P., WUYANG, J., TING, L., XIAOWEN, H., LIU, X. & YUXIANG, C. **2008**. A critical role of CCR7 in invasiveness and metastasis of SW620 colon cancer cell in vitro and in vivo. *Cancer Biology & Therapy,* 7**,** 1037-1043.

SIEGEL, R. L., MILLER, K. D. & JEMAL, A. **2017**. Cancer Statistics, 2017. *CA: A Cancer Journal for Clinicians,* 67**,** 7-30.

SIPOS, B., KOJIMA, M., TIEMANN, K., KLAPPER, W., KRUSE, M. L., KALTHOFF, H., SCHNIEWIND, B., TEPEL, J., WEICH, H., KERJASCHKI, D. & KLOPPEL, G. **2005**. Lymphatic spread of ductal pancreatic adenocarcinoma is independent of lymphangiogenesis. *Journal of Pathology,* 207**,** 301-12.

SLETTENAAR, V. I. & WILSON, J. L. **2006**. The chemokine network: a target in cancer biology? *Adv Drug Deliv Rev,* 58**,** 962-74.

SMITH, M. R., SAAD, F., COLEMAN, R., SHORE, N., FIZAZI, K., TOMBAL, B., MILLER, K., SIEBER, P., KARSH, L., DAMIAO, R., TAMMELA, T. L., EGERDIE, B., VAN POPPEL, H., CHIN, J., MOROTE, J., GOMEZ-VEIGA, F., BORKOWSKI, T., YE, Z., KUPIC, A., DANSEY, R. & GOESSL, C. **2012**. Denosumab and bone-metastasis-free survival in men with castration-resistant prostate cancer: results of a phase 3, randomised, placebo-controlled trial. *Lancet,* 379**,** 39-46.

SOZZANI, S., BOSISIO, D., MANTOVANI, A. & GHEZZI, P. **2005**. Linking stress, oxidation and the chemokine system. *European Journal of Immunology,* 35**,** 3095-8.

SPERVESLAGE, J., FRANK, S., HENEWEER, C., EGBERTS, J., SCHNIEWIND, B., BUCHHOLZ, M., BERGMANN, F., GIESE, N., MUNDING, J., HAHN, S. A., KALTHOFF, H., KLOPPEL, G. & SIPOS, B. **2012**. Lack of CCR7 expression is rate limiting for lymphatic spread of pancreatic ductal adenocarcinoma. *International Journal of Cancer,* 131**,** E371-81.

STEEG, P. S. **2016**. Targeting metastasis. *Nature Reviews: Cancer,* 16**,** 201-218.

STEEN, A., LARSEN, O., THIELE, S. & ROSENKILDE, M. M. **2014**. Biased and G protein-independent signaling of chemokinereceptors. *Frontiers in Immunology,* 5.

STOCK, A. M., TROOST, G., NIGGEMANN, B., ZANKER, K. S. & ENTSCHLADEN, F. **2013**. Targets for anti-metastatic drug development. *Current Pharmaceutical Design,* 19**,** 5127-34.

STRINGER, S. E., FORSTER, M. J., MULLOY, B., BISHOP, C. R., GRAHAM, G. J. & GALLAGHER, J. T. **2002**. Characterization of the binding site on heparan sulfate for macrophage inflammatory protein 1alpha. *Blood,* 100**,** 1543-50.

SU, M. L., CHANG, T. M., CHIANG, C. H., CHANG, H. C., HOU, M. F., LI, W. S. & HUNG, W. C. **2014**. Inhibition of chemokine (C-C motif) receptor 7 sialylation suppresses CCL19-stimulated proliferation, invasion and anti-anoikis. *PloS One,* 9**,** e98823.

SULLIVAN, L. B. & CHANDEL, N. S. **2014**. Mitochondrial reactive oxygen species and cancer. *Cancer & Metabolism,* 2**,** 17.

SUN, J. S., ZHANG, X. L., YANG, Y. J., NIE, Z. G. & ZHANG, Y. **2015**. Hypoxia promotes C-X-C chemokine receptor type 4 expression through microRNA-150 in pancreatic cancer cells. *Oncology Letters,* 10**,** 835-840.

SUN, Y.-X., WANG, J., SHELBURNE, C. E., LOPATIN, D. E., CHINNAIYAN, A. M., RUBIN, M. A., PIENTA, K. J. & TAICHMAN, R. S. **2003**. Expression of CXCR4 and CXCL12 (SDF-1) in human prostate cancers (PCa) in vivo. *Journal of Cellular Biochemistry,* 89**,** 462-473.

TAFANI, M., SANSONE, L., LIMANA, F., ARCANGELI, T., DE SANTIS, E., POLESE, M., FINI, M. & RUSSO, M. A. **2016**. The Interplay of Reactive Oxygen Species, Hypoxia, Inflammation, and Sirtuins in Cancer Initiation and Progression. *Oxidative Medicine and Cellular Longevity,* 2016**,** 18.

TAICHMAN, R. S., COOPER, C., KELLER, E. T., PIENTA, K. J., TAICHMAN, N. S. & MCCAULEY, L. K. **2002**. Use of the Stromal Cell-derived Factor-1/CXCR4 Pathway in Prostate Cancer Metastasis to Bone. *Cancer Research,* 62**,** 1832.

TAKANAMI, I. **2003**. Overexpression of CCR7 mRNA in nonsmall cell lung cancer: correlation with lymph node metastasis. *International Journal of Cancer,* 105**,** 186-189.

TAKEKOSHI, T., FANG, L., PARAGH, G. & HWANG, S. T. **2012**. CCR7-expressing B16 melanoma cells downregulate interferon-[gamma]-mediated inflammation and increase lymphangiogenesis in the tumor microenvironment. *Oncogenesis,* 1**,** e9.

TAN, K. X., DANQUAH, M. K., SIDHU, A., ONGKUDON, C. M. & LAU, S. Y. **2017**. Towards targeted cancer therapy: Aptamer or oncolytic virus? *European Journal of Pharmaceutical Sciences,* 96**,** 8-19.

TSAI, Y. P. & WU, K. J. **2012**. Hypoxia-regulated target genes implicated in tumor metastasis. *Journal of Biomedical Science,* 19**,** 102.

TURNER, L., SCOTTON, C., NEGUS, R. & BALKWILL, F. **1999**. Hypoxia inhibits macrophage migration. *European Journal of Immunology,* 29**,** 2280-7.

TUTUNEA-FATAN, E., MAJUMDER, M., XIN, X. & LALA, P. K. **2015**. The role of CCL21/CCR7 chemokine axis in breast cancer-induced lymphangiogenesis. *Molecular Cancer,* 14.

UEDA, M., SHIMADA, T., GOTO, Y., TEI, K., NAKAI, S., HISA, Y. & KANNAGI, R. **2010**. Expression of CC-chemokine receptor 7 (CCR7) and CXC-chemokine receptor 4 (CXCR4) in head and neck squamous cell carcinoma. *Auris, Nasus, Larynx,* 37**,** 488-95.

ULVMAR, M. H., HUB, E. & ROT, A. **2011**. Atypical chemokine receptors. *Experimental Cell Research,* 317**,** 556-68.

VARIA, M. A., CALKINS-ADAMS, D. P., RINKER, L. H., KENNEDY, A. S., NOVOTNY, D. B., FOWLER, W. C. & RALEIGH, J. A. **1998**. Pimonidazole: A Novel Hypoxia Marker for Complementary Study of Tumor Hypoxia and Cell Proliferation in Cervical Carcinoma. *Gynecologic Oncology,* 71**,** 270-277.

VAUGHAN, M. M., TOTH, K., CHINTALA, S. & RUSTUM, Y. M. **2010**. Double Immunohistochemical Staining Method for HIF-1α and its Regulators PHD2 and PHD3 in Formalin Fixed Paraffin Embedded Tissues. *Applied immunohistochemistry & molecular morphology : AIMM / official publication of the Society for Applied Immunohistochemistry,* 18**,** 375-381.

VAUX, E. C., METZEN, E., YEATES, K. M. & RATCLIFFE, P. J. **2001**. Regulation of hypoxia-inducible factor is preserved in the absence of a functioning mitochondrial respiratory chain. *Blood,* 98**,** 296.

VELA, M., ARIS, M., LLORENTE, M., GARCIA-SANZ, J. A. & KREMER, L. **2015**. Chemokine Receptor-Specific Antibodies in Cancer Immunotherapy: Achievements and Challenges. *Frontiers in Immunology,* 6.

VERMORKEN, J. B. & SPECENIER, P. **2010**. Optimal treatment for recurrent/metastatic head and neck cancer. *Annals of Oncology,* 21 Suppl 7**,** vii252-61.

VILLA, P., TRIULZI, S., CAVALIERI, B., DI BITONDO, R., BERTINI, R., BARBERA, S., BIGINI, P., MENNINI, T., GELOSA, P., TREMOLI, E., SIRONI, L. & GHEZZI, P. **2007**. The interleukin-8 (IL-8/CXCL8) receptor inhibitor reparixin improves neurological deficits and reduces long-term inflammation in permanent and transient cerebral ischemia in rats. *Molecular Medicine,* 13**,** 125-33.

VILLABLANCA, E. J., RACCOSTA, L., ZHOU, D., FONTANA, R., MAGGIONI, D., NEGRO, A., SANVITO, F., PONZONI, M., VALENTINIS, B., BREGNI, M., PRINETTI, A., STEFFENSEN, K. R., SONNINO, S., GUSTAFSSON, J.-A., DOGLIONI, C., BORDIGNON, C., TRAVERSARI, C. & RUSSO, V. **2010**. Tumor-mediated liver X receptor-[alpha] activation inhibits CC chemokine receptor-7 expression on dendritic cells and dampens antitumor responses. *Nature Medicine,* 16**,** 98-105.

VINADER, V. & AFARINKIA, K. **2012**. A beginner's guide to chemokines. *Future Medicinal Chemistry,* 4**,** 845-852.

VIOLA, A. & LUSTER, A. D. **2008**. Chemokines and Their Receptors: Drug Targets in Immunity and Inflammation. *Annual Review of Pharmacology and Toxicology,* 48**,** 171-197.

VIVES, R. R., CRUBLET, E., ANDRIEU, J. P., GAGNON, J., ROUSSELLE, P. & LORTAT-JACOB, H. **2004**. A novel strategy for defining critical amino acid residues involved in protein/glycosaminoglycan interactions. *Journal of Biological Chemistry,* 279**,** 54327-33.

VOKES, E. E. & ATHANASIADIS, I. **1996**. Chemotherapy of squamous cell carcinoma of head and neck: the future is now. *Annals of Oncology,* 7**,** 15-29.

WANG, J., SEETHALA, R. R., ZHANG, Q., GOODING, W., VAN WAES, C., HASEGAWA, H. & FERRIS, R. L. **2008**. Autocrine and paracrine chemokine receptor 7 activation in head and neck cancer: implications for therapy. *Journal of the National Cancer Institute,* 100**,** 502-12.

WANG, J., XI, L., HUNT, J. L., GOODING, W., WHITESIDE, T. L., CHEN, Z., GODFREY, T. E. & FERRIS, R. L. **2004**. Expression pattern of chemokine receptor 6 (CCR6) and CCR7 in squamous cell carcinoma of the head and neck identifies a novel metastatic phenotype. *Cancer Research,* 64**,** 1861-6.

WANG, J., ZHANG, X., THOMAS, S. M., GRANDIS, J. R., WELLS, A., CHEN, Z. G. & FERRIS, R. L. **2005**. Chemokine receptor 7 activates phosphoinositide-3 kinase-mediated invasive and prosurvival pathways in head and neck cancer cells independent of EGFR. *Oncogene,* 24**,** 5897-904.

WANG, R., ZHOU, S. & LI, S. **2011**. Cancer therapeutic agents targeting hypoxia-inducible factor-1. *Current Medicinal Chemistry,* 18**,** 3168-89.

WEIDLE, U. H., BIRZELE, F., KOLLMORGEN, G. & RUGER, R. **2016**. Molecular Mechanisms of Bone Metastasis. *Cancer Genomics & Proteomics,* 13**,** 1-12.

WEK, R. C. & STASCHKE, K. A. **2010**. How do tumours adapt to nutrient stress? *The EMBOJournal,* 29**,** 1946-1947

WELLS, T. N., POWER, C. A., SHAW, J. P. & PROUDFOOT, A. E. **2006**. Chemokine blockers--therapeutics in the making? *Trends in Pharmacological Sciences,* 27**,** 41-7.

WENDT, M. K., COOPER, A. N. & DWINELL, M. B. **2008**. Epigenetic silencing of CXCL12 increases the metastatic potential of mammary carcinoma cells. *Oncogene,* 27**,** 1461-71.

WENDT, M. K., JOHANESEN, P. A., KANG-DECKER, N., BINION, D. G., SHAH, V. & DWINELL, M. B. **2006**. Silencing of epithelial CXCL12 expression by DNA hypermethylation promotes colonic carcinoma metastasis. *Oncogene,* 25**,** 4986-4997.

WERMUTH, C. G. **2004**. Multitargeted drugs: the end of the 'one-target-one-disease' philosophy? *Drug Discovery Today,* 9**,** 826-827.

WHO. 2017 World health organization. *cancer* [Online]. [Accessed 2017].

WHO. 2014 World health organization. *cancer* [Online]. [Accessed 2017].

WICHMANN, G., CEDRA, S., SCHLEGEL, D., KOLB, M., WIEGAND, S., BOEHM, A., HOFER, M. & DIETZ, A. **2017**. Cilengitide and Cetuximab Reduce Cytokine Production and Colony Formation of Head and Neck Squamous Cell Carcinoma Cells Ex Vivo. *Anticancer Research,* 37**,** 521-527.

WIGERUP, C., PAHLMAN, S. & BEXELL, D. **2016**. Therapeutic targeting of hypoxia and hypoxia-inducible factors in cancer. *Pharmacology & Therapeutics,* 164**,** 152-69.

WILEY, H. E., GONZALEZ, E. B., MAKI, W., WU, M. T. & HWANG, S. T. **2001**. Expression of CC chemokine receptor-7 and regional lymph node metastasis of B16 murine melanoma. *Journal of the National Cancer Institute,* 93**,** 1638-43.

WILSON, J. L., BURCHELL, J. & GRIMSHAW, M. J. **2006**. Endothelins induce CCR7 expression by breast tumor cells via endothelin receptor A and hypoxia-inducible factor-1. *Cancer Research,* 66**,** 11802-7.

WILSON, W. R. & HAY, M. P. **2011**. Targeting hypoxia in cancer therapy. *Nature Reviews: Cancer,* 11**,** 393-410.

WORBS, T. & FÖRSTER, R. **2007**. A key role for CCR7 in establishing central and peripheral tolerance. *Trends in Immunology,* 28**,** 274-280.

WU, D. & YOTNDA, P. **2011**. Induction and Testing of Hypoxia in Cell Culture. *J Vis Exp***,** 2899.

WU, X., LEE, V. C., CHEVALIER, E. & HWANG, S. T. **2009**. Chemokine receptors as targets for cancer therapy. *Current Pharmaceutical Design,* 15**,** 742-57.

XIA, X., LIU, K., ZHANG, H. & SHANG, Z. **2014**. Correlation between CCR7 expression and lymph node metastatic potential of human tongue carcinoma. *Oral Diseases*.

XIAO, Z., LUO, G., LIU, C., WU, C., LIU, L., LIU, Z., NI, Q., LONG, J. & YU, X. **2014**. Molecular Mechanism Underlying Lymphatic Metastasis in Pancreatic Cancer. *BioMed Research International,* 2014**,** 15.

XU, G. G., GUO, J. & WU, Y. **2014**. Chemokine Receptor CCR5 Antagonist Maraviroc: Medicinal Chemistry and Clinical Applications. *Current Topics in Medicinal Chemistry,* 14**,** 1504-14.

XU, Y., LIU, L., QIU, X., JIANG, L., HUANG, B., LI, H., LI, Z., LUO, W. & WANG, E. **2011**. CCL21/CCR7 Promotes G2/M Phase Progression via the ERK Pathway in Human Non-Small Cell Lung Cancer Cells. *PloS One,* 6**,** e21119.

XU, Y., LIU, L., QIU, X., LIU, Z., LI, H., LI, Z., LUO, W. & WANG, E. **2012**. CCL21/CCR7 Prevents Apoptosis via the ERK Pathway in Human Non-Small Cell Lung Cancer Cells. *PloS One,* 7**,** e33262.

YAGUCHI, T., SUMIMOTO, H., KUDO-SAITO, C., TSUKAMOTO, N., UEDA, R., IWATA-KAJIHARA, T., NISHIO, H., KAWAMURA, N. & KAWAKAMI, Y. **2011**. The mechanisms of cancer immunoescape and development of overcoming strategies. *International Journal of Hematology,* 93**,** 294-300.

YE, Q., YAN, Z., LIAO, X., LI, Y., YANG, J. & SUN, J. **2011**. MUC1 induces metastasis in esophageal squamous cell carcinoma by upregulating matrix metalloproteinase 13. *Laboratory Investigation,* 91.

YOSHIDA, R., NAGIRA, M., KITAURA, M., IMAGAWA, N., IMAI, T. & YOSHIE, O. **1998**. Secondary lymphoid-tissue chemokine is a functional ligand for the CC chemokine receptor CCR7. *Journal of Biological Chemistry,* 273**,** 7118-22.

ZABLOCKA, A. & JANUSZ, M. **2008**. [The two faces of reactive oxygen species]. *Postepy Hig Med Dosw (Online),* 62**,** 118-24.

ZHANG, H., WU, H., GUAN, J., WANG, L., REN, X., SHI, X., LIANG, Z. & LIU, T. **2015**. Paracrine SDF-1alpha signaling mediates the effects of PSCs on GEM chemoresistance through an IL-6 autocrine loop in pancreatic cancer cells. *Oncotarget,* 6**,** 3085-97.

ZHANG, L., WANG, D., LI, Y., LIU, Y., XIE, X., WU, Y., ZHOU, Y., REN, J., ZHANG, J., ZHU, H. & SU, Z. **2016**. CCL21/CCR7 Axis Contributed to CD133(+) Pancreatic Cancer Stem-Like Cell Metastasis via EMT and Erk/NF-κB Pathway. *PLoS One,* 11**,** e0158529.

ZHAO, B., CUI, K., WANG, C. L., WANG, A. L., ZHANG, B., ZHOU, W. Y., ZHAO, W. H. & LI, S. **2011**. The chemotactic interaction between CCL21 and its receptor, CCR7, facilitates the progression of pancreatic cancer via induction of angiogenesis and lymphangiogenesis. *J Hepatobiliary Pancreat Sci*.

ZHAO, W., DARMANIN, S., FU, Q., CHEN, J., CUI, H., WANG, J., OKADA, F., HAMADA, J., HATTORI, Y., KONDO, T., HAMURO, J., ASAKA, M. & KOBAYASHI, M. **2005**. Hypoxia suppresses the production of matrix metalloproteinases and the migration of human monocyte-derived dendritic cells. *European Journal of Immunology,* 35**,** 3468-77.

ZHOU, S., SHEN, Z., WANG, Y., MA, H., XU, S., QIN, J., CHEN, L., TAO, H., ZHEN, Z., CHEN, G., ZHANG, Z., LI, R., XIAO, H., ZHONG, C., YANG, Y. & LIANG, C. **2013**. CCR7 expression and intratumoral FOXP3+ regulatory T cells are correlated with overall survival and lymph node metastasis in gastric cancer. *PloS One,* 8**,** e74430.

ZIEGLER, E., OBERBARNSCHEIDT, M., BULFONE-PAUS, S., FORSTER, R., KUNZENDORF, U. & KRAUTWALD, S. **2007**. CCR7 signaling inhibits T cell proliferation. *Journal of Immunology,* 179**,** 6485-93.

ZLOTNIK, A., BURKHARDT, A. M. & HOMEY, B. **2011**. Homeostatic chemokine receptors and organ-specific metastasis. *Nature Reviews: Immunology,* 11**,** 597-606.

Appendix:

Appendix I: Media used for each cell line.

Five types of media (Sigma) were used for growing cell:

- RPMI: Roswell Park Memorial Institute
- DMEM: Dulbecco's Modified Eagle Medium
- DMEM- F12: Dulbecco's Modified Eagle Medium: Nutrient Mixture F-12
- McCoy's 5A
- MEME: Minimum Essential Medium Eagle

Glutamine and sodium pyruvate were not added to media if incomplete media was originally supplemented.

Cell line	Media incomplete	Additives to complete media
PC-3	RPMI	FBS, glutamine, sodium pyruvate
DU-145	RPMI	FBS, glutamine, sodium pyruvate
U-87 MG	RPMI	FBS, glutamine, sodium pyruvate
PANC-1	DMEM	FBS, glutamine, sodium pyruvate
DLD-1	RPMI	FBS, glutamine, sodium pyruvate
SW480	RPMI	FBS, glutamine, sodium pyruvate
MCF-7	RPMI	FBS, glutamine, sodium pyruvate
MDA-231	RPMI	FBS, glutamine, sodium pyruvate
COLO 205	RPMI	FBS, glutamine, sodium pyruvate
OSC-19	RPMI	FBS, glutamine, sodium pyruvate
FaDu	MEME	FBS, glutamine, sodium pyruvate, non-essential amino acids
Detroit-256	MEME	FBS, glutamine, sodium pyruvate, non-essential amino acid
A-253	McCoy’s 5A	FBS, glutamine, sodium pyruvate
SCC-4	DMEM-F12	FBS, hydrocortisone,, sodium pyruvate

Appendix II: Preparation of MTT stock solution.

3-(4,5-dimethylthiazol-2-yl)-2,5-diphenyltetrazolium bromide (MTT; 5

mg/ml) was prepared by dissolving MTT powder (sigma) in distilled water, which was then passed through 0.2 µm sterile syringe filter (corning incorporated). The solution was covered with aluminum paper to protect it from light and kept at 4ºC until used for a period of 4 weeks.

Appendix III: Preparation of Methylcellulose.

The preparation of methylcellulose solution is very important for obtaining well-defined rounded spheroids. Methylcellulose is used to enhance cell matrix assembly. Otherwise, several small spheroids or unrounded cell aggregates will be formed in each drop. Methylcellulose (6 g) was autoclaved in a 500ml flask containing a magnetic stirrer. The autoclaved methylcellulose is then mixed in preheated 250 ml 60°C medium for 30 min. Then, another 250 ml medium was added and stirred for another 30 min at R.T. The methylcellulose solution was left for 1-2 h at 4°C to ensure complete solution. The 500 ml of methylcellulose solution was then centrifuged (5000 g, 2 h, R.T.). The clear highly viscous supernatant was then taken and kept at 4°C.

Appendix IV: Morphology of 2D cultured, spheroid forming ability of head and neck cell lines and growth curves.

Cell line	Monolayer	Spheroid formation
OSC-19	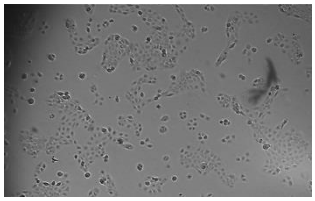	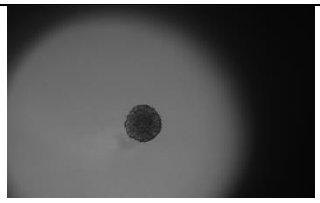
SCC-4	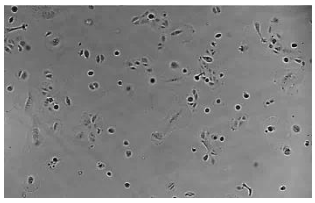	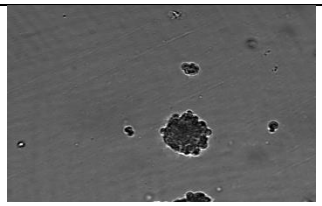
FaDu	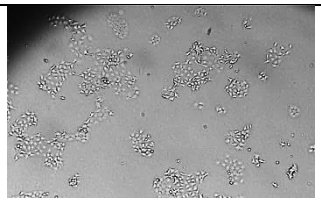	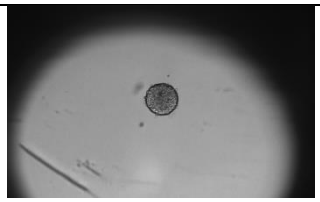
Detroit 256	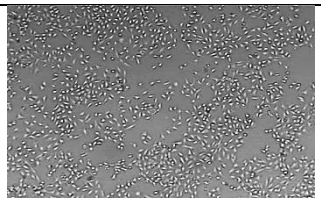	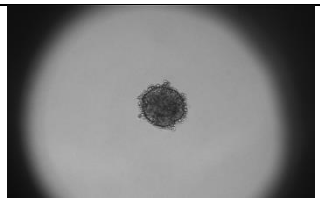
A-253	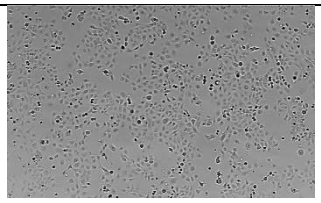	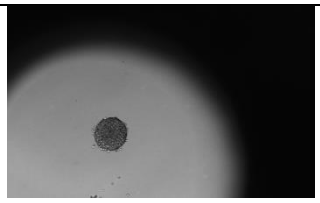

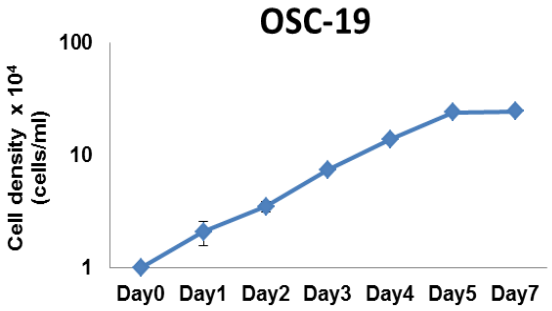
OSC-19
Cell density x 10⁴ (cells/ml)
100
10
1
Day0 Day1 Day2 Day3 Day4 Day5 Day7

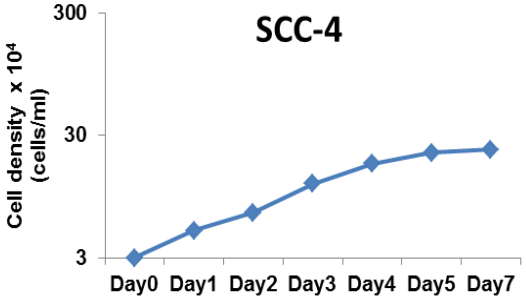
SCC-4
Cell density x 10⁴ (cells/ml)
300
30
3
Day0 Day1 Day2 Day3 Day4 Day5 Day7

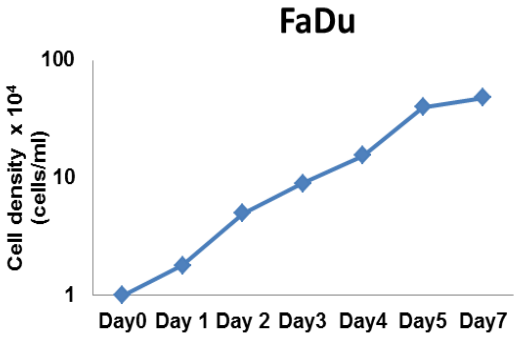
FaDu
Cell density x 10⁴ (cells/ml)
100
10
1
Day0 Day 1 Day 2 Day3 Day4 Day5 Day7

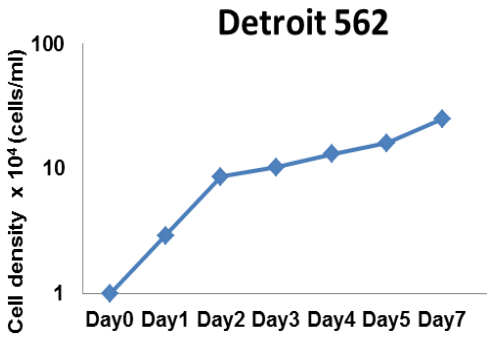
Detroit 562
Cell density x 10⁴ (cells/ml)
100
10
1
Day0 Day1 Day2 Day3 Day4 Day5 Day7

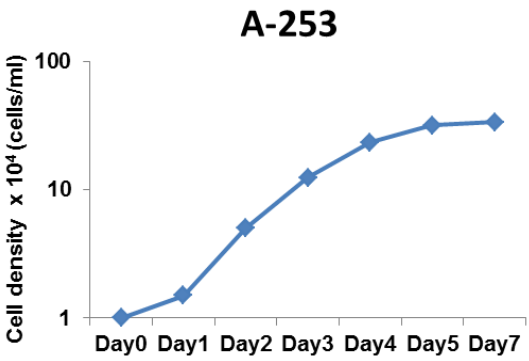
A-253
Cell density x 10⁴ (cells/ml)
100
10
1
Day0 Day1 Day2 Day3 Day4 Day5 Day7

Appendix V: Haematoxylin and Eosin Staining.

Sections were de-paraffinised with xylene (2 × 5 min) and 50% xylene/ethanol (1 × 5 min) rehydrated using 100% ethanol (1 × 5 min) 90% ethanol (1 × 2 min) and 70% ethanol (1 × 2 min). Later, sections were stained with Harris' haematoxylin (Sigma) for 10 min and then washed with running water for 5 min. The excess stain was removed from the section by acid alcohol (0.5% HCl in 70% ethanol) by immersing in 5s. This will help to differentiate the cytoplasm from nucleus. Next, Slides were washed with running water for 5 min and immersing in Scott's Tap Water for 2 min to colour development Sections were counterstained in Eosin for 1 min before a final wash in running tap water. Finally, the sections were dehydrated using 100%, 90% and 70% ethanol each for (1 x 1 min, 1 x 3 min), 50% xylene/ethanol (1 × 3 min), xylene (1 × 3 min, 1 × 5 min) and mounted using diphenylxylene.

PANC-1	U-87 MG
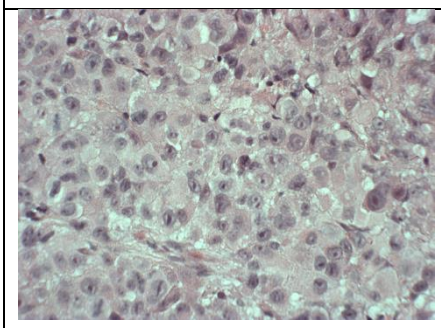	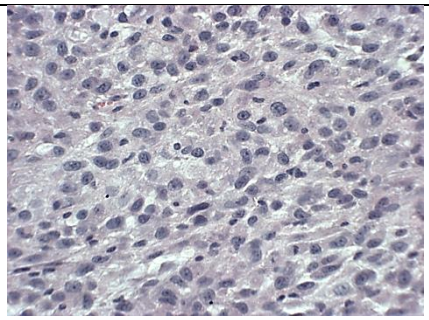
DU-145	**PC-3**
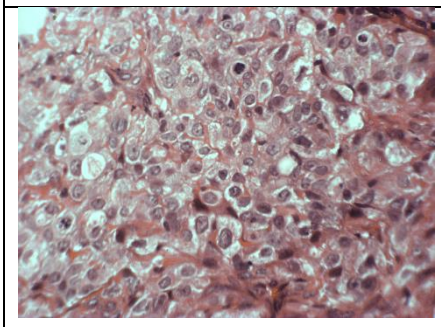	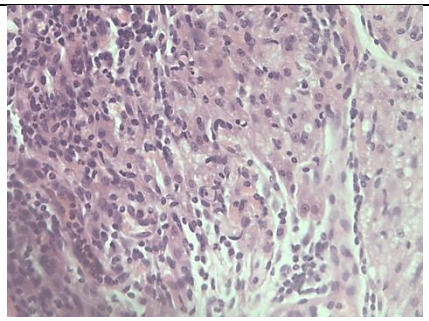
MDA-MB- 231	**MCF-7**
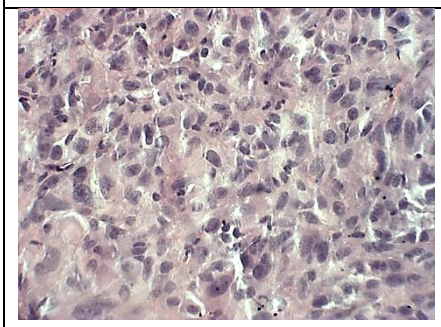	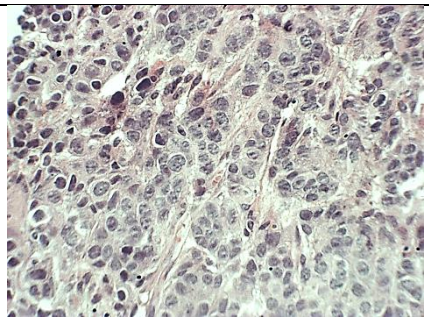
FaDu	**OSC-19**
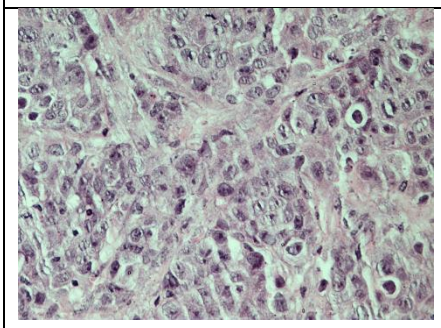	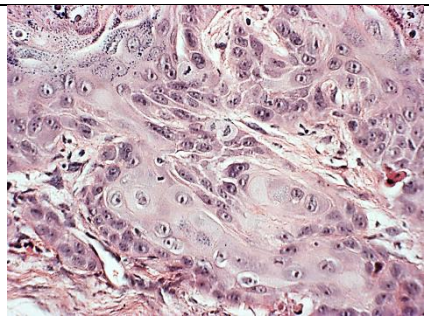

Detroit 562	A-253
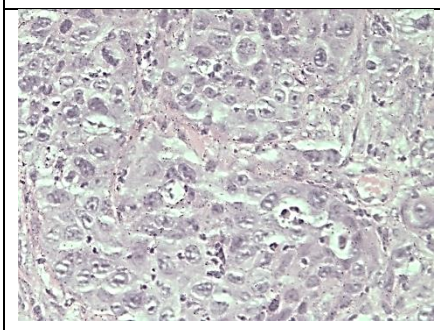	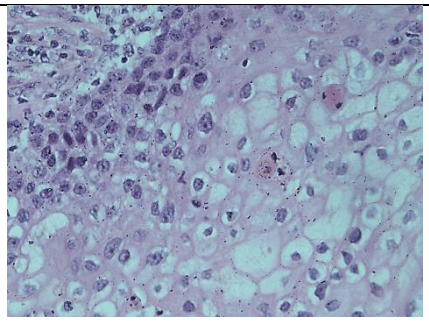
DLD-1	**HT-29**
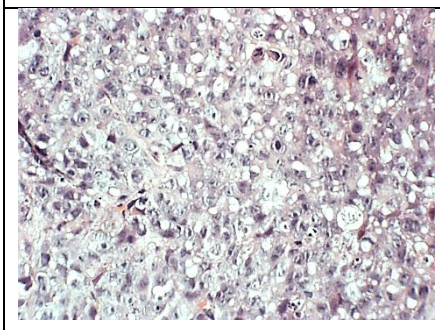	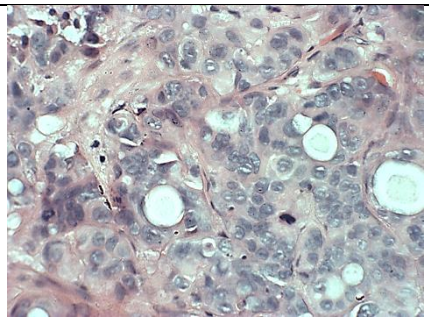
COLO-205	
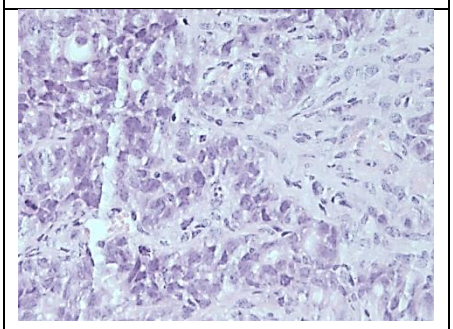	

Appendix VI: Agarose preparation and 96 well plate coating

1.5 g of agarose (Sigma) was added to 100 ml of PBS, stirred on a hot plate under sterile conditions to avoid clumping. The solution was brought to its boiling point to ensure that the agarose is completely dissolved. Then was allowed to cool to 50-55°C, where it was still in its liquid state. Next 50 µl of this solution were added to 96 flat bottom 96 well plates. Agarose was solidified and cooled down to R.T in 20 min to create a concave surface. Plates were kept at 4°C until the spheroid seeding day. Plates were taken out and incubated for 5 min in humidified atmosphere with 5% CO_2 in air at 37°C before adding the cell suspension.

Appendix VII: Characteristics of microarrays clinical sample

position	sex	age	organ	pathology	grade	stage	tnm	type
A1	F	61	Oral cavity	Squamous cell carcinoma of palate	1	I	T1N0M0	Malignant
A2	M	61	Lip	Squamous cell carcinoma of lower lip	1	I	T1N0M0	Malignant
A3	M	77	Lip	Squamous cell carcinoma of lower lip	1	I	T1N0M0	Malignant
A4	F	75	Oral cavity	Squamous cell carcinoma of upper jaw	1	I	T1N0M0	Malignant
A5	M	67	Oral cavity	Squamous cell carcinoma of right palate	1	II	T2N0M0	Malignant
A6	M	50	Tongue	Squamous cell carcinoma of root of tongue	1	III	T3N1M0	Malignant
A7	M	66	Pharynx	Squamous cell carcinoma of pharynx	1	IVA	T3N2M0	Malignant
A8	M	49	Gingiva	Squamous cell carcinoma of right gingiva	1	IVA	T4N0M0	Malignant

A9	M	55	Pharynx	Squamous cell carcinoma of epiglottis	1	IVA	T4N0M0	Malignant
A10	M	57	Pharynx	Squamous cell carcinoma of oropharynx	1	IV	T4N0M0	Malignant
B1	M	74	Nose	Squamous cell carcinoma of root of nose	2	II	T2N0M0	Malignant
B2	M	90	Cheek	Squamous cell carcinoma of cheek	-	II	T2N0M0	Malignant
B3	M	72	Larynx	Squamous cell carcinoma of larynx	1	II	T2N0M0	Malignant
B4	F	61	Oral cavity	Squamous cell carcinoma of right mandible	1	II	T2N0M0	Malignant
B5	M	50	Larynx	Squamous cell carcinoma of larynx	1	III	T2N1M0	Malignant
B6	M	67	Larynx	Squamous cell carcinoma of larynx	2	III	T3N1M0	Malignant
B7	M	58	Larynx	Squamous cell carcinoma of larynx	2	III	T3N1M1	Malignant
B8	M	52	Nose	Squamous cell carcinoma of nasopharynx	2	I	T1N0M0	Malignant

B9	M	60	Tongue	Squamous cell carcinoma of tongue	2	II	T2N0M0	Malignant
B10	M	60	Tongue	Squamous cell carcinoma of tongue	2	II	T2N0M0	Malignant
C1	M	67	Larynx	Squamous cell carcinoma of throat	3	II	T2N0M0	Malignant
C2	M	48	Cheek	Squamous cell carcinoma of cheek	1	II	T2N0M0	Malignant
C3	M	70	Oral cavity	Squamous cell carcinoma of right mandible	2	II	T2N0M0	Malignant
C4	M	43	Oral cavity	Squamous cell carcinoma of right mandible	2	II	T2N0M0	Malignant
C5	M	56	Pharynx	Squamous cell carcinoma of pharynx	2	II	T2N0M0	Malignant
C6	M	45	Cheek	Squamous cell carcinoma of right cheek	-	II	T2N0M0	Malignant
C7	M	47	Larynx	Squamous cell carcinoma of larynx	2	II	T2N0M0	Malignant
C8	M	61	Pharynx	Squamous cell carcinoma of epiglottis	-	II	T2N0M0	Malignant

C9	M	50	Larynx	Squamous cell carcinoma of larynx	2	II	T2N0M0	Malignant
C10	F	38	Lip	Squamous cell carcinoma of lower lip	2	II	T2N0M0	Malignant
D1	M	47	Larynx	Squamous cell carcinoma of larynx	3	III	T2N1M0	Malignant
D2	F	50	Pharynx	Squamous cell carcinoma of hypopharynx	2	III	T2N1M0	Malignant
D3	M	71	Pharynx	Squamous cell carcinoma of hypopharynx	2	III	T2N1M0	Malignant
D4	M	44	Pharynx	Squamous cell carcinoma of hypopharynx	2	III	T2N1M0	Malignant
D5	M	61	Pharynx	Squamous cell carcinoma of epiglottis	2	III	T2N1M0	Malignant
D6	M	54	Oral cavity	Squamous cell carcinoma of left upper jaw	2	III	T3N0M0	Malignant
D7	M	61	Pharynx	Squamous cell carcinoma of hypopharynx	3	III	T3N0M0	Malignant
D8	M	58	Larynx	Squamous cell carcinoma of larynx	3	III	T3N0M0	Malignant

D9	M	63	Pharynx	Squamous cell carcinoma of epiglottis	2	III	T3N1M0	Malignant
D10	M	71	Pharynx	Squamous cell carcinoma of epiglottis	3	III	T3N1M0	Malignant
E1	M	51	Pharynx	Squamous cell carcinoma of left pharynx	2	III	T3N1M0	Malignant
E2	M	55	Larynx	Squamous cell carcinoma of larynx	2	III	T3N1M0	Malignant
E3	M	75	Oral cavity	Squamous cell carcinoma of maxillary sinus	2	IV	T4N0M0	Malignant
E4	M	56	Pharynx	Squamous cell carcinoma of epiglottis	1	IVA	T4N0M0	Malignant
E5	M	57	Larynx	Squamous cell carcinoma of larynx	-	IVA	T4N0M0	Malignant
E6	M	49	Larynx	Squamous cell carcinoma of larynx	3	IVA	T4N1M0	Malignant
E7	F	69	Cheek	Squamous cell carcinoma of right cheek	2	I	T2N0M0	Malignant
E8	M	29	Larynx	Squamous cell carcinoma of larynx	-	II	T2N0M0	Malignant

E9	F	56	Lip	Squamous cell carcinoma of oral lip	2	II	T2N0M0	Malignant
E10	M	50	Oral cavity	Squamous cell carcinoma of maxillary sinus	2	II	T2N0M0	Malignant
F1	M	50	Tongue	Squamous cell carcinoma of tongue	3	II	T2N0M0	Malignant
F2	M	64	Larynx	Squamous cell carcinoma of larynx	3	II	T2N0M0	Malignant
F3	M	49	Larynx	Squamous cell carcinoma of larynx	3	III	T2N1M0	Malignant
F4	F	42	Nose	Squamous cell carcinoma of nasal sinus	3	III	T3N0M0	Malignant
F5	M	50	Larynx	Squamous cell carcinoma of larynx	3	III	T3N1M0	Malignant
F6	M	58	Larynx	Squamous cell carcinoma of larynx	3	IV	T2N2N0	Malignant
F7	M	75	Nose	Squamous cell carcinoma of nasal sinus	3	IV	T4N0M0	Malignant
F8	M	48	Pharynx	Squamous cell carcinoma of hypopharynx	3	IV	T4N0M0	Malignant

F9	M	74	Pharynx	Squamous cell carcinoma of hypopharynx	-	IV	T4N0M0	Malignant
F10	M	65	Larynx	Squamous cell carcinoma of larynx	3	IV	T3N2M0	Malignant
G1	F	32	Oral cavity	Carcinoma sarcomatodes of maxillary sinus	-	II	T2N0M0	Malignant
G2	F	40	Lymph node	Metastatic mucoepidermoid carcinoma	-	-	-	Metastasis
G3	M	67	Lymph node	Metastatic mucoepidermoid carcinoma	-	-	-	Metastasis
G4	M	45	Lymph node	Metastatic mucoepidermoid carcinoma	-	-	-	Metastasis
G5	M	47	Lymph node	Metastatic squamous cell carcinoma	1	-	-	Metastasis
G6	M	48	Lymph node	Metastatic squamous cell carcinoma	2	-	-	Metastasis
G7	M	53	Lymph node	Metastatic squamous cell carcinoma	3	-	-	Metastasis
G8	F	45	Lymph node	Metastatic squamous cell carcinoma	2	-	-	Metastasis

G9	F	52	Lymph node	Metastatic acinic cell carcinoma	-	-	-	Metastasis
G10	M	38	Tongue	Adjacent normal tongue tissue	-	-	-	NAT
H1	M	28	Tongue	Tongue tissue	-	-	-	Normal
H2	F	27	Tongue	Tongue tissue	-	-	-	Normal
H3	M	48	Tongue	Tongue tissue	-	-	-	Normal
H4	F	42	Tongue	Adjacent normal tongue tissue	-	-	-	NAT
H5	F	15	Tongue	Tongue tissue	-	-	-	Normal
H6	F	19	Tongue	Tongue tissue	-	-	-	Normal
H7	M	35	Tongue	Tongue tissue	-	-	-	Normal
H8	F	18	Tongue	Tongue tissue	-	-	-	Normal
H9	F	19	Tongue	Tongue tissue	-	-	-	Normal
H10	M	28	Tongue	Tongue tissue	-	-	-	Normal

Appendix VIII: western blot solutions

-RIPA lysis buffer stock solution

150 mM NaCl, 1.0% IGEPAL® CA-630, 0.5% sodium deoxycholate, 0.1% SDS (GE Healthcare), 50 mM Tris, pH 8.0.

-RIPA lysis buffer working solution

940 µl RIPA buffer, 50 µl protease inhibitor (1x cOmplete mini EDTA free, S8830) , 10 µl 1x phosphatase inhibitor (P5726)

-4x sample loading buffer (Lammeli buffer)

300 mM Tris-HCl pH 6.8, 35% glycerol (GE Healthcare), 12% SDS, 0.02% bromophenol blue, 6% mercaptoethanol, made up to 20 ml with deionised water.

-1.5M Tris-HCL (pH 8.8):

36.6g Tris, 200ml of distilled H_2O, Adjust pH with HCL.

-10% (w/v) ammonium persulfate (APS):

100g of APS, 1ml of distilled H_2O.

-10% (w/v) SDS (10ml):

1g SDS, 10ml of distilled H_2O.

-Preparation of resolving and stacking gel:

10% Resolving gel for 20 ml	
H_2O	7.9 ml
30% acrylamide mix	6.7 ml
1.5 M Tris-HCl (pH 8.8)	5.0 ml
10% SDS (GE Healthcare)	0.2 ml
10% ammonium persulfate	0.2 ml
TEMED	0.008 ml

12% Resolving gel for 20 ml	
H_2O	6.6 ml
30% acrylamide mix	8.0 ml
1.5 M Tris-HCl (pH 8.8)	5.0 ml
10% SDS (GE Healthcare)	0.2 ml
10% ammonium persulfate	0.2 ml
TEMED	0.008ml

5% Stacking gel for 10 ml	
H_2O	6.8 ml
30% acrylamide mix	1.7 ml
1.5 M Tris-HCl (pH 8.8)	1.25 ml
10% SDS (GE Healthcare)	0.1 ml
10% ammonium persulfate	0.1ml
TEMED	0.01 ml

-10x Running buffer

15 g Tris base, 72 g Glycine and 5 g SDS (GE Healthcare) in 500 ml deionised water.

-10x Transfer buffer

30 g Tris base and 144 g Glycine in 1 L deionised water.

-1X Running buffer

100 mL running buffer stock 10x and 900 ml distillate H_2O

-1x Transfer buffer

100 ml 10x Transfer buffer, 200 ml methanol, 10 ml 10% SDS (GE Healthcare) and 690 ml deionised water.

-PBS Tween 20 (PBST)

1 ml of Tween 20 in 1 L PBS (pH 7.4)

-5% blocking solution

5 g milk (less than 0.1% fat) in 100 ml of 0.1% PBST.

-Developing solution

50 ml multigrade developer (ILFORD) in 500 ml distilled H_2O.

-Fixation solution

50 ml rapid fixer (ILFORD) in 500 ml distilled H_2O.